THÈSE POUR OBTENIR LE GRADE DE DOCTEUR DE L'UNIVERSITÉ DE MONTPELLIER

En Chimie et Physico-Chimie des Matériaux

École doctorale Sciences Chimiques Balard ED 459

Unité de recherche Institut Européen des Membranes

Development of Highly Efficient Artificial Water Channels for Water Desalination

Présentée par Dmytro STRILETS
Le 24 Novembre 2021

Sous la direction de Mihail BĂRBOIU

Devant le jury composé de

Stéphane VINCENT, Professeur, Université de Namur ASBL	Président du jury
Mihail BĂRBOIU, Directeur de Recherche, CNRS-IEM	Directeur de thèse
Sophie CERNEAUX, Maîtresse de Conférences, ENSCM	Co-encadrante de thèse
Nicolas GIUSEPPONE, Professeur, Institut Charles Sadron	Rapporteur
Narcis AVARVARI, Directeur de Recherche, Université d'Angers	Rapporteur
Andreea PASC, Professeur, Université de Lorraine	Examinateur
Sébastien ULRICH, Chargé de recherche, Université de Montpellier	Examinateur

UNIVERSITÉ DE MONTPELLIER

THÈSE POUR OBTENIR LE GRADE DE DOCTEUR DE L'UNIVERSITÉ DE MONTPELLIER

En Chimie et Physico-Chimie des Matériaux

École doctorale Sciences Chimiques Balard ED 459

Unité de recherche Institut Européen des Membranes

Development of Highly Efficient Artificial Water Channels for Water Desalination

Présentée par Dmytro STRILETS
Le 24 Novembre 2021

Sous la direction de Mihail BĂRBOIU

Devant le jury composé de

Stéphane VINCENT, Professeur, Université de Namur ASBL	**Président du jury**
Mihail BĂRBOIU, Directeur de Recherche, CNRS-IEM	**Directeur de thèse**
Sophie CERNEAUX, Maîtresse de Conférences, ENSCM	**Co-encadrante de thèse**
Nicolas GIUSEPPONE, Professeur, Institut Charles Sadron	**Rapporteur**
Narcis AVARVARI, Directeur de Recherche, Université d'Angers	**Rapporteur**
Andreea PASC, Professeur, Université de Lorraine	**Examinateur**
Sébastien ULRICH, Chargé de recherche, Université de Montpellier	**Examinateur**

Acknowledgements

I would like to thank a number of people for their help and support during the production of this thesis.

I would like to express my sincere gratitude to my thesis supervisor Dr. Mihail Barboiu. His patience, enthusiasm, co-operations and suggestions made me present this research work to produce in the present form. His brilliant, skilful supervision enriched this study higher than my expectation. I could not remain any more without giving heartfelt thanks to Dr. Barboiu for his painstaking supervision throughout the study period. This research work would not be possible without his stimulation, inspiration and cooperation.

Gratitude is due towards our collaborator who worked together with us on various projects, as so I would like to thank Prof. Tomoki Ogoshi and Dr. Marc Baaden.

I would like to thank my thesis co-director Dr. Sophie Cerneaux for investing time and effort into trying to find solutions for our joint research work. I would like to thank my current and former colleagues, Iuliana Marilena Andrei, Cristina Ion, Sanaa Daakour, Omar Samhari, Libo Huang, Dandan Su, Maxime Leclere, Kelvinraj Nursiah, Romain Dupuis, Maria di Vincenzo and for their involvement and for making the group a more welcoming place. Additional thanks to Maria di Vincenzo, who helped me understand membrane fabrication process and for tea times with nice talks during my stay in this group.

I would like to say thank you to all members of jury: Prof. Nicolas Giuseppone, Dr. Narcis Avarvari, Prof. Andreea Pasc, Prof. Stéphane Vincent and Dr. Sébastien Ulrich for participation in the defence and for fruitful discussion

Also I would like to thank my friend Erol-Dan Licsandru, who encouraged me to continue my research career.

Last, but not least, my warm and heartfelt thanks go to my family and friends for their tremendous support and hope they had given to me. Without that hope, this thesis would not have been possible. Thank you all for the strength you gave me.

Resume - *version en français*

La déplétion des sources de l'eau douce a la cause de la pollution environnementale, et la croissance de la population et de l'industrie, a encouragé les scientifiques et les ingénieurs de développer des nouvelles directions pour la désalinisation de l'eau.

Les méthodes modernes de désalinisation membranaire sont capables de réduire la consommation d'énergie proche du niveau d'un minimum thermodynamique. Le développement de nouvelles membranes biomimétiques à base de protéines de transport naturelles – les aquaporines – ou de ses analogues synthétiques – les canaux d'eau artificiels – permet les méthodes de désalinisation d'arriver à un nouveau niveau de consommation énergétique efficace.

Le but de ce travail a été la conception de nouveaux types de canaux d'eau artificiels auto-assemblés à haute efficacité, d'étudier leur permsélectivité de l'eau et leur mécanisme de transport. A la fin, l'objectif fut la transition suivante des canaux d'eau artificiels du niveau nanométrique au niveau macroscopique en montrant la possibilité de fabrication de membranes incorporées à l'AWC. Deux concepts de canaux d'eau artificiels auto-assemblés sont présentés ici, dont ont montré une capacité élevée de transport sélectif de l'eau. Les tentatives d'incorporation de Pillar[5]arene dans la membrane de désalinisation ont conduit au développement des membranes en polyamide de dessalement amélioré incorporant AWC avec une perméabilité à l'eau significativement élevée et un rejet presque complet des ions dans des conditions d'osmose inverse.

Le manuscrit est divisé en quatre chapitres. Le premier chapitre fournit une étude bibliographique complète mettant en évidence les principales caractéristiques structurelles de la protéine naturelle de transport Aquaporin, couvrant la totale connaissance actuelle du domaine des canaux d'eau artificiels avec un aperçu sur les stratégies possibles d'incorporation d'Aquaporin, ainsi que des canaux d'eau artificiels dans membranes polymères pour la purification de l'eau et la désalinisation.

Les chapitres II-IV comprennent trois articles scientifiques, qui constituent le noyau expérimental de cette thèse.

Le deuxième est concentré sur l'étude des capacités de transport de l'eau/des ions et de la nature du mécanisme de transport des dimères tubulaires discrets auto-assemblés de peralkyl-carboxylate-pillar[5]arène (PAD). En utilisant des méthodes avancées telles que la cristallographie aux rayons X et la simulation MD combinées complémentairement avec les techniques d'investigation du transport des ions d'eau comme la méthode Stopped flow et la spectroscopie de fluorescence, on a montré que ces canaux sont capables de former des pores toroïdaux à l'intérieur de la bicouche lipidique, qui pourraient transporter sélectivement les molécules d'eau vers le haut. à 5,21 $\times \cdot 10^7$ H_2O/s/canal.

Le troisième chapitre montre l'incorporation de Pillar[5]arène dans des matrices polymères pour obtenir des matériaux fonctionnels pour la désalinisation de l'eau. La méthode d'agrégation et de polymérisation inter faciale in situ – isAGRIP a été utilisé. Nous avons réussi d'incorporer de manière homogène des canaux d'eau artificiels en PA[5], ce qui a conduit à une augmentation de ~ 40 % de la perméance à l'eau avec une excellente productivité de 50 $L \cdot m^{-2} \cdot h^{-1}$ sous 17,5 bar de pression appliquée, tout en maintenant une sélectivité élevée de 99,4 %. .

Le quatrième chapitre a rapporté l'expansion de la famille des canaux d'eau artificiels par la synthèse de nouveaux dérivés uréido hydrophobes et leur mélange avec des I-quartets hautement efficaces afin de construire de nouveaux canaux d'eau supramoléculaires hybrides auto-assemblés. Les études sur le transport de l'eau et des ions ont montré que les systèmes bi-composants ont multiplié par plusieurs fois la perméabilité monocanale par rapport aux systèmes à un seul composé, alors qu'aucun transport d'ions significatif n'a été détecté. La performance la plus élevée a été montrée par le système HC8/S8-8 formé par le mélange des dérivés d'imidazole et de benzsulfonamine avec une perméabilité de près de 8,2 × 10^7 H_2O/s/canal.

En conclusion, ce travail présente plusieurs systèmes AWC qui fonctionnent avec succès comme filtres à eau sélectifs au niveau moléculaire ainsi qu'au niveau macro.

Summary - *English version*

Depletion of fresh water supplies due to environmental pollution, population and industrial growth, encouraged scientists and engineers to develop new directions in water desalination.

Modern membrane desalination methods are able to reduce energy consumption close to the level of a thermodynamic minimum. Development of novel biomimetic membranes based on natural transport proteins – Aquaporins – or its synthetic analogues – artificial water channels – aims to bring desalination methods on a new level of efficient energy consumption.

This work aims to design new types of highly efficient self-assembled artificial water channels, investigate their water permselectivity, and transport mechanism. Consequently, it follows the transition of artificial water channels from nanoscale to macroscale level by proposing a potential way of fabricating AWC-incorporated membranes. Here, the design of self-assembled artificial water channels based on two perspective platforms is presented: Pillar[5]arene and alkylureido derivatives. Both of them displayed high selective water transport ability. The attempts to incorporate Pillar[5]arene into desalination membrane led to development of enhanced desalination polyamide membranes incorporating AWC with significant high water permeability and almost complete ion rejection under reverse osmosis conditions.

The manuscript is divided into four chapters. Chapter I provides a comprehensive bibliographic study highlighting the key structural features of the natural transport protein Aquaporin, covering current developments of the field of artificial water channels. An overview of both possible strategies for water purification and desalination, the incorporation of Aquaporin, as well as artificial water channels into polymer membranes.

The following Chapters II-IV include three scientific articles, which constitute the experimental core of this thesis.

The Chapter II focused on the investigation of water/ion transport abilities and nature of the transport mechanism of self-assembled discrete tubular dimers of rim-differentiated peralkyl-

carboxylate-pillar[5]arenes (PADs). The objective was the assessment of water transport and selectivity, as well as the description of the functioning and structural existence/stability of PADs as perspective artificial water channels in lipidic systems. By using advanced methods as X-Ray crystallography and MD simulation combined with water and ion transport investigation techniques as Stopped-flow methods and fluorescence spectroscopy, it was demonstrated that the channels form toroidal pores inside lipid bilayer, which selectively transport water molecules up to 5.21 $\times \cdot 10^7$ H_2O/s/channel.

Chapter III presents the successful attempt to incorporate pillar[5]arenes into polymeric matrices to obtain functional materials for water desalination experiments using in-situ aggregation-interfacial polymerization method – isAGRIP. We succeeded to incorporate homogeneously PA[5] artificial water channels, which led to a ~40 % increase in water permeance with an excellent productivity of 50 $L \cdot m^{-2} \cdot h^{-1}$ under 17.5 bar applied pressure, while maintaining high selectivity of 99.4 %.

Chapter IV reported the expansion of artificial water channel family by synthesis of new hydrophobic ureido derivatives. These molecules were combined with high efficient I-quartets in order to construct novel hybrid supramolecular self-assembled water channels. Water and ion transport investigations showed that bi-component systems have a multiple times increased single channel permeability compared to single compound systems, while no significant ion transport was detected. The highest performance was shown by the system HC8/S8-8 formed by combination for imidazol and benzsulfonamine derivatives with permeability of almost 8.2 $\times 10^7$ H_2O/s/channel.

In conclusion, this work presents several AWC systems that successfully function as selective water filters both on molecular as well as macro-level.

Abstract

The objective of this work is the design new types of highly efficient self-assembled artificial water channels (AWC) and the investigation of their water permselectivity and transport mechanism aiming for the transition from nanoscale to macroscale by showing of possibility of AWC-incorporated membrane fabrication.

The starting point focused on the investigation of water/ion transport abilities and nature of transport mechanism of self-assembled discrete tubular dimers of rim-differentiated peralkyl-carboxylate-pillar[5]arenes (PADs). The objective was the assessment of water transport and selectivity of the transport, by describing the functioning and structural existence/stability of PADs in lipidic systems as perspective artificial water channels. By using advanced methods as X-Ray crystallography and MD simulation combined with water and ion transport investigation techniques such as Stopped-flow methods and fluorescence spectroscopy, it was proven that those channels able to form toroidal pores inside lipide bilayer, which could selectively transport water molecules up to 5.21 $\times \cdot 10^7$ H_2O/s/channel.

Inspired by those results, an attempt was made to incorporate pillar[5]arenes into polymeric matrices to obtain functional materials for water desalination experiments using in-situ aggregation-interfacial polymerization method – isAGRIP. We succeeded to incorporate homogeneously PA[5] artificial water channels, which led to a ~40 % increase in water permeance with an excellent productivity of 50 L $m^{-2}h^{-1}$ under 17.5 bar of applied pressure, while maintaining high selectivity of 99.4 %.

Finally, this work focused on expanding the artificial water channel family by synthesising new hydrophobic ureido derivative. These were combined with highly efficient I-quartets in order to construct novel hybrid supramolecular self-assembled water channels. Water and ion transport investigations showed that bi-component systems presents a multiple time increase single channel permeability compared to single compound systems, while no significant ion transport was detected. The highest performance was shown by the system HC8/S8-8 formed by combination of imidazol and benzsulfonamine derivatives with a permeability of almost 8.2 $\times \cdot 10^7$ H_2O/s/channel.

In conclusion, this work has described several AWC systems that function as selective water filters both on a molecular as well as on macro-level.

Keywords: artificial water channels; biomimetic membranes; reverse osmosis; water purification; thin-film composite, Pillar[5]arene, I-quartets, water permeability

Table of content

Abbreviations

ABMs	Aquaporin biomimetic membranes
AFM	Atomic force microscope
AQP	Aquaporin
ar/R	Aromatic arginine constriction
AWC	Artificial water channel
BWRO	Brackish water reverse osmosis
CNTP	Carbon nanotube porins
DCM	Dichloromethane
DI	Deionized water
DLS	Dynamic light scattering
DMF	Dimethylformamide
DMPC	1,2-dimyristoyl-sn-glycero-3-phosphocholine
DMSO	Dimethyl sulfoxide
DOPC	Dipalmitoylphosphatidylcholine
DOTAP	1,2-dioleoyl-3-trimethylammonium-propane
ED	Electrodialysis
EDX	Energy dispersive X-ray spectroscopy
EYPC	Egg yolk L-α-phosphatidylcholine
FO	Forward osmosis
FTIR	Fourier Transform Infrared spectroscopy
gA	Gramicidin A
HEPES	4-(2-hydroxyethyl)-1-piperazineethanesulfonic acid
HPTS	8-Hydroxypyrene-1,3,6-trisulfonic acid trisodium salt
IP	Interfacial polymerization
isAGRIP	In-situ aggregation-interfacial polymerization
KscA	K channel of streptomyces A
LbL	Layer-by-layer
LMV	Large multilamellar liposome
LPRO	Low pressure reverse osmosis
LUV	Large unilamellar vesicles
mCLRs	Molar Channel-to-lipid ratio
MD	Molecular dynamic simulation
MPD	M-phenylenediamine

m-PE	Hexa(m-phenylene ethynylene)
MWCO	Molecular weight cut-off
NF	Nanofiltration
NMR	Nuclear magnetic resonance spectroscopy
NPA	Asparagine-proline-alanine motive
PA	Polyamide
PA5	Pillararene
PADs	Dimers of rim-differentiated peralkyl-carboxylate-pillar[5]arenes
PAH4	Peptide-appended hybrid[4]arene
PAH5	Hydrazide-appended pillar[5]arenes
PAP5	Peptide-appended pillar[5]arene
PB-b-PEO	Poly(1,2-butadiene) and poly(ethylene oxide)
PBS	Phosphate buffered saline
PC	Phosphatidylcholine
PCTE	Polycarbonate track etch
PDMS	Poly(dimethylsiloxane)
PES	Poly(ether sulfone)
PMOXA	Poly(2-methyl-2-oxazoline)
POCs	Porous organic cages
PS	Phosphatidylserine
PSf	Polysulfone
RO	Reverse osmosis
SEM	Scanning electronic microscopy
SF	Selective filter
SLBs	Supported lipid bilayers
SWRO	Sea water reverse osmosis
TEM	Transmission electron microscopy
TFC	Thin film composite membrane
TMC	Trimesoylchloride
XRD	X-Ray diffraction analysis

Introduction

Our planet Earth is also known as the “Blue planet”, since 71% of its surface is covered by water. However, 97% is sea water, which is unsuitable for drinking and industrial use, and only 1% accounts for accessible fresh water out of 1.39 billion km^3. In the 21^{st} century, humanity thus is facing three most troubling problems: water scarcity, accelerated population growth and climate changes. The last two challenges adversely affect the first one therefore immediate action is required to solve water scarcity, otherwise it threatens our survival. The problem of water sustainability could be solved by finding new purification methods and seek for alternative water resources.

Regarding the fact that seawater is dominant on our planet, water desalination of saline water is the most attractive way to provide clean drinkable water. Currently, there are many methods of desalination that are thermal processes and membrane desalination processes. The common methods of membrane desalination are reverse osmosis (RO), forward osmosis (FO), electrodialysis (ED), and nanotechnology-based processes. In the literature, methods such as humidification dehumidification, vapor compression, multi-stage flash and multi-effect distillation are also described to desalinate water. Evaporation and condensation of water are the main principles involved in thermal processes. These processes require energy that is cost-effective to produce fresh water in large quantity. With the objective to lower this energy consumption, membrane technology development has risen.[1] In addition, the development of energy recovery devices, more efficient pumps and membranes, and the development of improved configurations has made it possible to significantly increase the energy efficiency of membrane desalination in recent years.[2-3] Thus, just for the desalination stage, the development of high-efficiency membranes has reduced energy consumption to a level of 1.8 kWh/m^3, allowing 50% of freshwater recovery.[4] Nonetheless, taking into account the magnitude of the world's desalination capacity, the total cost of energy remains significant.

The discovery of aquaporins, natural water transporting proteins, has offered hope as a solution to the energy consumption issue. Due to their unique properties, such as high transport and selectivity towards water, they were found attractive for the development of new membrane desalination technologies. However, challenges related to protein production, incorporation difficulty and membrane stability due to their aggregation in unnatural polymeric matrixes, do not allow to totally solve the problem of energy efficiency. Moreover, the AQPs do not show high permeability per unity of areas necessary to develop highly performant membranes for desalination

Artificial water channels (AWCs) are synthetic analogues of aquaporins, which fully or partially mimic structure and/or transport function of natural proteins. Highly efficient AWC-incorporated water desalination membranes were fabricated, being characterized by a water transport efficiency one order of magnitude superior than the currently available commercial membranes. The discovery of aquaporins and the subsequent development of artificial water channels opened a new chapter in membrane desalination technologies.

The three main objectives of the PhD project described in this thesis were as follows:

I) the assessment of water transport and selectivity, description of the functioning and structural existence/stability of self-assembled discrete tubular dimers of rim-differentiated peralkyl-carboxylate-pillar[5]arenes (PADs) as perspective artificial water channels in lipidic systems;

II) incorporation of pillar[5]arene into polymeric matrices to obtain functional materials for water desalination experiments;

III) expanding the artificial water channel family by exploring different design approaches by synthesizing new hydrophobic molecules and combination of them for the construction of novel supramolecular self-assembled water channels.

The manuscript is divided into four chapters. Chapter I provides a comprehensive bibliographic study highlighting the key structural features of natural transport protein Aquaporin, covering current state-of-art of the field of artificial water channels with following overview of possible strategies of incorporation of Aquaporin, as well as artificial water channels into polymer membranes for water purification and desalination.

The following Chapters II-IV include three scientific articles, which are the experimental core of this thesis.

The Chapter II focused on investigation of water/ion transport abilities and nature of transport mechanism of self-assembled discrete tubular dimers of rim-differentiated peralkyl-carboxylate-pillar[5]arenes (PADs). The objective is the assessment of water transport and selectivity, description of the functioning and structural existence/stability of PADs as perspective artificial water channels in lipidic systems.

Chapter III dedicated to the incorporation of pillar[5]arene into polymeric matrices to obtain functional materials for water desalination experiments using in-situ aggregation-interfacial polymerization method – isAGRIP.

Chapter IV reported expanding of artificial water channel family by synthesis of new hydrophobic ureido derivatives and combination of them with high efficient I-quartets in order to construct a novel hybrid supramolecular self-assembled water channels.

Finally, we will conclude on the development of several AWC systems that are able to function as function as selective water filters both at molecular and macroscale levels.

Chapter I. Current State of the Art of Artificial Water Channels and Biomimetic Membranes

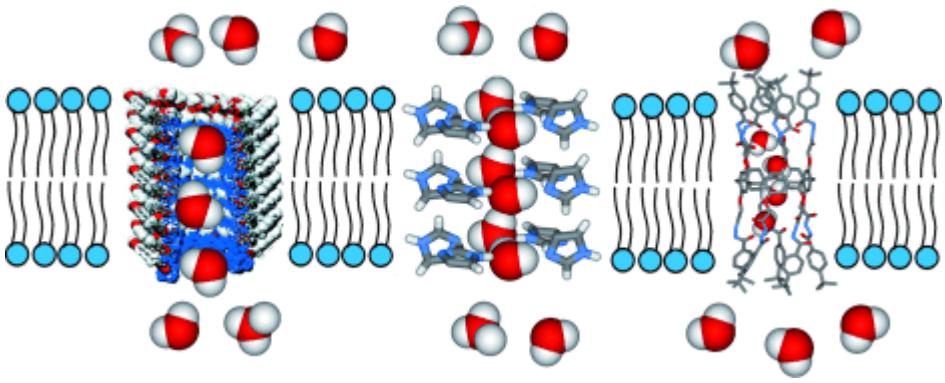

Water is essential for life, the main part of all human cells as well as all other plants, vertebrates, invertebrates and unicellular organisms. The cell membrane is the main barrier to the translocation of water between cells, however the mechanism of absorption/resorption of water from the cells remains unknown. For a long time, this problem has been debated by physiologists and biophysicists, and it was agreed that water transport through lipid membrane occurs by simple diffusion.[5]

Nonetheless, some scientists were convinced that specific water-selective pores are needed for high water permeability as was observed in many organs as for example in red blood cells and renal tubules.[6] Furthermore, an activation energy of this process was the same as for diffusion of water in bulk solution, around 5 kcal/mol. Moreover, there was known the specific antidiuretic hormone, vasopressin, which is involved in regulation of water transport through specialized tissues such as mammalian collecting duct or amphibian bladder. However, several attempts[7] to isolate or clone water transport proteins have allowed to explain the water transport mechanism with excluding protons (H_3O^+, hydronium ions).

1 Natural water channels

1.1 Aquaporins discovery

The discovery of Aquaporin1-AQP1, 28 kDa integral membrane protein in red cells and renal tubules, [8] was a first structural proof about existence of molecular water channels. This protein AQP1 exists as a tetramer with organization similar to several ion channel proteins and has intracellular N- and C-termini.[9] Two tandem repeats were revealed in the primary cDNA sequence, each containing three bilayer α-helices. [10] The loops connecting the second and third transmembrane segments in each repeat contained several highly conserved residues and an asparagine-proline-alanine (NPA) signature motif.

To confirm the water transport abilities of discovered water transport protein through the cell, AQP1 was tested on low-permeable Xenopus laevis oocytes. Those experiments showed highly remarkable increasing of water permeability after transferring laevis oocytes containing cRNA into hypoosmotic buffer, which could be reversibly inhibited by Hg^{2+}.[11] Besides, isolated and purified AQP1 were incorporated into lipid vesicles mimicking natural cell membrane and tested on water permeability. The water permeability of APQ1-containing vesicles was extremely high, $\sim 3\times10^9$ water molecules per subunit per second, although the transport of ions and other solutes was insignificant[12-13]. The same experiments without incorporated proteins also showed water permeability; however, Xenopus laevis oocytes and lipid vesicles containing AQP1 had 100 times increased water transport, which suggests that both theories, simple diffusion through the cell and the existence of hypothetical water channels, are partially correct and over the debates about water transport mechanism across the cell. Nowadays, AQP1 is known as first identified natural water channel that inspired many scientists for future researches in biology and chemistry.

1.2 The hourglass form and water transport function

Water molecules could pass through the cell membrane inside or outside under different physiological conditions, thus molecular structure of water channels must explain bi-directionality. Inhibition by mercury ions indicates on the presence of a free sulfhydryl within the water channel protein, which could react with Hg^{2+}, and, as result, block water transport and could be unblocked by reducing reaction. Structure analysis of primary amino acids sequence of AQP1 shows four cysteines, however only one group (C189) can be responsible of the mercury sensitivity to transport proteins, as it may be in the active part of the channel.[14] Several studies were focused on defining the protein topology[9,15], which helped to establish that APQ1 has a pseudo bi-fold symmetric structure with six α-helices surrounding the water pore, formed by two loops containing NPA, which enter the bilayer from opposite sides and overlap at the junction of two NPA motifs, which was later called ‘hourglass model’.[16] Advanced X-Ray crystal analysis and atomic force microscopy of purified AQP1 helped to

confirm suggestions of existence of 'hourglass model' and found that red cell water transport protein exists as tetramer of four AQP1 monomers, each containing six tilted, bilayer-spanning α-helices surrounding the two NPA-containing loops which enter the membrane from the opposite surfaces and are juxtaposed in the center.[17-24] Molecular dynamics simulations of water transport by AQP1 by two different groups[25-26] have led to an advanced understanding of how water can be rapidly transported across membranes while protons (H_3O^+) are repelled.

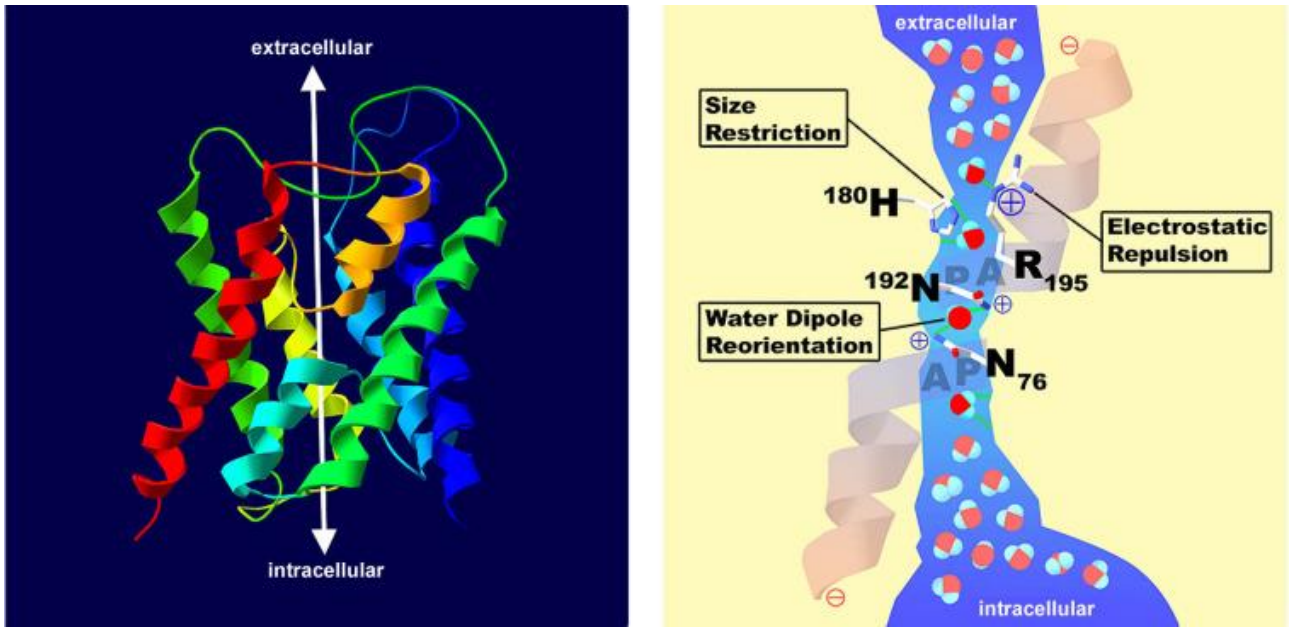

Figure 1. AQP1 subunit structure and water transport scheme. Left: strip model of AQP1 monomer showing six oblique bilayer domains and two pore-forming loops. Right: The overflow of water from the extracellular chambers into the intracellular ones occurs through a narrow column. Proton conduction (hydronium ion, H_3O^+) is prevented by size limitation and electrostatic repulsion (H180 and R195), as well as in the center of the channel, where partial positive dipoles are introduced by short α-helices lining the pores and two highly conserved asparagines (N76 and N192) in the signature motif NPA cause a temporary dipole reorientation of an isolated water molecule. Image adapted from reference [27].

The transport protein AQP1 mostly formed by hydrophobic residues, which concentrated on the widest inner part of 20 Å - length pore, but towards the center of the pore (~8 Å), the channel narrows forming the selectivity filter and there is a smooth transition from hydrophobic to hydrophilic part within diameter of 2.8 Å, which is close to the Van der Waals diameter of a single water molecule and performs the function of size restriction and electrostatic repulsion. This narrowest segment is formed by several amino acids, the most important of them being arginine R195 (from one of the NPA motifs) and histidine H180,

which provide a size restriction for molecules larger than water, and fixed positive charges to repel protons and other cations. Besides, the presence of phenylalanine residue F56 facilitates the passage of water due to hydrophobic effects. In addition, a string of four carbonyl oxygens of the peptide backbone (glycine G188, cysteine C189, glycine G190, and isoleucine I191) line the pore, serving as energetically favourable substitutes for hydrogen bonding (Figure 2).

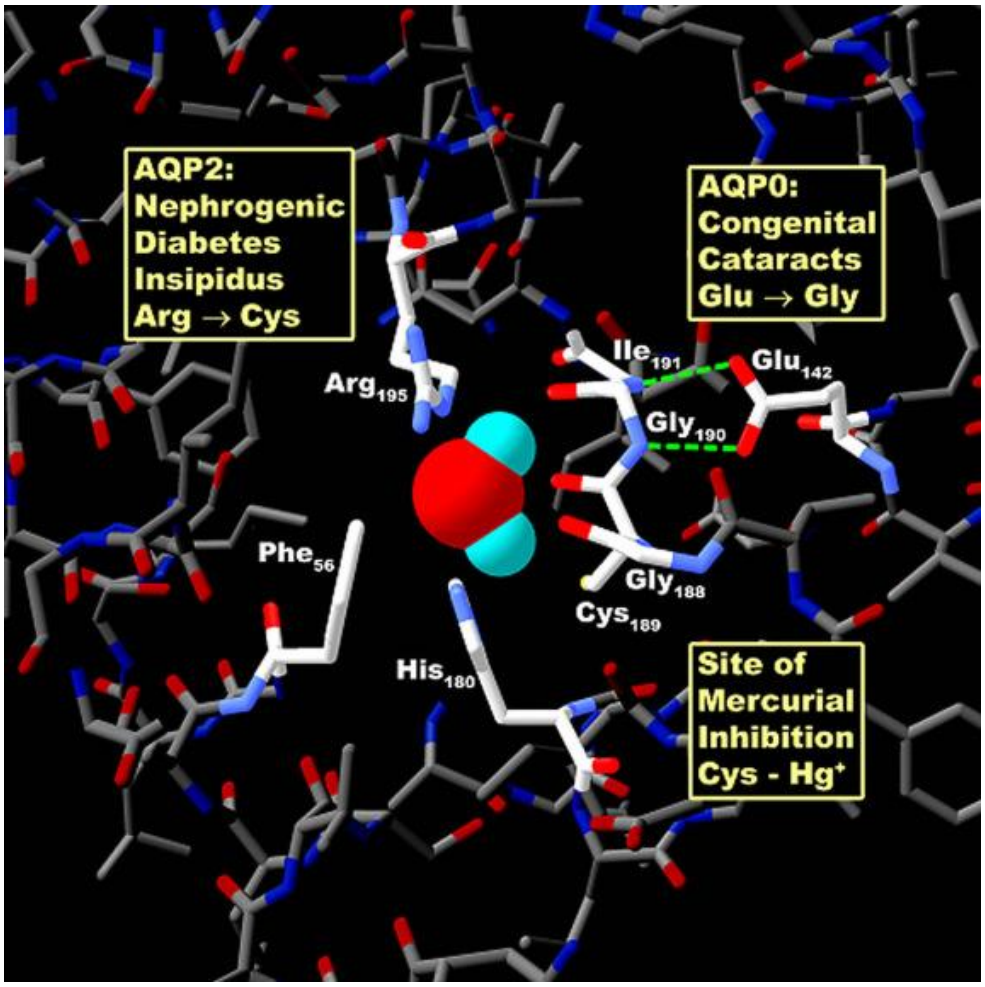

Figure 2. Horizontal cross-section representation of narrowest segment of AQP1. A single water molecule at the narrowest segment of the channel surrounded by functionally important residues (F56, R195, H180, and C189). Hydrogen bonding occurs between carbonyl oxygens on the peptide backbone (G188, C189, G190, and I191) at the other surface of the pore. Image adapted from reference [27].

2 Artificial water channels

Despite the fact that protein transport channels such as aquaporins can be synthesized using traditional bioprocessing techniques, production of protein-based membranes could be expensive and complex, due to the difficulty of purification methods involving many steps. These proteins can easily denature and loose functionality, hence it could affect the stability and create additional problems during membrane synthesis and use. Furthermore, biological channels are not necessarily the most optimal in terms of pore-loading efficiency and functionality for industrial processes. Synthetic, bioinspired channels could overcome the instability and poor processability of their biological analogous and provide a greater opportunity to tune performance for target applications.

Artificial Water channels-AWCs are synthetic counterparts, consisting of unimolecular or self-assembled channels presenting an inner water conducting pore and an outer hydrophobic exterior in interaction with the lipid bilayer or polymeric membranes. The artificial water channels (AWCs) can be divided into two main groups: unimolecular channels and self-assembled supramolecular channels. [28-29] Additionally, AWCs could be classified according to translocation mechanism as hydrophobic, hydrophilic and hybrid pores. In this section, it will be reviewed synthetic water channels, considering their design strategies and resultant transport properties.

2.1 Self-assembled supramolecular channels

Self-assembled supramolecular channels consist of a number of building blocks that connect themselves into a tubular structure by intermolecular forces such as hydrophobic interactions or hydrogen bonding. Early research on artificial water channels started from the development of self-assembling channels due to structural simplicity.

2.1.1 Dendritic dipeptide pores

The first known AWCs, dendritic dipeptide aquapores were proposed as a model water channel by Percec et al. in the 2000s. [30-31] The series of compound consists of amphiphilic

dendritic dipeptides which able to self-assemble into tubular structures by H-bonds formation between dipeptide dendrons with open pores of 12.8 Å. However, this AWCs have two main disadvantages: a) the necessity of creation of specific conditions for self-assembly as non-polarized and H-bond free media (cyclohexane, aliphatic component of lipid bilayer) and b) the thermal stability of self-assembled pores due to dynamic equilibrium states of dendron monomers between trans and gauche conformers at approximately 22 ºC (Figure 3).

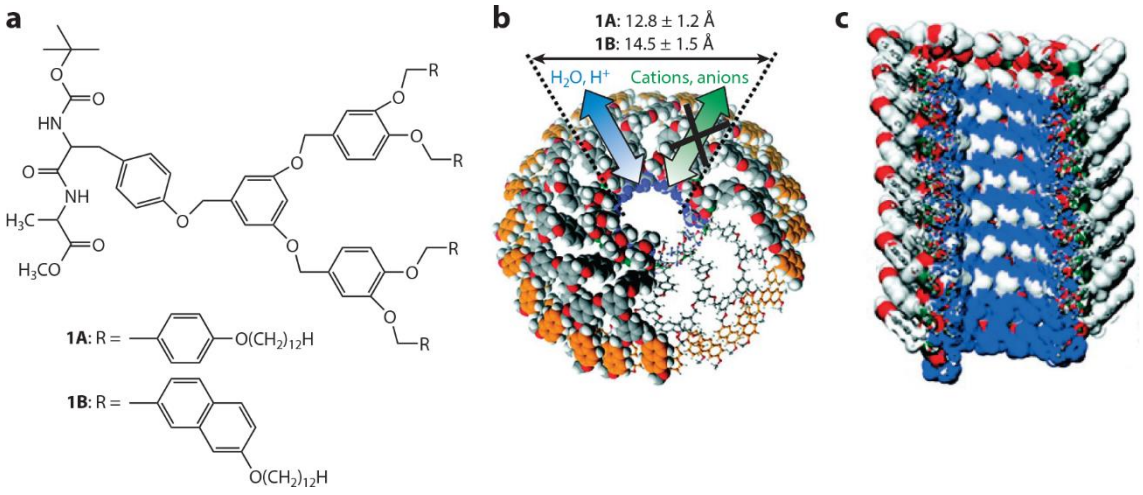

Figure 3. Dendritic dipeptide pores. (a) Chemical structures (1A and 1B, modified) of dendritic dipeptides with different dendritic periphery arms. (b) top and (c) cross-sectional views of simulation model of dendritic hydrophobic pores. Image adapted with permission from reference [31].

The possibility to incorporate dendritic dipeptide pores into the lipid bilayer allowed to test proton transport by monitoring the translocation of protons across lipid bilayers via pH-sensitive fluorescent dyes. These synthetic channels showed proton permeability comparable to that of the gramicidin A (gA) biological proton channel, a well-characterized membrane protein. [32-34] No water permeability through these channels was reported, however, in virtue of these experiments, it can also be argued that they can conduct water through the lipid membrane since proton transport is known to be accompanied by water transport. [35]

The thermal stability issue was solved by replacing benzyl ether moity by naphthyl groups that were located at the periphery of helical pores to induce π-π stacking interactions so that

the entire structure could be stabilized. This modification led to an increase of the thermal stability from 20 ºC to 40 ºC, but also affected the pore size slightly by increasing it up to 14.5 Å. Modified dendritic aquapores showed selective water and proton transports over Li^+, Na^+, and Cl^- monovalent ions; such selectivity was attributed to a hydrophobic effect near the channel entrance rather than the steric hindrance.

2.1.2 Imidazole quartet channels

Barboiu et al have previously reported that alkylureido-imidazole organic molecules can be used as scaffolds for the self-assembly of imidazole quartets (I-quartets) mutually stabilized by water wires. [36-38] They are similar to Influenza A M2 proton channels, a membrane protein that facilitates water and proton diffusion through water-filled pores, which have the imidazole quartet (I-quartet) motif in the histidine quartet selectivity filter and promote the transport of protons across the membrane.[39-43] As a result, it was developed ureido imidazole systems which could be self-assembled into transmembrane channels in lipid bilayer due to urea-urea, imidazole-imidazole and imidazole-water H-bonds formations and construct dipolar water wire arrays inside the tubular imidazole architectures. Those unique artificial systems have 2.6 Å inner diameter, which completely correlate with Van der Waals water molecule diameter, and, as a consequence, these channels could accommodate single water wire and enable to reject all kinds of ions except protons.

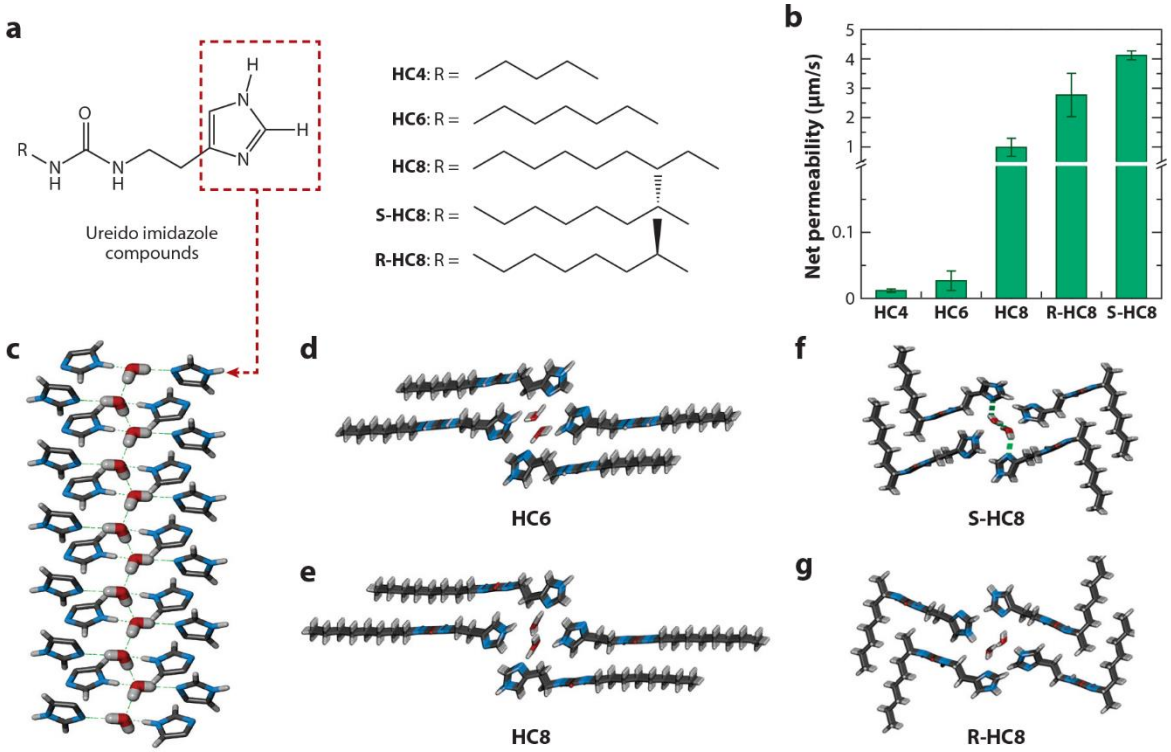

Figure 4. Imidazole quartet (I-quartet) channels. (a) Chemical structures of ureido imidazole compounds with various alkyl chain tails in terms of chain length and chirality. (b) I-quartet channel–embedded vesicular membrane water permeabilities. (c) Columnar assembly of imidazole moieties inside hydrophobic environments. (d–g) Hydrated crystal structures of (d) HC6, (e) HC8, (f) S-HC8, and (g) R-HC8, which contain dipolar water wires. Image adapted with permission from reference [43].

Currently, the family of I-quartet systems contains more than 5 compounds, which differ in terms of length and chirality of alkyl tails. Water transport abilities are improving with increasing of the alkyl chain length, which could be explained by rising of stability in lipid vesicles due to affinity to inner hydrophobic nature of lipid bilayer. Furthermore, chirality also improves the stability of the final channels and brings maximum increase in channel water permeability within ~1.5 × 10^6 H_2O molecules per second per channel for S-HC8, which is only two orders of magnitude lower than that of the classical mammalian AQP1.

The relevantly high water transport ability and incredible rejection properties are explained by H-bonding of water inside the channel with formation of tiny water arrays and the I-quartet channel's restricted pore structure, which is compatible with water molecules (which are 2.7 Å in size), suggesting that ~3 Å is the limited pore diameter for future desalination applications of artificial channel–based membranes.

2.1.3 Hexa(m-phenylene ethynylene) channels

Another self-assembled platform for development of high-efficient synthetic channels is represented by columnar nanopores that are less than 2 nm in diameter, with a straightforward strategy of stacking them coaxially. Gong et al. presented a family of macrocycles based on hexa(m-phenylene ethynylene) (m-PE), which have ability to self-assemble into columnar channels in solid state and hydrophobic media, such as lipid bilayer (Figure 5). [44]

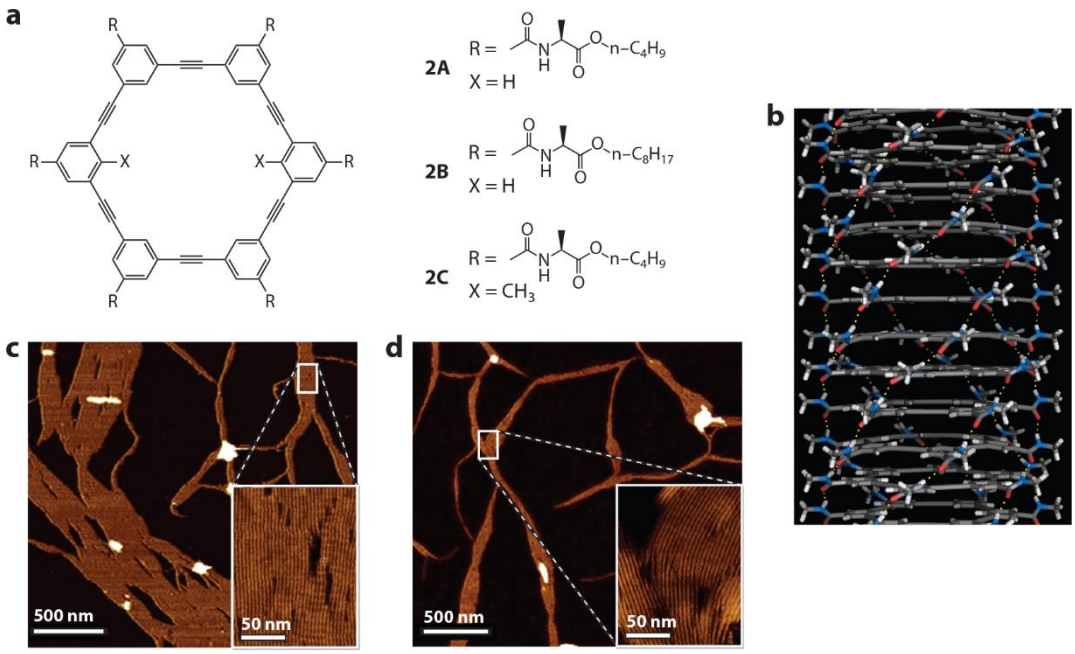

Figure 5. Hexa(m-phenylene ethynylene) (m-PE) channels. (a) Chemical structures of m-PE-based planar macrocycles. (b) A snapshot of quantum molecular dynamic simulations for the stacked columnar pore structure 2A. (c,d) Atomic force microscopy images of the assembled pillar structures (c) 2A and (d) 2B on a mica substrate in CCl_4. Image adapted from reference [44].

High stability of this class of channels is explained by H-bonding between amide groups present in side chains, as well as π-π stacking interactions of acetylene fragments and benzene rings. In lipid bilayer, 9 or 10 m-PE macrocycles could stack into columnar nanopore (~3.6 nm, 3.6 Å per π-π interaction) within 6.4 Å and 3.7 nm inner and outer diameters respectively, that perfectly fit the thickness of bilayer (~4 nm). [45] Water transport experiments using lipid bilayer incorporation method showed approximately 4.9 x 10^7 water molecules/s/channel or ~ 22% that of Aquaporin-AQP1 and ion channel transport activities: the conductance reaches ~ 5.8 pS for K^+, while no conductance is measured for Li^+ or Na^+ cations.

Another advantage of this type of AWC is the possibility of chemical modification of synthons. m-PE macrocycles have 2 sites for tuning: I) hydrogen of benzene rings (X, fig 5a) could be replaced by methyl group, which in turn reduces the inner pore diameter and brings more water/ion selectivity due to steric factor and II) external alkyl chains, which could be extended from $–C_4H_9$ to $–C_8H_{17}$, and, as result would increase pore stability in lipid bilayer without any conformational disruption to columnar pores.

2.1.4 Aquafoldamers

Zeng et al. were inspired by extraordinary features of the folding process of helical molecules as selective molecular recognition[46-48] and prompted to develop pyridine-based foldamers, which allow to stack into tubular channels and recognize H_2O molecules. [49-50] Investigation of aquafoldamers structure showed that this class of foldamers had helical 3D structure with inner pore size of 2.8 Å, which is comparable with AQP's selective filter. There are 2 main driving forces of pyridine-based foldamers self-assembly into helical tubular pores: I) 'sticky-end' approach, where each synthon has 2 functional groups - one is an ester and the other one is a rigid phenyl ring, which is involved in H-bond intermolecular interaction between the oxygen of one carboxyl group and one or two hydrogens from the benzene ring, and allow to elongate the overall helical structure for spanning the lipid bilayer and II) π-π aromatic stacking interactions between pyridine fragments of synthons, which is responsible for stability of tubular structure in lipid bilayer. Additional straight of channels comes from amid-water and water-water H-bond interactions inside the pore; combination of all of those interactions is contributing to maintaining 1D columnar stacks.

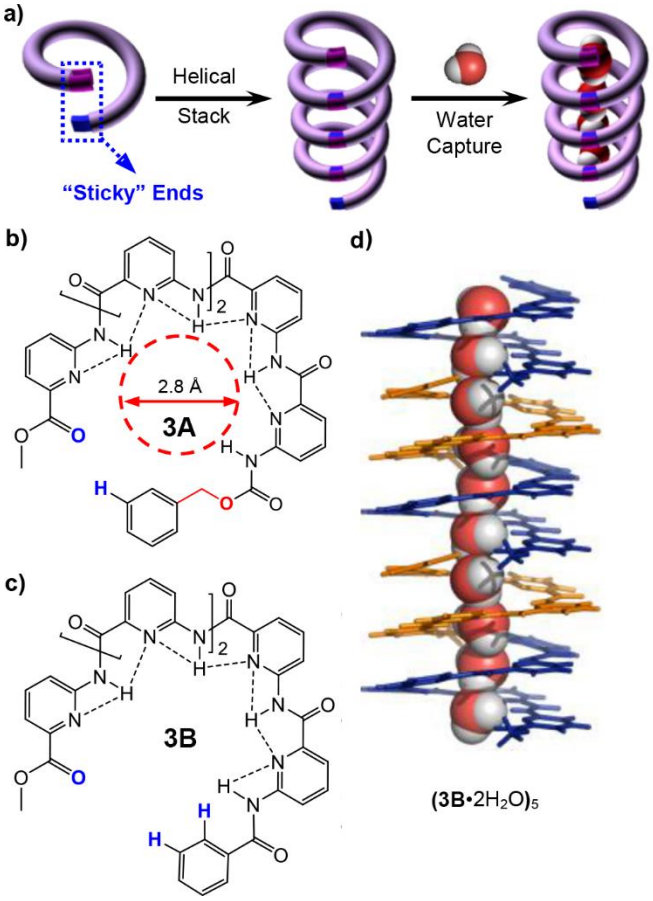

Figure 6. Chemical structure of synthons and crystal structures of aquafoldamer-based synthetic water channels. a) A "sticky end"-mediated molecular strategy for creating self-assembled 1D nanotubes for water transport. b) Chemical structure of **3A**. c) Chemical and d) crystal structures of **3B**, encapsulating 1D chain of water molecules. Image adapted from reference [51].

Recent investigation of aquafoldamers water transport ability by using stopped-flow method (shrinking mode) demonstrates incredible permeability of this class of AWC: two tested aquafoldamers **3A** and **3B** (Figure 6) showed single channel permeability of 3.0×10^9 H_2O molecules per second per channel and 2.2×10^8 H_2O molecules per second per channel, respectively, where in case of aquafoldamer **3A**, it reaches 50% capacity of AQP water permeability. [51]

Fluorescence HPTS (8-Hydroxypyrene-1,3,6-trisulfonic acid trisodium salt) assay was used for monitoring ion transport across lipid bilayer and compared with gramicidin-A (gA), a natural ion transport channel. This observation demonstrated that, unlike gA that can transport H^+, Na^+ and K^+ ions, aquafoldamer **3A** does not transport both Na^+ and K^+ ions, as well as Cl^- ion. However, previous investigation of aquafoldamer transport abilities showed

substantial proton conduction across the bilayer membranes when higher proton concentration was imposed at one side of the membranes (specific values were not reported), that suggests that I-quartet systems and aquafoldamers could transport water and protons with exclusion of other ions; the proton transport comes from Grotthuss mechanism, where protons can pass from one water molecule to another by analogy with the conductivity of electrons in a copper plate.

2.2 Unimolecular transmembrane channels

Unimolecular channels are single supramolecular compounds that have tubular pore structures which mimic properties of AQP. In general, this class of AWC is challenging to synthesize, however covalent-bonded framework is more favourable for future development of membrane for water treatment due to higher stability compared with self-assembled AWC.

2.2.1 Carbon nanotube porins

It was proven that nearly to Angstrom level, Hagen-Poiseuille flow model, classical model of Newtonian fluid flow, is not respected and the water flow through nano- or angström-scale hydrophobic cylindric pipes can be orders of magnitude faster[52-53] than the one calculated from the Hagen-Poiseuille flow model due to boundary slip mechanism. Therefore, carbon nanotube porins (CNTPs) became the object of research as a new promising platform for the selective and fast transport of water. [54-57] CNTPs are basically rolled up graphene sheets into perfect cylinders with variable diameter up to 8 Å.

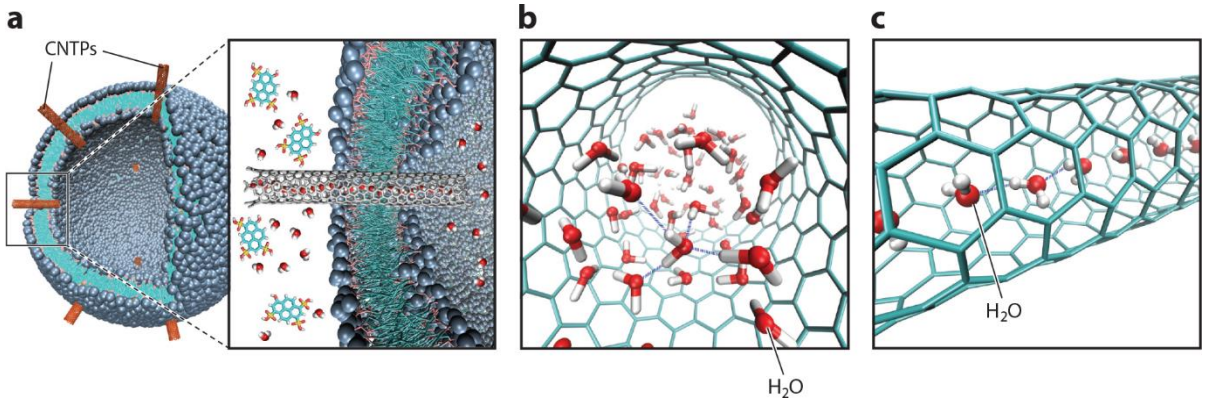

Figure 7. Carbon nanotube porins (CNTPs). (a) Illustration of CNTP-incorporated vesicles and transport of water through lipid membrane. Representation of (b) bulk water inside wCNTPs and (c) single file water inside the nCNTP from MD simulation. Image adapted from reference [57].

The water permeability of narrow CNTPs (nCNTPs) was determined as 2.3×10^{10} H_2O molecules per second per channel, which exceeds almost 6 times the value of AQP1. Interestingly, that wide CNTPs (wCNTPs with diameter of ~16 Å) single channel permeability equals to 2×10^{9} H_2O molecules per second per channel, which is one order of magnitude less than nCNTPs. [58] It could be explained by the fact that water exists as 1D chain inside nCNTPs, while water flows as bulk solution through wCNTPs; since bulk-state water molecules typically have higher number of H-bonds (3.9 on average) than do single-file water molecules (1.8 on average), less confined water resulted in a higher energy barrier for water transport.

Further, CNTPs do not show AQP-like salt and proton rejections, ion transport rates are strongly related to the level of ionic strength of the solutions and the hydration shell radii of the cations. However, CNTPs block anion transport, even at salinity that exceeds seawater level, and their ion selectivity can be tuned to configure them into switchable ionic diodes. These properties make CNTPs a promising material for developing highly permeable membrane for separation technologies.

2.2.2 Pillar(n)arene-based synthetic water channels

Pillar[n]arene-based systems play an important role in supramolecular chemistry, since they have well-defined electron-rich cavities, which in turn allow to accommodate different ions and molecules. [59] Due to their symmetrical structure and flexibility in modification, this class of molecules has inspired supramolecular chemists to design and synthesize pore-like tubular constructions with high aspect ratios and restricted pore sizes by extending side chains on pillararene templates. This simple strategy has been showed as a promising way to design efficient single-molecular water channel systems [60-61].

2.2.2.1 Hydrazide-appended pillar[5]arenes

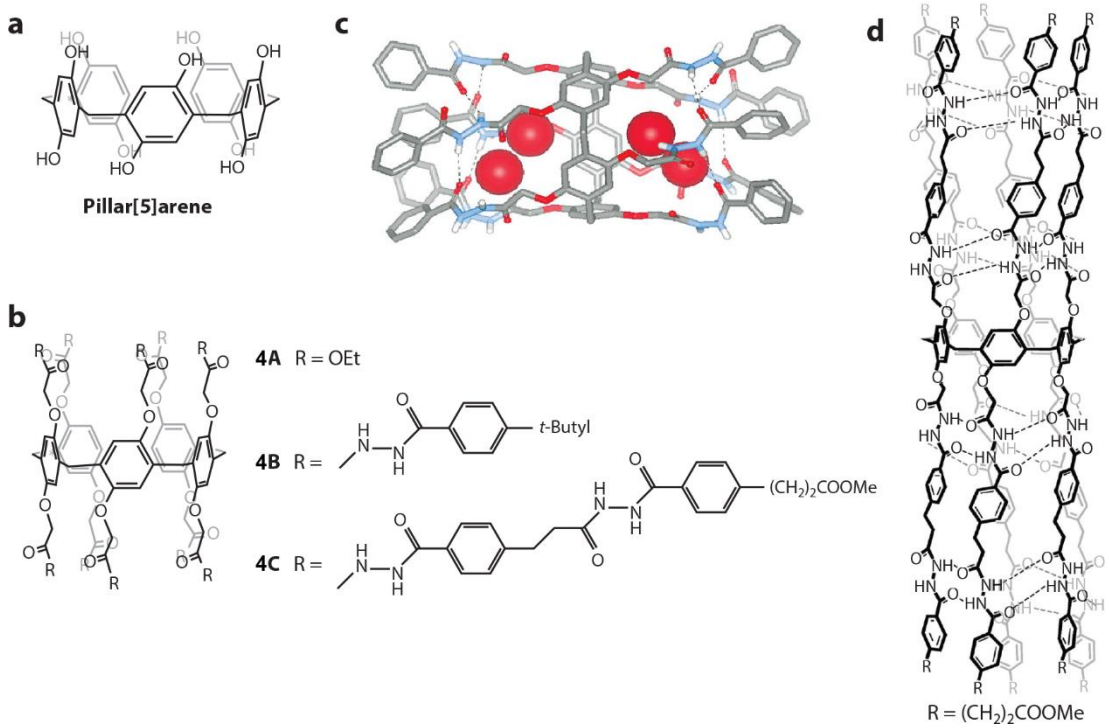

Figure 8. Hydrazide-appended pillar[5]arenes (PAH5). a) Crystal structure of pillar[5]arene. b) A series of PAH5. c) Chemical structure of **4B**. d) Schematic tubular conformation of **4C**. Image adapted from reference [61].

The first successful unimolecular synthetic water channels was hydrazide-appended pillar[5]arenes (PAH5) that was developed by Hou et al. [62] This class of pillararene-based compounds was obtained by synthesis of ester-substituted pillar[5]arene **4A**, which has the behaviour of water channels due to formation of continuously forming single-file water wire inside the pore. [63-64] This observation prompted the subsequent expansion of the compound library by replacing side chains of pillararene with hydrazine substitutes, where each structure

was clearly defined as having intramolecular H-bonds between hydrazide side chains, forming intact tubular structures. Crystal structure analysis of **4B** revealed unexpected details of water accommodation inside the channel: the water wires are cut at the middle of channels by H-bonding of water to hydrazide backbones, which might mean that PAH5 has ability to exhibit repulsion of protons due to disruption of the water wire. This structural information was confirmed experimentally, which gave the right to call these channels complete synthetic analogues of aquaporin, which showed the water transport ability with ion exclusion including the smallest cation – proton. [26, 65] However, attempts to extend the side hydrazine chain with the aim of overlapping the lipid bilayer (the length of **4C** is 5 nm, while the thickness of lipid bilayer is ~4 nm[29]) dramatically affected the water conductance; the single channel permeability was approximately 40 H_2O molecules per second per channel for structure **4C**, which explained by multiple H-bonds formation between water and repeating hydrophilic hydrazide groups or the possible denaturation of the cylindric structure of the pillars.

2.2.2.2 Peptide-appended pillar[5]arene

Next generation of pillararene-based channels by Hou et al. decided to replace the hydrazide backbones with hydrophobic poly-phenylalanine peptidic substitute, leaving pillar[5]arene as the central core of the channel.[66] Those changes led to an increase of single water permeability up to the level of natural aquaporins: novel peptide-appended pillar[5]arene had the average single channels osmotic water permeability of 3.5×10^8 water molecules per second, while permeability of AQP1 is 4×10^9 water molecules per second (one order of magnitude more than PAP5) and AQP0 has 3.4×10^8 water molecules per second per channel. MD simulation highlighted the mechanism of water transport through PAP5 channels; the water conductance occurred by wetting–dewetting transitions, preventing continuous water diffusion over extended periods of time, what distinguishes these pores from other AWCs.

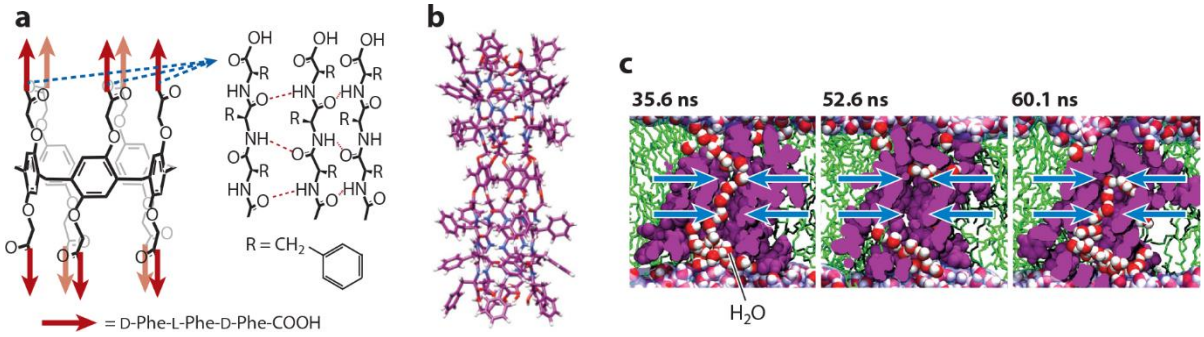

Figure 9. a) Structure of the peptide-appended pillar[5]arene (PAP) channel. b) Molecular modeling of the PAP[5] channel. c) Wetting/dewetting observation of a PAP channel from MD simulation of water transport in a POPC bilayer. Image adapted from reference [66].

Despite incredible water transport ability, PAP5 presents a drawback when it comes to ionic selectivity, which is attributed to the pore size of pillar[5]arene (~5 Å), that is in excellent agreement with a previous hypothesis that 3 Å is the critical pore diameter for efficient ion rejection.[37] They allow the passage of ions with selectivity according to their hydration energy: $NH_4^+ > Cs^+ > Rb^+ > K^+ > Na^+ > Li^+ > Cl^-$.

2.2.2.3 Peptide-appended hybrid[4]arene

Next artificial water channel cannot be called fully pillararene-based, due to the fact that Hybrid[4]arene were used instead of Pillar[n]arene to form the backbone in the design of this channel. Previous attempts to create the perfect artificial channel performed by Hou et al. pushed to develop peptide-appended hybrid[4]arenes (PAH4s).[67] The difference between PAP5 and PAH4 is that hybrid[4]arene was used as the core of the channel, an arene of alternating resorcinol and catechol subunits (2 each, 4 subunits total), linked alternately at the meta and ortho positions, with keeping 8 peptide appendages.

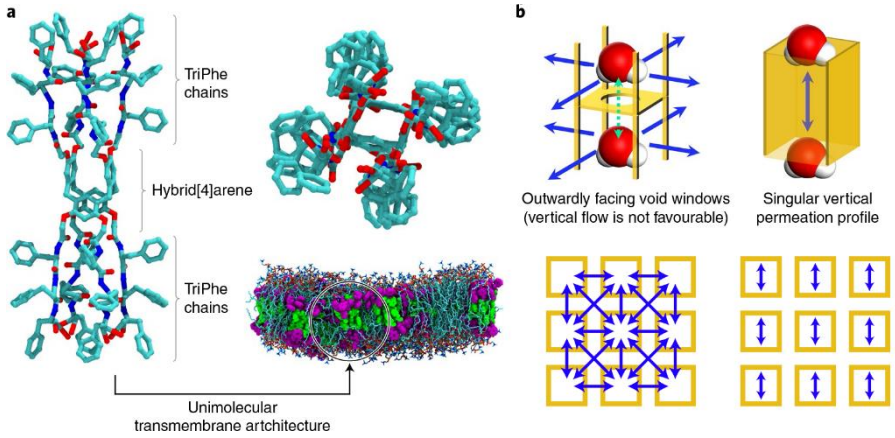

Figure 10. a) Molecular model of the peptide-pillar[4]arene, PAH[4]. b) Proposed water permeation conduits (blue arrows) between PAH[4] (left) and traditional AWC (right) configuration. Image adapted from reference [67].

Changing of backbone from pillar[5]arene to hybrid[4]arene led to the formation of the narrowest part of the channel with dimension ~3 Å × ~5 Å, and ability to create dense clusters within amphiphilic matrices. MD simulation showed interesting water transport mechanism: the center of the channel is relevantly impermeable, however presence of dynamic voids of 2 – 4 Å width allows for interconnected water-wire pathways to hop between channels. This is explaining extremely high water permeability measured by stopped-flow technique – 3.7×10^9 water molecules per second per channel. Sodium permeability through the pores was undetectable, while chloride permeability was not significant. Based on reported chloride and water permeations, PAH[4]- incorporated pristine biomimetic membranes could theoretically achieve water-salt selectivity of at least $\sim 10^8$, far exceeding the current 10^4–10^5 desalination membranes water/salt selectivity. [68]

2.2.2.4 Artificial aquaporin

Excellent work was done by Hou et al. who developed new synthetic analogues of aquaporin using pillar[5]arene platform.[69] They used positively-charged amino groups as side substituents connecting to pillar[5]arene backbone via alkyl chains. For this new type of synthetic channels, tryptophan (Trp) residues were introduced to enhance their membrane-incorporation ability.

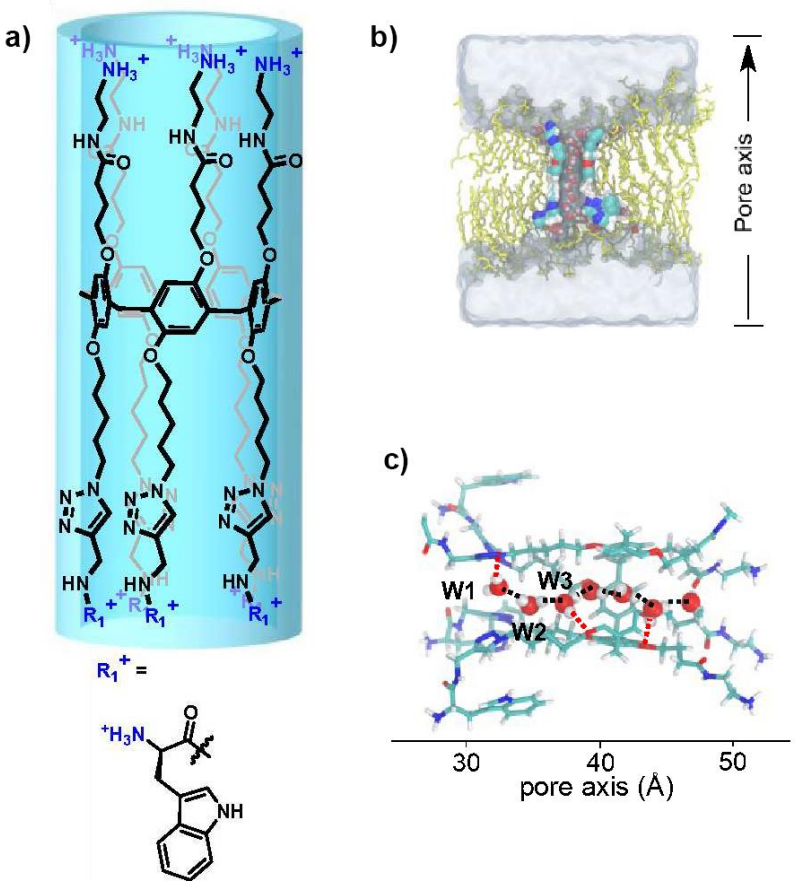

Figure 11. Artificial aquaporin used in medical applications. a) Chemical structure of artificial AQP. b) MD simulation of artificial AQP in a palmitoyloleoyl-phosphocholine (POPC) lipid bilayer. c) Molecular structure and interactions of synthetic channel with water-wire file. Image adapted from reference [69].

This elegant and successful solution made it possible to completely mimic the structure and properties of natural aquaporins. The observed water permeability was determined as 2.7 × 10^9 water molecules per second for each channel, which is more than 50% capacity of AQP1. Besides, positively-charged entrance of channel does not allowto pass protons through the artificial AQP. Crystal structure showed formation of single water-wire file inside the pore, and MD simulation established the formation of 'hourglass' structure inside the palmitoyloleoyl-phosphocholine lipid bilayer. Thus, these channels have all the key features of natural aquaporins including high water permeability and selectivity toward protons, structural features as hourglass-like cavity, ability to form single water file and critical pore

size to generate steric obstruction. Remarkably, the high water permeability and selectivity enable the healing of impaired cells.

Table 1. Overview of the features of current reported water channels. This table is adapted from reference [84]

Channel	Pore size	Type according structure	Type according transport mechanism	Water permeability	Selectivity
AQP[70]	2.8 Å	Unimolecular natural protein	Hybrid hydrophobic/hydrophilic	4×10^9 H_2O/s/channel	Rejection all ions including proton
Dendritic dipeptides[30-31]	14.5 Å	Self-assembled	Hydrophobic	N/A	Water ions/ selectivity (except protons)
I-quartets[28, 37-38]	2.6 Å		Hydrophilic	1.5×10^6 H_2O/s/channel	Rejection all ions excluding proton
m-PE[44]	6.4 Å		Hydrophobic	4.7×10^7 H_2O/s/channel	No selectivity for water; high conduction for K+ and protons
Aquafoldamers[51]	2.8 Å		Hydrophilic	3.0×10^9 H_2O/s/channel	Rejection of all ions excluding proton
CNTP[58]	nCNTP – 6.8 Å wCNTP – 13.5 Å	Unimolecular	Hydrophobic	nCNTP – 2.3×10^{10} H_2O/s/channel wCNTP – 1.9×10^9 H_2O/s/channel	nCNTP – concentration depending selectivity, ion rejection for diluted solution; wCNTP – no water selectivity
PAH5[62]	4.7 Å		Hybrid hydrophobic/hydrophilic	40 H_2O/s/channel	no selectivity for water; good conduction for alkali cations
PAP5[66]	4.7 Å		Hydrophobic	3.5×10^8 H_2O/s/channel (Swelling mode) $3.7 \times 10^6 H_2O$/s/channel (Shrinking mode)	Low ion rejection
PAH4[67]	~3 Å × ~5 Å		Hydrophobic	3.7×10^9 H_2O/s/channel	~10^8 water/salt selectivity
Artificial AQP[69]	~4.7 Å		Hybrid hydrophobic/hydrophilic	2.7×10^9 H_2O/s/channel	Rejecting all ions including proton

3 Biomimetic desalination technologies

With the development of industry and the rapid growth of the population, one of the main problems of humanity in the 20th and 21st centuries has become the lack of clean water[70-72], which prompts scientists and engineers to develop new affordable and sustainable water treatment technologies. Nowadays, membrane separation systems are the most demanded in the field of water purification due to their energy efficiency[73], which became possible mainly due to the development of polymer science. Combination of advanced membrane technologies with high performing and selective natural or artificial water channel contributes to the developing of a new direction - biomimetic desalination technologies, which opens a new chapter in membrane-based water filtration.

3.1 Aquaporin-assisted synthetic membranes for water purification

After a detailed study of the structures and functions of aquaporins, the idea of channels integration into synthetic membranes for water desalination was not long in coming[74-75], and as a result, aquaporin biomimetic membranes (ABMs) were developed. In order to achieve the goal of incorporating aquaporins, a three-component membrane system has been proposed:

-Water transport protein aquaporin itself, enhancing the water permeability across the membrane; unfortunately its role of selectivity filter was not yet proven.- amphiphilic lipides of polymers forming liposomes in which the aquaporins are embedded due to the affinity of transport proteins with a hydrophobic medium;- a polymeric support and a polyamide thin layer used for the mechanical resistance.

In general, there are two types of molecules that self-assemble to form channel-incorporating matrices (Figure 12): amphiphilic natural (chicken egg phosphatidylcholine or porcine brain phosphatidylserine) or synthetic (DOPC, 1,2-dioleoyl-3-trimethylammonium-propane (DOTAP) or 1,2-dimyristoyl-sn-glycero-3-phosphocholine (DMPC) lipids and block copolymers. Polymer matrices are formed by diblock or triblock copolymers, which consist of poly(2-methyl-2-oxazoline) (PMOXA) as the hydrophilic block and poly(dimethylsiloxane)

(PDMS) as the hydrophobic block, but sometimes comprising poly(1,2-butadiene) and poly(ethylene oxide) (PB-b-PEO).[76]

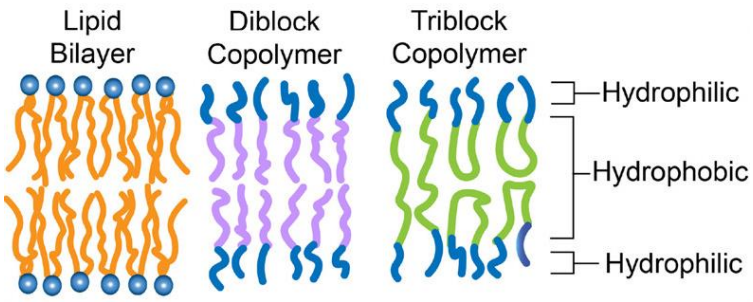

Figure 12. Biomimetic compositions for the amphiphilic channel insertion matrix. Image adapted from reference [76].

The forward osmosis (FO) membrane with high selectivity was developed by Ding et al[77] using covalently attached aquaporin Z-incorporated supported lipid bilayers (SLBs) to a polydopamine-coated porous polysulfone (PSf) support (Figure 13a). Although that covalent linkage offers stability to selective layer, the lipid layer undergoes degradation upon contact with detergent-containing solution, which enables the use of this membrane under real condition of water purification. Separation performance was tested using cross-section FO measurements and showed significant water flux of 23 $L \cdot m^{-2} \cdot h^{-1}$ (LMH) with reverse salt flux of 3.1 $g \cdot m^{-2} \cdot h^{-1}$ (gMH).

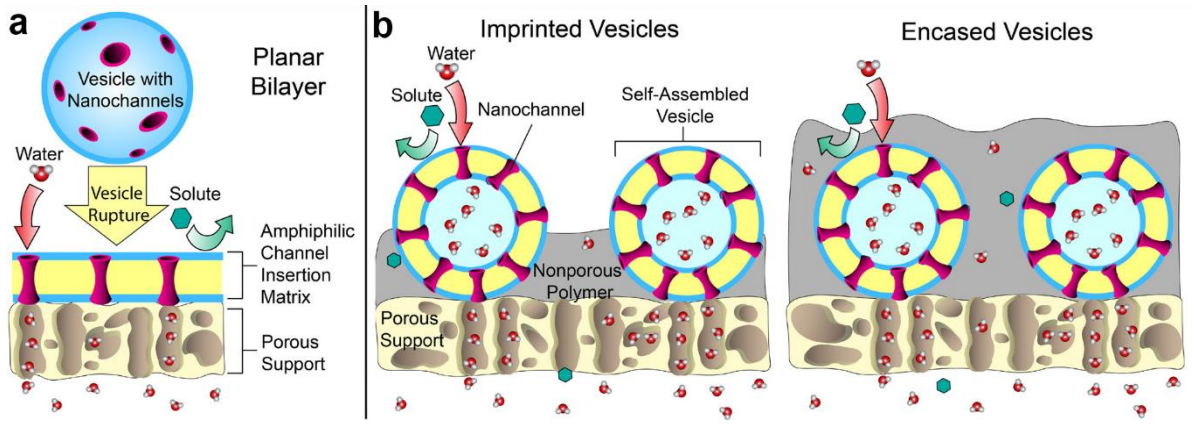

Figure 13. Design considerations for common biomimetic membrane formation strategies. (a) Pore-spanning planar layer format. (b) Vesicle-encapsulated mixed-matrix formats. Image adapted from reference [76].

Changing matrix from amphiphilic lipids to block copolymers could partially solve stability problems of AQP-incorporated membranes. Thus, Wang et al.[78] demonstrated the fabrication of FO membrane with AqpZ proteins reconstituted into ABA block copolymer blends on polycarbonate track etch (PCTE) support. ABA copolymer consisted of poly-(2-methyloxazoline)-block-poly-(dimethylsiloxane)-block-poly-(2-methyloxazoline) (PMOXA–PDMS–PMOXA) with acrylate or disulfide end group. This approach increased membrane mechanical resistance and showed high water flux (17.6 LMH) with moderate salt retention (91.8%) when using 6000 ppm NaCl as the feed and 0.8 M sucrose as the draw solute in the forward osmosis operation. We note that most of the time, low salinity conditions less than 8000 ppm are used for testing the AQP incorporating membranes which most probably are not resisting to harsh high salinity conditions of seawater desalination (35 000 ppm NaCl).

Notwithstanding the using polymeric vesicles for aquaporin incorporation, the stability challenge remained unsolved. Chasing a trade-off between stability and performance of aquaporin biomimetic membranes, a series of studies on using mixed matrix approach was reported.[79-81] Aquaporin-incorporated vesicles were trapped into traditional polyamide thin films, which made it possible to use membranes for reverse osmosis desalination (Figure 13b). Nielsen et al[79] achieved water permeability values up to 4 LMH/bar with a salt rejection of ~97% at applied pressure of 5 bar. Wang et al.[80] introduced the aquaporin-based hollow fiber composite membrane with water flux of ~8 LMH/bar (rejection 97%) at same pressure, and one year after they presented the thin-film composite membrane, which could work under 10 bar applied pressure with performance of ~4 LMH/bar (rejection remained at the level of 97%)[81]. As can be noted, despite high levels of water permeability, these membranes can only be used for low pressure reverse osmosis (LPRO) desalination due to their fragility. In addition, lipid vesicles trapping contributed to the formation of defects in the active layer, which can be seen from low rejection values.

Most modern AQP membrane designs use a polymeric matrix that can make them scalable and industrially applicable. However, a vital part of AQP membranes is not commercially available yet, as well as AQP, which are challenging for mass production. Another limitation is the surface to channel ratio of these proteins. To have one channel, the AQP protein occupies approximately 6 nm^2 on the surface. From a chemical engineering point of view, this can create limitations when trying to obtain highly functional membrane surfaces. Thus, the use of aquaporin biomimetic membranes is beneficial, but in the long term, the technology may suffer from limitations that make them less attractive options for fabrication of desalination membranes.

3.2 Biomimetic desalination membranes with incorporated AWC

In relation to the challenges of natural transport proteins incorporation, the artificial channels, reviewed in section 1.3 of the present chapter, are more appealing options for the development of novel biomimetic membranes. Indeed, some AWCs have come close to the performance and selectivity of natural aquaporins by mimicking their structure in part (aquafoldamers) or in whole (artificial AQP). Since this area is quite recent, there are only a few studies related to incorporation of AWC into membrane for water purification and desalination that were reported.

PAP5 channels became one of the first AWCs embedded into synthetic membrane models at microscale level.[82] Carboxylic-functionalized PAP5 channels were incorporated into flat micrometric crystalline sheets of PB-b-PEO diblock copolymers as aggregated microphases leading to hybrid membranes with a diameter of 1 cm (Figure 14a). Presence of carboxylic groups allowed to laminate micrometric-scale layers onto poly(ether sulfone) (PES) microfiltration support by a layer-by-layer (LbL) technique using polyethyleneimine. Those membranes showed high water permeability of ~65 LMH/bar with molecular weight cut-off (MWCO) of ~450 Da but no selectivity for sub nanometric separation as requested by desalination technology.

Another method of providing multilayer for full coverage of the active layer is based on the revision of the matrix composition.[83] A crosslinkable polyisoprene-b-poly-(ethylene oxide)-b-polyisoprene triblock copolymer was spin-coated onto a silicon wafer for self-assembly into well-aligned multilayer lamellas lying parallel to the surface. These lamellas were transferred onto an aluminum oxide porous substrate to afford the composite membrane (Figure 14b). In this system, the BAB pattern (i.e., hydrophobic-hydrophilic-hydrophobic) was used to stimulate and stabilize multilayer formation by stimulating the formation of polymer bridges between adjacent hydrophobic domains. Membranes with PAP5 had increased water permeability and showed again MWCO ~ 450 Da.

The above-described disadvantage of this class of artificial water channels does not allow their use for RO distillation, however, PAP5-based membranes ccould find their application in the nanofiltration (NF) area, if the scale up of the membranes will be further developped. In addition, the methods of incorporation shown on the example of PAP5 could be applied to other artificial water channels.

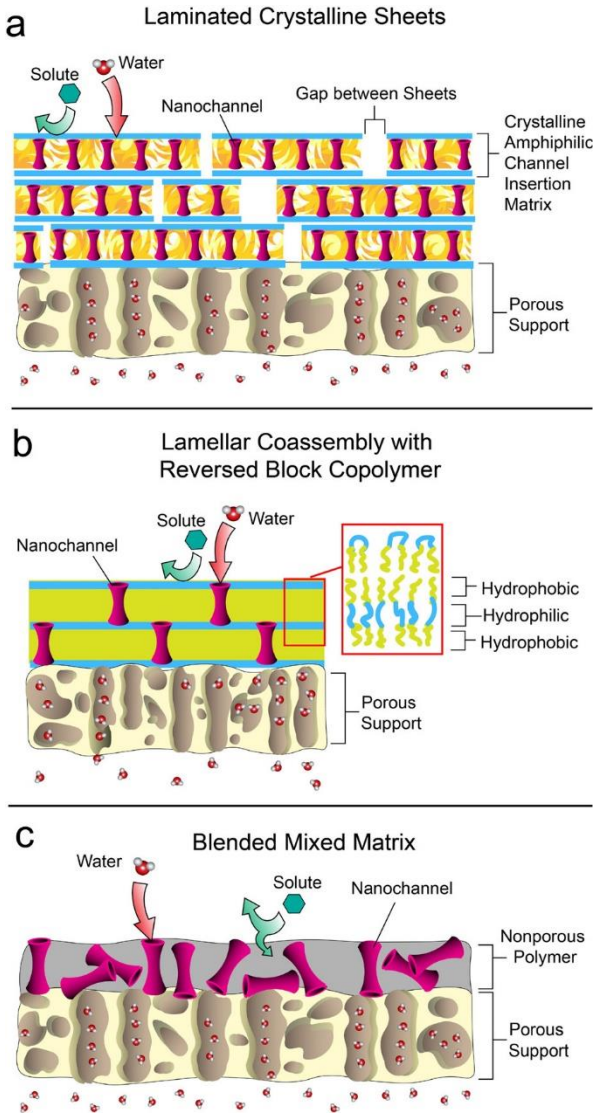

Figure 14. Alternative biomimetic membrane formats. (a) Laminated crystalline sheets, where sheets of up to ~1 μm in side-length are layered for full coverage. (b) Co-assembly of multilayer lamellar block copolymer. Biological membranes follow an ABA (hydrophilic−hydrophobic−hydrophilic) pattern, whereas, here, a BAB (hydrophobic− hydrophilic−hydrophobic) block copolymer is used to promote multilayered self-assembly. (c) Blended mixed matrix, where channels are blended into a polymer solution before interfacial polymerization of polyamide. Random alignment of nanochannels occurs. Image adapted from reference -

The most successful AWC incorporation technique was presented by Barboiu et al, that was based on I-quartet systems.[84-85] The ability to form a stable cluster of channels in the solid state made it possible to homogeneously incorporate highly selective pores into the polyamide membrane with formation blended mixed matrix (Figure 14c). Remarkable that there is no need to use protection for AWC as lipid vesicles or copolymers, which is a huge advantage compared to aquaporins. The mechanism of incorporation was defined as in-situ crystallization during interfacial polymerization due to the diffusion of organic solvent into a colloidal water-alcohol

solution of I-quartets. Optimization of incorporation made it possible to obtain highly efficient SWRO membranes for desalination with a water permeability of 75 LMH at 65 bar applied pressure with 35000 ppm NaCl feed solution, which is two times higher than the values of commercially available membranes for water desalination, while salt rejection is up to 99.8%. This work showed successful transition from nano-scale level of high performing AWC to ultra rapid and selective macro-scale synthetic membranes for water desalination.

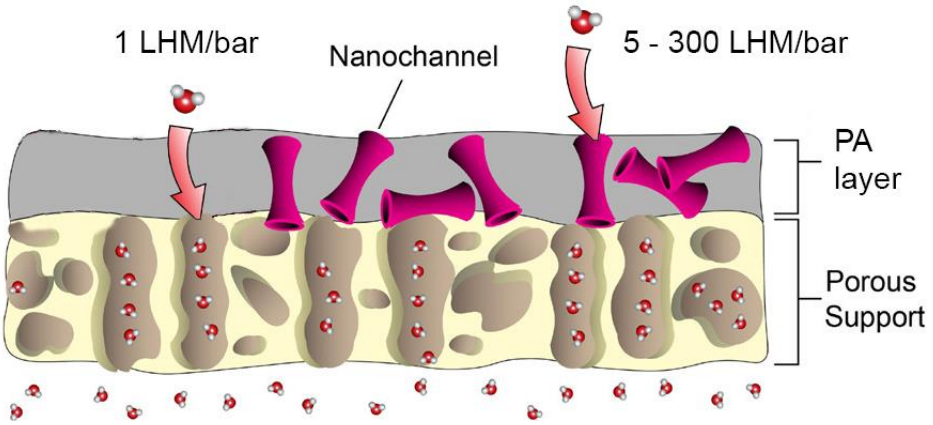

Figure 15. Theoretical comparison of water permeability through PA layer and synthetic nanochannel. Image adapted from reference [84]

As a conclusion, the development of biomimetic membranes based on transport proteins, as well as AWC-incorporated membranes, is still challenging, which, in general, related to water permselectivity and membrane stability trade-off. However, biomimetic membrane fabrication studies reviewed in this subchapter opens new horizons in this field. One of the perspective directions of AWC-incorporated desalination membranes fabrication is direct embedding of selective pores into PA matrix. The theoretical calculations of water flux through AWC-PA selective layer predict the value of up to 300 LMH/bar based on MD simulation[86], while self-supportive PA membrane has permeability 1 LMH/bar (Figure 15).[87] This breakthrough leads to new incomes in AWCs studies, towards the development of high-performance selective membranes for desalination.

4 Objectives and strategy

The aim of this PhD thesis is to develop new desalination technology by designing of new classes of artificial water channels and integration them into real RO desalination membranes.

The research development strategy was initially implemented on the basis of previously obtained results. By choosing perspective pillar[n]arene platform for artificial water channel design, first of all, we focused on investigation of water/ion transport abilities and nature of transport mechanism of self-assembled discrete tubular dimers of rim-differentiated peralkyl-carboxylate-pillar[5]arenes, developed in collaboration with Prof. Tomoki Ogoshi (Department of Synthetic Chemistry and Biological Chemistry Graduate School of Engineering, Kyoto University, Japan). Originally, those pillar[5]arene-modified dimers were designed as capsules for host–guest chemistry.[88] However, having discovered such unique structure, we anticipated that they will be able to form supramolecular self-assembled pores inside lipid bilayer membranes fitting perfectly for water or/and ion translocation. As so, the option to study the PAD derivatives inside vesicular systems by stopped-flow and fluorescence assays was chosen, as it offers the possibility to determine whether or not the compounds are capable of water transport across the lipid bilayer of the vesicles. The next step was to obtain and analyse solid state structural information through X-ray crystallography of PAD with different alkyl substitutes. It followed to describe the water channels transport abilities and structure/performance relationship of water transport across lipid bilayers.

After determining that the PAD derivatives are indeed able to water transport, we started to investigate the mechanism of water movement through the formed pores inside lipid bilayers. To achieve this goal, we started a collaboration with Marc Baaden (Institut de Biologie Physico-Chimique de Paris), an expert in molecular dynamics. We proposed to study through molecular dynamics simulations the structural behavior of the initial solid state like structures of the channels when placed in a lipid environment.

In the meanwhile, the second significant objective was to verify the possibility of upscaling from molecular level studies and try to transfer the artificial water channels onto the

macroscopic level. As objective for future research, it was selected a non-modified pillar[5]arene. The main reasons of choosing this compound were: ability formation of self-assembled tubular structures in solid state with pore size close to critical value for water/ion selectivity (~3 Å), mentioned in present Chapter; relevant simplicity and low cost of non-modified pillar[5]arene synthesis. Thus, the design and optimisation of fabrication of membrane materials containing pillar[n]arene artificial water channels for water desalination was proposed.

Last but not least objective of this PhD thesis was to propose the design and synthesis of functional organic molecules that could self-assemble into functional hydrophobic channels in a same way as or in a mixture with the imidazole compounds. We proposed the synthesis of new synthons mainly through the modification of the functional head of the ureido derivative compounds to obtain similar small organic compounds capable of self-assembling into water channels. The compounds were studied for their ability to form water channels in solid state and tested for water and ion transport capabilities in the same fashion as for the I-quartet channels. After that it was decided to combine obtained hydrophobic alkylureido derivatives with highly effective hydrophilic I-quartet channels in order to achieve hybrid hydrophobic/hydrophilic pores.

The experimental part of the PhD thesis is organized in 3 chapters:

Chapter II. Biomimetic Approach for Highly Selective Artificial Water Channels Based on Tubular Pillar [5] arene Dimers

Chapter III. Enhanced desalination polyamide membranes incorporating Pillar[5]arene via in-situ aggregation-interfacial polymerization-isAGRIP

This chapter is adapted from submitted article Dmytro Strilets, Sophie Cerneaux, Mihail Barboiu*, Enhanced desalination polyamide membranes incorporating Pillar[5]arene via in-situ aggregation-interfacial polymerization-isAGRIP .

Chapter IV. Synergetic self-assembly of bi-component alkylureido systems into artificial water channels

This chapter is adapted from manuscript Dmytro Strilets, Mihail Barboiu*, Synergetic self-assembly of bi-component alkylureido systems into artificial water channels.

References

1. Kesieme, U. K.; Milne, N.; Aral, H.; Cheng, C. Y.; Duke, M., Economic analysis of desalination technologies in the context of carbon pricing, and opportunities for membrane distillation. *Desalination* **2013,** *323*, 66-74.

2. Council, N. R., *Desalination: A national perspective*. National Academies Press: 2008.

3. Hafez, A.; El-Mariharawy, S., Design and performance of the two-stage/two-pass RO membrane system for chromium removal from tannery wastewater. Part 3. *Desalination* **2004,** *165*, 141-151.

4. WA, E. M. P., The future of seawater desalination: Energy, technology, and the environment Science 333712. Elimelech, M., and Phillip, WA (2011). The future of seawater desalination: Energy, technology, and the environment. *Science* **2011,** *333*, 712.

5. Lieb, W.; Stein, W., The molecular basis of simple diffusion within biological membranes. In *Current topics in membranes and transport*, Elsevier: 1972; Vol. 2, pp 1-39.

6. Baylis, P., Water movement through lipid bilayers, pores and plasma membranes: Theory and reality.(Distinquished lecture series of the society of general physiologists, volume 4). Alan Finkelstein, John Wiley and Sons Ltd: New York. 228 pages,£ 38.45 (1987). Wiley Online Library: 1988.

7. Benga, G., Water channel proteins (later called aquaporins) and relatives: past, present, and future. *IUBMB life* **2009,** *61* (2), 112-133.

8. Denker, B. M.; Smith, B. L.; Kuhajda, F. P.; Agre, P., Identification, purification, and partial characterization of a novel Mr 28,000 integral membrane protein from erythrocytes and renal tubules. *Journal of Biological Chemistry* **1988,** *263* (30), 15634-15642.

9. Smith, B. L.; Agre, P., Erythrocyte Mr 28,000 transmembrane protein exists as a multisubunit oligomer similar to channel proteins. *Journal of Biological Chemistry* **1991,** *266* (10), 6407-6415.

10. Preston, G. M.; Agre, P., Isolation of the cDNA for erythrocyte integral membrane protein of 28 kilodaltons: member of an ancient channel family. *Proceedings of the National Academy of Sciences* **1991,** *88* (24), 11110-11114.

11. Preston, G. M.; Carroll, T. P.; Guggino, W. B.; Agre, P., Appearance of water channels in Xenopus oocytes expressing red cell CHIP28 protein. *Science* **1992**, 385-387.

12. Zeidel, M. L.; Ambudkar, S. V.; Smith, B. L.; Agre, P., Reconstitution of functional water channels in liposomes containing purified red cell CHIP28 protein. *Biochemistry* **1992,** *31* (33), 7436-7440.

13. Van Hoek, A.; Verkman, A., Functional reconstitution of the isolated erythrocyte water channel CHIP28. *Journal of Biological Chemistry* **1992,** *267* (26), 18267-18269.

14. Preston, G. M.; Jung, J. S.; Guggino, W.; Agre, P., The mercury-sensitive residue at cysteine 189 in the CHIP28 water channel. *Journal of Biological Chemistry* **1993,** *268* (1), 17-20.

15. Preston, G. M.; Jung, J. S.; Guggino, W. B.; Agre, P., Membrane topology of aquaporin CHIP. Analysis of functional epitope-scanning mutants by vectorial proteolysis. *Journal of Biological Chemistry* **1994,** *269* (3), 1668-1673.

16. Jung, J. S.; Preston, G. M.; Smith, B. L.; Guggino, W. B.; Agre, P., Molecular structure of the water channel through aquaporin CHIP. The hourglass model. *Journal of Biological Chemistry* **1994,** *269* (20), 14648-14654.

17. Cheng, A.; Van Hoek, A.; Yeager, M.; Verkman, A.; Mitra, A., Three-dimensional organization of a human water channel. *Nature* **1997,** *387* (6633), 627-630.

18. de Groot, B. L.; Engel, A.; Grubmüller, H., A refined structure of human aquaporin-1. *Febs Letters* **2001,** *504* (3), 206-211.

19. Fu, D.; Libson, A.; Miercke, L. J.; Weitzman, C.; Nollert, P.; Krucinski, J.; Stroud, R. M., Structure of a glycerol-conducting channel and the basis for its selectivity. *science* **2000,** *290* (5491), 481-486.

20. Mitsuoka, K.; Murata, K.; Walz, T.; Hirai, T.; Agre, P.; Heymann, J. B.; Engel, A.; Fujiyoshi, Y., The structure of aquaporin-1 at 4.5-Å resolution reveals short α-helices in the center of the monomer. *Journal of structural biology* **1999,** *128* (1), 34-43.

21. Murata, K.; Mitsuoka, K.; Hirai, T.; Walz, T.; Agre, P.; Heymann, J. B.; Engel, A.; Fujiyoshi, Y., Structural determinants of water permeation through aquaporin-1. *Nature* **2000,** *407* (6804), 599-605.

22. Walz, T.; Hirai, T.; Murata, K.; Heymann, J. B.; Mitsuoka, K.; Fujiyoshi, Y.; Smith, B. L.; Agre, P.; Engel, A., The three-dimensional structure of aquaporin-1. *Nature* **1997,** *387* (6633), 624-627.

23. Walz, T.; Smith, B. L.; Zeidel, M. L.; Engel, A.; Agre, P., Biologically active two-dimensional crystals of aquaporin CHIP. *Journal of Biological Chemistry* **1994,** *269* (3), 1583-1586.

24. Sui, H.; Han, B.-G.; Lee, J. K.; Walian, P.; Jap, B. K., Structural basis of water-specific transport through the AQP1 water channel. *Nature* **2001,** *414* (6866), 872-878.

25. de Groot, B. L.; Grubmüller, H., Water permeation across biological membranes: mechanism and dynamics of aquaporin-1 and GlpF. *Science* **2001,** *294* (5550), 2353-2357.

26. Tajkhorshid, E.; Nollert, P.; Jensen, M. Ø.; Miercke, L. J.; O'Connell, J.; Stroud, R. M.; Schulten, K., Control of the selectivity of the aquaporin water channel family by global orientational tuning. *Science* **2002,** *296* (5567), 525-530.

27. Kozono, D.; Yasui, M.; King, L. S.; Agre, P., Aquaporin water channels: Atomic structure and molecular dynamics meet clinical medicine(Review). *Journal of Clinical Investigation* **2002,** *109* (11), 1395-1399.

28. Barboiu, M., Artificial water channels–incipient innovative developments. *Chemical Communications* **2016,** *52* (33), 5657-5665.

29. Si, W.; Xin, P.; Li, Z.-T.; Hou, J.-L., Tubular unimolecular transmembrane channels: construction strategy and transport activities. *Accounts of chemical research* **2015,** *48* (6), 1612-1619.

30. Kaucher, M. S.; Peterca, M.; Dulcey, A. E.; Kim, A. J.; Vinogradov, S. A.; Hammer, D. A.; Heiney, P. A.; Percec, V., Selective transport of water mediated by porous dendritic dipeptides. *Journal of the American Chemical Society* **2007,** *129* (38), 11698-11699.

31. Percec, V.; Dulcey, A. E.; Balagurusamy, V. S.; Miura, Y.; Smidrkal, J.; Peterca, M.; Nummelin, S.; Edlund, U.; Hudson, S. D.; Heiney, P. A., Self-assembly of amphiphilic dendritic dipeptides into helical pores. *Nature* **2004,** *430* (7001), 764-768.

32. Allen, T. W.; Andersen, O. S.; Roux, B., Energetics of ion conduction through the gramicidin channel. *Proceedings of the National Academy of Sciences* **2004,** *101* (1), 117-122.

33. Burkhart, B.; Li, N.; Langs, D.; Pangborn, W.; Duax, W., The conducting form of gramicidin A is a right-handed double-stranded double helix. *Proceedings of the National Academy of Sciences* **1998,** *95* (22), 12950-12955.

34. Roux, B., Computational studies of the gramicidin channel. *Accounts of chemical research* **2002,** *35* (6), 366-375.

35. Agmon, N., The grotthuss mechanism. *Chemical Physics Letters* **1995,** *244* (5-6), 456-462.

36. Le Duc, Y.; Michau, M.; Gilles, A.; Gence, V.; Legrand, Y. M.; van der Lee, A.; Tingry, S.; Barboiu, M., Rücktitelbild: Imidazole-Quartet Water and Proton Dipolar Channels (Angew. Chem. 48/2011). *Angewandte Chemie* **2011,** *123* (48), 11744-11744.

37. Licsandru, E.; Kocsis, I.; Shen, Y.-x.; Murail, S.; Legrand, Y.-M.; Van Der Lee, A.; Tsai, D.; Baaden, M.; Kumar, M.; Barboiu, M., Salt-excluding artificial water channels exhibiting enhanced dipolar water and proton translocation. *Journal of the American Chemical Society* **2016,** *138* (16), 5403-5409.

38. Kocsis, I.; Sorci, M.; Vanselous, H.; Murail, S.; Sanders, S. E.; Licsandru, E.; Legrand, Y.-M.; van der Lee, A.; Baaden, M.; Petersen, P. B., Oriented chiral water wires in artificial transmembrane channels. *Science advances* **2018,** *4* (3), eaao5603.

39. Schnell, J. R.; Chou, J. J., Structure and mechanism of the M2 proton channel of influenza A virus. *Nature* **2008,** *451* (7178), 591-595.

40. Stouffer, A. L.; Acharya, R.; Salom, D.; Levine, A. S.; Di Costanzo, L.; Soto, C. S.; Tereshko, V.; Nanda, V.; Stayrook, S.; DeGrado, W. F., Structural basis for the function and inhibition of an influenza virus proton channel. *Nature* **2008,** *451* (7178), 596-599.

41. Phongphanphanee, S.; Rungrotmongkol, T.; Yoshida, N.; Hannongbua, S.; Hirata, F., Proton transport through the influenza A M2 channel: three-dimensional reference interaction site model study. *Journal of the American Chemical Society* **2010,** *132* (28), 9782-9788.

42. Hu, F.; Luo, W.; Hong, M., Mechanisms of proton conduction and gating in influenza M2 proton channels from solid-state NMR. *Science* **2010,** *330* (6003), 505-508.

43. Pinto, L. H.; Dieckmann, G. R.; Gandhi, C. S.; Papworth, C. G.; Braman, J.; Shaughnessy, M. A.; Lear, J. D.; Lamb, R. A.; DeGrado, W. F., A functionally defined model for the M2 proton channel of influenza A virus suggests a mechanism for its ion selectivity. *Proceedings of the National Academy of Sciences* **1997,** *94* (21), 11301-11306.

44. Zhou, X.; Liu, G.; Yamato, K.; Shen, Y.; Cheng, R.; Wei, X.; Bai, W.; Gao, Y.; Li, H.; Liu, Y., Self-assembling subnanometer pores with unusual mass-transport properties. *Nature communications* **2012,** *3* (1), 1-8.

45. Li, X.; Yang, K.; Su, J.; Guo, H., Water transport through a transmembrane channel formed by arylene ethynylene macrocycles. *RSC advances* **2014,** *4* (7), 3245-3252.

46. Ren, C.; Maurizot, V.; Zhao, H.; Shen, J.; Zhou, F.; Ong, W. Q.; Du, Z.; Zhang, K.; Su, H.; Zeng, H., Five-fold-symmetric macrocyclic aromatic pentamers: high-affinity cation recognition, ion-pair-induced columnar stacking, and nanofibrillation. *Journal of the American Chemical Society* **2011,** *133* (35), 13930-13933.

47. Qin, B.; Sun, C.; Liu, Y.; Shen, J.; Ye, R.; Zhu, J.; Duan, X.-F.; Zeng, H., One-pot synthesis of hybrid macrocyclic pentamers with variable functionalizations around the periphery. *Organic letters* **2011,** *13* (9), 2270-2273.

48. Shen, J.; Ma, W.; Yu, L.; Li, J.-B.; Tao, H.-C.; Zhang, K.; Zeng, H., Size-dependent patterned recognition and extraction of metal ions by a macrocyclic aromatic pyridone pentamer. *Chemical Communications* **2014,** *50* (84), 12730-12733.

49. Zhao, H.; Sheng, S.; Hong, Y.; Zeng, H., Proton gradient-induced water transport mediated by water wires inside narrow aquapores of aquafoldamer molecules. *Journal of the American Chemical Society* **2014,** *136* (40), 14270-14276.

50. Zhao, H.; Ong, W. Q.; Fang, X.; Zhou, F.; Hii, M. N.; Li, S. F. Y.; Su, H.; Zeng, H., Synthesis, structural investigation and computational modelling of water-binding aquafoldamers. *Organic & biomolecular chemistry* **2012,** *10* (6), 1172-1180.

51. Shen, J.; Ye, R.; Romanies, A.; Roy, A.; Chen, F.; Ren, C.; Liu, Z.; Zeng, H., Aquafoldmer-based aquaporin-like synthetic water channel. *Journal of the American Chemical Society* **2020,** *142* (22), 10050-10058.

52. Hummer, G.; Rasaiah, J. C.; Noworyta, J. P., Water conduction through the hydrophobic channel of a carbon nanotube. *Nature* **2001,** *414* (6860), 188-190.

53. Joseph, S.; Aluru, N., Why are carbon nanotubes fast transporters of water? *Nano letters* **2008,** *8* (2), 452-458.

54. Holt, J. K.; Park, H. G.; Wang, Y.; Stadermann, M.; Artyukhin, A. B.; Grigoropoulos, C. P.; Noy, A.; Bakajin, O., Fast mass transport through sub-2-nanometer carbon nanotubes. *Science* **2006,** *312* (5776), 1034-1037.

55. Majumder, M.; Chopra, N.; Andrews, R.; Hinds, B. J., Enhanced flow in carbon nanotubes. *Nature* **2005,** *438* (7064), 44-44.

56. Secchi, E.; Marbach, S.; Niguès, A.; Stein, D.; Siria, A.; Bocquet, L., Massive radius-dependent flow slippage in carbon nanotubes. *Nature* **2016,** *537* (7619), 210-213.

57. Fornasiero, F.; Park, H. G.; Holt, J. K.; Stadermann, M.; Grigoropoulos, C. P.; Noy, A.; Bakajin, O., Ion exclusion by sub-2-nm carbon nanotube pores. *Proceedings of the National Academy of Sciences* **2008,** *105* (45), 17250-17255.

58. Tunuguntla, R. H.; Henley, R. Y.; Yao, Y.-C.; Pham, T. A.; Wanunu, M.; Noy, A., Enhanced water permeability and tunable ion selectivity in subnanometer carbon nanotube porins. *Science* **2017,** *357* (6353), 792-796.

59. Ogoshi, T.; Kanai, S.; Fujinami, S.; Yamagishi, T.-a.; Nakamoto, Y., para-Bridged symmetrical pillar [5] arenes: their Lewis acid catalyzed synthesis and host–guest property. *Journal of the American Chemical Society* **2008,** *130* (15), 5022-5023.

60. Behera, H.; Yang, L.; Hou, J. L., Pillar [n] arenes: chemistry and their material applications. *Chinese Journal of Chemistry* **2020,** *38* (2), 215-217.

61. Ogoshi, T.; Kakuta, T.; Yamagishi, T. a., Applications of Pillar [n] arene-Based Supramolecular Assemblies. *Angewandte Chemie International Edition* **2019,** *58* (8), 2197-2206.

62. Chen, L.; Si, W.; Zhang, L.; Tang, G.; Li, Z.-T.; Hou, J.-L., Chiral selective transmembrane transport of amino acids through artificial channels. *Journal of the American Chemical Society* **2013,** *135* (6), 2152-2155.

63. Si, W.; Chen, L.; Hu, X. B.; Tang, G.; Chen, Z.; Hou, J. L.; Li, Z. T., Selective artificial transmembrane channels for protons by formation of water wires. *Angewandte Chemie International Edition* **2011,** *50* (52), 12564-12568.

64. Si, W.; Hu, X.-B.; Liu, X.-H.; Fan, R.; Chen, Z.; Weng, L.; Hou, J.-L., Self-assembly and proton conductance of organic nanotubes from pillar [5] arenes. *Tetrahedron letters* **2011,** *52* (19), 2484-2487.

65. Burykin, A.; Warshel, A., What really prevents proton transport through aquaporin? Charge self-energy versus proton wire proposals. *Biophysical journal* **2003,** *85* (6), 3696-3706.

66. Shen, Y.-x.; Si, W.; Erbakan, M.; Decker, K.; De Zorzi, R.; Saboe, P. O.; Kang, Y. J.; Majd, S.; Butler, P. J.; Walz, T., Highly permeable artificial water channels that can self-assemble into two-dimensional arrays. *Proceedings of the National Academy of Sciences* **2015,** *112* (32), 9810-9815.

67. Song, W.; Joshi, H.; Chowdhury, R.; Najem, J. S.; Shen, Y.-x.; Lang, C.; Henderson, C. B.; Tu, Y.-M.; Farell, M.; Pitz, M. E., Artificial water channels enable fast and selective water permeation through water-wire networks. *Nature nanotechnology* **2020,** *15* (1), 73-79.

68. Park, H. B.; Kamcev, J.; Robeson, L. M.; Elimelech, M.; Freeman, B. D., Maximizing the right stuff: The trade-off between membrane permeability and selectivity. *Science* **2017,** *356* (6343).

69. Yan, Z.-J.; Wang, D.; Ye, Z.; Fan, T.; Wu, G.; Deng, L.; Yang, L.; Li, B.; Liu, J.; Ma, T., Artificial Aquaporin That Restores Wound Healing of Impaired Cells. *Journal of the American Chemical Society* **2020,** *142* (37), 15638-15643.

70. Mekonnen, M. M.; Hoekstra, A. Y., Four billion people facing severe water scarcity. *Science advances* **2016,** *2* (2), e1500323.

71. Eliasson, J., The rising pressure of global water shortages. *Nature News* **2015,** *517* (7532), 6.

72. Schewe, J.; Heinke, J.; Gerten, D.; Haddeland, I.; Arnell, N. W.; Clark, D. B.; Dankers, R.; Eisner, S.; Fekete, B. M.; Colón-González, F. J., Multimodel assessment of water scarcity under climate change. *Proceedings of the National Academy of Sciences* **2014,** *111* (9), 3245-3250.

73. Geise, G. M.; Lee, H. S.; Miller, D. J.; Freeman, B. D.; McGrath, J. E.; Paul, D. R., Water purification by membranes: the role of polymer science. *Journal of Polymer Science Part B: Polymer Physics* **2010,** *48* (15), 1685-1718.

74. Tang, C.; Zhao, Y.; Wang, R.; Hélix-Nielsen, C.; Fane, A., Desalination by biomimetic aquaporin membranes: Review of status and prospects. *Desalination* **2013,** *308*, 34-40.

75. Habel, J.; Hansen, M.; Kynde, S.; Larsen, N.; Midtgaard, S. R.; Jensen, G. V.; Bomholt, J.; Ogbonna, A.; Almdal, K.; Schulz, A., Aquaporin-based biomimetic polymeric membranes: approaches and challenges. *Membranes* **2015,** *5* (3), 307-351.

76. Porter, C. J.; Werber, J. R.; Zhong, M.; Wilson, C. J.; Elimelech, M., Pathways and challenges for biomimetic desalination membranes with sub-nanometer channels. *ACS nano* **2020,** *14* (9), 10894-10916.

77. Ding, W.; Cai, J.; Yu, Z.; Wang, Q.; Xu, Z.; Wang, Z.; Gao, C., Fabrication of an aquaporin-based forward osmosis membrane through covalent bonding of a lipid bilayer to a microporous support. *Journal of Materials Chemistry A* **2015,** *3* (40), 20118-20126.

78. Wang, H.; Chung, T. S.; Tong, Y. W.; Jeyaseelan, K.; Armugam, A.; Chen, Z.; Hong, M.; Meier, W., Highly permeable and selective pore-spanning biomimetic membrane embedded with aquaporin Z. *small* **2012,** *8* (8), 1185-1190.

79. Zhao, Y.; Qiu, C.; Li, X.; Vararattanavech, A.; Shen, W.; Torres, J.; Helix-Nielsen, C.; Wang, R.; Hu, X.; Fane, A. G., Synthesis of robust and high-performance aquaporin-based biomimetic membranes by interfacial polymerization-membrane preparation and RO performance characterization. *Journal of Membrane Science* **2012,** *423*, 422-428.

80. Li, X.; Chou, S.; Wang, R.; Shi, L.; Fang, W.; Chaitra, G.; Tang, C. Y.; Torres, J.; Hu, X.; Fane, A. G., Nature gives the best solution for desalination: Aquaporin-based hollow fiber composite membrane with superior performance. *Journal of Membrane Science* **2015,** *494*, 68-77.

81. Qi, S.; Wang, R.; Chaitra, G. K. M.; Torres, J.; Hu, X.; Fane, A. G., Aquaporin-based biomimetic reverse osmosis membranes: Stability and long term performance. *Journal of Membrane Science* **2016,** *508*, 94-103.

82. Shen, Y.-x.; Song, W.; Barden, D. R.; Ren, T.; Lang, C.; Feroz, H.; Henderson, C. B.; Saboe, P. O.; Tsai, D.; Yan, H., Achieving high permeability and enhanced selectivity for Angstrom-scale separations using artificial water channel membranes. *Nature communications* **2018,** *9* (1), 1-11.

83. Lang, C.; Ye, D.; Song, W.; Yao, C.; Tu, Y.-m.; Capparelli, C.; LaNasa, J. A.; Hickner, M. A.; Gomez, E. W.; Gomez, E. D., Biomimetic separation of transport and matrix functions in lamellar block copolymer channel-based membranes. *ACS nano* **2019,** *13* (7), 8292-8302.

84. Di Vincenzo, M.; Tiraferri, A.; Musteata, V.-E.; Chisca, S.; Sougrat, R.; Huang, L.-B.; Nunes, S. P.; Barboiu, M., Biomimetic artificial water channel membranes for enhanced desalination. *Nature Nanotechnology* **2021,** *16* (2), 190-196.

85. Huang, L.-B.; Di Vincenzo, M.; Li, Y.; Barboiu, M., Artificial Water Channels-towards Biomimetic Membranes for Desalination. *Chemistry-A European Journal* **2020**.

86. Murail, S.; Vasiliu, T.; Neamtu, A.; Barboiu, M.; Sterpone, F.; Baaden, M., Water permeation across artificial I-quartet membrane channels: from structure to disorder. *Faraday discussions* **2018,** *209*, 125-148.

87. Yang, Z.; Ma, X.-H.; Tang, C. Y., Recent development of novel membranes for desalination. *Desalination* **2018,** *434*, 37-59.

88. Fa, S.; Sakata, Y.; Akine, S.; Ogoshi, T., Non-Covalent Interactions Enable the Length-Controlled Generation of Discrete Tubes Capable of Guest Exchange. *Angewandte Chemie International Edition* **2020,** *59* (24), 9309-9313.

Chapter II. Biomimetic approach for highly selective artificial water channels based on tubular Pillar[5]Arene dimers

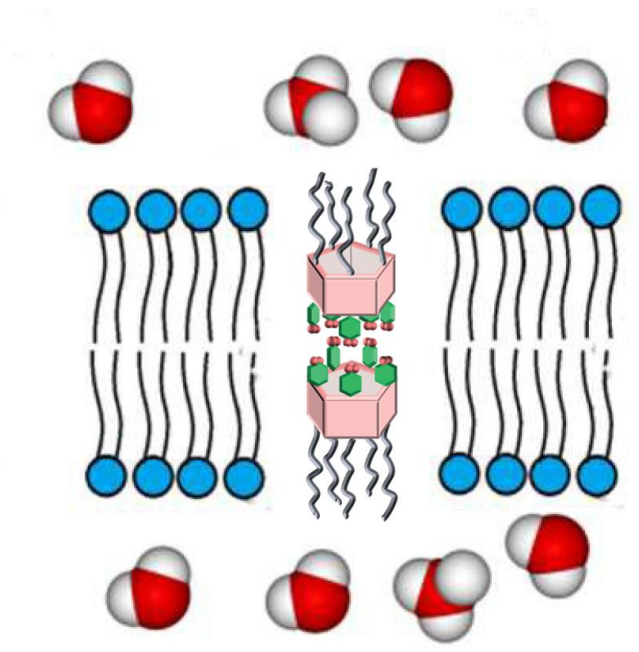

Contribution to Publication

The contribution of the Ph.D. candidate to the manuscript “Biomimetic approach for highly selective artificial water channels based on tubular Pillar[5]Arene dimers” is related to the identification of empirical strategies toward the obtainment of the objective of the research project for which he performed most of the experimental work, including (i) analysing structure of Pillar[5]arene dimers (PAD), (ii) defining strategy insertion of PAD into lipid bilayer, (iii) performing water transport evaluation by using Stopped-flow method and analysing obtained results, (iv) investigation of ion transport by using fluorescence HPTS assay and (v) planar bilayer experiments.

This chapter is adapted *with permission from* D. Strilets, S. Fa, A. Hardiagon, M. Baaden T. Ogoshi*, **M. Barboiu***, Biomimetic approach for highly selective artificial water channels based on tubular Pillar[5]Arene dimers" **Very Important Paper**. *Angew. Chem*. **2020** DOI: 10.1002/ange.202009219; *Angew. Chem. Int. Ed.* **2020**, *59(51),* 23213-23219. DOI: 10.1002/anie.202009219.

Biomimetic approach for highly selective artificial water channels based on tubular Pillar[5]Arene dimers

Dmytro Strilets,[a] Shixin Fa,[b] Arthur Hardiagon,[d,e] Marc Baaden, [d,e] Tomoki Ogoshi,* [b,c] Mihail Barboiu[a]*

D. Strilets, Dr. M Barboiu

Institut Europeen des Membranes, Adaptive Supramolecular Nanosystems Group, University of Montpellier, ENSCM-CNRS Place E. Bataillon CC047, 34095 Montpellier (France)

E-mail: mihail-dumitru.barboiu@umontpellier.fr

Dr. S. Fa, Prof. Tomoki Ogoshi

Department of Synthetic Chemistry and Biological Chemistry Graduate School of Engineering, Kyoto University, Katsura, Nishikyo-ku, Kyoto 615-8510 (Japan)

E-mail: ogoshi@sbchem.kyoto-u.ac.jp

WPI Nano Life Science Institute, Kanazawa University, Kakuma-machi, Kanazawa, 920-1192, Japan (Japan)

A. Hardiagon, Dr. Marc Baaden

CNRS, Université de Paris, UPR 9080, Laboratoire de Biochimie Théorique, 13 rue Pierre et Marie Curie, F-75005, Paris, France

Institut de Biologie Physico-Chimique-Fondation Edmond de Rotschild, PSL Research University, Paris, France

Abstract: Nature provides answers for efficient transport of water by using Aquaporins AQPs as the translocation relays. Artificial Water Channels biomimicking natural AQPs, can be used for both selective and fast transport of water. Here, we use complementary synthetic methods, X-ray structural data, transport assays to quantify the transport performances of peralkyl-carboxylate-pillar[5]arenes dimers in bilayer membranes. They are able to transport

~10^7 water molecules/channel/second, within one order of magnitude of AQPs' rates, rejecting Na+ and K+ cations. The dimers have an tubular structure, superposing larger pillar[5]arene pores of 5 Å diameter with narrowest twisted carboxy-phenyl pores of 2.8 Å diameter. This exceptional channel biomimetic platform, with variable pore dimensions within the same structure, offers size restriction reminiscent to natural proteins. It allows water molecules to selectively transit and prevent bigger hydrated cations to pass through the 2.8 Å pore. Molecular simulations probe that dimeric or multimeric honeycomb aggregates are stable in the membrane and form water pathways through the bilayer. Over time, a significant shift of the upper vs. lower layer of occurs initiating new unexpected water permeation events through novel toroidal pores. Altogether, uncovering the interplay between supramolecular construction and transport performances, the novel PAD channels described here are critical to accelerate the systematic discovery for artificial water channels for water desalting.

Keywords: Artificial water channels, pillar[5]arene, aquaporins, bilayer membranes

Natural channels allow ion/water translocation across biological membranes.[1] The transport is regulated by proteins, converting the ion-water interactions into ion-selectivity filter ones.[2] Because of the high significance of the related processes, the design of synthetic unimolecular or self-assembled channels with water-ion[3] or ion-ion selectivity have become areas of expanding interest. Very attractive strategies have been developed based on the self-assembly, towards supramolecular capsules presenting conductance states in bilayer membranes. Barboiu et al.,[6] Fyles et al.,[7] Kim et al.,[8] Gokel et al.[9] and Furkawa et al.[10] demonstrated the efficiency of integrated capsules as selectivity ion filters across lipid bilayers.

The easily accessible Pillar[n]arenes-PA play an important role in supramolecular chemistry, towards the generation of light-harvesting or drug delivery systems, transmembrane channels, separation and storage materials, etc.[11,12] Hou et al. firstly realized that PAs, with their unique hollow pillar-shape and tuneable size cavities with fine-tuneable rims, could be suitable platforms to construct artificial channels.[13-24] Most of them, are positioning the PA scaffolding relay in the middle of the membrane, whereas functional groups attached to aromatic rings form unimolecular pillared channels. Significant progress has been obtained in a very short time, as the single-channel osmotic water permeability for peptide-PAPs,[25,26] is close to natural aquaporins and superior to other synthetic water channel analogues.[27] Their drawback it relates to their low ion-water selectivity.

Innovative design approaches for the construction of PA-boxes[28] or PA-tubular dimers[29] were proposed. We recently described the dimerization of rim-differentiated pillar[5]arene *via* hydrogen bonding (Figure 1), producing expanded length-controlled tubular superstructures,[29] reminiscent to calixarenecapsules. [30]

Pursuing our endeavors to design original supramolecular channels with efficient and selective transport properties, we recently got interested in the possibility to make use of a directional structuring of such tubular PA platforms, towards the generation of directional channels within lipid bilayer membranes. We anticipated they are able to form supramolecular

self-assembled pores inside lipid bilayer membranes. As observed for alkyl-pyrogallol-arenes, the pore formation is strongly depending on the nature of grafted alkyl chains and probably

more than on type of aggregates form efficient ion channels.[9]

We know that a pore with a diameter of $\sim$ 3 Å is a critical prerequisite to selectively accommodate and transport water-wires.[27] Pillar[5]arene platform presents a hydrophobic cavity of 5 Å diameter, which in turn is much bigger to selectively accommodate single waterwires.[12,29] Having an inner pore size of ~5 Å, they allow the passage of cations according to their hydration energy.[23-25]

Herein we concentrate our efforts on investigation of water/ion transport abilities of selfassembled discrete tubular dimers of rim-differentiated peralkyl-carboxylate-pillar[5]arenes **PAD4**, **PAD8** and **PAD12** (Figure 1a) through bilayer lipid membrane. Interestingly, the analysis of x-ray single structure of **PAD4** show that two dimeric tubular architectures. It results in the formation of tubular carboxylic dimers pS-pS and pR-pR and of bilayer dimers form via two different H-bonding vs hydrophobic binding modes, respectively (Figure 1b, red). The 15 hydrogen bonds between the carboxyl groups and water molecules and adopts closely spaced carboxy-phenyl groups with a fivefold helical conformation,[29] which in turn superpose the pillar[5]arene relay of 5 Å diameter with a narrowest twisted hydrophobic pore of 2.8 Å diameter (Figure 1c). This affords a size restricted control of translocation along tubular channels at narrowest selectivity filter level, offering size restriction. The biological KscA[2a] or Aquaporin[2b] channels, have hydrophobic conical pores with variable diameter with the selectivity filter in the middle of the channel, affording closely spaced binding sites for temporarily coordinating the partly dehydrated cations or water molecules, respectively. We anticipated, **PAD4**, **PAD8** and **PAD12** dimers, with a variable pore diameter would allow to control of the transport activity as for natural proteins, within the selectivity filter. A reverse bilayer dimer of PADs may form (Figure 1b, red), allowing phospholipid polar head-groups of

the membrane to be in contact with the carboxylic rims in the polar region of the bilayer and of the butyl chains hydrophobic interactions inside the bilayer (Figure 1b, blue).

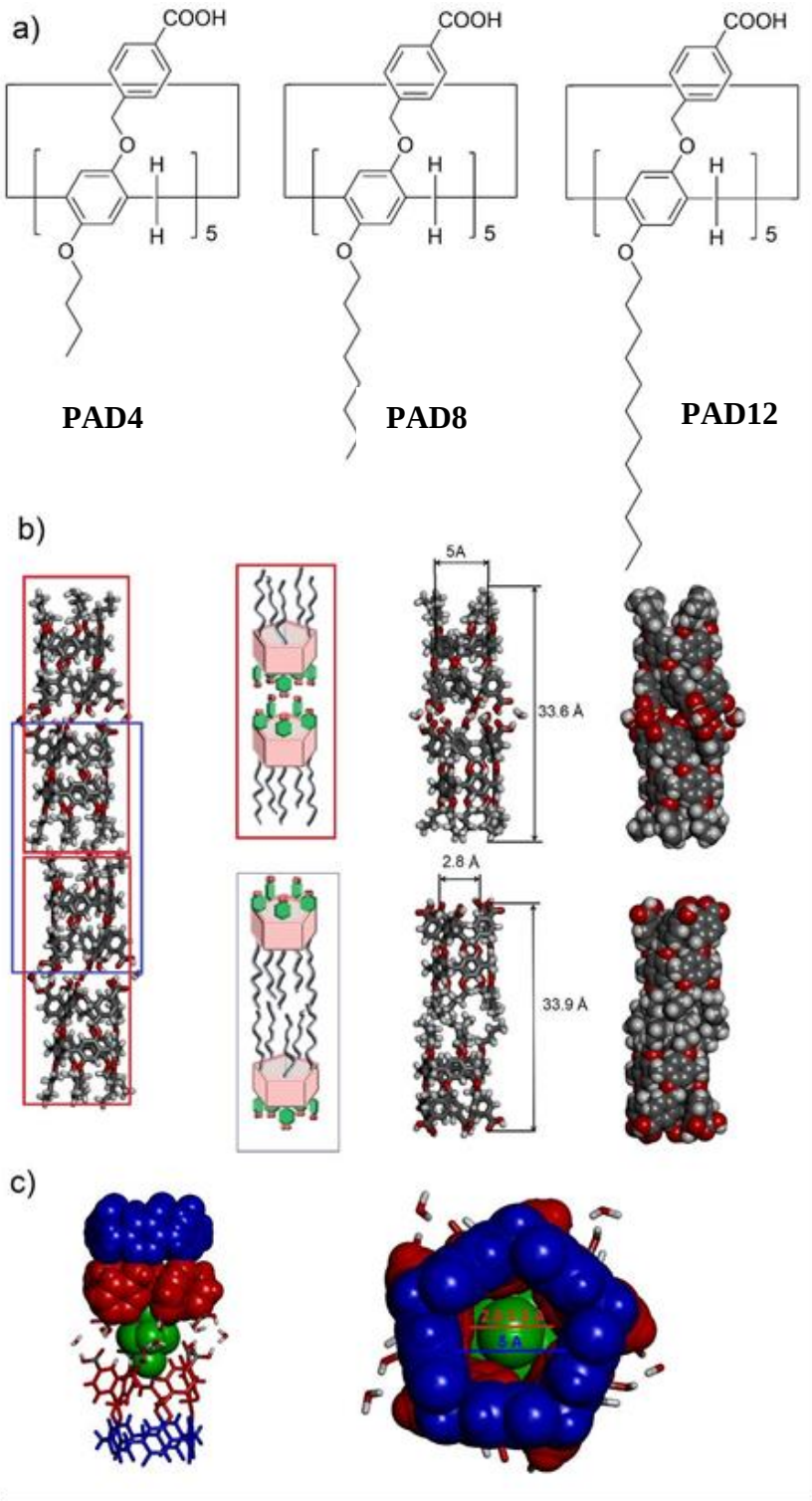

Figure 1. a) Structures of peralkylcarboxylate-pillar[5]arenes **PAD4**, **PAD8** and **PAD12** and b) X-ray single crystal structure of PAD4.[29] Crystal packing along c-axis emphasizing self-assembled tubular carboxylate H-bonding (b, red) and bilayer hydrophobic (b, blue) dimers in stick and CPK representations Crystalline solid state structures show dimeric structures of 34 Å length and c) a variable pore geometry composed of Pillar[5]arene platform (blue) of 5 Å diameter and of narrowest twisted carboxy-phenyl pore of 2.8 Å diameter (red). Green $CHCl_3$ molecules in CPK representation are perfectly positioning a Cl atom fitting the narrowest carboxy-phenyl pore, while the other atoms are disordered in the larger junction formed via hydrogen bonding of the carboxylate groups.

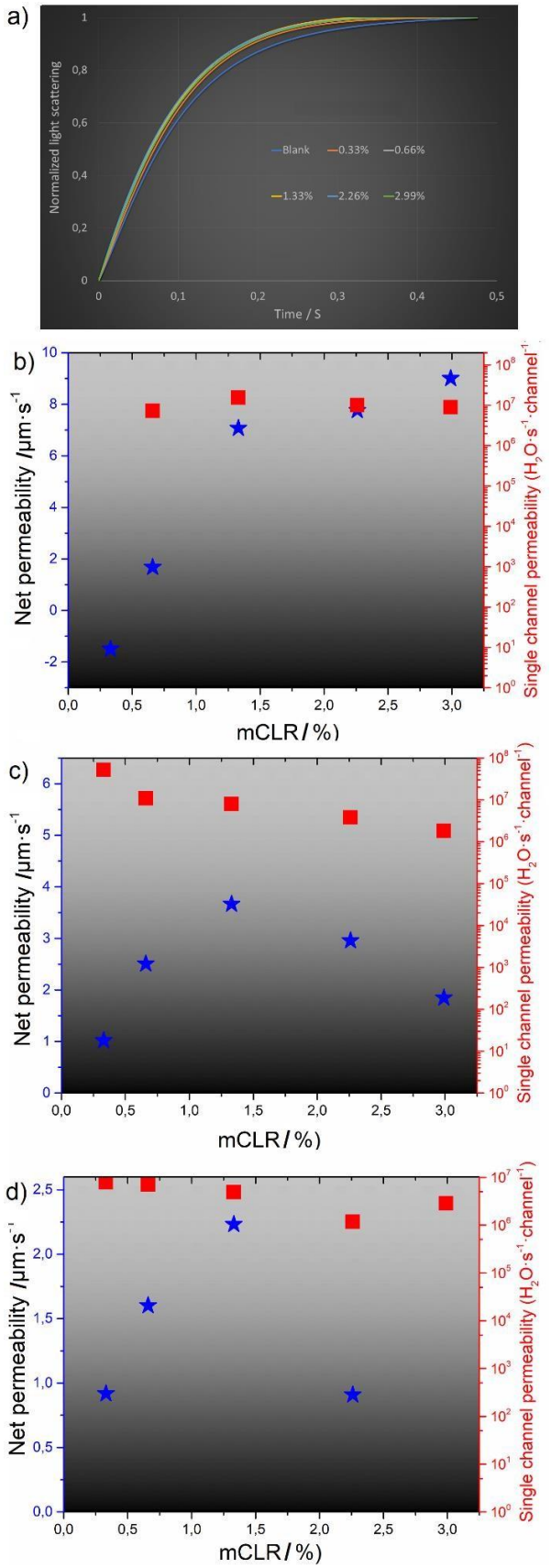

Figure 2. Water-transport activity in liposomes: a) Representative stopped-flow light-scattering experimental traces of liposome post-mix assays at different mCLRs of **PAD4** after abrupt exposure to a hypertonic solution of 200-mM KCl. The net (blue stars) and single water (red squares) permeabilities of the liposomes containing b) **PAD4**, c) **PAD8** and d) **PAD12** channels at different mCLRs, measured under hypertonic conditions abruptly exposed to a hypertonic solution of 100-mM KCl from the post-mix assays.

Longer alkyl chains in **PAD12** might stabilize the bilayer conformation, while shorter alkyl chains in **PAD4** should strongly stabilize the tubular dimers in the bilayer. It is important to note that the thickness of the insulating bilayer membrane (30-35 Å)[1] is quite similar to the length of the dimeric **PAD4** (Figure 1), while the hydrophobic interactions between the longer alkyl chains in **PAD8** and **PAD12** and the bilayer stabilize their positionings.

PAD4, **PAD8** and **PAD12** assemble into functional water-permeable channels in liposomes and increase the overall water permeability relative to the background lipid permeability.[31] Their water transport rates are strongly dependent on the nature of hydrophobic alkyl tails grafted onto pillar[5]arene platform. **PAD4**, **PAD8** and **PAD12** channels were reconstituted into phosphatidylcholine (PC) lipid vesicles (100 nm in diameter) with different molar ratios of compound to lipids (0.33%, 0.66%, 1.33%, 2.26% and 2.99% mCLRs) in which channels were added by simple addition of the dimethylsulfoxide DMSO solutions of the **PADs** derivatives to pre-formed vesicle suspensions. Then the vesicles were exposed to outwardly directed osmotic pressure gradients (shrinking mode of the vesicles). Under hypertonic conditions driven by outwardly 10 mM HEPES buffer solution 100, 200 mM KCl osmolate, the shrinkage of the liposomes under osmotic gradients of 100, 200 mOsm increased the lightscattering signal (Figure 2a). The net permeabilities increase when mCLRs ratios increase and with increasing osmolarity. The permeabilities present a maximum of 9.00 μm/s at high mCLR=3.00 for **PAD4** which is the most permeable toward water in the dimeric tubular configuration in the series, whereas for **PAD8**, and **PAD12**, the maxima values are lower: 3.66 μm/s and 2.23 μm/s respectively and they can be detected at mCLR=1.33% (Figure 2b-d). We further estimated the single-channel permeability, P_s of each channel [27] (see Supporting information for details). In the shrinking mode, **PAD4**, **PAD8** and **PAD12** show a tendency of P_s increasing with osmolarity as it was with net permeability. For example permeabilities of

$1.54 \cdot 10^7$, $5.21 \cdot 10^7$ and $7.95 \cdot 10^6$ water molecules/s/channel, are obtained for **PAD4** (mCLR=1.33), **PAD8**, (mCLR=0.33) and **PAD12** (mCLR=0.33) respectively, which are only one orders of magnitude lower than that of AQPs (~10^8-10^9 water molecules/s/channel).[2b] It

can be noticed that with increasing of mCLR the single channel permeability is decreasing, but remains on the same level of magnitude. Thus, the tendency for dropping of single channel permeability can be explained by progressive higher aggregation or lower solubility of **PAD** channels at high concentration, while using low concentration for incorporation into lipid bilayer prevents its aggregation. Water transport activities decrease substantially as the grafted alkyl chain length increases (**PAD4**>>**PAD8**>**PAD12**), implying the formation variable architectures of permeable tubular dimers for **PAD4** and less permeable bilayer configuration for **PAD12,** whereas **PAD8** present an intermediate situation. An unfavorable hindering wrapping of the hydrophobic tails inside the selective pore of the **PADs** or around at the interface with the bilayers, can be presumed for longer chains. Indeed, the tail length seemed to be optimal for *butyl* chains while longer chains led to aggregation when mixed with lipids.

In order to have more precise structural support for the in-membrane contentions we further prepared the carboxylate Na^+ or Li^+ salts of **PAD4**.[32] Oppositely to carboxyl functionalized PAD4, for the carboxylate salt of **PAD4** the hydrogen-bonding driven dimerization would not be possible. **PAD4Na** or **PADLi** salts could dimerize only through the interdigitation of the alkyl chains, having the carboxylate groups interacting with the polar heads of the phospholipids. Their net and single channel permeabilities at 1.33% mCLRs are 13.00 μm/s and $2.83 \cdot 10^7$water molecules/s/channel, respectively, which is almost double to that observed for **PAD4** counterpart, providing clear evidence two distinguish both models. For the carboxylate appended bilayer dimers the average fraction of channels filled with water is increasing due the presence of hydrophilic carboxylate groups, remaining accessible to water from both sides of the membrane.

Ion (Na^+ and K^+) transport activities across the bilayer membranes incorporating **PAD4**, **PAD8** and **PAD12** channels reconstituted into phosphatidylcholine (PC) lipid vesicles (100 nm) at the same mCRLs as used for water transport, were assessed using standard HPTS fluorescence assays.[33] Indeed, when tested with NaCl or KCl on external buffer, the **PAD4**,

PAD8 and **PAD12** channels had an unexpected behaviour: after the compound injection at t=20 s, the internal pH remains stable and only the creation of a pH gradient, applied at t=40 s, induce an abrupt increase of the internal pH, reminiscent with a low H^+ efflux (A_{max} = 0.06 for **PAD4**, 0.10 for **PAD8** and 0.03 for **PAD12** at 300 s) (Figure S7) and then the internal pH remains quasi-stable, independent on the nature of the channel or transported cation. Accordingly, the addition of base in the extravesicular solution induces a rapid deprotonation of carboxyl groups of the channel in the bilayer membrane, which synergistically induce HPTS deprotonation and generate the observed abrupt increase in fluorescence. After pH equilibration, dose-response experiments show the constant absorbance behaviors. It is noteworthy that, K^+ and Na^+ cations are not transported and channel structuration is no effective to induce Na^+ or K^+ /H^+ antiport conductance states along the assembled channel.

Single channel planar lipid bilayer experiments confirm the complete inactivity for K^+ transport under applied potential in range of 50 - 200 mV for tested solutions of **PAD4** (Figure S8). The transport activity is rather impossible to initiate, both in terms of length of operating periods and the concentration of **PAD4** in the membrane.

Overall, the **PAD4**, **PAD8** and **PAD12** dimers, obtained using simple chemistry, can be assembled into highly selective artificial water channels and remain stable in lipid membranes. Previously, the seminal discovery of pillar[5]arene PAP unimolecular channels by Hou et al.[15]are at long last beginning to meet encouraging signs for high water permeability (10^6-10^8 water molecules/second/channel), while most of these channels present ionic transport activity, thus not yet selectivity. Natural AQP channels present an hourglass structure offering size SF restriction of ~3 Å and selectivity against cations, reinforced through electrostatic repulsion in the region known as the aromatic arginine (ar/R) constriction.[2b] In this study a simple modification of rims of pillar[5]arene backbone of 5 Å diameter led to the construction of a supplementary narrowest hydrophobic pore of 2.6-2.8 Å diameter within the same structure, affording a size restriction control of translocation along tubular dimers at this selectivity filter

level. The water permeability of **PAD4**, **PAD8** and **PAD12** channels (~ 10^7 water molecules/s/channel) is only one orders of magnitude lower than that of AQPs, and more important they are rejecting alkali cations. Differently to previous selective I-quartets where water molecules are interacting along the whole structure of the channel of ~2.8 Å, herein the narrowest pore structure of **PAD4**, **PAD8** and **PAD12** channels in precisely located at the two narrowest regions of the pore, which remains larger along the resting length of the pore. The narrowest diameter of the pore itself is large enough for the water molecules to pass having themselves a diameter of ~2.8 Å, but restrictive enough to block the passage of hydrated Na^+ or K^+ cations.

We set up computer simulations to probe the behavior of **PAD4** dimers in an explicit lipid bilayer environment. Simulation results are summarized in Figure 3. As a first test we inserted a single H-bonding carboxylate or hydrophobic butyl dimers. Neither isolated dimer was stable in the membrane, leading either to a tilted but stable membrane-embedded structure for carboxylate (Figure 3a) or to a shifted side-by-side aggregated for butyl dimer losing its butyl connections (Figure 3b). In the latter case we hypothesize the competition with the lipid molecules to weaken the hydrophobic interactions between the butyls. Next, we tested whether larger assemblies provide increased stabilization within the membrane environment, which was indeed the case. For this purpose, we built a honeycomb arrangement where a central dimer is surrounded by a hexagon of 6 others, as schematically depicted in Figure 3c. Both dimer assemblies form water pathways through the bilayer. At the beginning of the simulation, the carboxylate dimer honeycomb shows water wetting-dewetting forming water wires through the tubular dimers as selective pores (Figure 1d). Over time, a significant shift of the upper vs. lower layer of monomers occurs, which brings water penetration and accumulation to a halt in the region of where the carboxylic groups are present. The carboxylate dimer honeycomb does experience a tilt that is not quite as pronounced as the one observed for the monomer, but most importantly initiates water permeation events. Initially these water paths are through the dimeric pathways (Figure 1e), whereas later on alternative pathways, leading to the formation

of a toroidal pore through the bilayer are observed as well (Figure 1f). The permeation rate is at its maximum around 250 ns, when the tilted structure allows a continuous water pathway around carboxylate groups. The permeation time duration varies from 2 ns to 175 ns.

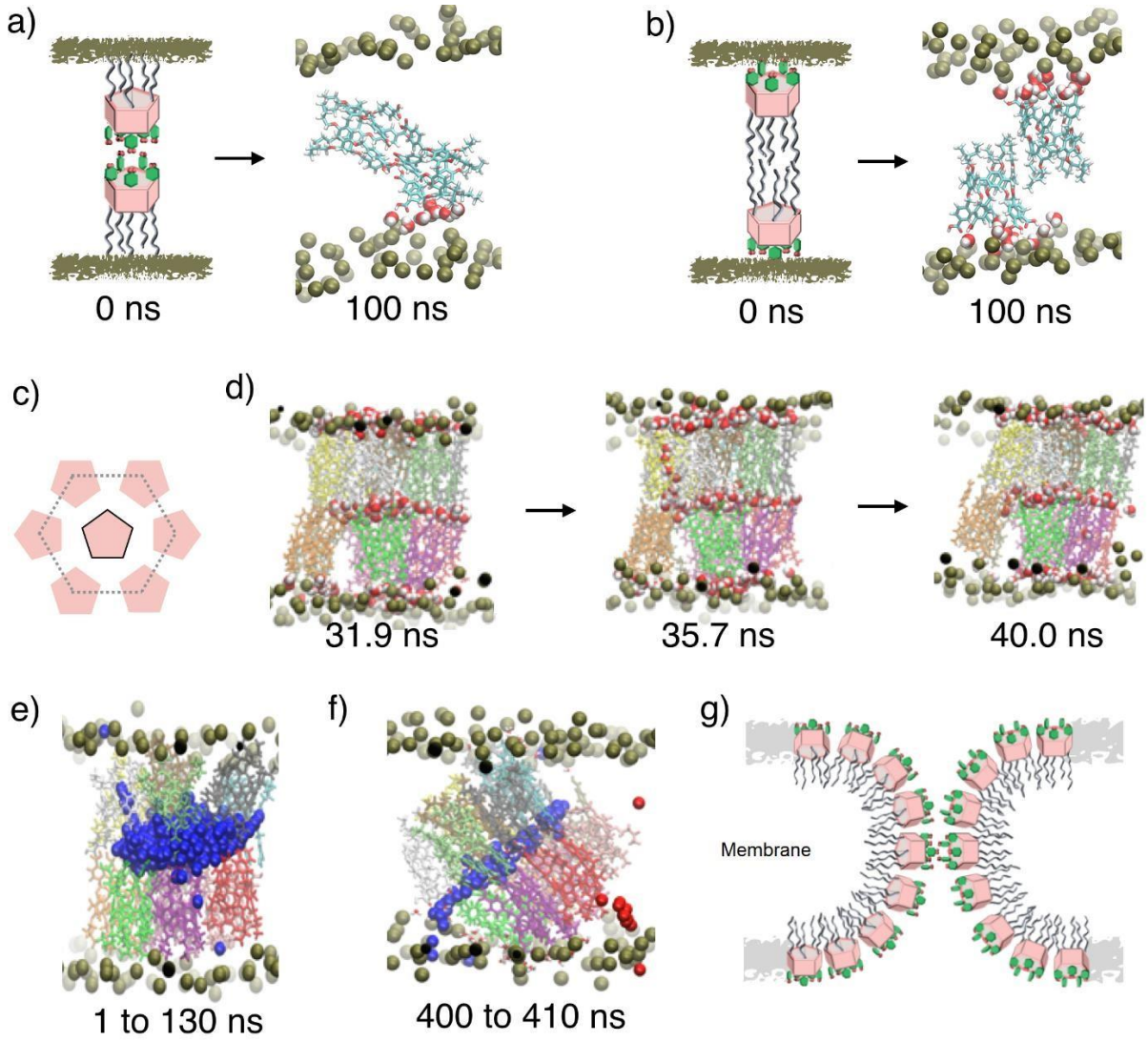

Figure 3. a) Carboxylic H-bonding dimer in a 100 ns molecular dynamics simulation in the lipid bilayer. b) Lipophilic bilayer dimer shifts side-to-side. c) Top view of honeycomb hexametric arrangement around a central dimer. d) Wetting-dewetting events in the first 50 ns of the carboxylic dimer. e) Water-wire pathway in the beginning 1 ns after releasing constraints on the system. through the carboxyli dimer channel (around 130 ns) in the central region and the exit in a lateral exposed lipid area. f), two water pathways are shown around 400ns after equilibration. The blue pathway accounts for a permeation event through the toroidal COOH pore (during around 10 ns) and the red pathway accounts for a permeation event in the lipid area. g) ideal schematic representation of a toroidal pore in the bilayer membrane

Artificial toroidal pores have been pionieered by Colombini[34a,b] for the pores formed by natural ceramide and by our group[34c] for the pores formed by artificial self-assembled crown ethers. The inner walls of the pore would be lined with carboxylate groups and with the external

butyl tails projecting into the lipid hydrocarbon region, maximizing favorable interactions with the environment for both polar and lipophilic moieties. The relatively large number of the polar carboxyl groups relative to the hydrocarbon tail would stabilize the positive curvature required on the inside of the torus (Figure 1b). Based on their physico-chemical properties, one may hypothesize that a toroidal pore would stabilize clusters of water which probably is favored by more hydrophilic ones as proved by increased permeation rates of **PADLi** or **PADNa**. The honeycomb assembly we probed is likely not the optimal. Longer and different simulations setups will be required to investigate novel toroidal complex assemblies and are beyond the scope of the present contribution.

The present results show that, using a rationally designed pillar[5]arene platform and a simple restriction mechanism, it becomes possible to control the selectivity of water translocation in a manner reminiscent of that of proteins capable of selectively transport Å scale species. This is a very intriguing system. It is very tempting to equate the two types of structures in the solid state (hydrogen bonded and hydrophobic dimers) and the two types of channels in the bilayer membrane (dimeric H-bonded PA and a discrete large toroidal pore). The unifying assumption is that an H-bonding dimer would form preferentially and is stable in the membrane. Stacks of these dimers would lead to the dominant toroidal structure in a membrane environment providing hybrid pathways for water translocation through the dimeric water-wires and on alternative pathways encapsulating self-protective water clusters through a toroidal pore.

I -quartet-embedded water sponges were the first example in literature taking into account the formation of 3D water sponges/clusters displaying high water/ion selectivity.[35] They make the intrinsic features of water sponges [35] or clusters[3d] particularly self-protective against ions. The water translocation events lead to the change in shape of the channel conduits in bilayer membranes from a single water-wires to fully aggregated toroidal water clusters, which confer to these channels the self-adaptive behaviours.

The **PAD** channels showed no transport of Na^+ and K^+ cations, making them a viable option for desalination. The observed ionic-exclusion of these channels suggests that the channel selectivity performance is of outmost importance in translating molecular transport properties to performant membranes optimized by using chemical engineering approaches. **PAD** channels described here, hold significant promise for the incipient development of the innovative materials based on artificial synthetic scaffolds mimicking the functions of natural water channels. On the other hand, precise-triggered shape changes of aggregated channels also amount to coupling and transduction between geometric water clusters and selective translocation events, a feature of much interest for supramolecular translocation of water in membranes used for desalination.

Acknowledgements. This work was supported by Agence Nationale de la Recherche ANR18-CE06-0004-02, WATERCHANNELS, the Grant-in-Aid for Scientific Research on Innovative Areas: Soft Crystal (JP18H04510 and JP20H04670), and Kiban A (JP19H00909) from MEXT Japan, JST CREST (JPMJCR18R3), and the World Premier International Research Center Initiative (WPI), MEXT, Japan.

References

1. B. Hille, *Ion Channels of Excitable Membranes*, Sinauer Associates, Sunderland, MA, 3rd Ed, **2001**.

2. a) D. A. Doyle, J. Morais Cabral, R. A. Pfuetzner, A. Kuo, J. M. Gulbis, S. L. Cohen, B.T. Chait, R. MacKinnon, *Science* **1998**, *280*, 69-77; b) E. Tajkhoorshid, P. Nollert, M. O. M. Jensen, L. J. W. Miercke, J. O'Connell, R. M. Stroud, K. Schulten, *Science* **2002**, *296*, 525530.

3. a) Y. Le Duc, M. Michau, A. Gilles, V. Gence, Y.-M. Legrand, A. van der Lee, S. Tingry, M. Barboiu, *Angew. Chem.* **2011**, *123*, 11568-11574; *Angew. Chem. Int. Ed.* **2011**, *50*, 1136611372; b) M. Barboiu, A. Gilles, *Acc. Chem. Res.* **2013**, *46*, 2814–282; c) R. H. Tunuguntla, R. Y. Henley, Y. C. Yao, T. A. Pham, M. Wanunu, A. Noy, *Science* **2017**, *357*, 792-796; d) W. Song, H. Joshi, R. Chowdhury, J. S. Najem, Y. X. Shen, C. Lang, C. B.

Henderson, Y. M. Tu, M. Farell, M. E. Pitz, C. D. Maranas, P. S. Cremer, R. J. Hickey, S. A. Sarles, J. L. Hou, A. Aksimentiev, M. Kumar, *Nat. Nanotechnol*. **2020**, *15*, 73-79; e) J. Shen, R.J. Ye, A. Romanies, A. Roy, F. Chen, C. L. Ren, Z. Liu, H. Q. Zeng, *J. Am. Chem. Soc*. **2020**, *142*, 10050−10058

4. M. Barboiu, *Acc. Chem. Res.* **2018,** *51*, 2711−2718.

5. S.-P. Zheng, L.-B. Huang, Z. Sun, M. Barboiu, *Angew. Chem*. **2020**, DOI: 10.1002/ange.201915287; *Angew. Chem. Int. Ed.* **2020**, DOI: 10.1002/anie.201915287.

6. E. Mahon, S. Garai, A. Müller, M. Barboiu. *Adv. Mat.* **2015**, *27(3*5), 5165-5170.

7. T. M. Fyles, C. C. Tong, *New J. Chem.* **2007**, *31*, 655-661.

8. M. Jung, H. Kim, K. Baek, K. Kim, *Angew. Chem.* **2008**, *120*, 5839-5841; *Angew. Chem. Int. Ed.* **2008**, *47*, 5755-5757.

9. a) O. V. Kulikov, R. Li, G. W. Gokel, *Angew. Chem.* **2009**, *121*, 381-383; *Angew. Chem. Int. Ed.* **2009**, *48*, 375-377; S. Negin, M. M. Daschbach, O. V. Kulikov, N. Rath, G. W. Gokel, *J. Am. Chem. Soc.* **2011**, *133*, 3234-3237; b) R. Li, O. V. Kulikov, G. W. Gokel, *Chem. Commun.* **2009**, 6092-6094. c) O. V. Kulikov, M. M. Daschbach, C. R. Yamnitz, N. Rath, G. W. Gokel, *Chem. Commun.* **2009**, 7497-7499.

10. R. Kawano, N. Horike, Y. Hijikata, M. Kondo, A. Carné-Sánchez, P. Larpent, S. Ikemura, T. Osaki, K. Kamiya, S. Kitagawa, S. Takeuchi, S. Furukawa, *Chem* **2017**, *2*, 393-403.

11. a) T. Ogoshi, S. Kanai, S. Fujinami, T.-A.Yamagishi, Y. Nakamoto, *J. Am. Chem. Soc.* **2008,** *130* , 5022-5023; b) T. Ogoshi, T. Aoki, K. Kitajima, S. Fujinami, T.-A. Yamagishi, Y. Nakamoto, *J. Org. Chem.* **2011,** *76* (1), 328-331.

12. T. Ogoshi, T. Kakuta, T. A. Yamagishi, *Angew. Chem. Int. Ed.* **2019,** *58* (8), 2197-2206.

13. W. Si, P. Xin, Z. T. Li and J. -L. Hou, *Acc. Chem. Res*., **2015**, 48, 1612-1619.

14. W, Si. L, Chen. X.-B, Hu, G. Tang, Z. Chen, J.-L. Hou, Z.-T. Li, *Angew. Chem., Int. Ed*. **2011**, 50, 12564.

15. X. B. Hu, Z. Chen, G. Tang, J. -L. Hou and Z. T. Li, *J. Am. Chem. Soc*., **2012**, 134, 83848387.

16. L. Chen, W. Si, L. Zhang, G. Tang, Z. T. Li and J. -L. Hou, *J. Am. Chem. Soc*, **2013**, 135, 2152-2155.

17. W. Si, Z.-T. Li, and J.-L. Hou, *Angew. Chem. Int. Ed.*, **2014**, 53, 4578-4581

18. Y. Zhou, Y. Chen, P. P. Zhu, W. Si, J. -L. Hou, Y. Liu, *Chem. Commun.* **2017**, *53*, 3681-3684.

19. J.-Y. Chen, J.-L. Hou, *Org. Chem. Front.* **2018**, *5*, 1728-1736.

20. a) M. Zhang, P.-P. Zhu, P. Xin, W. Si, Z.-T. Li, and J.-L. Hou, *Angew. Chem. Int. Ed.*, **2017**, *56*, 2999 - 3003. b) W.-W. Haoyang, M. Zhang and J.-L. Hou, *Chin. J. Chem.*, **2019**, *37*, 25 - 29.

21. W. X. Feng, Z. Sun, M. Barboiu, *Israel. J. Chem.* **2018**, *58*, 1209-1218

22. H. Behera, L. Yang, J. L. Hou, *Chinese J. Chem.* **2020,** *38* (2), 215-217.

23. W.-X. Feng, Z.-H. Sun, Y. Zhang, Y.-M. Legrand, E. Petit, C.-Y. Su, M. Barboiu, *Org. Lett*. **2017**, *19*, 1438−1441

24. P. Xin, H. Kong, Y. Sun, L. Zhao, H. Fang, H. Zhu, T. Jiang, J. Guo, Q. Zhang, W. Dong, *Angew. Chem. Int. Ed.*, **2019**, *58*, 2779 - 2784.

25. Y.-X. Shen, W. Si, M. Erbakan, K. Decker, R. De Zorzi, P. O. Saboe, Y. J. Kang, S. Majd, P. J. Butler, T. Walz, A. Aksimentiev, J.-L. Hou and M. Kumar, *Proc. Natl. Acad. Sci*. USA, **2015**, *112*, 9810-9815.

26. W. Song, H. Joshi, R. Chowdhury, J. S. Najem, Y. X. Shen, C. Lang, C. B. Henderson, Y. M. Tu, M. Farell, M. E. Pitz, C. D. Maranas, P. S. Cremer, R. J. Hickey, S. A. Sarles, J. -L. Hou, A. Aksimentiev, M. Kumar, *Nat. Nanotechnol.* **2020**, 15, 73-79.

27. a) E. Licsandru, I. Kocsis, Y.-x. Shen, S. Murail, Y.-M. Legrand, A. van der Lee, D. Tsai, M. Baaden, M. Kumar, M. Barboiu, *J. Am. Chem. So*c., **2016**, *138*, 5403-5409; b) M. Barboiu, *Chem. Commun*. **2016,** *52*, 5657-5665.

28. D. Kaizerman-Kane, M. Hadar, N. Tal, R. Dobrovetsky, Y. Zafrani, Y. Cohen *Angew. Chem. Int. Ed.*, **2019**, *58*, 5302-5306; b) M. Hadar, D. Kaizerman-Kane, Y. Zafrani, Y. Cohen, *Chem. Eur. J.*, **2020**, 10.1002/chem.202000972.

29. S. Fa, Y.Sakata, S. Akine, T. Ogoshi, *Angew. Chem. Int. Ed.*, **2020**, *59*, 9309-9313

30. O. Mogck, V. Böhmer, W. Vogt, *Tetrahedron* **1996**, *52*, 8489- 8496.

31. M. L. Zeidel, S. V. Ambudkar, B. L. Smith, P. Agre, *Biochemistry* **1992,** *31*, 7436-7440.

32. G. Yu, M. Xue, Z. Zhang, J. Li C. Han, F. Huang, *J. Am. Chem. Soc.* **2012**, *134*, 13248–13251.

33. S. Matile, N. Sakai, In *Analytical Methods in Supramolecular Chemistry*, Schalley, C. A., Ed. Wiley -VCH: Weinheim, pp 381-418, **2007**.

34. (a) L. J. Siskind, A. Davvoody, N. Lewin, S. Marshall, M. Colombini, *Biophys J.* **2003**, *85*, 1560-1575; (b) L. Yang, T. A. Haroon, T.M. Weiss, L. Ding, H.W. Huang, *Biophys J.* **2001**, *85*, 1475-1485; c) A. Cazacu, C. Tong, A. van der Lee, T.M. Fyles, M. Barboiu, *J. Am. Chem. Soc*., **2006**, *128*, 9541-9548.

35. S. Murail, T. Vasiliu, A. Neamtu, M. Barboiu, F. Sterpone, M. Baaden, *Faraday Discuss.* **2018**, 209, 125–148.

Distinguishing Pillar[5]arene dimers with variable diameter SF interiors get spontaneously inserted into lipid bilayers, showing selective water conductance activity. The transport *via* the narrow pore gates ~2.8 Å, acting as selectivity filters, is perfectly sized for the water molecules to pass having themselves a diameter of ~2.8 Å, but restrictive enough to block the passage of hydrated Na^+ or K^+ cations

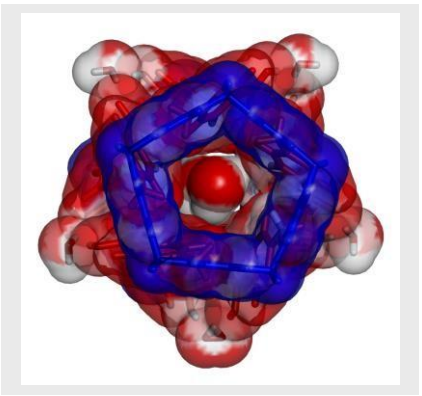

Dmytro Strilets, Shixin Fa, Arthur Hardiagon, Marc Baaden, Tomoki Ogoshi, Mihail Barboiu **

Page No. _ Page No.

Biomimetic approach for highly selective artificial water channels based on tubular Pillar[5]Arene dimers

Supporting Information

Biomimetic Approach for Highly Selective Artificial Water Channels Based on Tubular Pillar[5]arene Dimers

Dmytro Strilets, Shixin Fa, Arthur Hardiagon, Marc Baaden, Tomoki Ogoshi,* and Mihail Barboiu*

anie_202009219_sm_miscellaneous_information.pdf

General

All commercially available reagents and solvents were used as received. ^{1}H NMR and ^{13}C NMR spectra were recorded on JEOL JNM-ECS400 and JNM-ECZ500R spectrometers. Chemical shifts were reported in ppm versus tetramethylsilane. High-resolution ESI-MS was recorded on Thermo Fisher Scientific Exactive Plus mass spectrometer equipped with UltiMate 3000 HPLC.

Syntheses

Syntheses of compounds **PAD4** and **PAD12** have been reported,[S1] and the synthesis of **PAD8** followed this reported procedure.

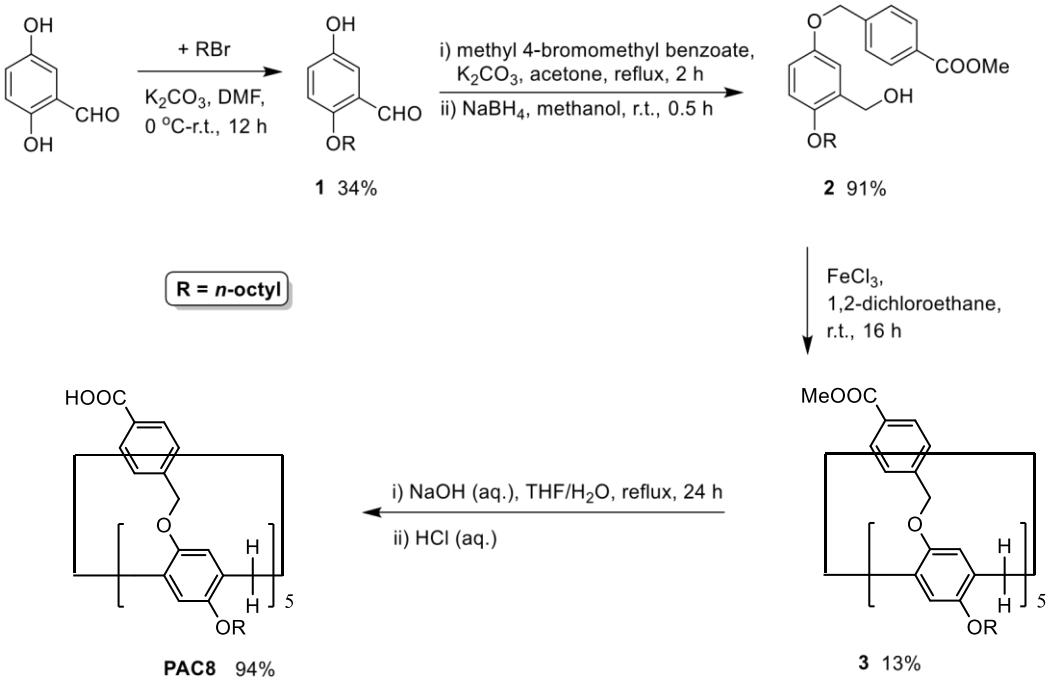

Scheme S1. Synthesis of **PAD8**.

Mono-substituted dihydroxybenzaldehyde 1. To a mixture of 2,5-dihydroxybenzaldehyde (5.0 g, 36.2 mmol) and 1-bromooctane (6.3 mL, 36.2 mmol) in dry DMF (50 mL) under 0 ℃ was added potassium carbonate (7.0 g, 50.7 mmol). The mixture was stirred in ice bath for 1 h, and then stirred at room temperature for 12 h. The solid was filtered off, and the filtrate was concentrated under reduce pressure. The residue was dissolved in ethyl acetate (100 mL) and washed with water (3 × 25 mL) and brine (25 mL), dried over anhydrous sodium sulfate and filtered. After removal of the solvent, the residue was chromatographed on a silica gel column using a mixture of *n*-hexane and ethyl acetate (from 10:1 to 5:1, v/v) as the mobile phase. The titled compound was obtained as white solid (3.05 g, 34%). ^{1}H NMR (500 MHz, $CDCl_3$): δ 10.44 (s, 1H), 7.37-7.33 (m, 1H), 7.13-7.06 (m, 1H), 6.90 (d, J = 9.0 Hz, 1H), 4.02 (t, J = 6.5 Hz, 2H), 1.86-1.77 (m, 2H), 1.51-1.42 (m, 2H), 1.39-1.23 (m, 16H), 0.92-0.86 (m, 3H). ^{13}C NMR (126 MHz, $CDCl_3$): δ 190.3, 156.5, 149.7, 125.3, 123.7, 114.6, 113.4, 69.3, 31.9, 29.4, 29.29, 29.28, 26.2, 22.7, 14.2. ESI-HRMS. Calcd for $C_{15}H_{22}O_3$ (m/z): $[M - H]^-$, 249.1496. Found: 249.1493.

Di-substituted dihydroxybenzyl alcohol 2. To a mixture of **1** (2.50 g, 10 mmol) and methyl 4-(bromomethyl) benzoate (2.75 g, 12 mmol) in acetone (100 mL) was added potassium carbonate (1.66 g, 12 mmol). The reaction mixture was stirred under reflux for 2 h. The solid was filtered off, and the filtrate was concentrated under reduced pressure. The residue was suspended in methanol (30 mL) and cooled down to 0 ℃ with an ice bath. Sodium borohydride (456 mg, 312 mmol) was then carefully added. The ice bath was removed, and the mixture was stirred at room temperature for 1 h. Brine (50 mL) was added to quench the reaction. The organic solvent was removed under reduced pressure, and the residue was extracted with dichloromethane (2 × 50 mL).The combined organic phase was washed with water (50 mL) and brine (50 mL), dried over anhydrous sodium sulfate and filtered. After removal of the solvent, the residue was chromatographed on a silica gel column using a mixture of *n*-hexane and acetone (from 10:1 to 5:1, v/v) as the mobile phase to get the titled compound as white solid (3.66 g, 91%). ^{1}H NMR (400 MHz, $CDCl_3$): δ 8.05 (d, J = 8.3 Hz, 2H), 7.49 (d, J = 8.0 Hz, 2H), 6.95 (d, J = 2.3 Hz, 1H), 6.82 (dd, J = 8.8, 2.8 Hz, 1H), 6.78 (d, J = 8.9 Hz, 1H), 5.08 (s, 2H), 4.66 (d, J = 6.6 Hz, 2H), 3.96 (t, J = 6.1 Hz, 2H) 3.92 (s, 3H), 2.45-2.36 (m, 1H), 1.831.73 (m, 2H), 1.49-1.41 (m, 2H), 1.39-1.22 (m, 8H), 0.93-0.85 (m, 3H). ^{13}C NMR (101 MHz, $CDCl_3$): δ 167.0, 152.4, 151.5, 142.6, 130.5, 130.0, 129.7, 127.0, 115.9, 114.2, 112.1, 70.1,

68.6, 62.4, 52.2, 31.9, 29.5, 29.4, 29.3, 26.3, 22.7, 14.2. ESI-HRMS. Calcd for $C_{24}H_{32}O_5$ (m/z):

$[M + Na]^+$, 423.2142. Found: 423.2145.

Rim-different pillar[5]arene ester 3. To a stirred solution of **2** (2.00g, 5 mmol) in 1,2dichloroethane (500 mL) was added anhydrous iron (III) chloride (82 mg, 0.5 mmol). The mixture was stirred at room temperature for 16 h before methanol (50 mL) was added to quench the reaction. The solution was washed by water (100 mL) and brine (100 mL), dried over anhydrous sodium sulfate, filtered and concentrated under reduced pressure. The residue was chromatographed on a silica gel column using a mixture of *n*-hexane and acetone (from 10:1 to 5:1, v/v) as the mobile phase to obtain the titled compound as white solid (245 mg, 13%). ^{1}H NMR (400 MHz, $CDCl_3$): δ 7.96 (d, J = 8.2 Hz, 10H), 7.33 (d, J = 8.2 Hz, 10H), 6.86 (s, 5H),

6.79 (s, 5H), 4.57-4.44 (m, 5H), 3.94-3.74 (m, 40H), 1.93-1.70 (m, 10H), 1.54-1.46 (m, 10H),

1.36-1.29 (m, 10H), 1.27-1.21 (m, 30H), 0.84-0.80 (m, 15H). ^{13}C NMR (101 MHz, $CDCl_3$): δ 166.8, 150.4, 149.2, 143.2, 129.8, 129.5, 128.5, 128.2, 127.0, 115.0, 69.6, 68.4, 52.2, 31.8, 31.7, 29.9, 29.6, 29.3, 26.4, 22.7, 14.2. ESI-HRMS. Calcd for $C_{120}H_{150}O_{20}$ (m/z): $[M + Na]^+$, 1934.0613. Found: 1934.0644.

PAD8. To the solution of **3** (96 mg, 0.05 mmol) in tetrahydrofuran (3 mL), sodium hydroxide (60 mg, 61.5 mmol) in water (3 mL) was added dropwise. The mixture was refluxed for 24 h. After the organic solvent was removed under reduced pressure, the solution was treated with aqueous HCl solution (1 M) until pH 1. The precipitate was collected by filtration, and washed with water (500 mL). After drying in vacuum, the product was obtained as white solid (87 mg, 94%).^{1}H NMR (400 MHz, $CDCl_3$): δ 8.00 (d, J = 7.8 Hz, 10H), 7.29 (d, J = 7.9 Hz, 10H), 6.89 (s, 5H), 6.87 (s, 5H), 4.77 (d, J = 13.7 Hz, 5H), 4.49 (d, J = 13.8 Hz, 5H), 4.04-3.79 (m, 20H), 1.94-1.75 (m, 10H), 1.62-1.49 (m, 10H), 1.42-1.35 (m, 10H), 1.34-1.25 (m, 10H), 1.24-1.09 (m, 20H), 0.89-0.77 (t, 15H). ^{13}C NMR (101 MHz, $CDCl_3$): δ 171.9, 150.4, 150.1, 144.5, 130.6, 128.81, 128.76, 128.4, 126.5, 115.8, 114.7, 70.8, 68.3, 31.8, 29.8, 29.6, 29.3, 26.4, 22.6, 14.2.

ESI-HRMS. Calcd for $C_{115}H_{140}O_{20}$ (m/z): $[M - H]^-$, 1839.9865. Found: 1839.9922.

Methods

Water transport experiments

LUV preparation: Preparation of unilamellar lipid vesiscles: Egg yolk L-α-phosphatidylcholine (EYPC) in $CHCl_3$ (25 mg/mL, 0.8 mL) was diluted with $CHCl_3$ (10 mL). The solution was evaporated under reduced pressure and the resulting thin film was further dried under high vacuum for 3 h. The lipid film was hydrated under vortex with HEPES buffer (2 mL, 10 mM HEPES buffer, pH = 7.0) at 25 ^{o}C for 5 min to give a milky suspension. The resulting suspension was subjected to six freeze-thaw cycles by using liquid N_2 to freeze and warm water bath to thaw. The suspension was extruded through polyethersulfone membrane (Whatman, UK, 0.1 μm) for nine times and then diluted with the same buffer into 40 mL. The final lipid concentration was 0.65 mM.

Stopped-flow water transport experiment: Water permeability of channels was measured with the stopped-flow instrument (SFM3000+MOS450, Bio-Logic SAS, Claix, France) by using stopped-flow light scattering experiments. Generally, the DMSO solution of **PAD4**, **PAD8** or **PAD12** (20 μL with required concentration) was added to the vesicle suspension (1.980 mL) to incorporate the channel molecules into the lipid bilayers. Then the vesicle sample and the hypertonic solutions (2.0 mL, 100 mM / 200 mM KCl, 10 mM HEPES buffer, pH 7.0) were loaded into two syringes. The size change of the vesicles was monitored through the light scattering intensity change with light of 365 nm wavelength and detection angle of 90°. The osmotic permeability (P_f) was calculated as following:

$$P_f = \frac{k}{\left(\frac{S}{V_0}\right) \times V_w \times \Delta Osm}$$

where k is the exponential coefficient of the change in the light scattering; S and V_0 are the initial surface area and volume of the vesicles, respectively; V_w is the molar volume of water, and Δ_{osm} is the osmolarity difference.

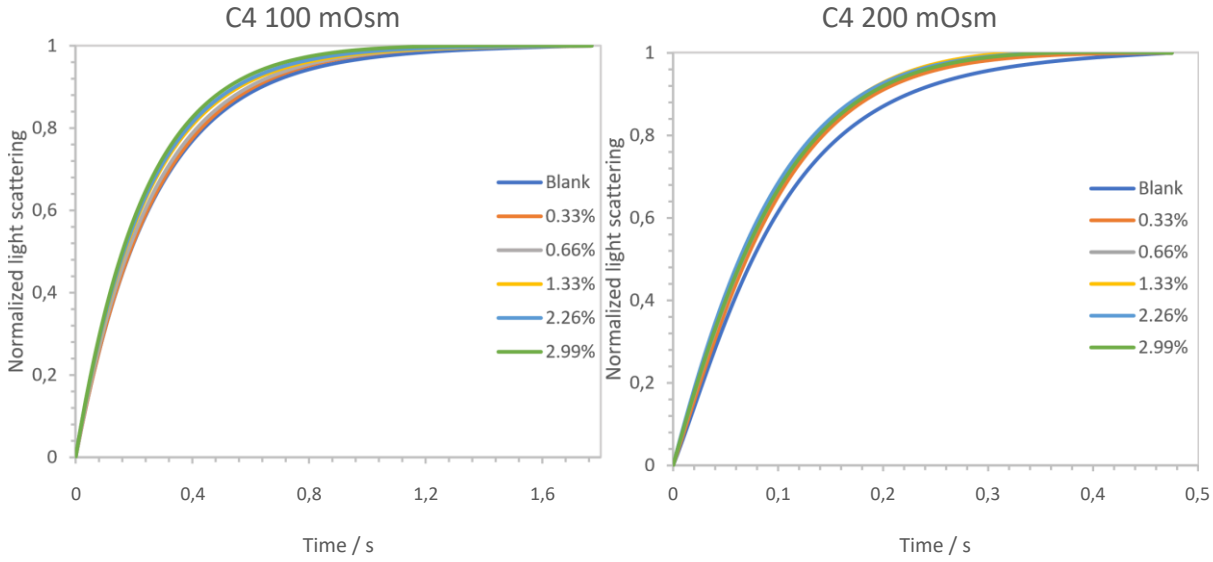

Figure S1. The stopped-flow traces from experiments on liposomes of **PAD4** with different mCLR and with 100 and 200 mOSM osmolarity gradients.

Table S1. Stopped-flow transport results for **PAD4** with 100 and 200 mOsm osmolality gradients

ΔO, mOsm	CLR, %	k_i	$P_{f(1)}$, μm·s^{-1}	Increase, %	Net permeability, μm·s^{-1}
100	BLANK	7.543	69.84		
	0.33	7.382	68.35	-2.14	-1.49
	0.66	7.724	71.52	2.40	1.68
	1.33	8.307	76.92	10.13	7.07
	2.26	8.382	77.61	11.12	7.76
	2.99	8.515	78.85	12.89	9.00
200	BLANK	9.129	42.26		
	0.33	9.397	43.51	2.94	1.24
	0.66	9.446	43.73	3.47	1.47
	1.33	9.557	44.25	4.69	1.98
	2.26	10.091	46.72	10.53	4.45
	2.99	9.542	44.18	4.53	1.91

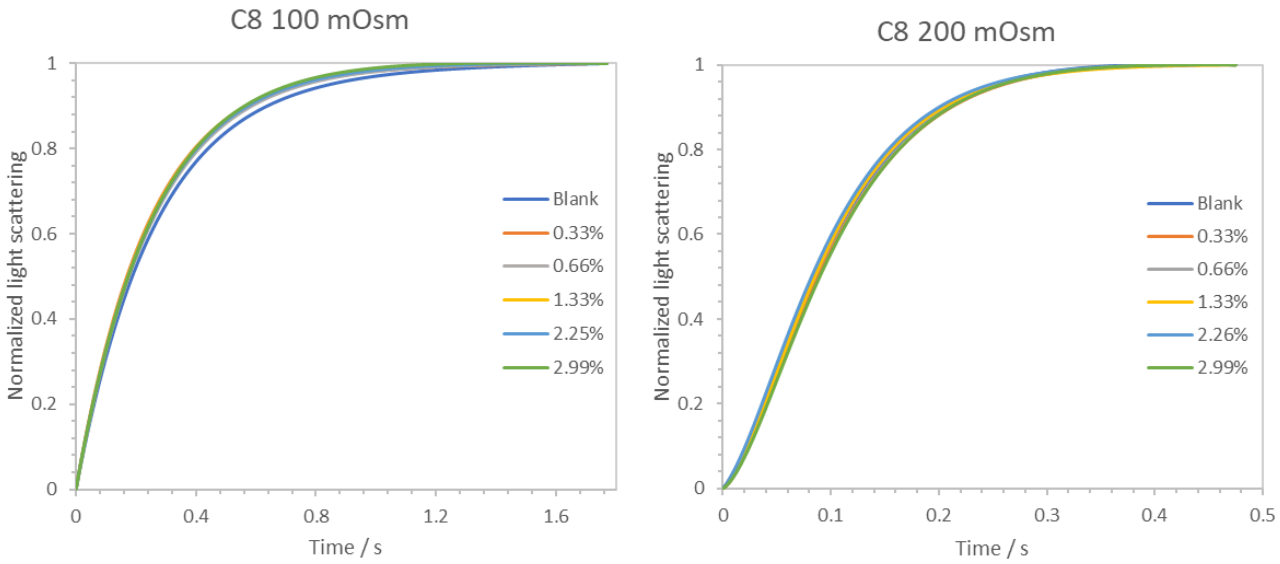

Figure S2. The stopped-flow traces from experiments on liposomes of **PAD8** with different mCLR and with 100 and 200 mOSM osmolarity gradients.

Table S2. Stopped-flow transport results for **PAD8** with 100 and 200 mOsm osmolality gradients

ΔO, mOsm	CLR, %	k_i	$P_{f(1)}$, µm·s^{-1}	Increase, %	Net permeability, µm·s^{-1}
100	BLANK	7.474	69.20	-	-
	0.33	7.573	70.12	1.33	0.92
	0.66	7.647	70.80	2.31	1.60
	1.33	7.715	71.43	3.23	2.23
	2.26	7.572	70.11	1.31	0.91
	2.99	7.786	72.09	4.18	2.89
200	BLANK	12.797	59.24	-	-
	0.33	11.603	53.72	-9.33	-5.53
	0.66	11.138	51.56	-12.96	-7.68
	1.33	10.593	49.04	-17.22	-10.20
	2.26	12.863	59.55	0.52	0.31
	2.99	12.007	55.59	-6.17	-3.66

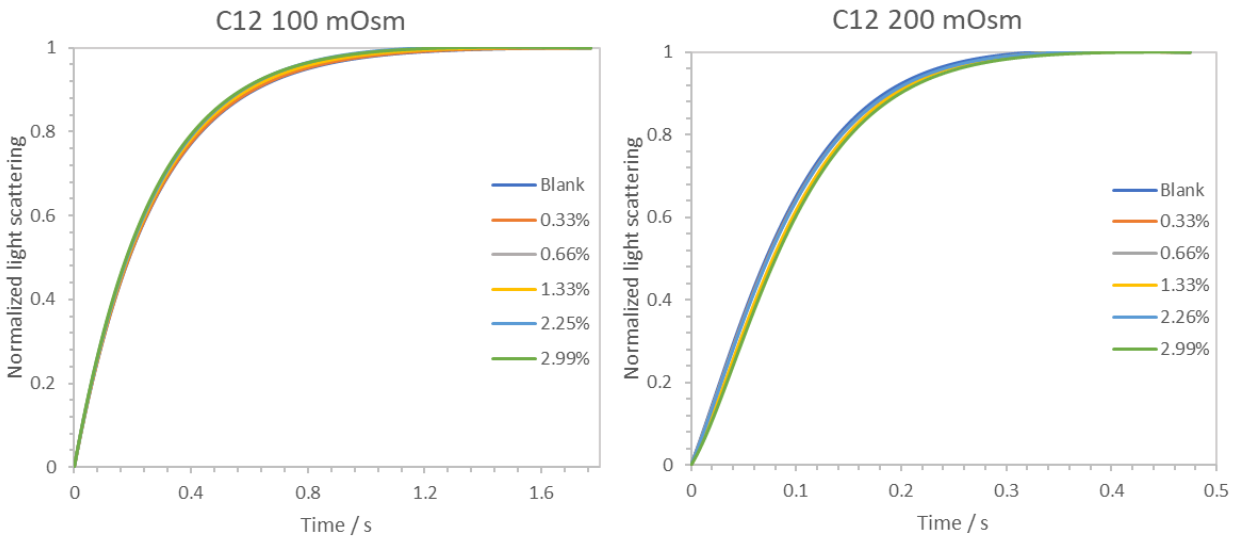

Figure S3. The stopped-flow traces from experiments on liposomes of **PAD12** with different mCLR and with 100 and 200 mOSM osmolarity gradients.

Table S3. Stopped-flow transport results for **PAD12** with 100 and 200 mOsm osmolality gradients

□ΔO, mOsm	CLR, %	k_i	$P_{f(1)}$, $\mu m \cdot s^{-1}$	Increase, %	Net permeability, $\mu m \cdot s^{-1}$
100	BLANK	7.474	69.20	-	-
	0.33	7.573	70.12	1.33	0.92
	0.66	7.647	70.80	2.31	1.60
	1.33	7.715	71.43	3.23	2.23
	2.26	7.572	70.11	1.31	0.91
	2.99	7.786	72.09	4.18	2.89
200	BLANK	12.797	59.24	-	-
	0.33	11.603	53.72	-9.33	-5.53
	0.66	11.138	51.56	-12.96	-7.68
	1.33	10.593	49.04	-17.22	-10.20
	2.26	12.863	59.55	0.52	0.31
	2.99	12.007	55.59	-6.17	-3.66

Single channel water permeability: The single channel permeability was calculated based on compound concentration and channel configuration in lipids. Take one sample of **C4** with mCLR = 1.33% as an example. The vesicles had diameter 100 nm in average after extrusion, the sum of outer and inner surface areas is $4\pi \cdot r + 4\pi \cdot (r-5) = 55{,}522\ nm^2$, assuming that the bilayer

thickness was 5 nm. The average cross-sectional area of a lipid in average was ~0.35 nm^2, and that of the was estimated as 0.786 nm^2. Taking on account that PAD**4** forms the channel from 2 molecules by self-assembling via Hydrogen bonds of carboxylic groups, the molar lipids to channel ratio was calculated as 150.94. The insertion number of the channel was ~810 per vesicle. If the overall net permeability by channels in liposomes was 7.07 μm/s, the singlechannel permeability was $4.62 \cdot 10^{-16}$ cm^3/s and $1.54 \cdot 10^7$ water molecules/s.

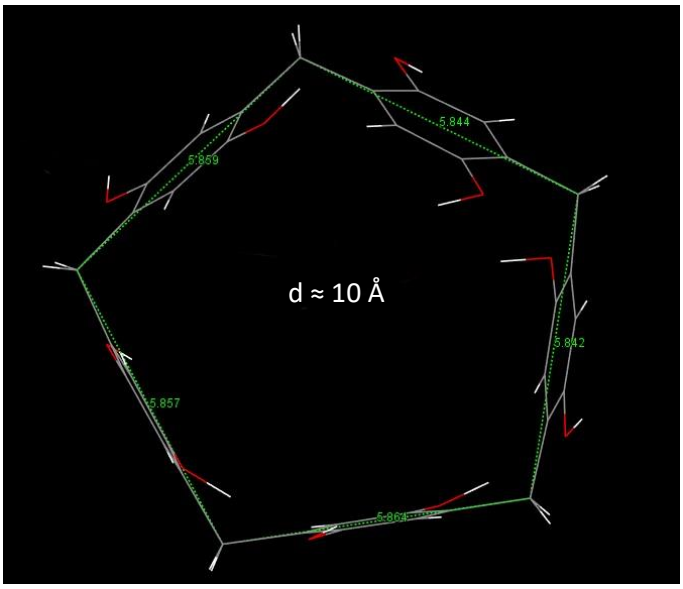

Figure S4. Crystal structure of Pillar[5]arene core.[S1] The cross-sectional surface of this molecule was calculated as 0.786 nm^2 based on its diameter. The value of cross-sectional surface was used for calculation of single channel permeability of Pillar[5]arenes dimers since pillar[5]arene is the core of these channels.

Table S4. Single channel permeability of PAD dimers at 100 mOsm osmolarity gradient

Compound	CLR, %	Net permeability, $\mu m \cdot s^{-1}$	P_{SINGLE}, cm^3/s	P_{SINGLE}, molecules H_2O/s
PAD4	0.33	-1.49	-	-
	0.66	1.68	$2.19 \cdot 10^{-16}$	$7.29 \cdot 10^{6}$
	1.33	7.07	$4.62 \cdot 10^{-16}$	$1.54 \cdot 10^{7}$
	2.26	7.76	$3.01 \cdot 10^{-16}$	$1.01 \cdot 10^{7}$
	2.99	9.00	$2.66 \cdot 10^{-16}$	$8.88 \cdot 10^{6}$
PAD8	0.33	6.02	$1.56 \cdot 10^{-15}$	$5.21 \cdot 10^{7}$
	0.66	2.51	$3.27 \cdot 10^{-16}$	$1.09 \cdot 10^{7}$
	1.33	3.67	$2.40 \cdot 10^{-16}$	$8.00 \cdot 10^{6}$
	2.26	2.95	$1.15 \cdot 10^{-16}$	$3.83 \cdot 10^{6}$
	2.99	1.85	$5.46 \cdot 10^{-17}$	$1.82 \cdot 10^{6}$
PAD12	0.33	0.92	$2.38 \cdot 10^{-16}$	$7.95 \cdot 10^{6}$
	0.66	1.60	$2.09 \cdot 10^{-16}$	$6.96 \cdot 10^{6}$
	1.33	2.23	$1.46 \cdot 10^{-16}$	$4.86 \cdot 10^{6}$
	2.26	0.91	$3.53 \cdot 10^{-17}$	$1.18 \cdot 10^{6}$
	2.99	2.89	$8.54 \cdot 10^{-17}$	$2.85 \cdot 10^{6}$

Table S5. Single channel permeability of PAD dimers at 200 mOsm osmolarity gradient

Compound	CLR, %	Net permeability, $\mu m \cdot s^{-1}$	P_{SINGLE}, cm^3/s	P_{SINGLE}, molecules H_2O/s
PAD4	0.33	1.24	$3.22 \cdot 10^{-16}$	$1.08 \cdot 10^{7}$
	0.66	1.47	$1.91 \cdot 10^{-16}$	$6.38 \cdot 10^{6}$
	1.33	1.98	$1.30 \cdot 10^{-16}$	$4.32 \cdot 10^{6}$
	2.26	4.45	$1.73 \cdot 10^{-16}$	$5.76 \cdot 10^{6}$
	2.99	1.91	$5.65 \cdot 10^{-17}$	$1.89 \cdot 10^{6}$
PAD8	0.33	1.53	$3.96 \cdot 10^{-16}$	$1.32 \cdot 10^{7}$
	0.66	4.33	$5.65 \cdot 10^{-16}$	$1.88 \cdot 10^{7}$
	1.33	8.27	$5.41 \cdot 10^{-16}$	$1.80 \cdot 10^{7}$
	2.26	4.74	$1.84 \cdot 10^{-16}$	$6.13 \cdot 10^{6}$
	2.99	3.21	$9.48 \cdot 10^{-17}$	$3.16 \cdot 10^{6}$
PAD12	0.33	-2.05	-	-
	0.66	0.38	$4.90 \cdot 10^{-17}$	$1.63 \cdot 10^{6}$
	1.33	0.65	$4.24 \cdot 10^{-17}$	$1.42 \cdot 10^{6}$
	2.26	1.75	$6.78 \cdot 10^{-17}$	$2.26 \cdot 10^{6}$
	2.99	0.82	$2.43 \cdot 10^{-17}$	$8.12 \cdot 10^{5}$

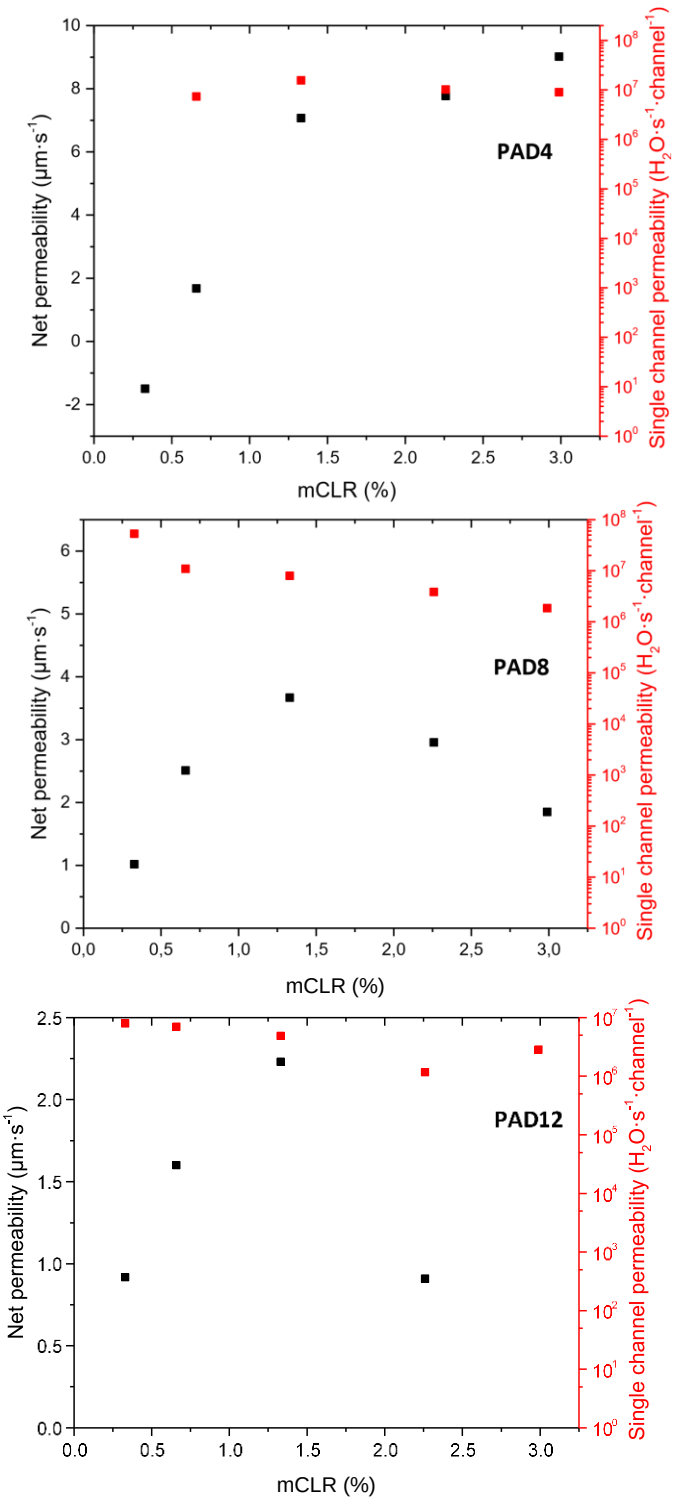

Figure S5. Net permeability versus Single channel permeability of **PAD4**, **PAD8**, **PAD12** channels at 100 mOsm osmolarity gradient

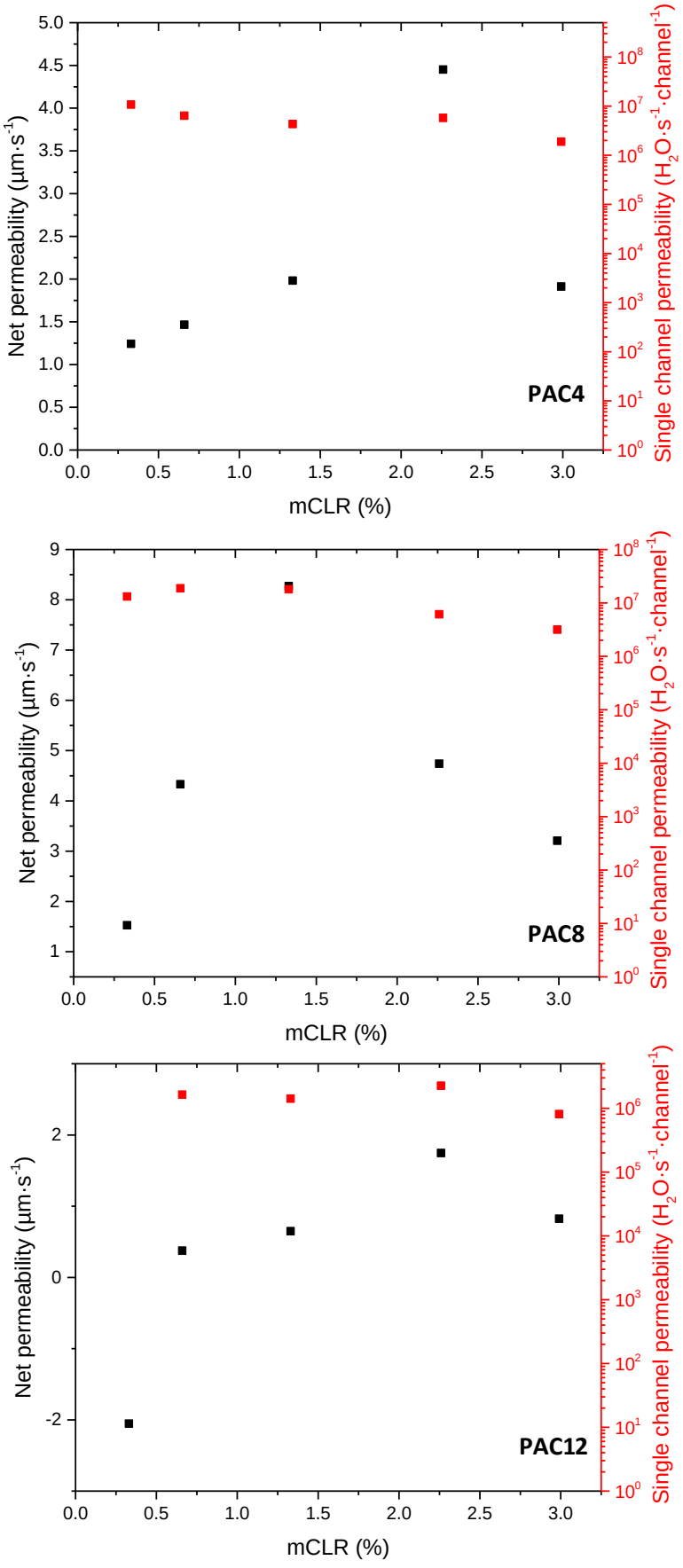

Figure S6. Net permeability and Single channel permeability of **PAD4**, **PAD8**, **PAD12** channels at 200 mOsm osmolarity gradient

LUV preparation for HPTS experiments: The large unilamellar vesicles (LUVs) were formed using egg yolk L-α-phosphatidylcholine (EYPC chloroform solution, 95%, 4 mL, 100 mg). To this solution was added 4 mL of MeOH and the solvent was slowly removed by evaporation under vacuum and dried overnight under high vacuum. The resulting thin film was hydrated with 2 mL of PBS buffer (10 mM sodium phosphate, pH 6.4, 100 mM NaCl) containing 10 μM HPTS (8-hydroxypyrene-1,3,6-trisulfonic acid trisodium salt). After hydrated for at least 30 minutes, the suspension was subject to 10 freeze-thaw cycles (liquid nitrogen and water at room temperature). The obtained white suspension was extruded 21 times through a 0.1 μm polycarbonate membrane in order to transform the large multilamellar liposome suspension (LMVs) into large unilamellar vesicles (LUVs) with an average diameter of 100 nm. The LUVs suspension was separated from extravesicular HPTS dye by using size exclusion chromatography (SEC, stationary phase Sephadex G-50, mobile phase: sodium phosphate buffer with 100 mM NaCl) and diluted with mobile phase to give 14 mL of 9.3 mM lipid stock solution (considering all the lipids have been incorporated).

HPTS assays for Ion Transport experiments: Here a fluorescent ratio data collection method was applied. 100 μL of stock vesicle solution was suspended in 1.85 mL of the corresponding buffer (10 mM sodium phosphate, pH 6.4, 100 mM of the analyzed cation KCl or NaCl) and placed into a quartz fluorimetric cell. The emission of HPTS at 510 nm was monitored at two excitation wavelengths (403 and 460 nm) simultaneously. An experiment involved two main events: injection of 20 μL of analysed sample (at 20 s after the start of experiment), then 29 μL of aqueous NaOH (0.5 M) (at 40 s) was added, resulting in a pH increase of about one unit in the extravesicular media. Finally, the vesicles were lysed with detergent (40 μL of 5% aqueous Triton X-100), in order to equilibrate the intravehicular and extravesicular solution.

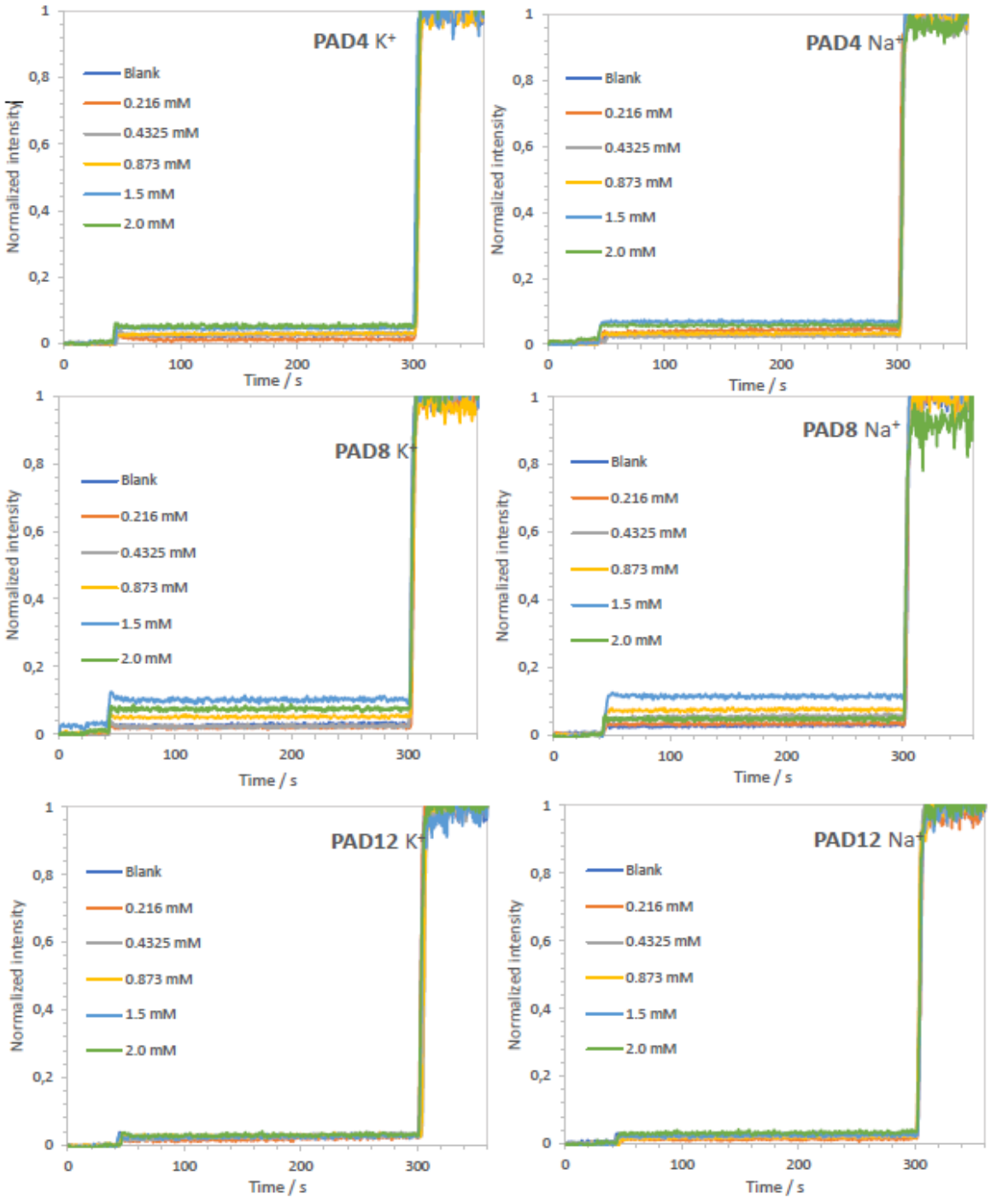

Figure S7. Normalized fluorescence intensity of HPTS as function of time associated with Na^+ and K^+ transport in the presence of **PAD4**, **PAD8**, **PAD12** channels.

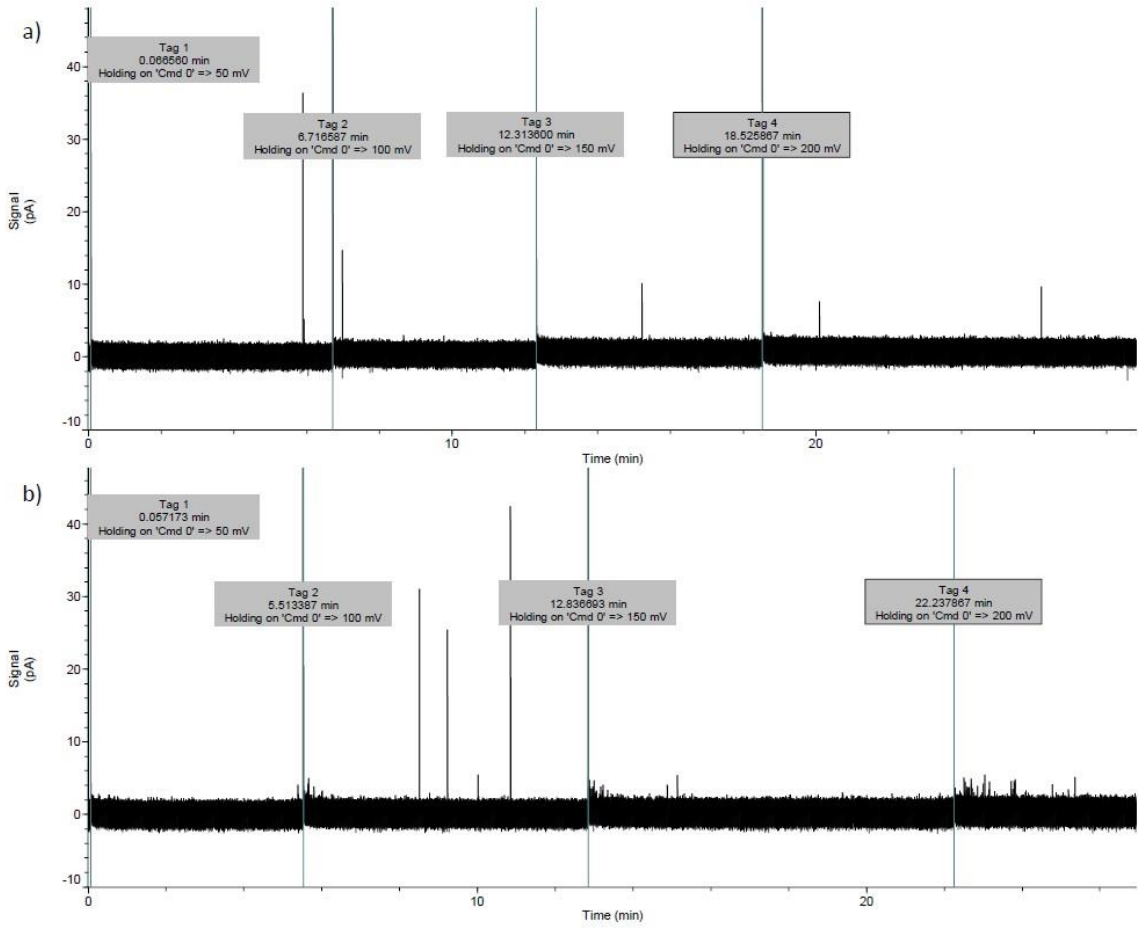

Figure S8. Single channel planar bilayer experiments. *Cis/trans* 1M KCl, diphytanoyl phosphatidylcholine (diPhyPC), a) 250 µM solution of **PAD4** in DMSO, b) 2.5 mM **PAD4** in THF, under applied potential in range of 50 - 200 mV.

MD simulations

All molecular dynamics simulations were performed under periodic boundary conditions with constant pressure. The CHARMM-36 force field [S2] was used for lipid molecules and the TIP3P model was chosen for water. To represent **PAD4** molecules and generate their topologies, we used the CHARMM General Force Field [S3] together with the ParamChem web service. [S4] The GROMACS 2019.4 software was used to run the simulations with all atoms, with an integration time step of 2fs. All bonds were constrained using the LINear Constraint Solver algorithm. Particle mesh Ewald electrostatics was used with a 12 Å cutoff with the Verlet buffer scheme for nonbonded interactions; the neighbor list was updated every 20 steps. Three baths (compounds, lipids, and water and ions) were coupled to a temperature of 310 K using the NoséHoover thermostat with a time constant t = 1 ps and a chain lengh of 4. Pressure in the x/y dimensions was scaled isotropically with Parrinello-Rahman barostat at 1 bar, and the z dimension was coupled independently to a reference pressure of 1 bar, t = 5.0 ps, and compressibility of 4.5 10^{-5} bar $^{-1}$. All systems were minimized for 5000 steps with a steepest descent algorithm and equilibrated for 3,5 ns, using decreasing position restraints of 1000, 400, 200, 100 and 40 kJ mol $^{-1}$ nm $^{-2}$ on heavy atoms, with the initial configuration as a reference. Production runs were finally computed for 500ns without any position restraints.

The molecular structures of dimers were extracted from X-ray single crystal structure data for **PAD4**. The initial configurations composed by seven dimers forming a hexagonal 2D packing were interactively assembled using the Unitymol software [S5] in virtual reality. The lipid composition is pure POPC and molecular ratio of compound to lipid was arbitrary set to mCLR=5 %, larger than the experimental value in order to limit the computational cost. All systems have been hydrated with a constant molar ratio of lipid : water equal to 28. Na^+ and Cl^- ions have been inserted using a Monte-Carlo scheme to neutralize the system and to obtain a concentration of solute equal to 0.15 M. All setups were assembled using the CHARMM-GUI web interface [S6] and format files were adapted to the Gromacs software using the online tool

services [S7].

The molecular dynamics trajectories were visually inspected and analysed using the VMD software [S8]. Analysis of the trajectories and permeation calculations were performed using custom scripts for the MDAnalysis library [S9, S10]. Fast computation and accuracy were accessed both using 0.1 ns as a sampling time for the analysis of water permeations.

References

S1. Fa, S.; Sakata, Y.; Akine, S.; Ogoshi, T. *Angew. Chem. Int. Ed.* **2020**, *59*, 9309–9313.

S2. Klauda JB, Venable RM, Freites JA, et al (2010) Update of the CHARMM All-Atom Additive Force Field for Lipids: Validation on Six Lipid Types. J Phys Chem B 114:7830–7843. https://doi.org/10.1021/jp101759q

S3. Vanommeslaeghe K, MacKerell AD (2012) Automation of the CHARMM General Force Field (CGenFF) I: Bond Perception and Atom Typing. J Chem Inf Model 52:3144–3154. https://doi.org/10.1021/ci300363c

S4 Vanommeslaeghe K, Raman EP, MacKerell AD (2012) Automation of the CHARMM General Force Field (CGenFF) II: Assignment of Bonded Parameters and Partial Atomic Charges. J Chem Inf Model 52:3155–3168. https://doi.org/10.1021/ci3003649

S5. Martinez X, Hardiagon A, Santuz H, et al (2020) Using Computer Simulations and Virtual Reality to Understand, Design and Optimize Artificial Water Channels. In: Piotto S, Concilio S, Sessa L, Rossi F (eds) Advances in Bionanomaterials II. Springer International Publishing, Cham, pp 78–99

S6. Jo S, Kim T, Iyer VG, Im W (2008) CHARMM-GUI: A web-based graphical user interface for CHARMM. J Comput Chem 29:1859–1865. https://doi.org/10.1002/jcc.20945

S7. Lee J, Cheng X, Swails JM, et al (2016) CHARMM-GUI Input Generator for NAMD, GROMACS, AMBER, OpenMM, and CHARMM/OpenMM Simulations Using the CHARMM36 Additive Force Field. J Chem Theory Comput 12:405–413. https://doi.org/10.1021/acs.jctc.5b00935

S8. Humphrey W, Dalke A, Schulten K (1996) VMD: Visual molecular dynamics. J Mol Graph 14:33–38. https://doi.org/10.1016/0263-7855(96)00018-5

S9. Gowers RJ, Linke M, Barnoud J, et al (2016) MDAnalysis: A Python Package for the Rapid Analysis of Molecular Dynamics Simulations. Proc 15th Python Sci Conf 98–105. https://doi.org/10.25080/Majora-629e541a-00e

S10. Michaud-Agrawal N, Denning EJ, Woolf TB, Beckstein O (2011) MDAnalysis: A toolkit for the analysis of molecular dynamics simulations. J Comput Chem 32:2319– 2327. https://doi.org/10.1002/jcc.21787.

Chapter III. Enhanced desalination polyamide membranes incorporating Pillar[5]arene via in-situ aggregation-interfacial polymerization-isAGRIP

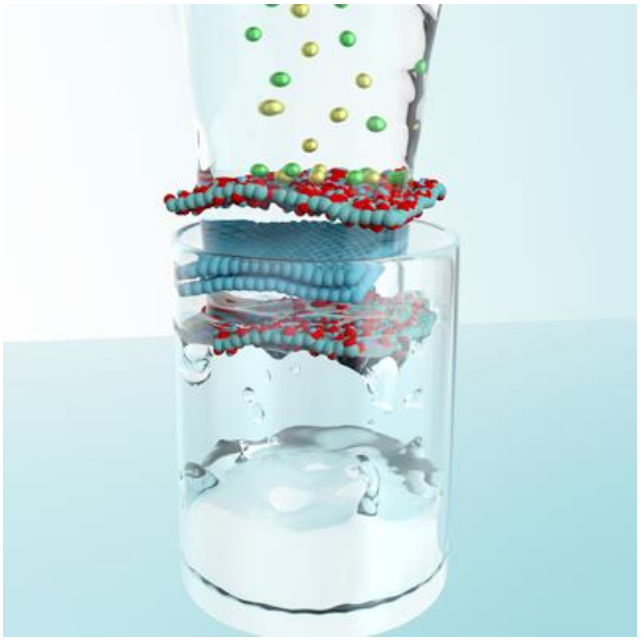

Contribution to Publication

The contribution of thePh.D. candidate to the manuscript “Enhanced desalination polyamide membranes incorporating Pillar[5]arene via in-situ aggregation-interfacial polymerization-isAGRIP” is related to the identification of empirical strategies toward the obtainment of the objective of the research project for which he performed most of the experimental work, including (i) membrane fabrication and optimization procedures, (ii) evaluation of optimal ratios for the casting solutions, (iii) observation of the nucleation process, (iv) elementary and nanostructural characterization of the bioinspired active layers (EDX, SEM, IR, XRD), and (v) BWRO filtration experiments.

Enhanced desalination polyamide membranes incorporating Pillar[5]arene via *in-situ* aggregation-interfacial polymerization-*is*AGRIP

Dmytro Strilets, Sophie CERNEAUX, Mihail Barboiu*

Institut Européen des Membranes, Adaptive Supramolecular Nanosystems Group,

University of Montpellier, ENSCM, CNRS, Place Eugène Bataillon, CC 047, F-34095,

Montpellier,

ORCID Mihail Barboiu: 0000-0003-0042-9483

Abstract

Membrane-based desalination has an important role in water purification. Inspired by highly performant biological proteins, artificial water channels (AWCs) have been proposed as active components to overcome the permeability/selectivity trade-off of desalination processes. Promising performances have been reported with Pillararene crystalline phases revealing impressive Å-scale separation performances, when used as selective porous materials. Herein, we demonstrate that self-assembled PA[5] AWCs are in-situ generated and macroscopically incorporated during the interfacial polymerization, within industrially relevant reverse osmosis polyamide-PA membranes. In particular, we explored the best combination between PA[5] aggregates and m-phenylenediamine (MPD) and trimesoylchloride (TMC) monomers to achieve their seamless incorporation in a defect-free hybrid PA[5]-PA membrane for enhanced desalination. The performances of the reference and hybrid membranes were evaluated by cross-flow filtration of brackish feed streams under real reverse osmosis conditions (15.5 bar of applied pressure) . The optimized membranes achieved a ~40 % improvement, with a water permeability of ~2.76±0.5 L $m^{-2} h^{-1} bar^{-1}$ and 99.5% NaCl rejection with respect to the reference TFC membrane and a similar water permeability compared to one of the best commercial BW30 membranes (3.0 L $m^{-2} h^{-1} bar^{-1}$ and 99.5% NaCl rejection).

Keywords: artificial water channels; self-assembly; pillararene; reverse osmosis; desalination

Water purification and desalination are important technologies to regulate the problems of freshwater scarcity.[1] Reverse osmosis (RO) membranes fabricated as supported polyamide-PA layers *via* interfacial polymerization-IP between diamine and acyl-chloride monomers (Figure 1), perform with exceptional performances in selective water desalination.[2] The effective transporting pathways dissolving and diffusing water *versus* ions with Å-scale selectivity are controlled by the PA layer structure and pores. It leads to a permeability-selectivity trade-off behaviour, reporting improved water permeability at the expense of lower selectivity, or vice-versa.[3,4] Numerous strategies have been tested to overcome the limitations of PA structure, including homogeneous fabrication *via* improved phase transfer of the monomers or *via* functional grafting on the PA. Efficient polymer spacing by the insertion of rigid molecular fillers,[5] or supramolecular macrocycles[6-9] and cages[10] were used to increase the free-volume of the composite membranes (Figure 1a) or porous polymeric powders.[11-15]

Filtration performances are controlled by the presence of defects at the boundaries between PA and nanoparticulate supramolecular fillers, limiting their selectivity to large molecular compounds (i.e. dyes, solvents, etc.). When fabricating a RO membrane for desalination, the inclusion of high density artificial water channels AWCs per unit area is directly impacting the membrane productivity and selectivity. The performance is related to important challenges in translating AWC self-assembly within PA matrix with the absence of defects. We postulated that one of the creative strategies for addressing such scale-up challenges and improving performances is the *in-situ* generation of aggregated AWCs colloidal soft particles that may be gently combined within the PA during the interfacial polymerization (IP) (Figure 1b). They generate multichannel continuous homogeneous architectures avoiding the formation of defects at the interfaces.[16]

Within this context, water/ions separation with Å-level selectivity is an important endeavor for desalination. Precise tuning of the pore size and distribution within PA matrix *via* nanoscale self-—assembly (Figure 1b) represent an alternative to the molecular grafting (Figure 1a) and an important premise to promote high selectivity control. We have previously shown

that self-assembled aggregated AWCs I-quartets [20-23] are active when embedded in PA, overcoming current RO-membrane limitations. [16]

Due to their unique functional design, the functionalized pillararenes with proven high-water permeability when embedded as unimolecular channels in lipid bilayers,[20-24] may inspire their incorporation as active artificial water channels in real desalination membranes. We know that permanent and uniform porosity of pillararene crystalline materials enable effective tunable fine molecular separations. [17-19] The crystal packing of PA[5] is revealing parallel sheets of self-assembled lamellar phases of tubular channels (Figure 2). The goal of the present study is to bridge the gap between unimolecular PA[5] channels and multichannel PA[5] solids, by introducing them with an optimal density distribution in functional polymeric layers, while retaining some of the desirable properties of porous PA[5] AWCs frameworks.

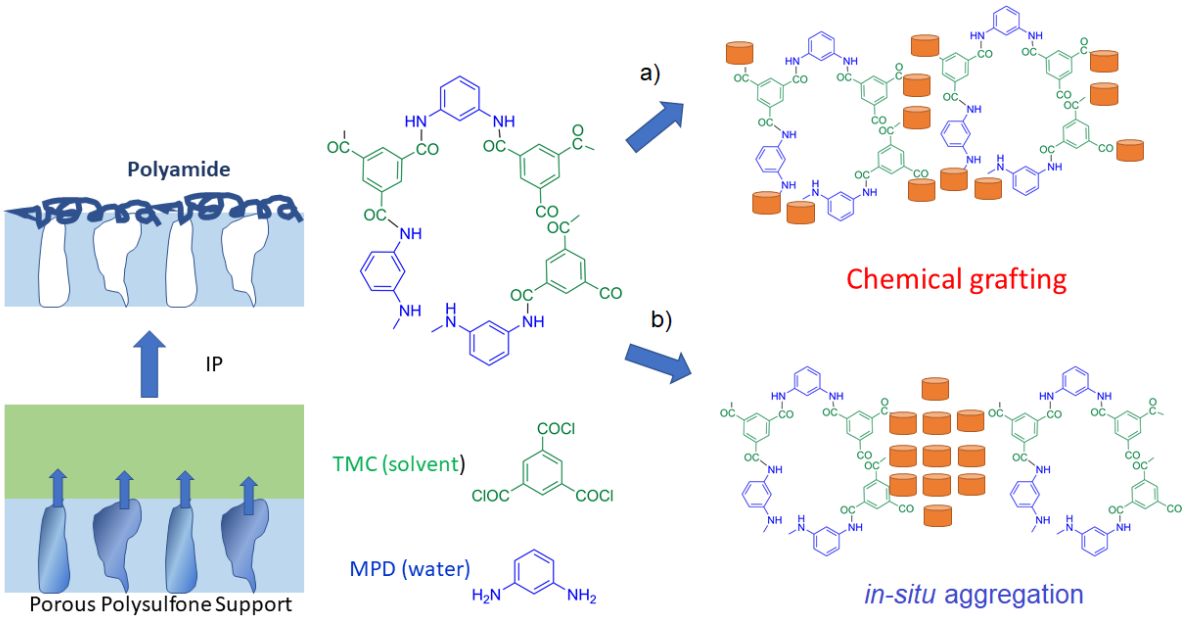

Figure 1. Interfacial polymerization (IP) between m-phenylene-diamine (MPD) and trimesoylchloride (TMC) monomers resulting in the formation of polyamide PA layers on the top of a polysulfone membrane support. Functional a) chemical grafting or b) *in-situ* supramolecular aggregation result in the formation of hybrid PA membrane materials.

In the present report, we describe an upscaling approach exploiting the self-assembled pillar[5]arene PA[5] channel aggregates, *in-situ* generated and embedded within PA layers during a streamlined IP procedure. The simple PA[5] platform has been chosen in order: a) to avoid complex synthetic steps used for the construction of its functionalized unimolecular

channel counterparts[25-28] and b) to take advantage of its self-assembly properties, generating H-bonded multichannel architectures in the solid state.[29-32] This work demonstrates the possibility to fabricate homogeneous hybrid PA[5]-PA thin-layer membranes of different morphologies and to tune their performances under real brackish water BWRO desalination filtration conditions. To increase the diversity, the synergistic self-assembly of various fabrication recipes with different compositions of PA[5] and former monomers is optimized to fabricate hybrid PA membranes *via in-situ* aggregation-interfacial polymerization *is*AGRIP method. The technological novelty here is related to the use of pre-aggregated PA[5] colloidal nanoparticles with nascent PA formation during the IP. It is resulting in a gentle defect-free incorporation of colloidal soft superstructures of PA[5] within PA host-matrix, going beyond those observed for solid nanoparticle (zeolite, ZIF8, graphene, etc.) incorporation in other literature reports.

Fabrication of hybrid PA[5]-PA membranes. The easy accessible pillar[5]arenes PA[5] discovered by Ogoshi et al. play an important role in supramolecular chemistry.[17-19] Hou et al. firstly discovered that the unique hollow pillar-shape cavities with fine-tuneable rims, could be used to construct artificial water channels.[24-28] They are positioning the PA as a scaffolding relay in the middle, whereas functional arms attached to aromatic rings form unimolecular pillared channels *via* self-assembly. Nonetheless, non-modified pillar[n]arenes could form low-dense, solid-state self-assembled structures via strong O-H···O, C-H···O, C-H···π, π···π interactions.[29-32] Pillar[5]arene-based supramolecular organic framework (PA[5]-SOF) shows great performance in CO_2/H_2 gas separation due to high porosity with Å-scale pore size and specific H-bonding between gas molecules and pillar[5]arene. Thus, those advantages of Ppillar[5]arene can be applicable for developing highly permeable and selective TFC membranes for water desalination.

The reference TFC membranes were prepared by interfacial polymerization (IP) of m-phenylenediamine (MPD) and trimesoyl chloride (TMC), resulting in the formation of polyamide (PA) layers onto a commercial polysulfone (PSf) support layer.

Table 1. Concentrations of PA[5] and MPD in the aqueous phase and TMC in the organic phase for the preparation of different membranes by interfacial polymerization.

MEMBRANE	PA[5]	MPD	TMC
	w/w %	w/w	w/w %
Control TFC H[a]	-	1.5	0.15
H-0.1	0.1	1.5	0.15
H-0.3	0.3	1.5	0.15
H-0.5	0.5	1.5	0.15
Control TFC L	-	1.2	0.1
L-0.01	0.01	1.2	0.1
L-0.025	0.025	1.2	0.1
L-0.05	0.05	1.2	0.1
L-0.1	0.1	1.2	0.1

[a] "H" and "L" stands for high and low PA[5], MPD and TMC concentrations

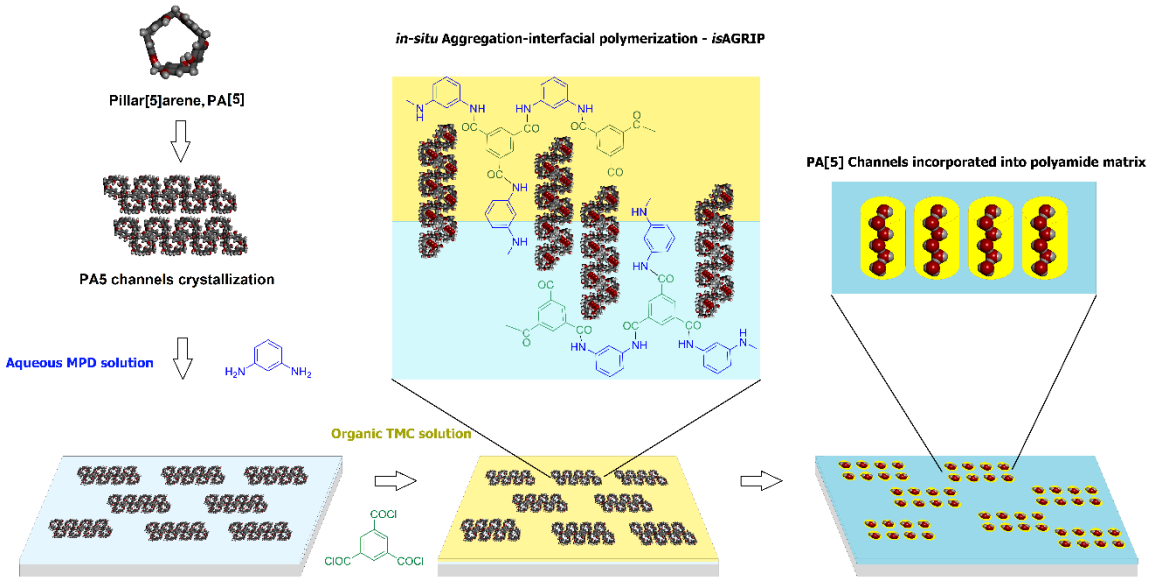

Figure 2. X-ray single-crystal structure and crystalline packing of PA[5].[29-32] Synthetic procedure for the hybrid PA/AWC membrane preparation: impregnation of PSf support with an ethanolic aqueous solution of PA[5], followed by IP with an aqueous MPD solution and with a hexane solution of TMC, resulting in the formation of hybrid PA[5]-PA layers *via in-situ* aggregation-interfacial polymerization-*is*AGRIP.

In this study, hybrid PA[5]-PA membranes have been prepared *via* the conventional IP procedure, preceded by the *in-situ* aggregation of self-assembled colloidal nanoparticles of PA[5] in ethanol/water solutions. Colloidal aggregates of D_h = 500 nm were observed at t= 0 h by dynamic light scattering (DLS) when variable amounts of water were added to ethanolic solutions of 0.3%-0.7% PA[5], resulting in the formation of clear solutions without any visible

precipitation. Then DLS analysis shows that higher aggregates (D_h =800-2500 nm) were obtained in time (t = 1-12 h) at low volume fraction of water, while smaller aggregates (D_h =200 nm) were constantly obtained for increasing amounts of water (Figure S1). It results in the formation of variable colloidal particles at different water contents, reminiscent of important H-bonding interactions between colloidal PA[5] aggregates at low water content, which are reduced in the presence of increasing amounts of water molecules. Solid particles of porous PA[5] may be further generated *via* dilution of these solutions with water, which is the most probable situation when a solution of MPD is added. Regarding the IP procedure, ethanolic aqueous solutions of PA[5] (EtOH:H_2O = 1:2 by weight) was thoroughly sonicated before being poured onto the PSf support and allowed to sit for 60 s to induce a partial evaporation of solutions, without the formation of solid crystallites at the surface of the membrane. Based on this information, high and low PA[5] or MPD/TMC concentrations were investigated to explore the effect of the composition on the resulting PA[5]-PA membrane layers (Table 1).

The PSf support containing the PA[5] colloidal solution was first immersed for 2 min in an aqueous solution at 1.5 w/w % (H) or 1.2 w/w% (L) of MPD. Then, the excess of solution was removed from the surface with an air gun. Finaly, the PA[5]-MPD-saturated support was immersed into a 0.15% w/w (H) or 0.10% w/w (L) TMC solution for 1 min to form the PA layer. In this step, the PA[5] colloidal aggregates migrate together with the MPD to the organic phase, favoring the IP reactions, while they synergistically might interact with the growing PA segments *via* H-bonding. The results of the *in-situ* crystallization process in the formation of homogeneous cross-linked PA[5]-PA regions of highly interpenetrated networks of PA[5] and PA hybrid components. Following the IP procedure, both the control and the hybrid membranes were cured in DI water at 95 °C for 2 min, dipped in a 200 ppm NaOCl aqueous solution for 2 min, and then dipped in a 1000 ppm $Na_2S_2O_5$ aqueous solution for 30 s. The membranes were finally rinsed and stored in DI water at 4 °C before testing.

Morphological / structural characterization of the hybrid membranes. The formation of the hybrid PA[5]-PA layers was confirmed by Fourier Transform Infrared FTIR spectroscopy

(Figures S2-S3). Vibration bands at 1504 cm^{-1} (amide-II, N–H in-plane bending) and 1656 cm^{-1} (amide-I, C=O stretching vibration) are associated with amide bonds of the PA. Evidence of PA[5] incorporation within hybrid PA is obtained from the presence of the vibration shifts at 1650-1700 cm^{-1} assigned to the C=C stretching of aromatic groups, as well as the $-CH_{2,as}$ and $-CH_{2,sym}$ stretches visible in the range 2850 and 2965 cm^{-1}, respectively. The large band in the range of 3700-3200 cm^{-1} with the peak at 3325 cm^{-1} is attributed to the O-H stretching vibration of strongly self-H-bonded within PA[5] crystals or H-bonded to water molecules present in the PA[5]-PA.

The elemental analysis obtained from Energy dispersive X-ray spectroscopy (EDX) analysis of hybrid membranes prepared with 0.025 % and 0.050 % PA[5] has been compared to the control TFC membranes presenting a content of C of 84 w %, N of 1.2 w % and O of 12 w %. For the hybrid PA[5]-PA layers the content of C of 86-87 w % was significantly higher, while the contents of N of 0.54 w % and Oof 10 w %, were significantly lower (Table S1). This result is expected because the C% of PA[5] is significantly high, providing evidence of its incorporation in PA[5]-PA layers of hybrid membranes.

The Scanning Electronic Microscopy-SEM micrographs (Figures S3-S12) suggest that all the hybrid PA[5]-PA layers are continuous and defect-free, consistent with the high salt rejections observed in the filtration tests described below. The nanostructure and micro-morphology of the layer are strongly dependent on the density and distribution of PA[5] crystals within the PA matrix, that can be modified by increasing the PA[5] amount deposited at the surface of the membrane before the IP procedure. In general, with an increasing content of PA[5], the top polyamide surface evolved from a typical “ridge-and-valley” morphology typical of the reference conventional PA layers in the reference TFC membrane, to a multilayer large voids structures with apparently lower density in PA[5]-PA hybrid membranes (Figure 3). The overall effect of the presence of increased PA[5] amounts during IP process, is related to an increased diffusion of the PA[5] into the organic phase, resulting in the formation of PA[5]-PA hybrid layers with a higher cross-linking degree.

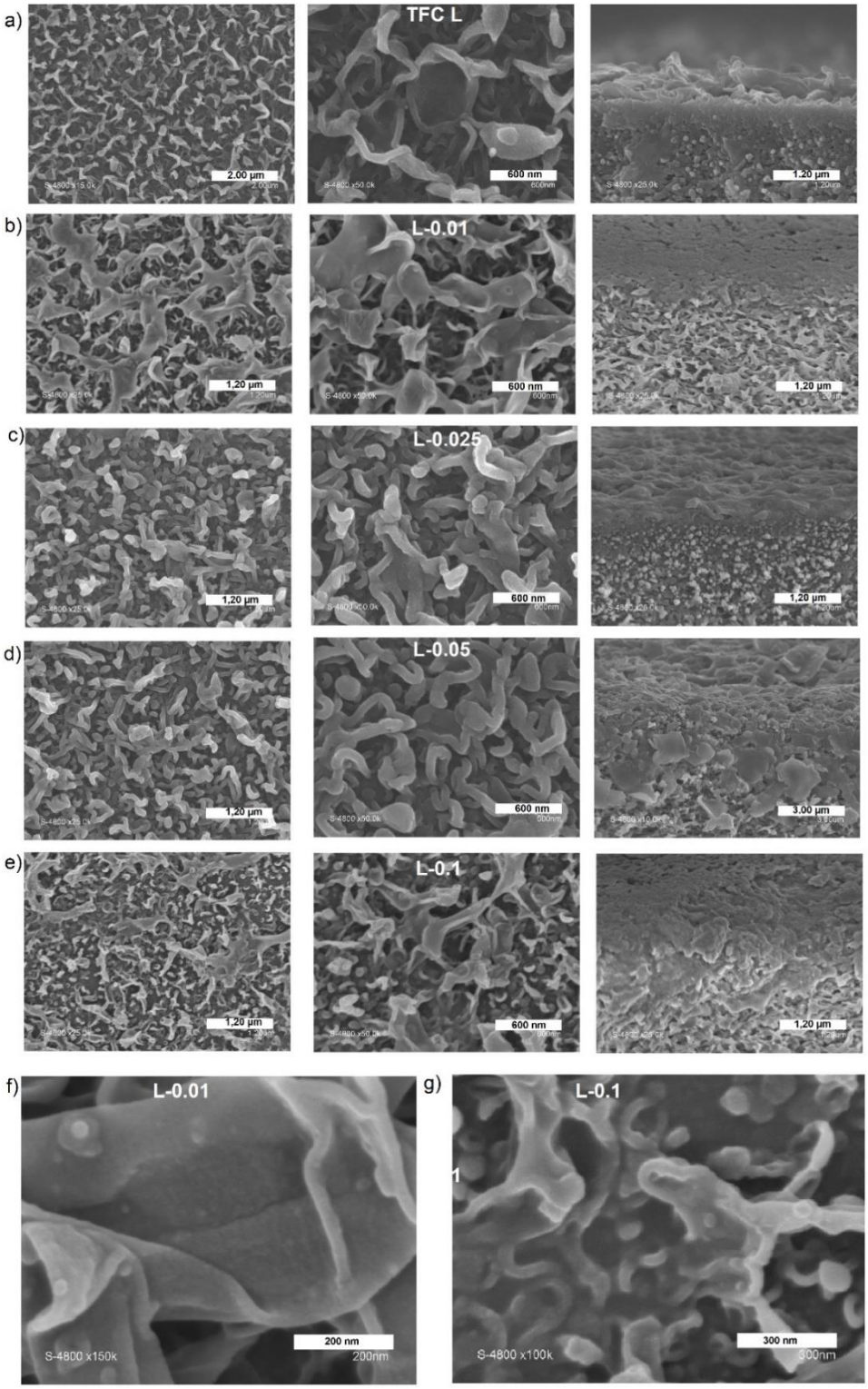

Figure 3. Representative surface SEM micrographs of (a) reference TFC; (b) 0.01 w/w % (c) 0.025 w/w % (d) 0.05 % w/w and (e) 0.1 % w/w PA[5] PA[5]-PA hybrid layers. High magnification details of (f) 0.01 w/w % and (g) 0.01 w/w % PA[5]-PA hybrids. MPD and TMC concentrations in the casting solutions were 1.2 w/w % and 0.1 w/w %, respectively.

In addition to a change of the surface roughness, the hybrid PA[5]-PA membranes with medium PA[5] loads (0.025 -0.05 % w/w) displayed a distinct, denser and more homogeneous nanoparticulate structure than the one observed for lower (0.01 % w/w) or higher (0.10 % w/w) PA[5] loads for which the morphology of the multilayers start to be inhomogeneous.

Importantly, all the layers prepared in the presence of PA[5] show a diffuse distribution of crystalline nanoparticles that are embedded with different densities within the whole active PA layer (Figure 3 f andg). Comparison of reference membrane surfaces prepared using 2 different application methods for PA[5] shows that membranes prepared using water-ethanol solution of MPD presents a more developed surface with smaller leaf-like formations (Figures S4 and S14), which could be explained by an improvement of the amine monomer diffusion in presence of ethanol. Moreover, membranes prepared with water-ethanol solution of PA[5] (0.5 w/w %) and MPD (1.2 w/w %) have a more inhomogeneous morphology compared to membranes prepared by sequential application of PA[5] and MPD (Figures S14-18). The best productivity and selectivity in experimental brackish water reverse osmosis tests were obtained for the hybrid layers with medium PA[5] contents. The dimensions of embedded nanoparticles as well as their distribution density, appeared to increase as expected, with increasing the PA[5] loads. Oppositely to homogeneous low content PA[5]% layers, bigger nanoparticles can be observed in a multi-layer structure of hybrid membrane prepared with high content of PA[5], while the micro-structure becomes more heterogeneous.

Performances of the membranes in BWRO filtration. The filtration performances (i.e., water permeability, water flux and NaCl rejection of saline solution) of reference and hybrid membranes prepared by varying the PA[5] loading from 0% (control TFC) to 0.1 % w/w (Series L) and then from 0.1 % to 0.5% (Series H), were measured for brackish water reverse osmosis (BWRO) desalination.[33] The MPD concentration in aqueous solution controls its diffusion into the organic phase and influences the self-assembly of PA[5] via H-bonding. For a series of high concentration membranes (Series H, 1.5 % w/w MPD and 0.15 % w/w TMC), increasing the PA[5] loading from 0.1 % w/w to 0.5% w/w led to a progressive lower water permeability (from 1.5 to 0.9 L m^{-2} h^{-1} bar^{-1}). This also impacts negatively the salt fluxes (decreasing from 24 to 14 L m^{-2} h^{-1}) and salt rejections (from 99% to 91%) with respect to the control TFC membrane. These results are rationalized with the high concentration of MPD and TMC and the high loading content of PA[5], which results in the formation of highly cross-linked hybrids

PA[5]– PA with respect to the control TFC membrane and the formation of defects at high PA[5] loading (Figure S20 and Table S2). In order to reduce the unfavourable cross-linking effects, lower concentrations of 1.2 % w/w MPD and 0.1 % w/w TMC, together with lower loadings of PA[5] from 0.01 to 0.1% w/w% were further used. Under the BWRO conditions, the water permeability increased significantly and reached a peak at ~2.76 L $m^{-2}h^{-1}bar^{-1}$ for the PA[5] concentration of 0.025% w/w, while maintaining higher observed NaCl rejection of 99.4 % (Figure 4 and Table S3). This result represents an exceptional ~40 % increase in water permeability at equivalent rejection, with respect to the reference TFC membrane and a similar water permeability compared to one of the best commercial BW30 membrane (permeability of ~3.0 L $m^{-2}h^{-1}bar^{-1}$ and 99.5% NaCl rejection). The filtration performances are lower for higher concentrations 0.05 and 0.1 % w/w of PA[5], confirming SEM observations that multilayer active structures are highly cross linked.

We noted that the membrane performances dropped rapidly by using high concentrations of PA[5] leading to high aggregation of PA[5] within the hybrid layers, that clearly shows that final layer morphology and transport performances are strongly correlated. Further experiments aimed at investigating the method of PA[5] implantation into a polyamide matrix by dissolving PA[5] in ethanol/water solution of MPD or adding PA[5] after soaking in the membrane with MPD solution. Both experiments led to a ~30-40 % decrease in water permeability and lower salt rejection (Table S4). The data suggest that an optimal PA[5] loading of 0.025 % w/w is needed to generate its optimal aggregation that can construct a homogeneous hybrid PA[5] – PA matrix and at the same time prevent the formation of defects in the selective layer. Also, it is a clear that adding the PA[5] dissolved in aqueous solution is not optimal since it results in the formation of molecularly dispersed and highly cross-linked materials with lower performances with respect to the reference TFC membrane.

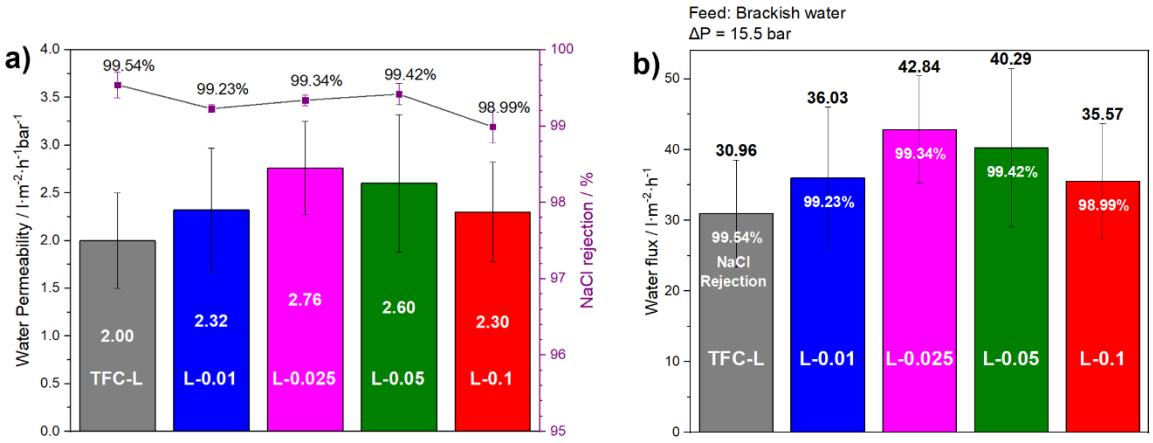

Figure 4. BWRO desalination performances at 15.5 bar with a 2000 ppm NaCl as feed solution: a) water permeability, b) flux of the saline solution and salt rejection for reference TFC and PA[5]-PA membranes prepared with 0.01 %, 0.025%, 0;05% and 0,01% w/w PA[5] solutions; MPD and TMC concentrations in the casting solutions were 1.2 w/w % and 0.1 w/w %, respectively.

The present study confirms that *in-situ* aggregation-interfacial polymerization-*is*AGRIP mechanistic strategy allows the homogeneous incorporation of PA[5] artificial water channels starting from their *in-situ* colloidal self-assembled superstructures. The formation of the hybrid PA[5]-PA layers may be further generated *via* the interaction of the PA[5] aggregates with nascent PA oligomers *via* H-bonding. It is leading to the formation of nanoparticles for which the distribution within hybrid PA[5] – PA is strongly depending on the PA[5] content. Under optimal conditions, they promote the synergistic incorporation of colloidal soft aggregates of PA[5] during the PA formation, whereby preventing the formation of defects, that is mostly observed when solid state nanoparticles are directly incorporated within PA.[16] A significant loss in the performances was observed for the membranes fabricated with too low or too high PA[5] loadings. Membranes fabricated using complex solution of PA[5] and MPD, resulted in the formation of homogeneous grafting of non-aggregated PA[5] molecules, exhibiting thus a low permeability. The pre-formation of PA[5] colloidal aggregates at the surface of the membrane led to distributed nanostructures into the PA layer. Such membranes provided the best performances in terms of water transport and selectivity, and the porous structure did not affect the mechanical resistance or the membrane properties under RO filtration. It can be concluded that the improved transport performances arise from a combination of higher porosity of the pre-organized PA[5] with less cross-linked PA-layer. However, overly high

loadings of PA[5], bigger nanoaggregates led to the formation of highly crosslinked PA and to defects, resulting in poorest performances. The PA[5] concentration had an important effect during membrane fabrication and performant hybrid layers were synthetized by adjusting this parameter to an optimal PA[5] concentration of 0.025 %w/w. In particular, the membranes provided a ~40 % increase in water permeability with an excellent productivity of 50 L $m^{-2}h^{-1}$ under 17.5 bar applied pressure, while maintaining a high selectivity of 99.4 %.

Ultimately, we demonstrated that *in-situ* aggregation-interfacial polymerization-*is*AGRIP previously used to fabricate bioinspired membranes incorporating I-quartet AWCs[16] owns its enormous potential by using hydrophobic PA[5] superstructures, that can be incorporated in homogeneous hybrid polyamides to target continuous flow applications by improving real reverse osmosis materials

Acknowledgements. This work was supported by Agence Nationale de la Recherche ANR-18-CE06-0004-02, WATERCHANNELS**.**

References

1. J. Imbrogno, G. Belfort, *Annu. Rev. Chem. Biomol. Eng.* **2016**, *7*, 29–64.

2. a) A. G. Fane, R. Wang, M. X. Hu, *Angew. Chem. Int. Ed.* **2015**, *54*, 3368–3386; b) W. J. Lau, S. Gray, T. Matsuura, D. Emadzadeh, J. P. Chen, A. F. Ismail, *Water Res.* **2015**, *80*, 306–324.

3. a) I. Kocsis, Z. Sun, Y. M. Legrand, M. Barboiu, *npj Clean Water* **2018**, *1*, 13; b) M. Barboiu A. Gilles, *Acc. Chem. Res.* **2013**, *46*, 2814–2823.

4. Z. Yang, H. Guo, C. Y. Tang, *J. Memb. Sci.* 2019, *590*.

5. M. F. Jimenez-Solomon, Q. Song, K. E. Jelfs, M. Munoz-Ibanez, A. G. Livingston, *Nature Mater.* **2016**, *15*, 760–767.

6. L. F. Villalobos, T. Huang, K.-V. Peinemann, *Adv. Mater.* **2017**, *29*, 1606641

7. T. Huang T. Puspasari, S. P. Nunes, K. V. Peinemann, *Adv. Funct. Mater.* **2020**, *30*, 1906797.

8 T. Huang, B. A. Moosa, P. Hoang, J. Liu, S. Chisca, G. Zhang, M. Al Yami, N. M. Khashab, S. P. Nunes, *Nature Commun.* **2020**, *11*, 5882.

9. J. Liu, D. Hua, Y. Zhang, S. Japip, T.-S Chung, *Adv. Mater.* **2018**, *30*, 1705933.

10. G. Liu, X. Zhang, Y.D. Yuan, H. Yuan, N. Li, Y. Ying, S.B. Peh, Y. Wang, Y. Cheng, Y. Cai, Z. Gu, H. Cai, D. Zhao, *ACS Materials Lett.* **2021**, *3*, 268-274.

11. A. Alsbaiee, B. J. Smith, L. Xiao, Y. Ling, D. E. Helbling, W. R. Dichtel, *Nature* **2016**, *529*, 190-194.

12. T. Huang, G. Sheng, P. Manchanda, A. H. Emwas, Z. Lai, S. P. Nunes, K.-V. Peinemann, *Sci. Adv.* **2019**, *5*, eaax6976.

13. S Abubakar, T. Skorjanc, D. Shetty, A. Trablosi, *ACS Appl. Mater. Interfaces* **2021**, *13*, 14802–14815.

14. X. Wang, L. Xie, K. Lin, W. Ma, T. Zhao, X. Ji, M. Alyami, N. M. Khashab, H. Wang, J. L. Sessler, *Angew. Chem. Int. Ed.* **2021**, *133*, 7264−7272.

15. B. B. Shi, H. X. Guan, L. Q. Shangguan, H. Wang, D. Y. Xia, X. Q. Kong, F. H. Huang, *J. Mater. Chem. A* **2017**, *5*, 24217−24222.

16. M. Di Vincenzo, A. Tiraferri, V.-E. Musteata, S.Chisca, R.Sougrat, L.-B. Huang, S. P. Nunes, M. Barboiu, *Nature Nanotechnol.* **2021**, *16*, 190-196.

17. T. Ogoshi, K. Saito, R. Sueto, R. Kojima, Y. Hamada, S. Akine, A. M. P. Moeljadi, H. Hirao, T. Kakuta, T. Yamagishi, *Angew. Chem. Int. Ed.* **2018**, *57*, 1592-1595.

18. T.Ogoshi, T. Kakuta; T. Yamagishi *Angew. Chem. Int. Ed.* **2019**, *58*, 2197-2206

19. T. Ogoshi, R. Sueto, M.Yagyu, R. Kojima, T. Kakuta, T. Yamagishi, K. Doitomi, A. K.Tummanapelli, H. Hirao, Y. Sakata, S. Akine, M. Mizuno, *Nature Commun*. **2019**, *10*, 479.

20. M. Barboiu and A. Gilles, *Acc. Chem. Res.*, **2013**, *46*, 2814–2823.

21. M. Barboiu, *Chem. Commun.* **2016**, *52*, 5657-5665.

22. E. Licsandru, I. Kocsis, Y. X. Shen, S. Murail, Y. M. Legrand, A. van der Lee, D. Tsai, M. Baaden, M. Kumar, M. Barboiu, *J. Am. Chem. Soc.* **2016**, *138*, 5403-5409.

23. I. Kocsis, M. Sorci, H. Vanselous, S. Murail, S. E. Sanders, E. Licsandru, Y. M. Legrand, A. Van der Lee, M. Baaden, P. B. Petersen, et al., *Sci. Adv.* **2018**, *4*, eaao5603.

24. X. B. Hu, Z. Chen, G. Tang, J. L. Hou, Z. T. Li, *J. Am. Chem. Soc.* **2012**, *134*, 8384–8387.

25. a) W. Si, P. Xin, Z. T. Li, J. L. Hou, *Acc. Chem. Res.* **2015**, *48*, 1612-1619.

26. W. Si, L. Chen, X.-B. Hu, G. Tang, Z. Chen, J.-L. Hou, Z.-T. Li, *Angew. Chem. Int. Ed.* **2011**, *50*, 12564-12568.

27. L. Chen, W. Si, L. Zhang, G. Tang, Z. T. Li, J. L. Hou, *J. Am. Chem. Soc.* **2013**, *135*, 2152-2155.

28. Z.-J. Yan, D. D. Wang, Z.J. Ye, T. Fan, G. Wu, L. Y. Deng, L. Yang, B. X. Li, J. W. Liu, T.H. Ma, C.Q. Dong, Z.-T. Li, L.H. Xiao, Y.F. Wang, W.N. Wang, and J.-L. Hou, *J. Am. Chem. Soc.* **2020**, *142*,15638-15643

29. L. L. Tan, H. Li, Y. Tao, S. X. A. Zhang, B. Wang, and Y. W. Yang, *Adv. Mat.* **2014** *26(41)*, 7027-7031

30. L. L. Tan, Y. Zhu, H. Long, Y. Jin, W. Zhang, and Y. W. Yang *Chem. Comm.* **2017** *53(48)*, 6409-6412.

31. L. L. Tan, Y. Zhu, Y. Jin, W. Zhang, and Y. W. Yang *Supramolecular Chemistry* **2018**, *30(7)*, 648-654.

32. T. Ogoshi, T. Aoki, K. Kitajima, S. Fujinami, T.-a. Yamagishi, Y. Nakamoto, *J. Org. Chem.* **2011**, *76*, 328–331

33. H. Yan, X. Miao, J. Xu, G. Pan, Y. Zhang, Y. Shi, M. Guo, Y. Liu, *J. Memb. Sci.* **2015**, *475*, 504–510;

34. S. Hermans, R. Bernstein, A. Volodin, I. F. J. Vankelecom, *React. Funct. Polym.* **2015**, *86*, 199–208.

Graphical Abstract

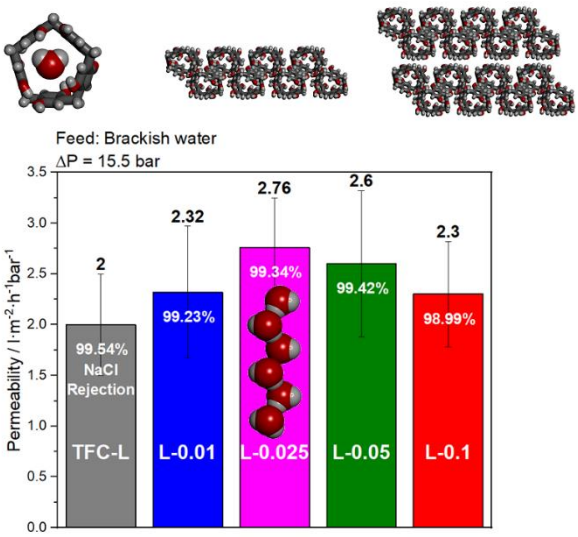

Supporting Information for

Enhanced desalination polyamide membranes incorporating Pillar[5]arene via *in-situ* aggregation-interfacial polymerization-*is*AGRIP

Dmytro Strilets, Sophie CERNEAUX, Mihail Barboiu*

Institut Européen des Membranes, Adaptive Supramolecular Nanosystems Group,

University of Montpellier, ENSCM, CNRS, Place Eugène Bataillon, CC 047, F-34095,

Montpellier,

ORCID Mihail Barboiu: 0000-0003-0042-9483

Chemicals. Commercial flat-sheet polysulfone (PSf) ultrafiltration membranes, PS35-GPP (Solecta, USA), were used as support layers for the fabrication of all the polyamide-based membranes. Trimesoyl chloride (TMC, 98%), m-phenylenediamine (MPD, flakes 99%), sodium chloride (NaCl) (≥99.5%), sodium metabisulfite ($Na_2S_2O_5$, 98%), were purchased from Sigma-Aldrich, France. Pillar[5]arene has been synthesized as previously reported.[29] All solvents used in this study were HPLC grade. Unless specified, all chemicals were dissolved in DI water obtained from a Milli-Q ultrapure water purification system (Millipore, France). All the reagents and solvents were used without any further purification.

Fabrication of Reference polyamide-based membranes (TFC): Reference polyamide active layers were cast on top of the commercial PSf ultrafiltration support. The support was taped onto a stainless-steel plate to leave only the topmost surface available for reaction and then contacting them with ethanol/water solution with ratio 1:2 (by volume). It was then placed in an amine aqueous solution (MPD: 1.2 w/w %) for 120 s. An air gun was used to remove the excess solution from the membrane surface. The membrane was then immersed in a hexane solution of TMC (0.1 w/w %) for 60 s. During this step, the ultrathin polyamide layer was formed. The composite membrane was then cured in DI water at 95 °C for 120 s, rinsed with a 200 ppm NaOCl aqueous solution for 120 s, followed by soaking in a 1000 ppm $Na_2S_2O_5$ aqueous solution for 30 s and a final wet curing step at 95 °C for 120 s in DI water. The TFC membranes were stored in DI water at 4 °C until their use.

Fabrication of the polyamide-based membranes incorporating pillar[5]arene (PA5).

We used 3 methods of PA[5] incorporation into the PA membrane during the interfacial polymerization:

1. A certain amount of pillar[5]arene was dissolved in ethanol followed by the addition of ultrapure water and ultrasonication to obtain 1:2 ethanol/water homogeneous solution with PA5 concentrations 0.01%, 0.025%, 0.05% and 0.1% (w/w). Further, PA5 solution was sprayed on PSf ultrafiltration support fixed on a stainless-steel plate. The following steps were done in the same way as it was for the reference TFC membrane including soaking in the MPD solution (1.2 w/w % in water), IP reaction in TMC solution and 2-step curing in the hot water.

2. Pillar[5]arene PA[5] was also incorporated as dissolved in the aqueous MPD/PA5 solution: the support was taped onto a stainless-steel plate to leave only the topmost surface available for reaction.

The fixed PSf support was soaked in the ethanol/water solution (MPD: 1.2 w/w %; PA5: 0.5 w/w %) and excess of solution was removed after 120 s by using an airgun. Interfacial

polymerization reaction and 2 steps curing in the hot water were applied as well as it was done for the reference polyamide-based membranes.

3. PA5 deposition have been applied after soaking in MPD solution: the support was taped onto a stainless-steel plate to leave only the topmost surface available for reaction. It was then placed in an amine aqueous solution (MPD: 1.2 w/w %) for 120 s. An airgun was used to remove the excess of MPD solution from the membrane surface. Fixed PSf support was contacted with PA5 ethanol/water solution with ratio 1:2 (by volume) for 15 s and the excess was removed with the airgun. The following steps of polyamide IF polymerization and curing procedure were done in the same way as for the reference polyamide-based membranes.

Membrane morphological and physio-chemical characterization.

Dynamic light scattering (DLS) measurements were performed using a Malvern Zetasizer with a 173° backscatter measurement angle and a quartz cuvette with a square aperture. The samples were prepared by dissolving the PA[5] in ethanol to achieve 0.3%, 0.5 % and 0.7% w/w. In order to investigate the formation of colloidal aggregates, different amounts of water were added to the PA[5]/ethanol solution under various conditions.

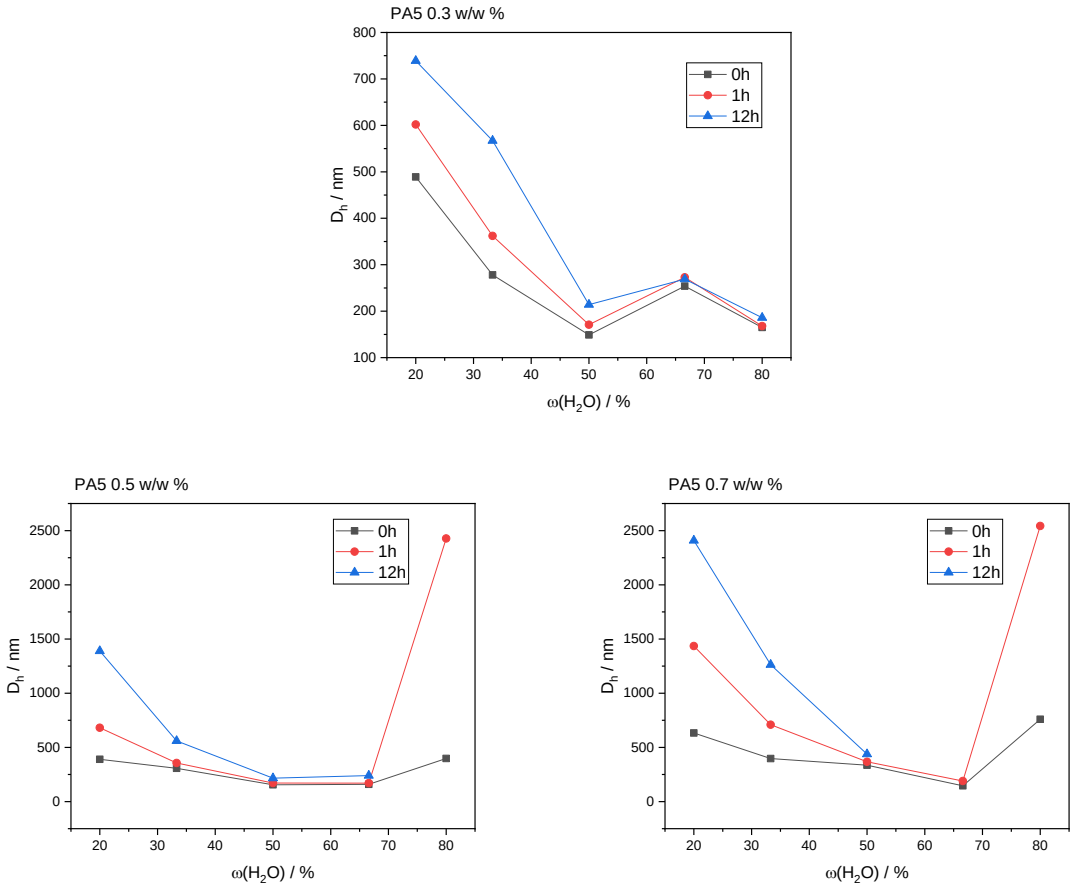

Figure S1. The size distribution of colloidal aggregates obtained by DLS measurements. The size distribution of hydrodynamic diameter (D_h) at t=0h, 1h and 12h after the addition under sonication of variable amounts of pure water to a) 0.3%, b) 0.5 % and c) 0.7% w/w PA[5] solution in 0.8 mL ethanol.

FTIR-ATR spectroscopy

ATR-FTIR spectra were recorded on a NEXUS spectrometer. The ATR accessory contained a monolithic diamond crystal at a nominal angle of incidence of 45°, yielding about 1 internal reflection at the sample surface. All spectra were recorded at 25 °C in the region 625 – 4000 cm^{-1}.

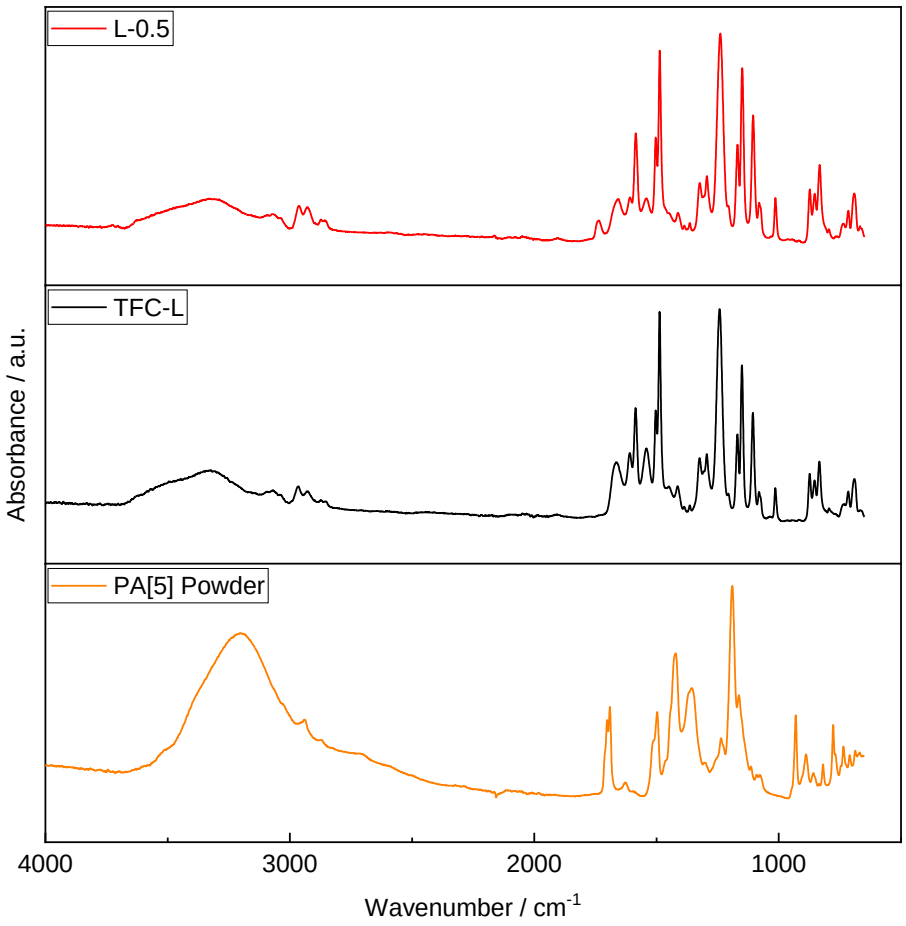

Figure S2. FTIR-ATR spectras of L-series TFC membranes (Reference TFC and L-0.5) and PA[5] powder (Membrane composition MPD 1.2 w/w %, TMC 0.1w/w %)

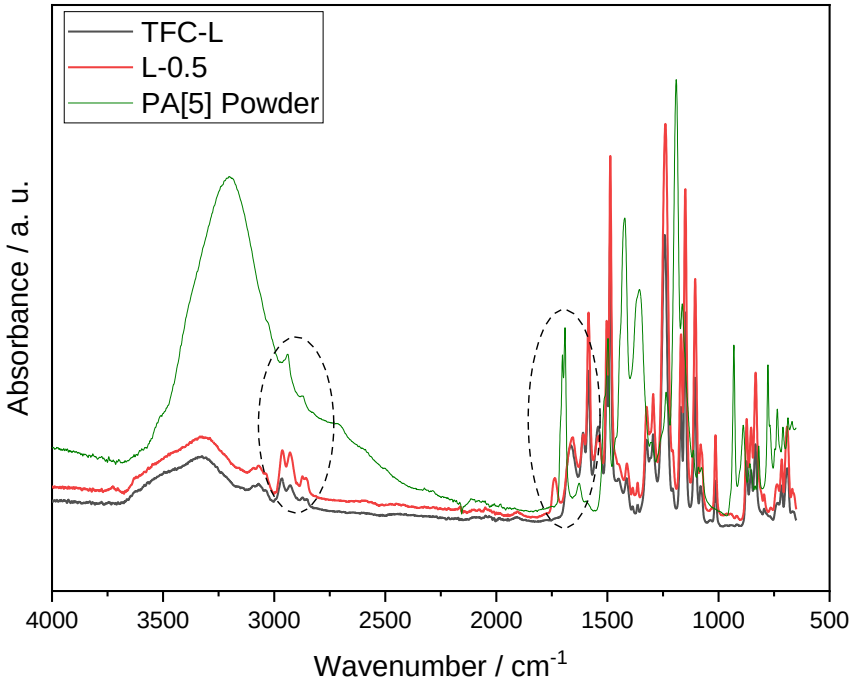

Figure S3. Comparison of FTIR-ATR spectra of PA[5] membrane with 0.5% PA[5] and the reference TFC membrane (membrane composition MPD 1.2 w/w % and TMC 0.1w/w %).

Energy Dispersive X-ray spectroscopy (EDX)

EDX was conducted with an AZTEC System, Oxford Instruments, UK, at an accelerating voltage of 10 kV and a working distance of 8.5 mm. At least three spectra were captured at different positions to calculate an average atomic percentage of %C, %N, and %O. Measurements of the atomic composition for PA[5] membranes are listed in Table S1.

Table S1. Atomic content of TFC and PA- PA[5]membranes by EDX

Membrane	C, %	N, %	O, %
TFC	83.95	1.21	12.02
PA-PA5 0.025%	86.13	0.54	10.62
PA-PA5 0.05%	86.9	0.54	10.16

Scanning electron microscopy (SEM): The incorporation of PA[5] aggregates in polyamide layers was verified by a high-resolution scanning electron microscope (SEM, HITACHI S-4800), at an accelerating voltage of 2 kV. For cross-sectional studies, membrane coupons were prepared by freeze-fracturing in liquid nitrogen and then dried in dry air for at least 24h. A 5 nm thick coating of chromium was sputtered (SC7620 Mini Sputter Coater,

Quorum Technologies Ltd.) under Ar atmosphere (10^{-1} mbar) to achieve a minimum conductivity for reliable SEM information.

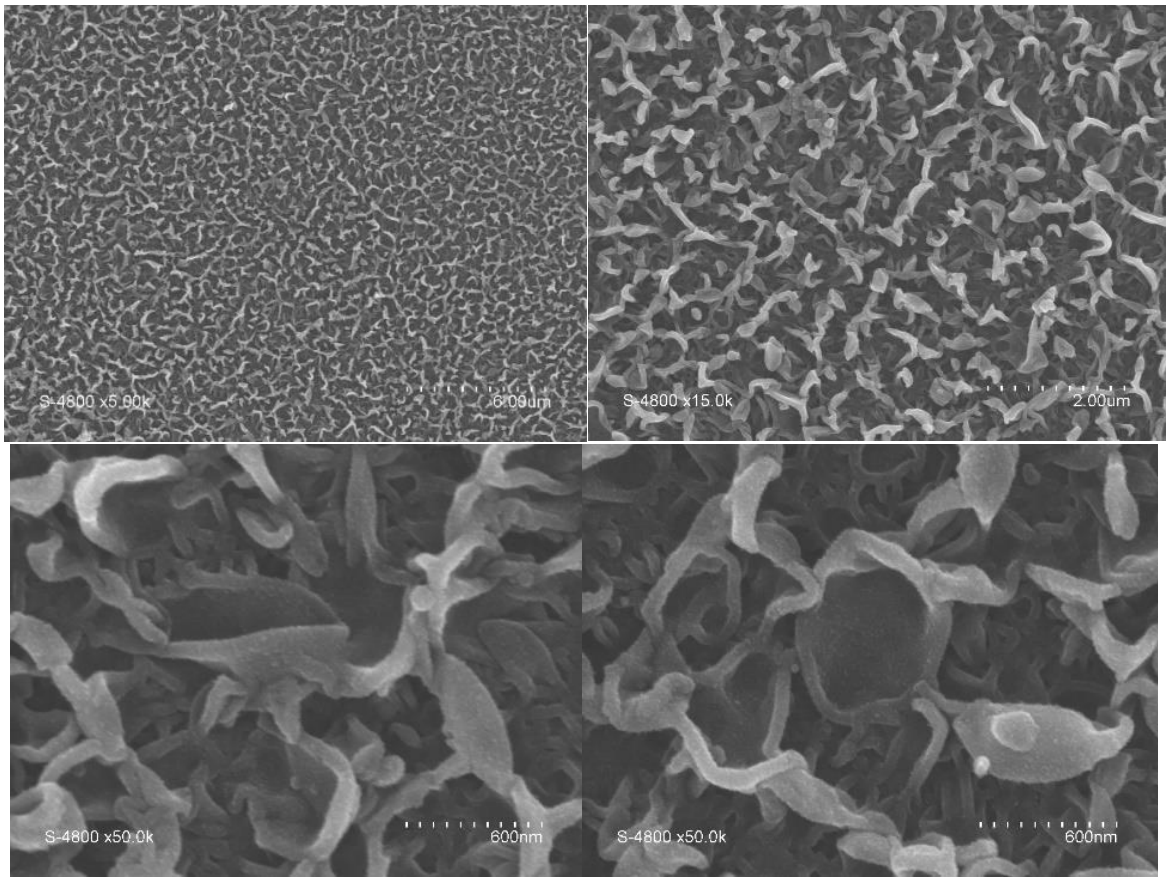

Figure S4. Surface SEM micrograph of the reference TFC membrane (membrane composition MPD 1.2 w/w % and TMC 0.1w/w %).

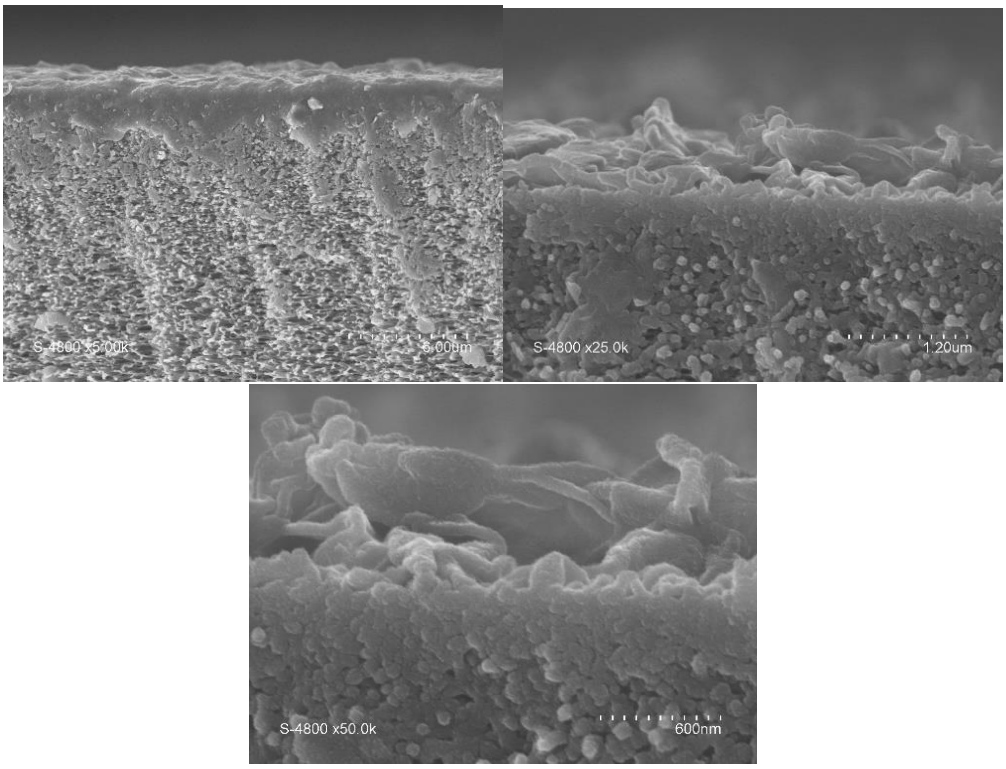

Figure S5. Cross-section SEM micrographs of the reference TFC membrane (membrane composition MPD 1.2 w/w % and TMC 0.1w/w %).

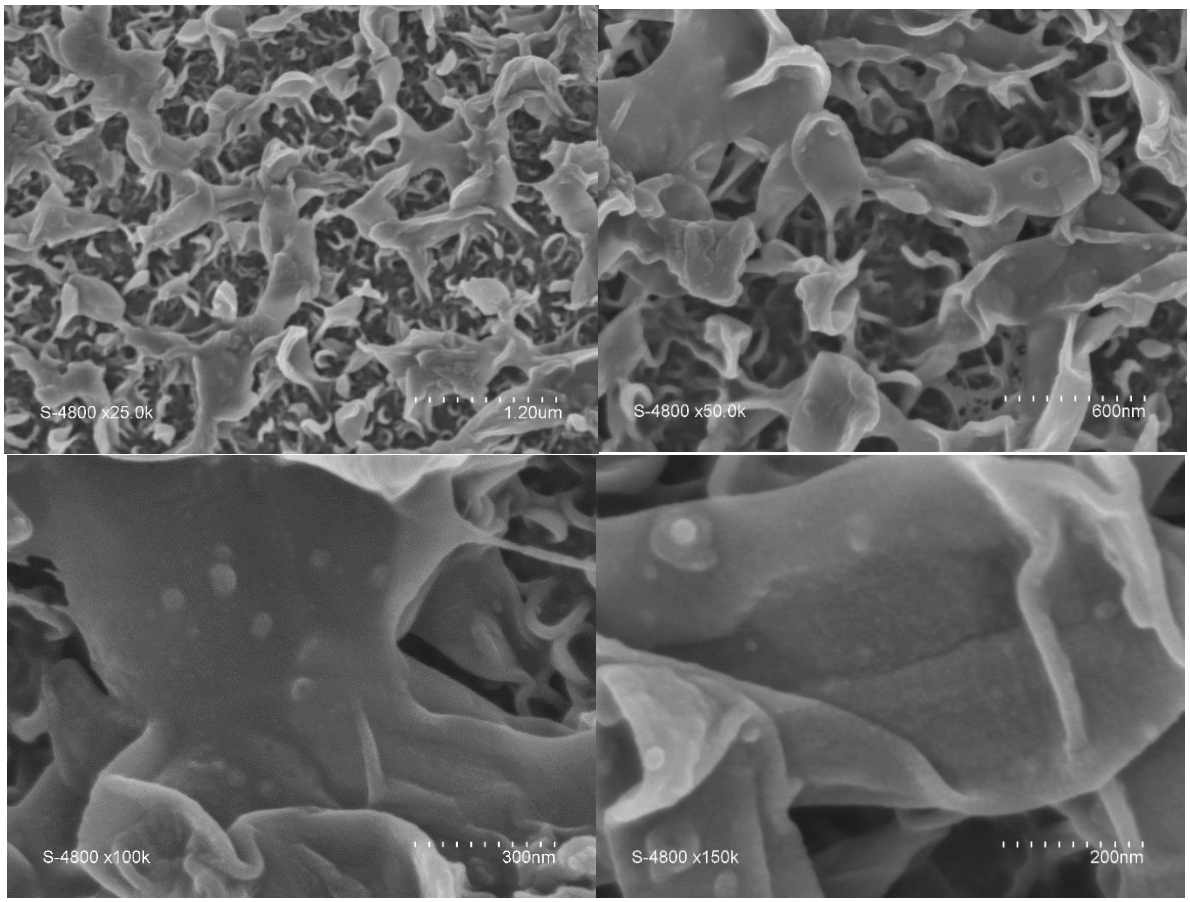

Figure S6. Surface SEM micrographs of PA-PA[5] membrane prepared using PA[5] 0.01% solution (membrane composition MPD 1.2 w/w % and TMC 0.1w/w %).

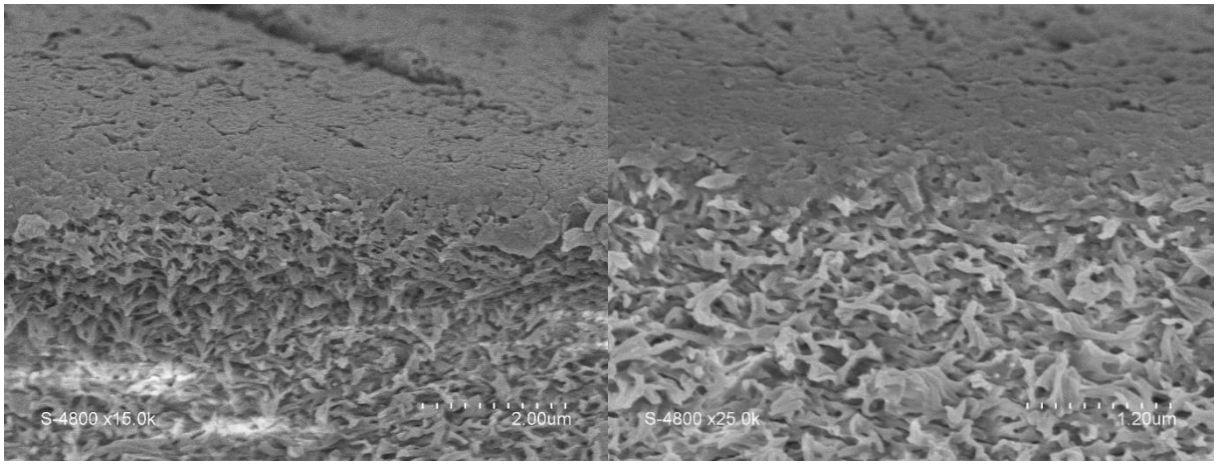

Figure S7. Cross-section SEM micrographs of PA-PA[5] membrane prepared using PA[5] 0.01% solution (membrane composition MPD 1.2 w/w % and TMC 0.1w/w %)

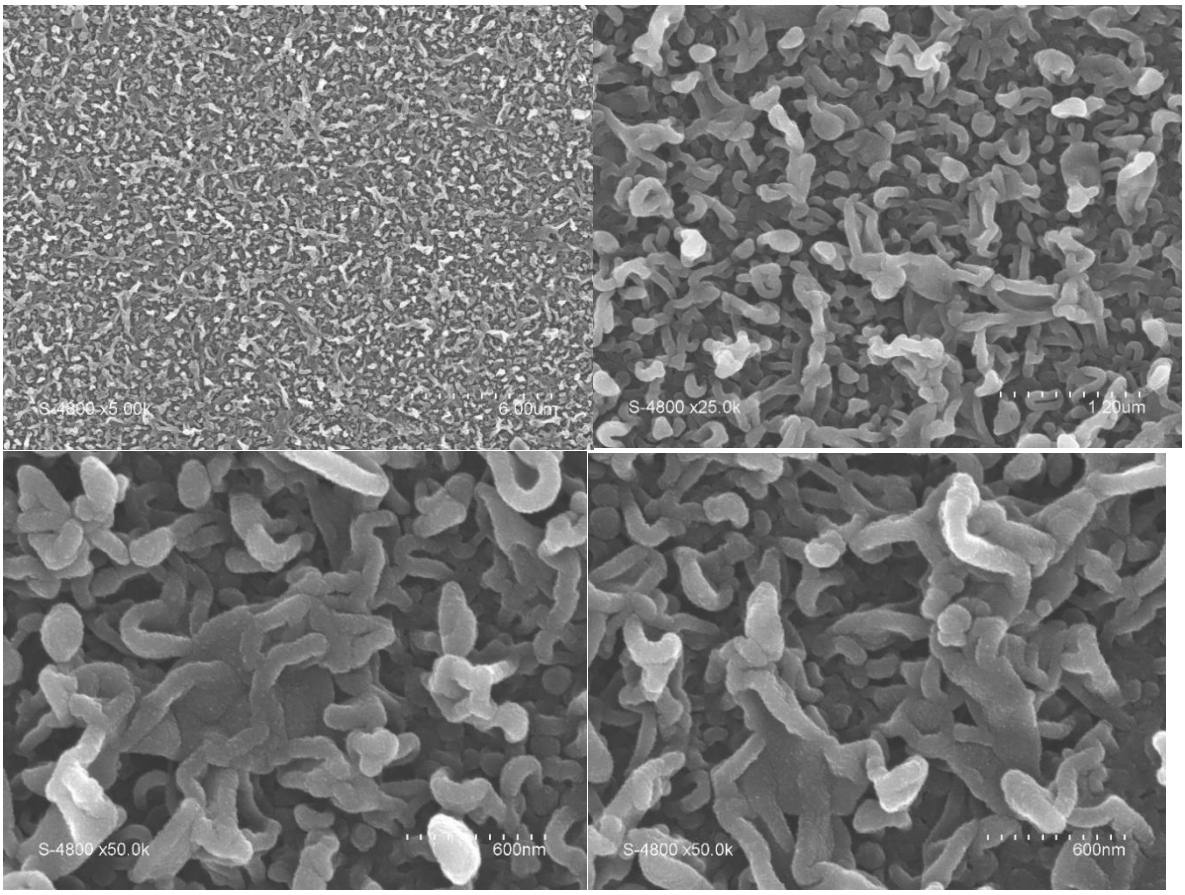

Figure S8. Surface SEM micrographs of PA-PA[5] membrane prepared using PA[5] 0.025% solution (membrane composition MPD 1.2 w/w % and TMC 0.1w/w %).

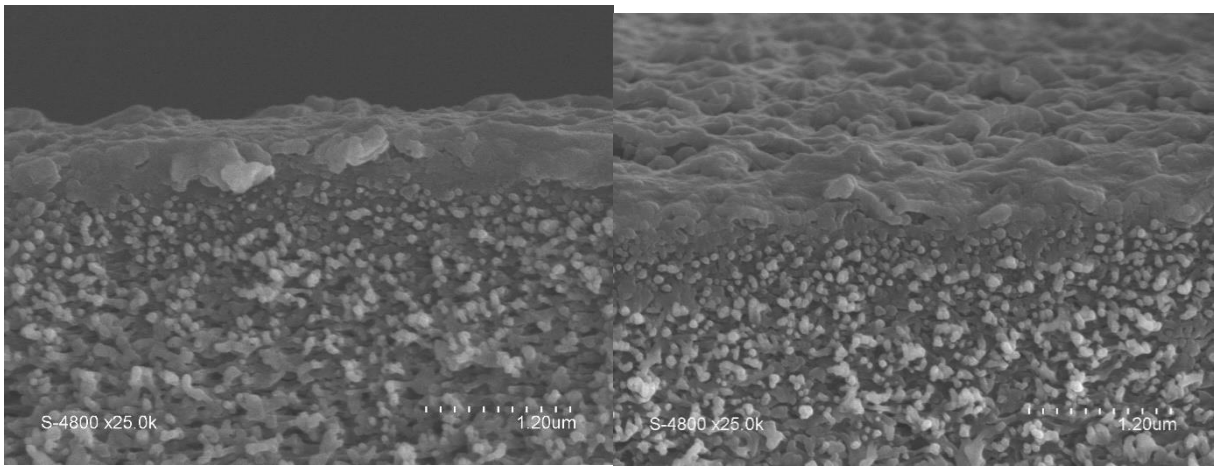

Figure S9. Cross-section SEM micrographs of PA-PA[5] membrane prepared using PA[5] 0.025% solution (membrane composition MPD 1.2 w/w % and TMC 0.1w/w %).

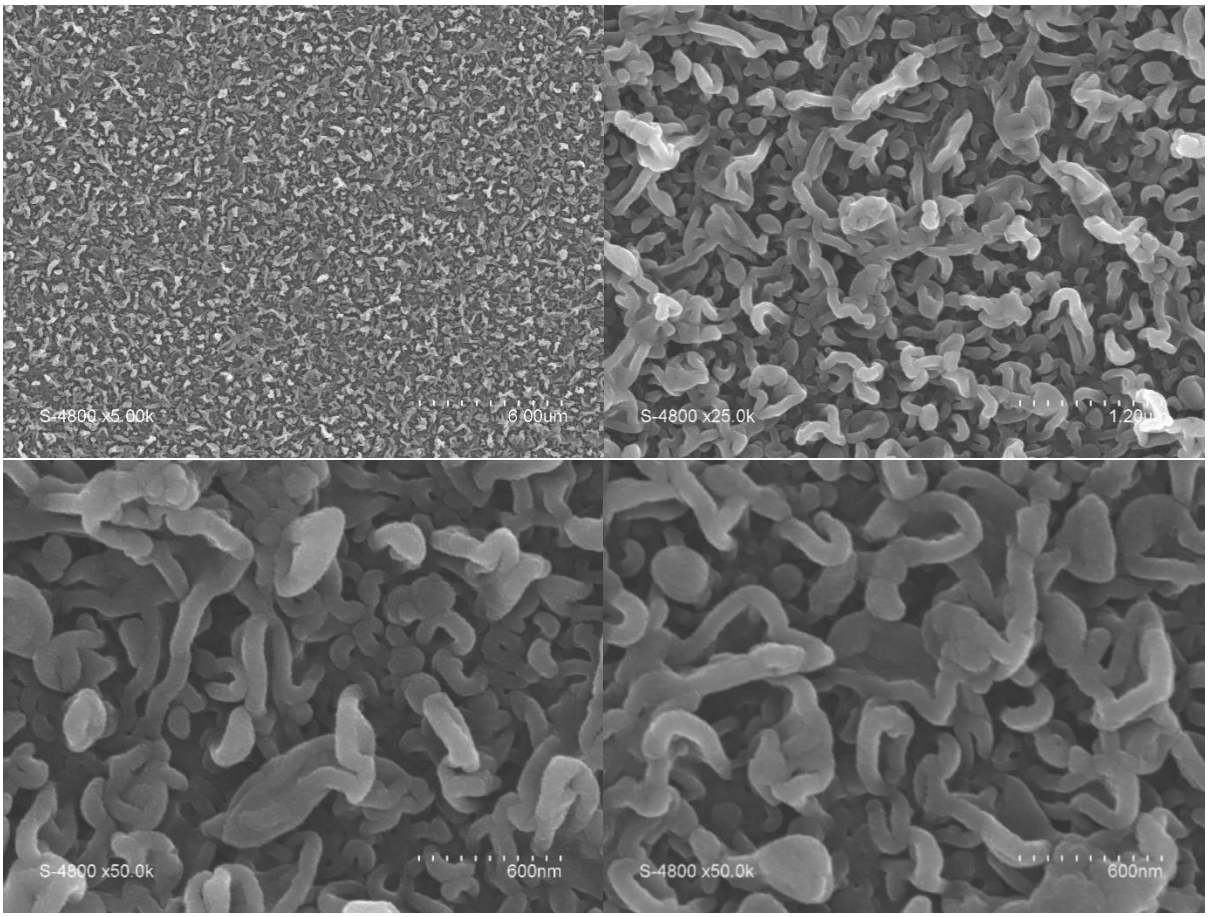

Figure S10. Surface SEM micrographs of PA-PA[5] membrane prepared using PA[5] 0.05% solution (Membrane composition MPD 1.2 w/w %, TMC 0.1w/w %)

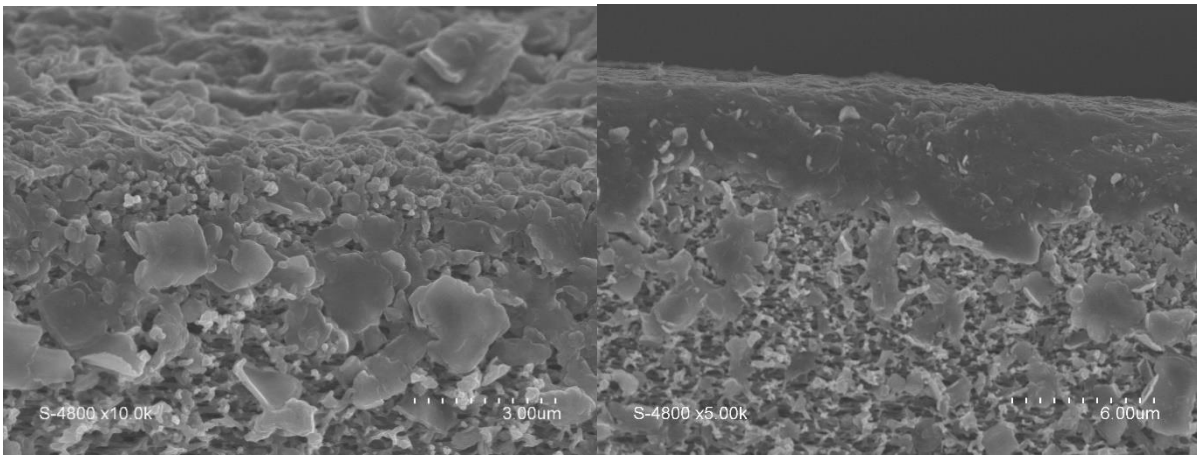

Figure S11. Cross-section SEM micrographs of PA-PA[5] membrane prepared using PA[5] 0.05% solution (Membrane composition MPD 1.2 w/w %, TMC 0.1w/w %)

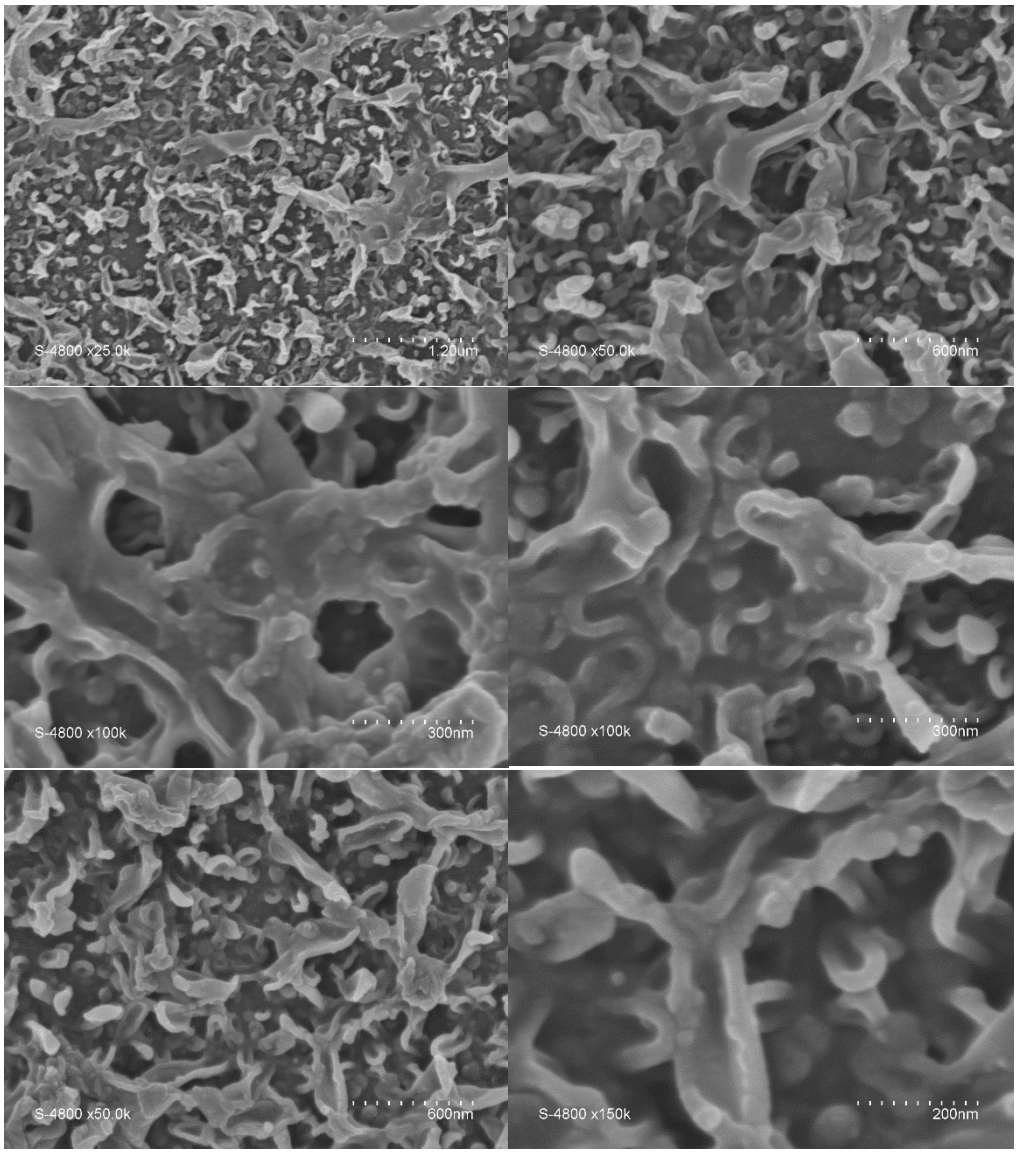

Figure S12. Surface SEM micrographs of PA-PA[5] membrane prepared using PA[5] 0.1% solution (Membrane composition MPD 1.2 w/w %, TMC 0.1w/w %)

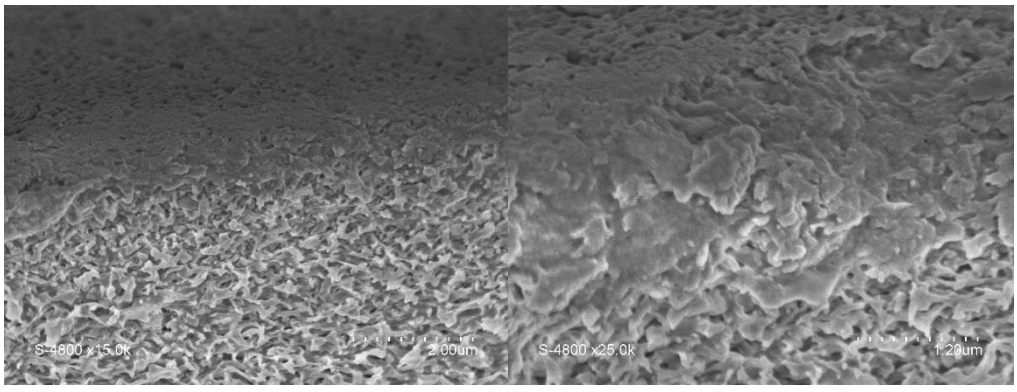

Figure S13. Cross-section SEM micrographs of PA-PA[5] membrane prepared using PA[5] 0.1% solution (Membrane composition MPD 1.2 w/w %, TMC 0.1w/w %)

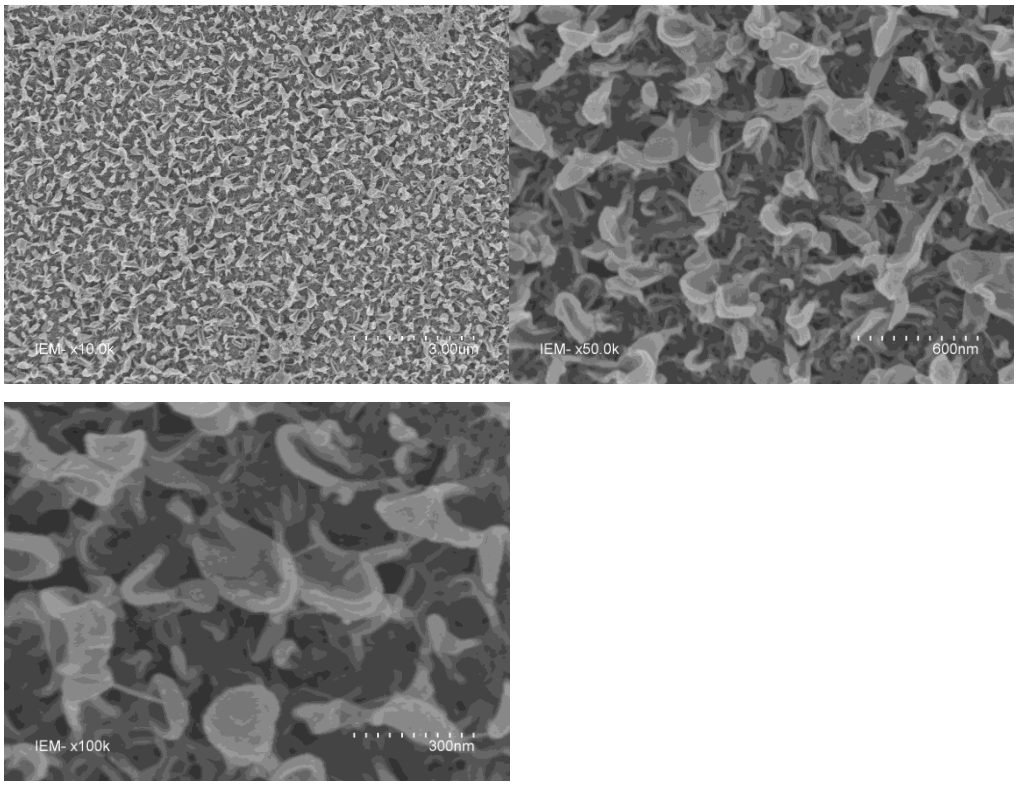

Figure S14. Surface SEM micrographs of Reference PA membrane prepared using Ethanol/water solution with ratio 1:2 w/w (Membrane composition MPD 1.2 w/w %, TMC 0.1w/w %)

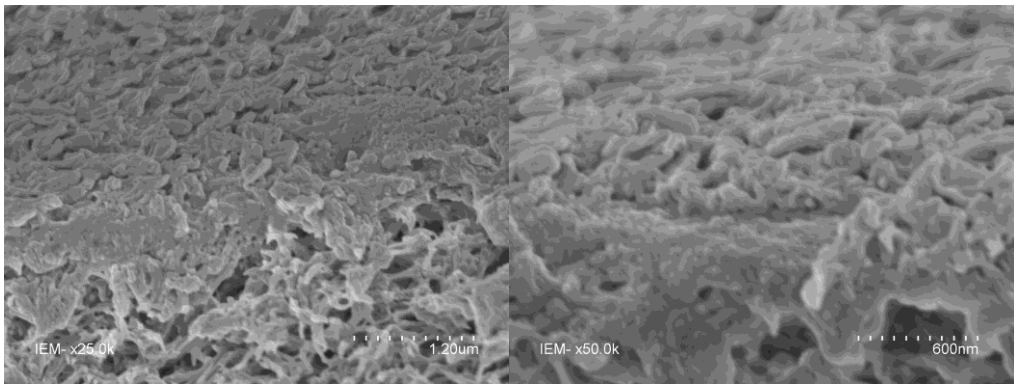

Figure S15. Cross-section SEM micrographs of Reference PA membrane prepared using Ethanol/water solution with ratio 1:2 w/w (Membrane composition MPD 1.2 w/w %, TMC 0.1w/w %)

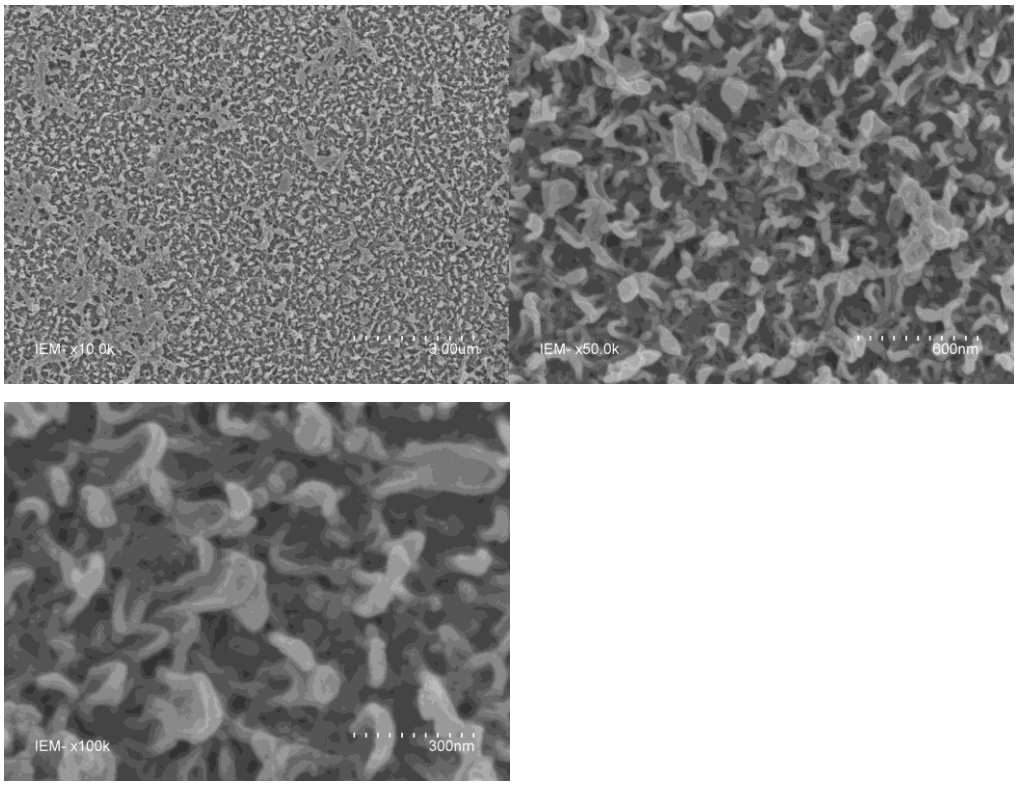

Figure S16. Surface SEM micrographs of PA-PA[5] membrane prepared using MPD-PA[5] 0.5% solution with Ethanol/Water ratio 1:2 (Membrane composition MPD 1.2 w/w %, TMC 0.1w/w %)

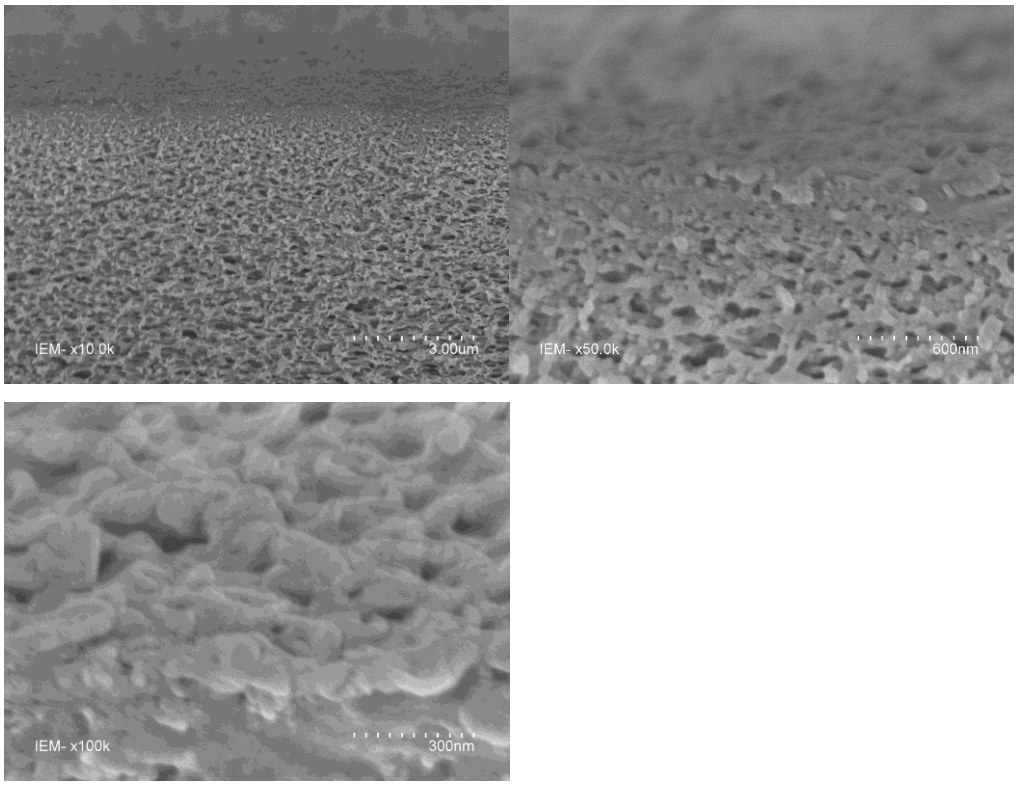

Figure S17. Cross-section SEM micrographs of PA-PA[5] membrane prepared using MPD-PA[5] 0.5% solution with Ethanol/Water ratio 1:2 (Membrane composition MPD 1.2 w/w %, TMC 0.1w/w %)

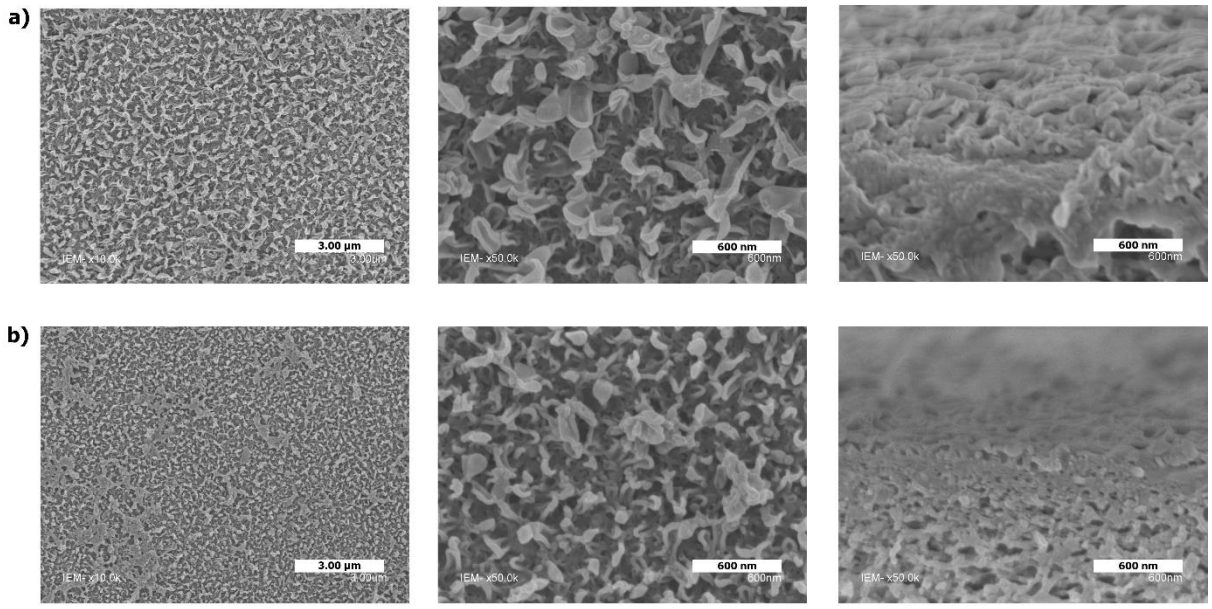

Figure S18. Representative surface (column 1 and 2) and cross-section (column 3) SEM micrographs of reference TFC membrane (a) and PA[5]-PA hybrid layers (b) with 0.5 w/w % PA[5]. Both membranes were prepared using Ethanol/Water (1:2 by weight) solution of MPD; PA[5] was dissolved together with MPD. MPD and TMC concentration in the casting solutions were 1.2 w/w % and 0.1 w/w %, respectively.

XRD

X-Ray diffraction analysis was performed using X'Pert3 MRD XL Materials Research X-ray Diffraction System (Malvern Panalytical, UK). XRD analysis of the reference TFC membrane and membranes containing PA5 does not provide any information about presence of nanocrystals in the membrane. It could be explained by the low content of PA5 in the membrane which cannot be detected with this technique.

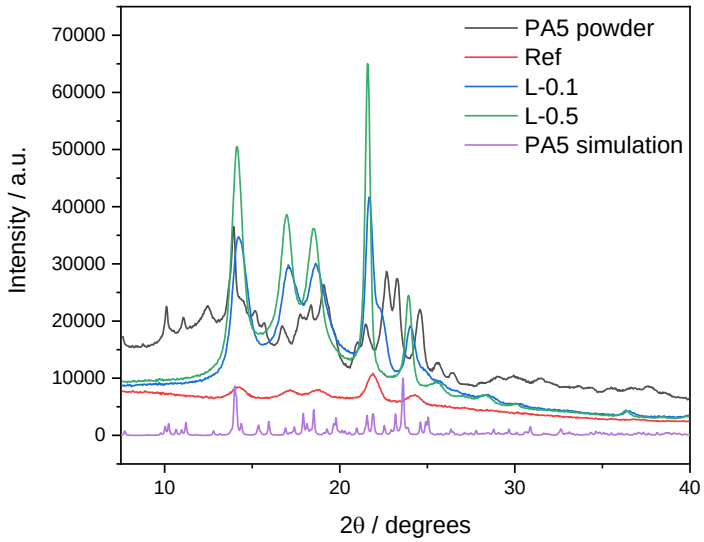

Figure S19. X-Ray diffraction comparison of PA5 powder, Reference TFC membrane, L-0.1 and L-0.5 membranes prepared using 0.1 w/w % and 0.5 w/w % PA5 solutions respectively.

Membrane performance evaluation. Intrinsic transport properties of control TFC and hybrid membranes were evaluated using a laboratory-scale cross-flow unit, comprising a high-pressure pump, a feed vessel, and a flat membrane housing cell. The housing cell consists of a 7.6 cm long, 2.8 cm wide, and 0.3 cm high rectangular channel. The effective membrane active area was 22 cm^2, the crossflow velocity was fixed at 0.9 m/s, and the temperature was constant at 25 ± 0.5 °C. Prior to each experiment, the membrane was immersed in water overnight. The filtration tests were conducted, referred to as "brackish water" tests. The membranes were compacted with DI water as feed at 17.5 bar (261 psi) of applied pressure, ΔP, until the permeate flux reached a steady-state. The pressure was then lowered to 15.5 bar (217 psi). The pure water flux, $J_{w,0}$, was calculated by dividing the volumetric permeate rate, obtained at steady-state, by the membrane active area. The pure water permeability was determined by dividing the water flux, $J_{w,0}$, by the applied pressure, $P = {J_{w,0}}/{\Delta P}$. Subsequently, for brackish water tests, NaCl was added from a 5 M stock solution to reach a final concentration of 100 mM (2000 ppm) and salt concentrations in the feed and permeate streams were measured using a calibrated conductivity meter (pHenomenal® CO 3100 H, VWR Instruments). Upon reaching steady-state, the permeate flux, J_w, was calculated by dividing the volumetric permeate rate by the membrane area. Observed rejection, R, was then computed from the concentrations determined in bulk feed, c_f, and in the permeate stream, c_p, for each ionic species or for global salinity (using conductivity as a proxy for salinity): $R = 1 - {c_p}/{c_f}$. The rejection values reported for each sample are the average of three filtration measurements of NaCl solution (V = 4L).

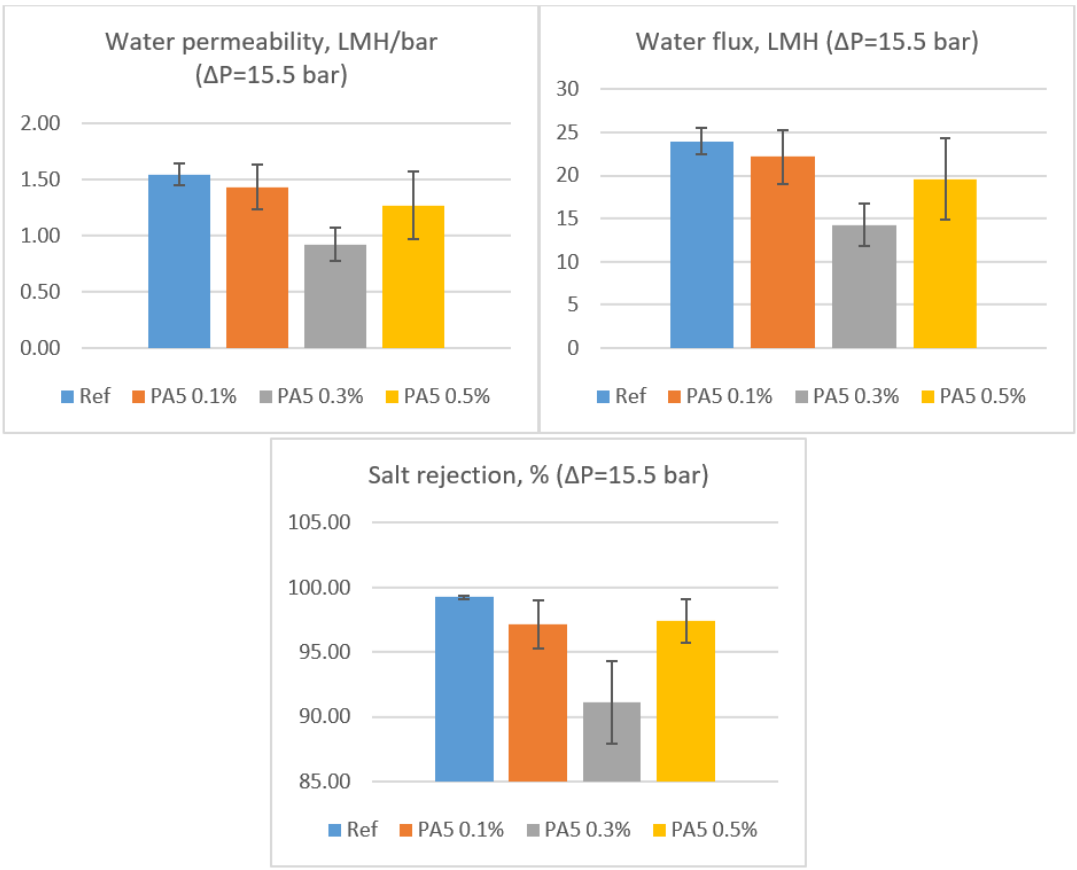

Figure S20. Water permeability, flux and salt rejection for the reference membrane REF and PA5 membranes prepared with 0.1%, 0.3% and 0;5% Pillar[5]arene solutions (w/w); membrane composition MPD 1,5 w/w % and TCM 0,15 w/w %.

Table S2. Filtration tests for REF and PA5 membranes (MPD 1,5 w/w %, TCM 0,15 w/w %)

Name	MPD, %	TMC, %	CPD, %	EtOH:H_2O	Pressure, bar	Flux (w/o NaCl), LMH	Permeability, LMH/bar	Flux (with NaCl), LMH	T, °C	Rejection		Average permeability, LMH/bar	Average salt rejection, %
										Test 1	Test 2		
REF 1 13/10	1.5	0.15	0	1:2	15.5	24.97	1.611	23.82	25	99.26	99.26	1.54 ± 0.10	99.23 ± 0.13
REF 3 13/10	1.5	0.15	0	1:2	15.5	21.55	1.39	20.46	25	99.2	99.21		
REF 4 13/10	1.5	0.15	0	1:2	15.5	25.15	1.623	24.37	25	99.25	99.25		
REF 5 13/10	1.5	0.15	0	1:2	15.5	25.24	1.628	23.61	25	99.46	99.46		
REF 2 12/10	1.5	0.15	0	1:2	15.5	23.74	1.532	22.82	25	99.5	99.51		
REF 3 12/10	1.5	0.15	0	1:2	15.5	21.76	1.404	20.04	25	99.18	99.18		
REF 4 12/10	1.5	0.15	0	1:2	15.5	25.18	1.625	23.53	25	98.77	98.75		
PA5-01-1	1.5	0.15	0.1	1:2	15.5	25.06	1.617	24.5	25	98.94	98.95	1.43 ± 0.20	97.15 ± 1.85
PA5-01-2	1.5	0.15	0.1	1:2	15.5	22.269	1.437	21.51	25	94.73	95.08		
PA5-01-3	1.5	0.15	0.1	1:2	15.5	25.45	1.642	24.37	25	97.95	97.92		
PA5-01-4	1.5	0.15	0.1	1:2	15.5	20.918	1.35	19.71	25	99.03	99.01		
PA5-01-5	1.5	0.15	0.1	1:2	15.5	21.909	1.413	20.76	25	98.43	98.37		
PA5-01-6	1.5	0.15	0.1	1:2	15.5	17.257	1.113	15.67	25	90.2	-		
PA5-03-1	1.5	0.15	0.3	1:2	15.5	12.845	0.829	12.31	25	84.57	-	0.92 ± 0.15	91.10 ± 3.19
PA5-03-2	1.5	0.15	0.3	1:2	15.5	13.175	0.85	12.82	25	91.38	91.35		
PA5-03-3	1.5	0.15	0.3	1:2	15.5	15.876	1.024	14.58	25	91.47	89.53		
PA5-03-4	1.5	0.15	0.3	1:2	15.5	15.246	0.984	14.71	25	94.68	94.72		
PA5-05-1	1.5	0.15	0.5	1:2	15.5	20.468	1.321	19.37	25	99.18	99.17	1.27 ± 0.30	97.40 ± 1.65
PA5-05-2	1.5	0.15	0.5	1:2	15.5	15.036	0.97	14.58	25	98.88	98.85		
PA5-05-3	1.5	0.15	0.5	1:2	15.5	23.019	1.485	21.43	25	98.97	98.99		
PA5-05-4	1.5	0.15	0.5	1:2	15.5	16.327	1.053	15.63	25	96.49	96.55		
PA5-05-5	1.5	0.15	0.5	1:2	15.5	23.199	1.497	20.88	25	93.31	93.63		

Table S3. Filtration tests for REF and PA5 membranes (MPD 1,2 w/w %, TCM 0,1 w/w %)

Name	MPD, %	TMC, %	CPD, %	EtOH:H_2O	Pressure, bar	Flux (w/o NaCl), LMH	Permeability, LMH/bar	Flux (with NaCl), LMH	T, °C	Rejection		Average permeability, LMH/bar	Average salt rejection, %
										Test 1	Test 2		
REF	1.2	0.1	-	1:2	15.5	29.89	1.929	25.87	25	99.33	99.33	2.00 ± 0.50	99.54 ± 0.17
	1.2	0.1	-	1:2	15.5	26.11	1.685	22.43	25	99.66	99.64		
	1.2	0.1	-	1:2	15.5	36.89	2.380	33.36	25	99.63	99.63		
PA5 0,01%	1.2	0.1	0.01	1:2	15.5	35.02	2.260	31.89	25	99.14	99.14	2.32 ± 0.65	99.23 ± 0.05
	1.2	0.1	0.01	1:2	15.5	28.27	1.824	25.63	25	99.23	99.24		
	1.2	0.1	0.01	1:2	15.5	37.25	2.403	33.78	25	99.26	99.27		
	1.2	0.1	0.01	1:2	15.5	43.58	2.811	39.50	25	99.30	99.29		
PA5 0,025%	1.2	0.1	0.025	1:2	15.5	50.57	3.263	44.71	25	99.47	99.51	2.76 ± 0.49	99.34 ± 0.07
	1.2	0.1	0.025	1:2	15.5	54.47	3.514	48.78	25	99.15	99.14		
	1.2	0.1	0.025	1:2	15.5	46.22	2.982	41.64	25	99.22	99.23		
	1.2	0.1	0.025	1:2	15.5	37.82	2.440	33.45	25	99.31	99.30		
	1.2	0.1	0.025	1:2	15.5	32.89	2.122	28.63	25	99.40	99.37		
	1.2	0.1	0.025	1:2	15.5	43.76	2.823	40.95	25	99.33	99.35		
	1.2	0.1	0.025	1:2	15.5	34.18	2.205	30.54	25	99.51	99.51		
PA5 0,05%	1.2	0.1	0.05	1:2	15.5	26.32	1.698	23.49	25	99.69	99.69	2.60 ± 0.72	99.42 ± 0.14
	1.2	0.1	0.05	1:2	15.5	34.54	2.229	31.60	25	99.06	99.03		
	1.2	0.1	0.05	1:2	15.5	55.40	3.574	49.08	25	99.51	99.51		
	1.2	0.1	0.05	1:2	15.5	40.34	2.602	36.68	25	99.56	99.56		
	1.2	0.1	0.05	1:2	15.5	49.70	3.206	43.66	25	99.44	99.44		
	1.2	0.1	0.05	1:2	15.5	35.44	2.287	32.64	25	99.24	99.25		
PA5 0,1%	1.2	0.1	0.1	1:2	15.5	35.11	2.265	32.31	25	99.12	99.13	2.30 ± 0.52	98.99 ± 0.21
	1.2	0.1	0.1	1:2	15.5	30.16	1.946	25.52	25	99.27	99.29		
	1.2	0.1	0.1	1:2	15.5	42.47	2.740	38.61	25	98.90	98.91		

Table S4. Filtration tests for REF, PA5-MPD and MPD-PA5 membranes (MPD 1,2 w/w %, TCM 0,1 w/w %)

Name	MPD, %	TMC, %	PA5, %	EtOH:H_2O	Pressure, bar	Flux (w/o NaCl), LMH	P, LMH/bar	Flux (with NaCl), LMH	T, °C	Rejection	
										Test 1	Test 2
REF 1 MPD/PA5	1.2	0.1	0	1:2	15.5	17.01	1.098	16.68	25	99.62	99.61
REF 2 MPD/PA5	1.2	0.1	0	1:2	15.5	21.3385	1.377	20.84	25	99.44	99.47
PA5/MPD	1.2	0.1	0.5	1:2	15.5	10.53	0.68	-	25	99.15	99.16
PA5/MPD	1.2	0.1	0.5	1:2	15.5	12.065	0.778	11.26	25	98.92	98.96
MPD-PA5-TMC	1.2	0.1	0.3	1:2	15.5	17.857	1.152	-	25	93.5	93.78
MPD-PA5-TMC	1.2	0.1	0.5	1:2	15.5	9.1236	0.589	-	25	-	-
MPD-PA5-TMC	1.2	0.1	0.5	1:2	15.5	45.498	2.935	42.23	25	75.12	75.28

Chapter IV. Synergistic self-assembly of bi-component alkylureido systems into artificial water channels

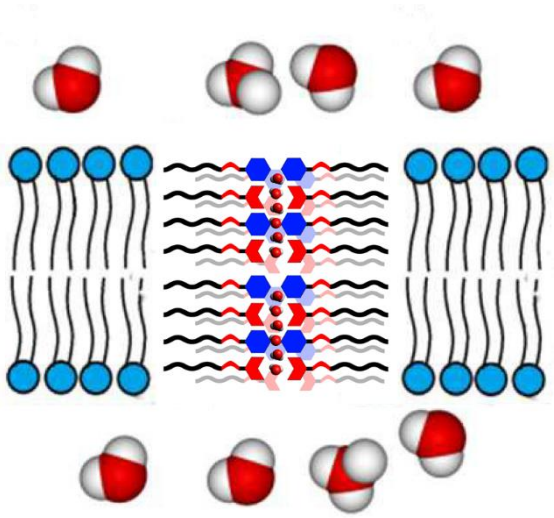

Contribution to Publication

The contribution of the Ph.D. candidate to the manuscript “Synergistic self-assembly of bi-component alkylureido systems into artificial water channels” is related to the identification of empirical strategies toward the obtainment of the objective of the research project for which he performed most of the experimental work, including (i) synthesis and characterization of hydrophobic alkylureido derivatives, (ii) defining the strategy of obtaining hybrid combination of alkylureido derivatives, (iii) performing water transport evaluation by using Stopped-flow method and analysing obtained results, (iv) investigation of ion transport by using fluorescence HPTS assay.

SYNERGISTIC SELF-ASSEMBLY OF BI-COMPONENT ALKYLUREIDO SYSTEMS INTO ARTIFICIAL WATER CHANNELS

Dmytro STRILETS, Sophie CERNEAUX, Mihail BARBOIU*

Institut Europeen des Membranes, Adaptive Supramolecular Nanosystems Group, ENSCM-UM- CNRS UMR 5635, Place Eugene Bataillon CC047,
34095 Montpellier, France

Water translocation through cell membranes plays an important role for living organisms. In cells, the transport of water molecules is carried out through water-transporting proteins, the aquaporins. Promising artificial water channels (AWCs) are Imidazole-quartet supramolecular systems whose hydrophilic channels within 2.6-Å pores are formed via self-assembly of alkylureido-ethylimidazole compounds. The size of the pore diameter, water permeability and ion rejection of these AWCs are on par with very efficient aquaporins.

Whilst the size restriction is still necessary, the specific water recognition is also needed to reach high level of selectivity. The selective binding of water can be obtained through the synergistic combination of donor-acceptor H-bonding binding components, while the permeability is determined by the friction-less translocation.

This work describes novel hydrophobic alkylureido AWCs and their bi-component optimal self-assembly containing I-quartets that induce the selective transport of water molecules against ions. A series of ureido derivatives was prepared by reacting aromatic amines containing donor and/or acceptor H-bonding fragments with alkyl isocyanates. The activity of the obtained derivatives and their combinations were evaluated in water and ion transports by using the stopped-flow method and fluorescent 8-Hydroxypyrene-1,3,6-trisulfonic acid trisodium salt (HPTS) assay, respectively. We noticed that water permeability for some bi-component systems is most of the time the sum of permeability of the individual compound systems, in particular two systems showed remarkable synergistic results. Indeed, a channel formed by imidazole and benzimidazole derivatives showed a water permeability of almost 10 times superior than the I-quartet itself being furthermore able to selectively transport 52 million water molecules per second. The second one is the combination of imidazole and benzosulfonamine derivatives that leads to the formation of a channel 33 times more efficient in terms of water permeability than I-quartet itself and able to transport 82 million molecules per second.

KEYWORDS: ARTIFICIAL WATER CHANNELS, ION TRANSPORT, FLUORESCENCE, SELF-ASSEMBLY, STOPPED-FLOW METOD, WATER PERMEABILITY

INTRODUCTION

Water plays an important role for living organisms.[1-3] In cells, the transport of water molecules is carried out through natural aquaporins (AQPs), that are cell water-transporting proteins discovered by Agre et al.[4], allowing the transfer of H_2O molecules over the physical barrier of cell membranes at significantly high rates of water permeation (> 10^9 H_2O molecules per second per channel) with selectivity for water toward ions to sustain homeostasis in the cell, which is demanding condition for the maintenance of life.[5-6]

Due to AQPs' ideal water / salt selectivity and spontaneous insertion in the cell membrane, the incorporation of this class of proteins into membranes is of great interest for desalination purposes.[7-8] Several scientific groups have successfully incorporated Aquaporins into desalination membranes.[9] However, the main challenge that limits the development of these proteins in membrane systems remains the integrity and translation of protein channel function that need to be conserved at a large scale [10].

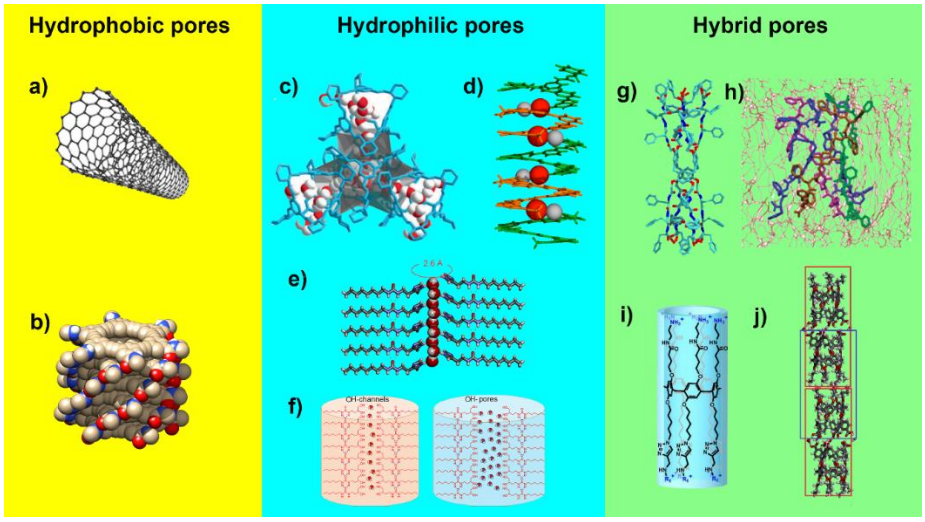

Figure 1. Classification of AWC by water translocation mechanism: Hydrophobic pores: a) Carbon nanotubes porins (CNTP), b) Hexa(m-phenylene ethynylene) (m-PE) macrocycles; hydrophilic pores: c) Porous organic cages (POC), d) Aquafoldamers, e) I-quartet systems, f) OH-Channels and OH-pores; Hybrid pores: g) Peptide-appended hybrid[4]arene (PAH[4]), h) peptide-appended pillar[5]arene (PAP), i) Pillar[5]arene-AQP, j) Pillar[5]arene dimers.

One alternative to biological water channels could be bioinspired Artificial Water Channels (AWCs), constructed as self-assembled or as unimolecular synthetic nanoscale architectures, which mimic the AQP functions.[11-16] AWCs have quickly appeared as a perspective platform for next generation desalination membranes. Based on structure and water transport studies of AQPs, it was proposed several molecular features as design criteria for AWCs, which include Angström-scale pore size, selective filter with specific H-bonding of water molecules and hydrophobic pore media.[14, 17] Stability and high pore packing density are the main advantages of AWC-incorporated membranes over membranes containing AQP, which make it more attractive for development of new type of selective polymer membranes. However, achieving both AQP-like single channel water permeability and selectivity remains a challenge that limits the development of AWC-incorporated desalination membranes.[18-20]

At the moment, numerous architectures were reported that fully or partially addressed the criteria mentioned above, among which are carbon nanotubes porins (CNTPs)[19, 21], m-PE macrocycles[22], pillar[5]arene (PAP5)[23-24], pillar[4]arene (PAH[4]) clusters[25], pillar[5]arene dimers[26], aquafoldamers[27], porous organic cages (POCs)[28], pillar[5]arene hydrazones (PAH5)[29], pillar[5]arene-AQPs[30], OH-channels[31] and Imidazole-quartet system (I-quartet)[18, 32] (**Figure 1**). Those channels can be separated in 3 groups according to their type of interaction with water as well as their transport mechanism (**Figure 1**): I) hydrophobic pores (CNTPs, **Figure 1a**, m-PE macrocycles **Figure 1b**), in which no H-bonding are occurring between the water and no interaction with the channels surfaces are observed; II) hydrophilic pores that specifically H-bond water molecules to the wall of the channel (I-quartet, **Figure 1e**; OH-channels, **Figure 1f**; POC **Figure 1c**; aquafoldamers **Figure 1d**); and III) hybrid pores, which mimic hourglass structure of AQPs with selective hydrophilic filter in the middle and hydrophobic side chains connected to the selective filter forming tubular water conductors

(pillar[5]arene hydrazones (PAH5), **Figure 1h**; Peptide-appended hybrid[4]arene PAH[4] , **Figure 1g**; pillar[5]arene-AQPs, **Figure 1i**; pillar[5]arene dimers, **Figure 1j**).

Imidazole-quartet systems are already very well-known AWCs with channels pores within 2.6 Å formed from the supramolecular organization of alkylureido ethylimidazole compounds that suits requirements to observe water permeability and ion rejection.[18, 32] On the other hand, AWCs based on carbon nanotubes showed incredibly high permeability values comparable or even exceeding those of natural channels without any selectivity though that may be explained by the repulsion of water molecules from the walls due to the high hydrophobicity of the channels.[19, 21]

The selective binding of water molecules can be obtained through the synergistic combination of donor-acceptor H-bonding components, while the permeability is determined by the friction-less translocation.[14]

This work describes novel synthetic routes to obtain new hybrid artificial water channels taking advantage of a synergistic combination of alkyl ureido derivatives that induce the selective transport of water against ions. We also decided to combine I-quartet channel with hydrophobic alkylureido derivatives, with the objective to gain in selectivity in hydrophilic pores and to enhance water permeability *via* hydrophobic pores.

Design of Bi-component Self-assembled Channels. Detailed investigation of AQP1 structure made by Agre[4] postulates that AQP1 consists of five inter-helical loop regions (**Figure 2**-A – E) that form the extracellular and cytoplasmic vestibules. [33] Loops B and E are hydrophobic loops that contain the asparagine–proline–alanine (NPA) motif, forming a 'hourglass' structure by overlapping the middle of lipid bilayer of cell membrane.[34] This overlap forms the narrow channel constriction site in the peptide, known as 'selectivity filter' or ar/R (aromatic/arginine) selectivity filter. The ar/R selectivity filter is a cluster of amino acids that helps transporting

water molecules by binding and excludes other molecules. Usually, this cluster consists of combination of Histidine (His), Arginine (Arg), Asparagine (Asn), Phenylalanine (Phe), Tryptophane (Try), etc.

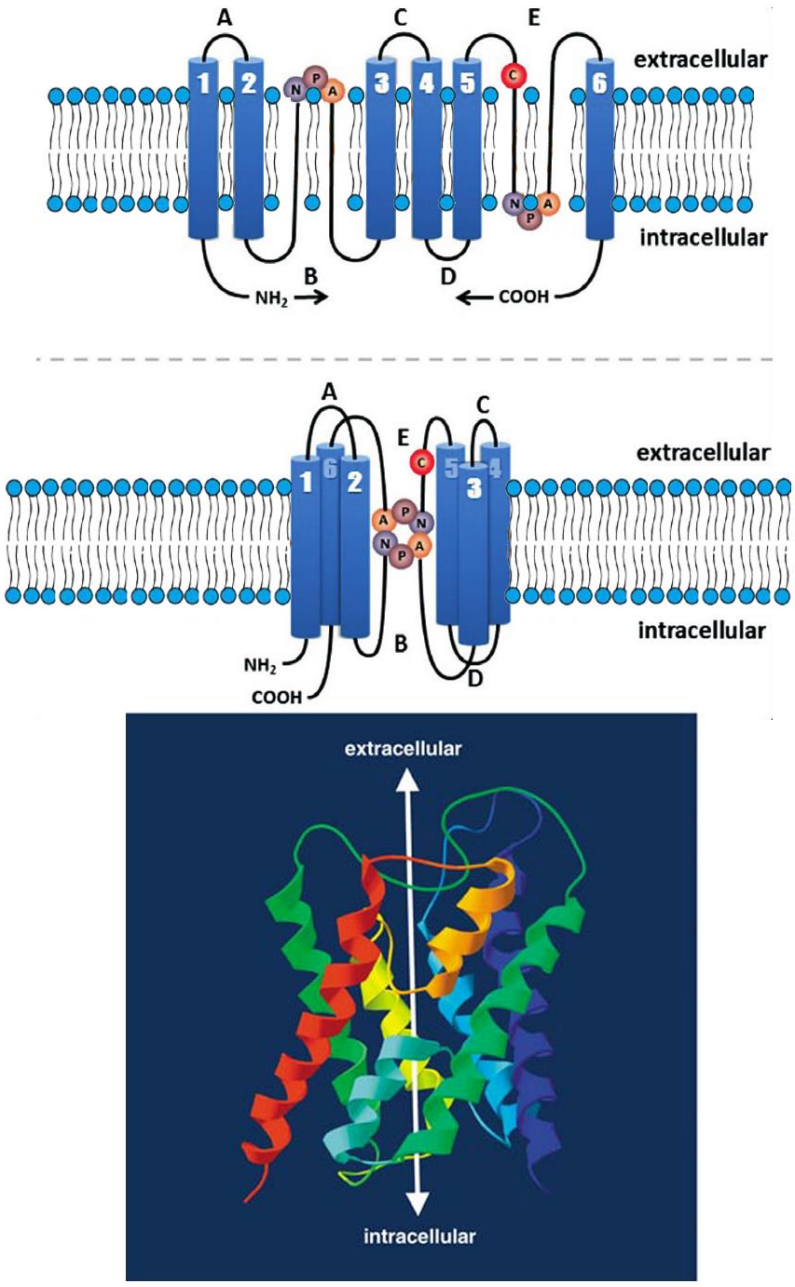

Figure 2. Hourglass model for the membrane topology of the AQP1 subunit. Top: Schematic representation of the folding of loops B and E; the loops overlap within the lipid bilayer to form a single aqueous pathway. Bottom: Ribbon model of the three-dimensional structure of the AQP1 subunit. Image adapted from reference [4].

I-quartet self-assembled AWC system mimic selective filter of AQP. The synthon of I-quartet consists of a histamine fragment, a mono-urea linkage and an alkyl tail. The histamine fragment form the hydrophilic core of I-quartet channel, which contributes to the formation of tetrameric I-quartet architectures, while mono-urea linkage aims to form tubular channels structure due to H-bonding. The alkyl tails promote better incorporation of the structure into the lipid membrane and also increase the channel stability (**Figure 3**).

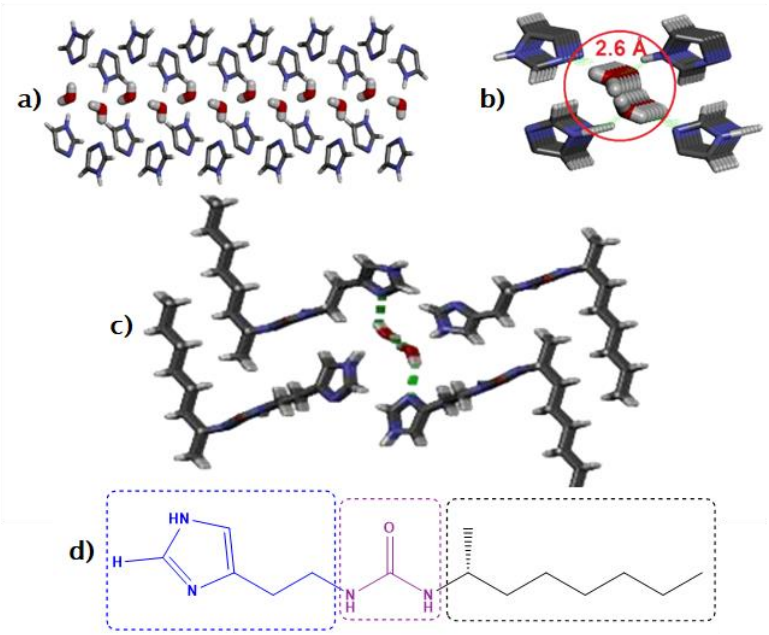

Figure 3. Side (a) and top (b) views of I-quartet water/proton channels that self-assemble into tetrameric tubular architectures confining dipolar oriented water wires. Top view (c) of water molecules confining I-quartet channel in stick representations consisting of S-Octylureido-ethylimidazole. Structure (d) of alkylureido-ethylimidazole compound by example of S-Octylureido-ethylimidazole: blue - Histamine fragment; purple – mono-urea linkage and black - alkyl substituents. Image adapted from reference [18].

It was decided to use I-quartet channels as a platform for developing new types of hybrid artificial channels by combination of I-quartets with compounds which have similar structures with hydrophobic properties. The main principle of self-assembly present in Imidazole-quartet systems was kept since the urea fragment plays an important role in supramolecular

organization and allows connection between I-quartets and hydrophobic alkylureido derivatives. In this case, Imidazole-quartet performs 2 functions: I) frame of bi-component systems due to tetrameric architecture and presence of urea fragments and II) selective filter by H-binding of water molecules and narrow pore size within 2.8 Å, while hydrophobic alkylurea units contribute to the friction-less passage of H_2O molecules. The ideal case of hybrid alkylureido derivative channels formation will be a configuration with sequences of I-quartets and hydrophobic derivatives that would allow the formation of stable pores with high water permeability and water selectivity.

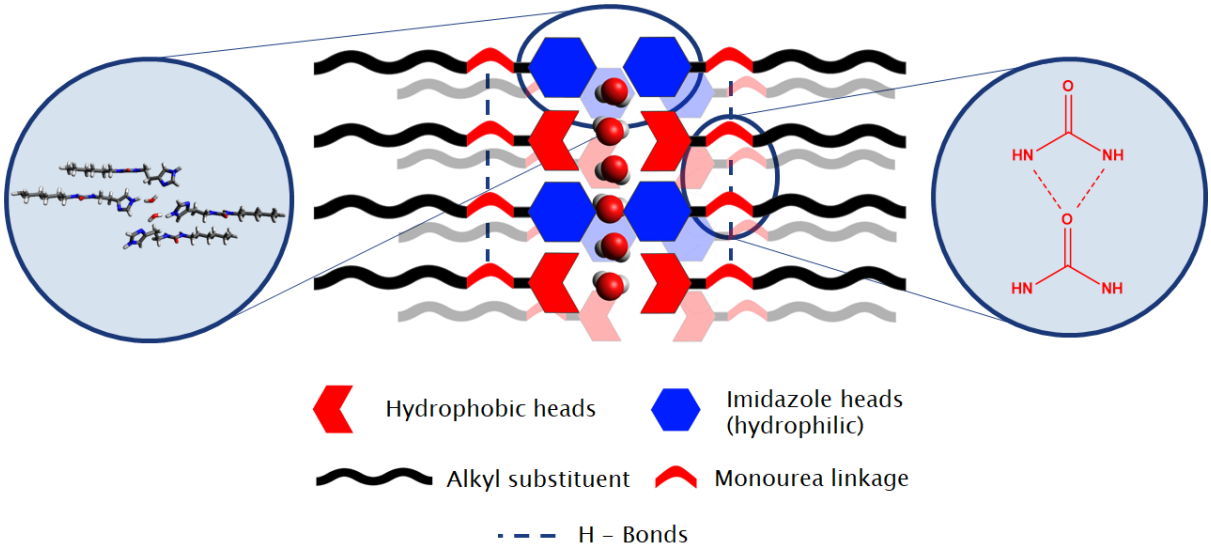

Figure 4. Design of bi-component self-assembled systems. I-quartet plays the role of selective filter and frame of channel, while hydrophobic alkylureido derivative is responsible for friction-less translocation of water molecules.

Sixteen compounds were synthesized for the study presented here (Scheme 1), which are divided in 2 groups according to their alkyl tail length, 8 compounds are bearing hexyl and 8 of them octyl tails. They were synthesized through a one-step reaction between hexyl or octyl isocyanates and different amines with hydrophobic properties such as tyramine, tryptamine, serotonin, 6-aminobenzoimidazol, 2-aminobenzoimidazol, 2-(2-aminoethyl)pyridine, 4-(2-aminoethyl)pyridine, 4-(2-aminoethyl)benzenesulfonamide. The ^{1}H and ^{13}C NMR spectra

agree with the proposed formulas (supporting information). Obtained compounds were mixed with I-quartet channels (HC6 and HC8) in a 1:1 molar ratio in DMSO with same length of alkyl tails. Finally, we performed lipid bilayer transport measurements to evaluate their efficiency.

Scheme 1. Compounds S1−S8, used as synthons for self-assembled hybrid channels formation

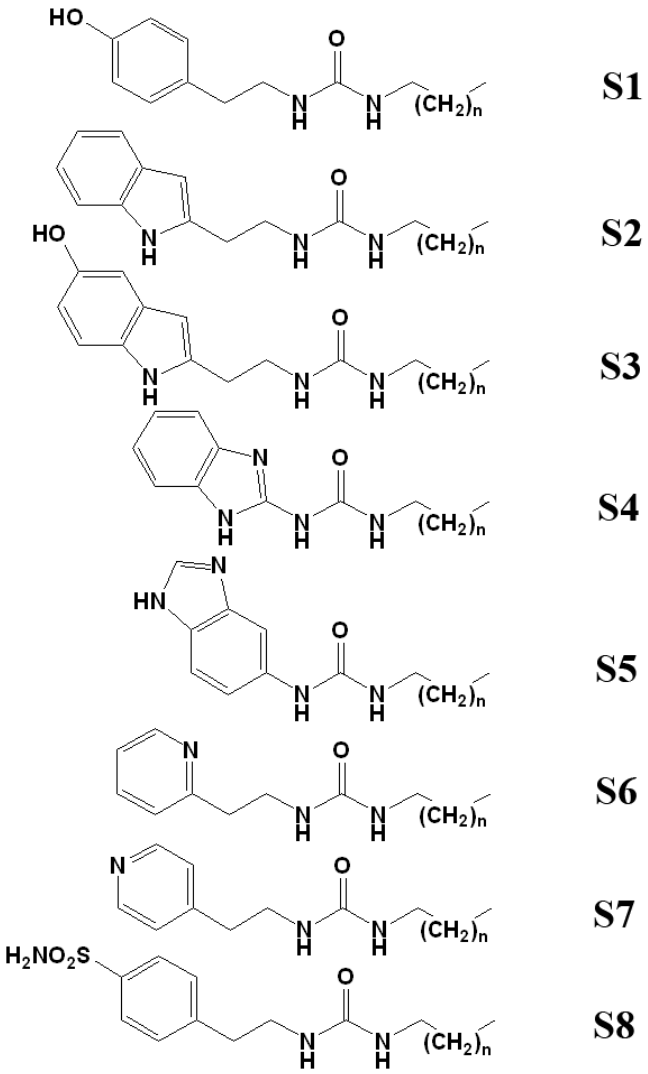

Transport experiments

Individual alkylureido and hybrid channels were reconstituted into phosphatidylcholine (PC) lipid vesicles (100 nm in diameter) in which channels were injected as an equimolar mixture of two compounds (in case of hybrid channels) into pre-formed liposomes with the aid of dimethylsulfoxide (DMSO). Then the vesicles were exposed to outwardly directed osmotic

pressure gradients (shrinking mode of the vesicles). Under hypertonic conditions driven by outwardly 10 mM Phosphate buffered saline (PBS) buffer solution (pH 6.4) 400 mM sucrose osmolyte, the shrinkage of the liposomes under osmotic gradients of 200 mOsm increased the light-scattering signal.

Analysis of stopped-flow experiments showed that some combinations of two compounds led to increasing water transport properties through the lipid membrane. For further research, it was decided to work with 8 systems which have positive changes of channel properties moving from individual compounds to combined systems: HC6/S3-6, HC6/S5-6, HC6-S6-8, HC6/S7-6, HC6/S8-6, HC8/S6-8, HC8/S7-8 and HC8/S8-8; the nomenclature of systems formed by name of corresponding imidazole-quartet (HC6 or HC8) and hydrophobic ureido derivative, where number '6' or '8' in the end displayed the length of alkyl chain, hexyl or octyl respectively. Comparison of individual compounds' and combined systems' transport abilities are presented at Figure 5. The most interesting results were found for systems formed by combination of HC6 and S5-6 compounds and combination of HC8 and S8-8. In the first case, the increasing of HC6/S5-6 system permeability was 9.5 times higher compared with HC6 alone and 2 times higher compared with S5-6 alone, giving a net water permeability of final system HC6/S5-6 of 21.8 μm/s (Figure 6b). Compound S5-6 is also an imidazole derivative as HC6, despite the fact that S5-6 has a benzene ring attached to the imidazole cycle, that brings hydrophobicity to the inner walls of the final system and, as a result, increases the water permeability through the lipid bilayer.

The system HC8/S8-8 showed the highest value of net water permeability from all series of tested systems, 33.2 μm/s, which is 33 times more than the HC8 net permeability (1.00 μm/s) and 1.33 times more than S8-8 (25 μm/s) (Figure 6c). Moreover, transition from compound with hexyl chain to compound having octyl chain improved the water transport ability of the system, which is clearly seen in the examples of systems HC6/S8-6 and HC8/S8-8: net water

permeability of HC6/S8-6 (hexyl derivatives system) was 4.83 µm/s and system HC8/S8-8 (octyl derivative system) showed 33.2 µm/s, 6.9 times more than for hexyl derivative. These results confirm the influence of the alkyl tails length on both the channel stability and transport properties.

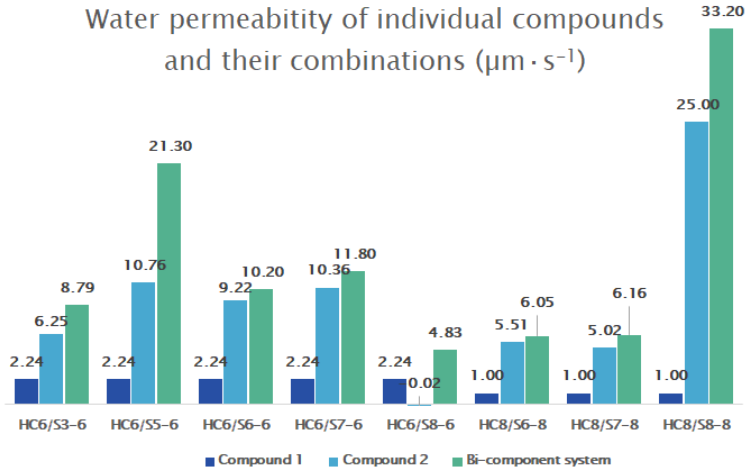

Figure 5. Comparison of net water permeability of individual compounds and combinations through lipid bilayer by using stopped-flow method (shrinking mode).

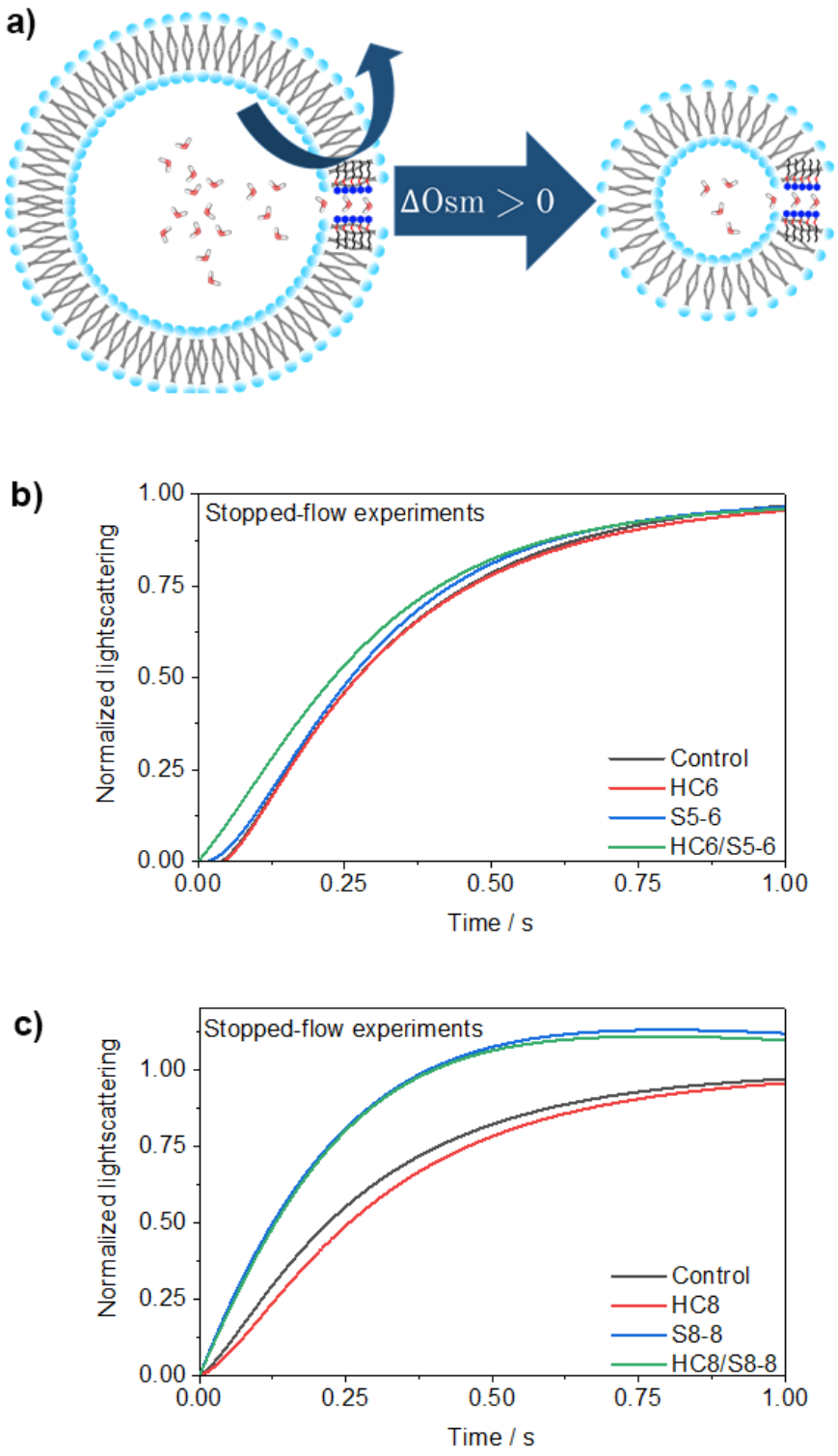

Figure 6. a) Schematic representation of principle of stopped-flow method (shrinking mode); stopped-flow light scattering traces of liposomes containing individual compounds and combination of HC6/S5-6 (b) and HC8/S8-8 (c), respectively.

Single channel permeability

Keeping in mind that Imidazole quartet plays the roles of frame and selective filter for bi-component combinations, we calculated the single channel permeability for each system. Two systems showed remarkable results for water transport per channel (Figure 7. The channel formed by the combination of HC6 and S5-6 compounds (imidazole and benzimidazole derivatives, respectively) is able to transport 52 million molecules per second, which is 4.8 times more compared with HC6 itself, and system HC8/S8-8 (combination for imidazole and benzosulfonamine derivatives) has a permeability of almost 82 million molecules per second or 16.7 times more than HC8 channel itself.

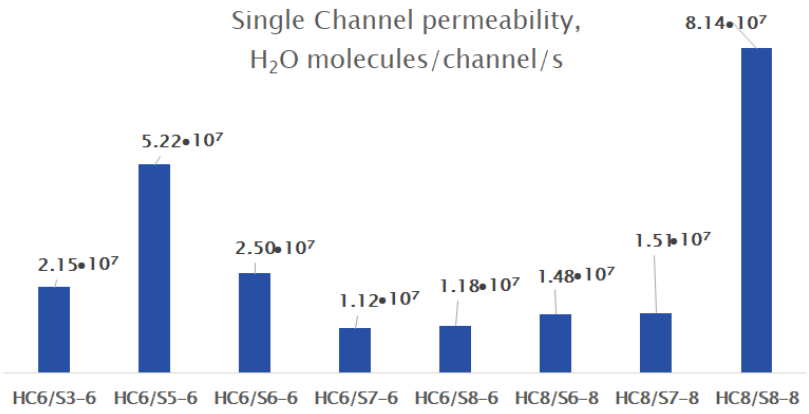

Figure 7. Comparison of single-channel permeability of synergistic combined channels

Cation transport experiments

Ions (Na^+ and K^+) transport activities across the bilayer membranes incorporating individual alkylureido derivatives and channels formed by combination of alkylureido derivatives reconstituted into phosphatidylcholine (PC) lipid vesicles (100 nm) at the same concentrations were assessed in water transport using standard 8-Hydroxypyrene-1,3,6-trisulfonic acid

trisodium salt (HPTS) fluorescence assay (Figure 8). Applying a gradient of pH between the inner and the outer media of vesicles initiates migration of ions through the channels. No transport activity was observed for combinations, which indicated that those channels were able to efficiently exclude alkali cations, which represents an ideal case for AWCs.

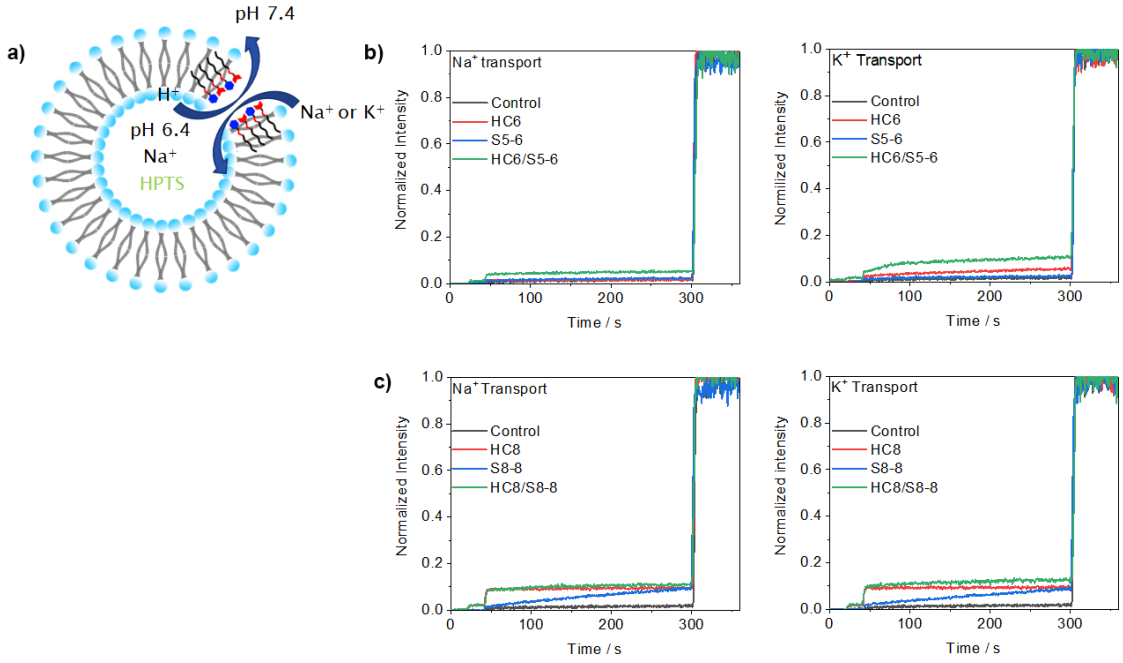

Figure 8. Schematic representation of antiport M^+/H^+ mechanisms (a) together with comparison of Na^+ and K^+ transport activities expressed as normalized fluorescence intensity of 5 mM of individual compounds or 5mM / 5mM for combined systems HC6/S5-6 (b) and HC8/S8-8 (c) in the extra-vesicular media containing 100 mM NaCl or KCl.

CONCLUSION

This work describes novel synthetic routes for obtaining a combination of hybrid artificial water channels by synergistic combination of alkyl ureido derivatives that induce the selective transport of water against ions. Water permeability (net permeability and single channel permeability) for selected bi-component systems are multiplying times higher compared to

single compound systems. Despite the fact that some compounds exhibit ionic activity individually, the systems of two compounds do not show any ion transport. The new class of hybrid Artificial Water Channels synthesized and presented in this work could be used to prepare novel biomimetic RO membranes that might form the basis for next-generation water purification technology with less energy consumption and better performances.

References

1. Ball, P., Water as an active constituent in cell biology. *Chemical reviews* **2008,** *108* (1), 74-108.

2. Zhong, D.; Pal, S. K.; Zewail, A. H., Biological water: A critique. *Chemical Physics Letters* **2011,** *503* (1-3), 1-11.

3. Pal, S. K.; Zewail, A. H., Dynamics of water in biological recognition. *Chemical Reviews* **2004,** *104* (4), 2099-2124.

4. Agre, P., Aquaporin water channels (Nobel lecture). *Angewandte Chemie International Edition* **2004,** *43* (33), 4278-4290.

5. Preston, G. M.; Carroll, T. P.; Guggino, W. B.; Agre, P., Appearance of water channels in Xenopus oocytes expressing red cell CHIP28 protein. *Science* **1992,** *256* (5055), 385-387.

6. Noda, Y.; Sohara, E.; Ohta, E.; Sasaki, S., Aquaporins in kidney pathophysiology. *Nature Reviews Nephrology* **2010,** *6* (3), 168-178.

7. Werber, J. R.; Osuji, C. O.; Elimelech, M., Materials for next-generation desalination and water purification membranes. *Nature Reviews Materials* **2016,** *1* (5), 1-15.

8. Park, H. B.; Kamcev, J.; Robeson, L. M.; Elimelech, M.; Freeman, B. D., Maximizing the right stuff: The trade-off between membrane permeability and selectivity. *Science* **2017,** *356* (6343).

9. Shen, Y.-x.; Saboe, P. O.; Sines, I. T.; Erbakan, M.; Kumar, M., Biomimetic membranes: A review. *Journal of Membrane Science* **2014,** *454*, 359-381.

10. Hélix-Nielsen, C., Biomimetic membranes as a technology platform: Challenges and opportunities. *Membranes* **2018,** *8* (3), 44.

11. Barboiu, M., Artificial water channels. *Angewandte Chemie International Edition* **2012,** *51* (47), 11674-11676.

12. Barboiu, M.; Gilles, A., From natural to bioassisted and biomimetic artificial water channel systems. *Accounts of chemical research* **2013,** *46* (12), 2814-2823.

13. Barboiu, M.; Le Duc, Y.; Gilles, A.; Cazade, P.-A.; Michau, M.; Legrand, Y. M.; Van Der Lee, A.; Coasne, B.; Parvizi, P.; Post, J., An artificial primitive mimic of the Gramicidin-A channel. *Nature communications* **2014,** *5* (1), 1-8.

14. Barboiu, M., Artificial water channels–incipient innovative developments. *Chemical Communications* **2016,** *52* (33), 5657-5665.

15. Song, W.; Lang, C.; Shen, Y.-x.; Kumar, M., Design considerations for artificial water channel–based membranes. *Annual Review of Materials Research* **2018,** *48*, 57-82.

16. Song, W.; Tu, Y.-M.; Oh, H.; Samineni, L.; Kumar, M., Hierarchical optimization of high-performance biomimetic and bioinspired membranes. *Langmuir* **2018,** *35* (3), 589-607.

17. Horner, A.; Zocher, F.; Preiner, J.; Ollinger, N.; Siligan, C.; Akimov, S. A.; Pohl, P., The mobility of single-file water molecules is governed by the number of H-bonds they may form with channel-lining residues. *Science advances* **2015,** *1* (2), e1400083.

18. Licsandru, E.; Kocsis, I.; Shen, Y.-x.; Murail, S.; Legrand, Y.-M.; Van Der Lee, A.; Tsai, D.; Baaden, M.; Kumar, M.; Barboiu, M., Salt-excluding artificial water channels exhibiting enhanced dipolar water and proton translocation. *Journal of the American Chemical Society* **2016,** *138* (16), 5403-5409.

19. Tunuguntla, R. H.; Henley, R. Y.; Yao, Y.-C.; Pham, T. A.; Wanunu, M.; Noy, A., Enhanced water permeability and tunable ion selectivity in subnanometer carbon nanotube porins. *Science* **2017,** *357* (6353), 792-796.

20. Freger, V., Selectivity and polarization in water channel membranes: lessons learned from polymeric membranes and CNTs. *Faraday discussions* **2018,** *209*, 371-388.

21. Li, Y.; Li, Z.; Aydin, F.; Quan, J.; Chen, X.; Yao, Y.-C.; Zhan, C.; Chen, Y.; Pham, T. A.; Noy, A., Water-ion permselectivity of narrow-diameter carbon nanotubes. *Science advances* **2020,** *6* (38), eaba9966.

22. Wang, Q.; Zhong, Y.; Miller, D. P.; Lu, X.; Tang, Q.; Lu, Z.-L.; Zurek, E.; Liu, R.; Gong, B., Self-assembly and molecular recognition in water: tubular stacking and guest-templated discrete assembly of water-soluble, shape-persistent macrocycles. *Journal of the American Chemical Society* **2020,** *142* (6), 2915-2924.

23. Chen, L.; Si, W.; Zhang, L.; Tang, G.; Li, Z.-T.; Hou, J.-L., Chiral selective transmembrane transport of amino acids through artificial channels. *Journal of the American Chemical Society* **2013,** *135* (6), 2152-2155.

24. Shen, Y.-x.; Si, W.; Erbakan, M.; Decker, K.; De Zorzi, R.; Saboe, P. O.; Kang, Y. J.; Majd, S.; Butler, P. J.; Walz, T., Highly permeable artificial water channels that can self-assemble into two-dimensional arrays. *Proceedings of the National Academy of Sciences* **2015,** *112* (32), 9810-9815.

25. Song, W.; Joshi, H.; Chowdhury, R.; Najem, J. S.; Shen, Y.-x.; Lang, C.; Henderson, C. B.; Tu, Y.-M.; Farell, M.; Pitz, M. E., Artificial water channels enable fast and selective water permeation through water-wire networks. *Nature nanotechnology* **2020,** *15* (1), 73-79.

26. Strilets, D.; Fa, S.; Hardiagon, A.; Baaden, M.; Ogoshi, T.; Barboiu, M., Biomimetic Approach for Highly Selective Artificial Water Channels Based on Tubular Pillar [5] arene Dimers. *Angewandte Chemie International Edition* **2020,** *59* (51), 23213-23219.

27. Shen, J.; Ye, R.; Romanies, A.; Roy, A.; Chen, F.; Ren, C.; Liu, Z.; Zeng, H., Aquafoldmer-based aquaporin-like synthetic water channel. *Journal of the American Chemical Society* **2020,** *142* (22), 10050-10058.

28. Di Yuan, Y.; Dong, J.; Liu, J.; Zhao, D.; Wu, H.; Zhou, W.; Gan, H. X.; Tong, Y. W.; Jiang, J.; Zhao, D., Porous organic cages as synthetic water channels. *Nature communications* **2020,** *11* (1), 1-10.

29. Hu, X.-B.; Chen, Z.; Tang, G.; Hou, J.-L.; Li, Z.-T., Single-molecular artificial transmembrane water channels. *Journal of the American Chemical Society* **2012,** *134* (20), 8384-8387.

30. Yan, Z.-J.; Wang, D.; Ye, Z.; Fan, T.; Wu, G.; Deng, L.; Yang, L.; Li, B.; Liu, J.; Ma, T., Artificial Aquaporin That Restores Wound Healing of Impaired Cells. *Journal of the American Chemical Society* **2020,** *142* (37), 15638-15643.

31. Huang, L.-B.; Hardiagon, A.; Kocsis, I.; Jegu, C.-A.; Deleanu, M.; Gilles, A.; van der Lee, A.; Sterpone, F.; Baaden, M.; Barboiu, M., Hydroxy Channels–Adaptive Pathways for Selective Water Cluster Permeation. *Journal of the American Chemical Society* **2021,** *143* (11), 4224-4233.

32. Kocsis, I.; Sun, Z.; Legrand, Y. M.; Barboiu, M., Artificial water channels—Deconvolution of natural aquaporins through synthetic design. *NPJ Clean Water* **2018,** *1* (1), 1-11.

33. Preston, G. M.; Agre, P., Isolation of the cDNA for erythrocyte integral membrane protein of 28 kilodaltons: member of an ancient channel family. *Proceedings of the National Academy of Sciences* **1991,** *88* (24), 11110-11114.

34. Jung, J. S.; Preston, G. M.; Smith, B. L.; Guggino, W. B.; Agre, P., Molecular structure of the water channel through aquaporin CHIP. The hourglass model. *Journal of Biological Chemistry* **1994,** *269* (20), 14648-14654.

Supporting Information for

SYNERGETIC SELF-ASSEMBLY OF BI-COMPONENT ALKYLUREIDO SYSTEMS INTO ARTIFICIAL WATER CHANNELS

Dmytro STRILETS,[†],and Mihail Barboiu*,[†]
†Institut Europeen des Membranes, Adaptive Supramolecular Nanosystems Group, University of Montpellier, ENSCM-CNRS, UMR5635, Place E. Bataillon CC047, 34095 Montpellier, France

Corresponding Author
*mihail-dumitru.barboiu@umontpellier.fr

General

Reagents were purchased from Sigma Aldrich and used as received. 1H NMR spectra were recorded on an ARX 300 MHz Bruker. Chemical shifts are reported as δ values (ppm) with DMSO-d6 1H NMR δ 2.50, solvent peak as an internal standard.

Synthesis

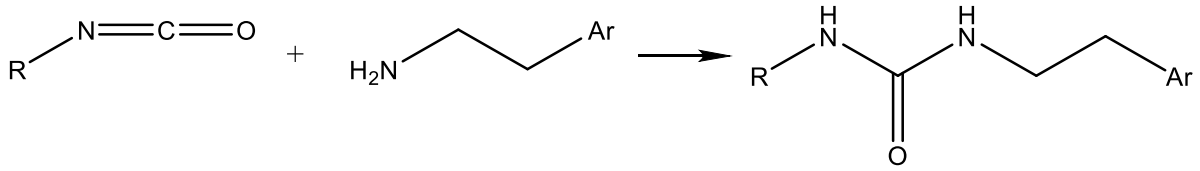

Scheme S1. General synthesis of alkylureido derivatives.

All compounds have been synthesized following the general scheme shown above in S1.

1.5 mmol of corresponding arylethyleneamine was dissolved in 20 mL of DMF, then equimolar amount of hexyl or octyl isocyanate was added dropwise to reaction solution. Reaction was left overnight at room temperature. 30 mL of DI water was added to quench the reaction. Obtained precipitate was filtrated, washed with DI water and dried under vacuum. Obtained alkylureido derivatives were purified by recrystallization from Dichloromethane (DMC)

Table S1. Chemical structure, formulas and molar mass of synthesized compounds.

Chemical structure	Name	Formula	MW, g/mol
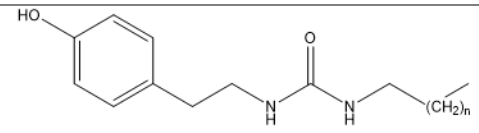	**(n = 4)** 1-(4-hydroxyphenethyl)-3-hexylurea **S1-6**	$C_{15}H_{24}N_2O_2$	264.36
	(n = 6) 1-(4-hydroxyphenethyl)-3-octylurea **S1-8**	$C_{17}H_{28}N_2O_2$	292.42
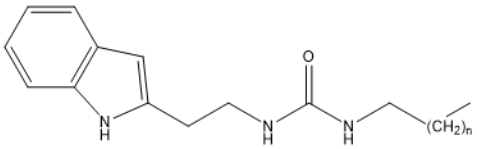	**(n = 4)** 1-(2-(1H-indol-2-yl)ethyl)-3-hexylurea **S2-6**	$C_{17}H_{25}N_3O$	287.40
	(n = 6) 1-(2-(1H-indol-2-yl)ethyl)-3-octylurea **S2-8**	$C_{19}H_{29}N_3O$	315.46
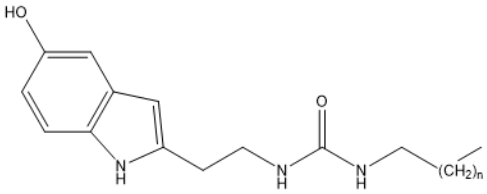	**(n = 4)** 1-(2-(5-hydroxy-1H-indol-2-yl)ethyl)-3-hexylurea **S3-6**	$C_{17}H_{25}N_3O_2$	303.40
	(n = 6) 1-(2-(5-hydroxy-1H-indol-2-yl)ethyl)-3-octylurea **S3-8**	$C_{19}H_{29}N_3O_2$	331.46
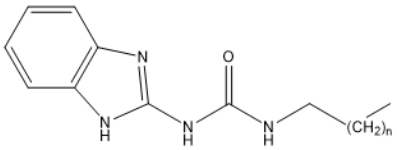	**(n = 4)** 1-(1H-benzo[d]imidazol-2-yl)-3-hexylurea **S4-6**	$C_{14}H_{20}N_4O$	260.34
	(n = 6) 1-(1H-benzo[d]imidazol-2-yl)-3-octylurea **S4-8**	$C_{16}H_{24}N_4O$	288.40
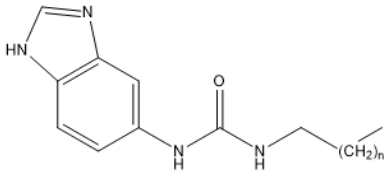	**(n = 4)** 1-(1H-benzo[d]imidazol-5-yl)-3-hexylurea **S5-6**	$C_{14}H_{20}N_4O$	260.34
	(n = 6) 1-(1H-benzo[d]imidazol-5-yl)-3-octylurea **S5-8**	$C_{16}H_{24}N_4O$	288.40
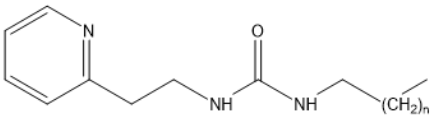	**(n = 4)** 1-(2-(pyridin-2-yl)ethyl)-3-hexylurea **S6-6**	$C_{14}H_{23}N_3O$	249.35
	(n = 6) 1-(2-(pyridin-2-yl)ethyl)-3-octylurea **S6-8**	$C_{16}H_{27}N_3O$	277.41
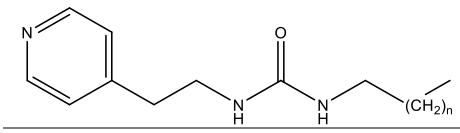	**(n = 4)** 3-(2-(pyridin-4-yl)ethyl)-3-hexylurea **S7-6**	$C_{14}H_{23}N_3O$	249.36
	(n = 6) 3-(2-(pyridin-4-yl)ethyl)-3-octylurea **S7-8**	$C_{16}H_{27}N_3O$	277.41
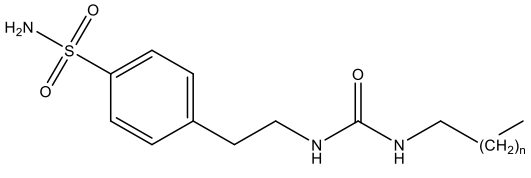	**(n = 4)** 4-(2-(3-hexylureido)ethyl)benzenesulfonamide **S8-6**	$C_{15}H_{25}N_3O_3S$	327.44
	(n = 6) 4-(2-(3-octylureido)ethyl)benzenesulfonamide **S8-8**	$C_{17}H_{29}N_3O_3S$	355.50

S1-6 (1-(4-hydroxyphenethyl)-3-hexylurea) **^{1}H-RMN (DMSO-d6, 400 MHz)** δ (ppm) = 0,87 (t, 3H, **CH$_3$**CH$_2$); 1,27-1.35 (m, 8H, CH$_3$**(CH$_2$)$_4$**CH$_2$); 2,54 (t, 2H, NH**CH$_2$**CH$_2$); 2,96 (q, 2H, CH$_2$**CH$_2$**NH); 3,12 (q, 2H, **CH$_2$**CH$_2$NH) 5,69 (t, 1H, **NH**CH$_2$);5.81 (t, 1H, **NH**CH$_2$); 6,68 (dt, 2 H, **CH** benzene ring); 6,97 (dt,1H, **CH** benzene ring); 9.15 (s, **1H**, **HO**-Ph); **^{13}C NMR (DMSO-*d6*, 200 MHz)** δ (ppm)= 14.38 (*CH$_3$*), 22.54, 26.46, 30.32, 31.57 (4x*CH$_2$*), 35.67 (*CH$_2$*NH), 40.01 (*C*H$_2$-Ph, among DMSO pick), 41.71 (*CH$_2$*NH), 115.53 (2x*CH* Benzene ring), 130.01 (2x*CH* Benzene ring) 130.26 (*C*-CH$_2$, Benzene ring), 155.67 (*C*-OH, Benzene ring) 158.74 (*C*=O).

S1-8 (1-(4-hydroxyphenethyl)-3-octylurea) **^{1}H-RMN (DMSO-d6, 400 MHz)** δ (ppm) = 0,86 (t, 3H, **CH$_3$**CH$_2$); 1,25-1.35 (m, 12H, CH$_3$**(CH$_2$)$_6$**CH$_2$); 2,54 (t, 2H, **NH**CH$_2$CH$_2$) ; 2,95 (q, 2H, **CH$_2$**CH$_2$NH) ; 3,14 (q, 2H, CH$_2$**CH$_2$**NH) 5,69 (t, 1H, **NH**CH$_2$) ;5.81 (t, 1H, **NH**CH$_2$) ; 6,67 (dt,2H, CH benzene ring) ; 6,97 (dt,2H, CH benzene ring); 9,15 (s,1H, HO-Ph). **^{13}C NMR (DMSO-*d6*, 100 MHz)** δ (ppm)= 14.45 (*CH$_3$*), 22.58, 26.87, 29.20, 29.26, 30.49, 31.73 (6x*CH$_2$*), 35.82 (*CH$_2$*NH), 40.42 (*C*H$_2$-Ph, among DMSO pick), 41.71 (*CH$_2$*NH), 115.53 (2x*CH* Benzene ring), 129.97 (2x*CH* Benzene ring) 130.24 (*C*-CH$_2$, Benzene ring), 156.01(*C*-OH, Benzene ring) 159.16 (*C*=O).

S2-6 (1-(2-(1H-indol-2-yl)ethyl)-3-hexylurea) **^{1}H-RMN (DMSO-d6, 400 MHz)** δ (ppm) = 0,87 (t, 3H, **CH$_3$**CH$_2$) ; 1,25-1.36 (m, 8H, CH$_3$(**CH$_2$**)$_4$CH$_2$) ; 2,77 (t, 2H, NHCH$_2$CH$_2$) ; 2,96 (q, 2H, CH$_2$CH$_2$NH) ; 3,28 (q, 2H, CH$_2$CH$_2$NH) 5,77 (t, 1H, NHCH$_2$) ;5.83 (t, 1H, NHCH$_2$) ; 6,97 (t,1H,**CH** benzene ring); 7,06 (t,1H,**CH** benzene ring) 7,12 (ds,1H,C**CH**C pyrrole ring) 7,33 (d,1H,CH benzene ring); 7,54 (d,1H,CH benzene ring) 10,78 (s, 1H, C**NH**C pyrrole ring). **^{13}C NMR (DMSO-*d6*, 100 MHz)** δ (ppm)= 14.39 (*CH$_3$*), 22.54, 26.44, 26.48, 30.35 (4x*CH$_2$*), 31.48 (*CH$_2$*NH), 40.11 (*C*H$_2$-Ph, among DMSO pick), 40.59 (*CH$_2$*NH), 111.82 (*CH*, pyrrole ring), 112.46 (*CH*, Benzene ring), 118.72 (*CH*, Benzene ring), 118.83 (*CH*, Benzene ring), 121.43 (*CH*, Benzene ring), 123.08 (*C*, Benzene ring), 127.68 (*C*, Benzene ring), 136.66 (*C*-CH$_2$, pyrrole ring), 158.81 (*C*=O).

S2-8 (1-(2-(1H-indol-2-yl)ethyl)-3-octylurea) **^{1}H-RMN (DMSO-d6, 400 MHz)** δ (ppm) = 0,86 (t, 3H, **CH$_3$**CH$_2$) ; 1,25-1.36 (m, 12H, CH$_3$(**CH$_2$**)$_6$CH$_2$) ; 2,78 (t, 2H, NH**CH$_2$**CH$_2$) ; 2,96 (q, 2H, CH$_2$**CH$_2$**NH); 3,28 (q, 2H, **CH$_2$**CH$_2$NH) 5,77 (t, 1H, NHCH$_2$) ;5.82 (t, 1H, NHCH$_2$) ; 6,97 (t,1H,**CH** benzene ring); 7,06 (t,1H,**CH** benzene ring) 7,12 (ds,1H,C**CH**C pyrrole ring) 7,33 (d,1H,CH benzene ring); 7,54 (d,1H,CH benzene ring) 10,80 (s, 1H, C**NH**C pyrrole ring). **^{13}C NMR (DMSO-*d6*, 100 MHz)** δ (ppm)= 14.46 (*CH$_3$*), 22.59, 26.64, 26.67, 26.90, 29.21,

29.27 (6x*CH₂*), 30.54 (*CH₂*NH), 31.74 (*C*H₂-Ph, among DMSO pick), 40.55 (*CH₂*NH, among DMSO pick), 111.79 (*CH*, pyrrole ring), 112.51 (*CH*, Benzene ring), 118.62 (*CH*, Benzene ring), 118.85 (*CH*, Benzene ring), 121.35 (*CH*, Benzene ring), 123.07 (*C*, Benzene ring), 127.75 (*C*, Benzene ring), 136.72 (*C*-CH₂, pyrrole ring), 158.54 (*C*=O).

S3-6 (1-(2-(5-hydroxy-1H-indol-2-yl)ethyl)-3-hexylurea) **^{1}H-RMN (DMSO-d6, 400 MHz)** δ (ppm) = 0,87 (t, 3H, **CH₃**CH₂) ; 1,25-1.36 (m, 8H, CH₃(**CH₂**)₄CH₂) ; 2,68 (t, 2H, NHCH₂CH₂) ; 2,97 (q, 2H, CH₂**CH₂**NH) ; 3,24 (q, 2H, **CH₂**CH₂NH) 5,75 (t, 1H, **NH**CH₂) ;5.82 (t, 1H, **NH**CH₂) ; 6,59 (dd,1H,**CH** benzene ring); 6,83 (d,1H,**CH** benzene ring) 7,01 (d,1H,CH benzene ring) 7,12 (ds,1H,C**CH**C pyrrole ring); 8,57 (s,1H, **HO**-Ph); 10,78 (s, 1H, C**NH**C pyrrole ring). **^{13}C NMR (DMSO-*d6*, 100 MHz)** δ (ppm)= 14.39 (*CH₃*), 22.54, 26.49, 26.55, 30.34 (4x*CH₂*), 31.47 (*CH₂*NH), 40.11 (*C*H₂-Ph, among DMSO pick), 40.37 (*CH₂*NH), 102.74 (*CH*, pyrrole ring), 111.46 (*CH*, Benzene ring), 111.69 (*CH*, Benzene ring), 112.17 (*CH*, Benzene ring), 123.60 (*CH*, Benzene ring), 128.33 (*C*, Benzene ring), 131.28 (*C*-CH₂, pyrrole ring), 150.46(*C*-OH, Benzene ring), 158.80 (*C*=O).

S3-8 (1-(2-(5-hydroxy-1H-indol-2-yl)ethyl)-3-octylurea) **^{1}H-RMN (DMSO-d6, 400 MHz)** δ (ppm) = 0,86 (t, 3H, **CH₃**CH₂) ; 1,25-1.37 (m, 12H, CH₃(**CH₂**)₆CH₂) ; 2,68 (t, 2H, NHCH₂CH₂) ; 2,97 (q, 2H, CH₂**CH₂**NH) ; 3,24 (q, 2H, **CH₂**CH₂NH) 5,75 (t, 1H, **NH**CH₂) ;5.82 (t, 1H, **NH**CH₂) ; 6,59 (dd,1H,**CH** benzene ring); 6,83 (d,1H,**CH** benzene ring) 7,01 (d,1H,CH benzene ring) 7,11 (ds,1H,C**CH**C pyrrole ring); 8,56 (s,1H, **HO**-Ph); 10,47 (s, 1H, C**NH**C pyrrole ring). **^{13}C NMR (DMSO-*d6*, 100 MHz)** δ (ppm)= 14.42 (*CH₃*), 22.54, 26.56, 26.82, 29.13, 29.19, 30.37 (6x*CH₂*), 31.68 (*CH₂*NH), 40.11 (*C*H₂-Ph, among DMSO pick), 40.38 (*CH₂*NH), 102.74 (*CH*, pyrrole ring), 111.46 (*CH*, Benzene ring), 111.69 (*CH*, Benzene ring), 112.17 (*CH*, Benzene ring), 123.59 (*CH*, Benzene ring), 128.33 (*C*, Benzene ring), 131.28 (*C*-CH₂, pyrrole ring), 150.46(*C*-OH, Benzene ring), 158.80 (*C*=O).

S4-6 (1-(1H-benzo[d]imidazol-2-yl)-3-hexylurea) **^{1}H-RMN (DMSO-d6, 400 MHz)** δ (ppm) = 0,88 (t, 3H, **CH₃**CH₂); 1,26-1.36 (m, 8H, CH₃(**CH₂**)₆CH₂); 1,48 (q, 2H, CH₂**CH₂**NH) ; 3,17 (q, 2H, **CH₂**CH₂NH) 6,09 (t, 1H, **NH**CH₂); 7,35 (m, 4H,**CH** benzene ring); 6,83 (d,1H,**CH** benzene ring) 9.74 (s, 1H, **NH**C); 11,45 (s, 1H, C**NH**C imidazole ring). **^{13}C NMR (DMSO-*d6*, 100 MHz)** δ (ppm)= 14.36 (*CH₃*), 22.50, 26.39, 29.83, 31.35 (4x*CH₂*), 40.20 (*CH₂*NH, among DMSO pick), 111.35 (2x*CH*, Benzene ring), 116.41 (2x*CH*, Benzene ring), 121.16 (2x*CH*, Benzene ring), 148.73 (*C*-NH, Imidazole ring), 154.73 (*C*=O).

S4-8 (1-(1H-benzo[d]imidazol-2-yl)-3-octylurea) **^{1}H-RMN (DMSO-d6, 400 MHz)** δ (ppm) = 0,88 (t, 3H, **CH$_3$**CH$_2$); 1,26-1.36 (m, 12H, CH$_3$(**CH$_2$**)$_6$CH$_2$); 1,48 (q, 2H, CH$_2$**CH$_2$**NH) ; 3,17 (q, 2H, **CH$_2$**CH$_2$NH) 6,09 (t, 1H, **NH**CH$_2$); 7,35 (m, 4H,**CH** benzene ring); 6,83 (d,1H,**CH** benzene ring) 9.74 (s, 1H, **NH**C); 11,45 (s, 1H, C**NH**C imidazole ring). **^{13}C NMR (DMSO-*d6*, 100 MHz)** δ (ppm)= 14.36 (*CH$_3$*), 22.50, 26.39, 29.08, 29.83, 31.35 (6x*CH$_2$*), 40.19 (*CH$_2$*NH, among DMSO pick), 111.35 (2x*CH*, Benzene ring), 116.41 (2x*CH*, Benzene ring), 121.16 (2x*CH*, Benzene ring), 148.73 (*C*-NH, Imidazole ring), 154.73 (*C*=O).

S5-6 (1-(1H-benzo[d]imidazol-5-yl)-3-hexylurea) **^{1}H-RMN (DMSO-d6, 400 MHz)** δ (ppm) = 0,88 (t, 3H, **CH$_3$**CH$_2$); 1,28-1.30 (m, 6H, CH$_3$(**CH$_2$**)$_3$CH$_2$) ; 1,43 (t, 2H, NH**CH$_2$**CH$_2$) ; 3,08 (q, 2H, **CH$_2$**CH$_2$NH) ; 6,05 (t, 1H, **NH**CH$_2$) ;6.98 (d,1H,**CH** benzene ring); 7,43 (d,1H,**CH** benzene ring); 7,82 (s,1H,**CH** benzene ring) 8,05 (s,1H,CH benzene ring) 8,35 (s, 1H, **NH**C); 12,22 (s, 1H, C**NH**C imidazole ring). **^{13}C NMR (DMSO-*d6*, 100 MHz)** δ (ppm)= 14.39 (*CH$_3$*), 22.54, 26.47, 30.17, 31.46 (4x*CH$_2$*), 41.11 (*CH$_2$*NH, among DMSO pick), 100.87 (*CH*, Benzene ring), 114.11 (*CH*, Benzene ring), 119.13 (*CH*, Benzene ring), 133.74 (*C*-NH, Benzene ring), 136.13 (*C*, Benzene/Imidazole ring), 138.05 (*C*, Benzene/Imidazole ring), 141.54 (*CH*, Imidazole ring), 154.73 (*C*=O).

S5-8 (1-(1H-benzo[d]imidazol-5-yl)-3-octylurea) **^{1}H-RMN (DMSO-d6, 400 MHz)** δ (ppm) = 0,88 (t, 3H, **CH$_3$**CH$_2$); 1,28-1.30 (m, 10H, CH$_3$(**CH$_2$**)$_5$CH$_2$); 1,43 (t, 2H, NH**CH$_2$**CH$_2$); 3,08 (q, 2H, **CH$_2$**CH$_2$NH) ; 6,05 (t, 1H, **NH**CH$_2$);6.98 (d,1H,**CH** benzene ring); 7,43 (d,1H,**CH** benzene ring); 7,82 (s,1H,**CH** benzene ring); 8,05 (s,1H,CH benzene ring) 8,35 (s, 1H, **NH**C); 12,22 (s, 1H, C**NH**C imidazole ring).**^{13}C NMR (DMSO-*d6*, 100 MHz)** δ (ppm)= 14.39 (*CH$_3$*), 22.54, 26.47, 30.05, 30.17, 31.46 (6x*CH$_2$*), 41.11 (*CH$_2$*NH, among DMSO pick), 100.87 (*CH*, Benzene ring), 114.11 (*CH*, Benzene ring), 119.13 (*CH*, Benzene ring), 133.74 (*C*-NH, Benzene ring), 136.13 (*C*, Benzene/Imidazole ring), 138.05 (*C*, Benzene/Imidazole ring), 141.54 (*CH*, Imidazole ring), 154.73 (*C*=O).

S6-6 (1-(2-(pyridin-2-yl)ethyl)-3-hexylurea) **^{1}H-RMN (DMSO-d6, 400 MHz)** δ (ppm) = 0,86 (t, 3H, **CH$_3$**CH$_2$) ; 1,25-1.37 (m, 8H, CH$_3$(**CH$_2$**)$_4$CH$_2$) ; 2,82 (t, 2H, NHCH$_2$CH$_2$) ; 2,95 (q, 2H, CH$_2$**CH$_2$**NH) ; 3,36 (q, 2H, **CH$_2$**CH$_2$NH) 5,79 (t, 1H, **NH**CH$_2$) ;5.84 (t, 1H, **NH**CH$_2$) ; 7,22 (m,2H,**CH** pyridine ring); 7,70 (td,1H,**CH** pyridine ring) 8,49 (dq,1H,CH pyridine ring). **^{13}C NMR (DMSO-*d6*, 100 MHz)** δ (ppm)= 14.38 (*CH$_3$*), 22.53, 26.45, 30.29, 31.46 (4x*CH$_2$*), 38.57 (*CH$_2$*NH), 40.03 (*C*H$_2$-Py, among DMSO pick), 40.20 (*CH$_2$*NH, among DMSO pick),

122.02 (*CH*, pyridine ring), 123.78 (*CH*, pyridine ring), 137.12 (*CH*, pyridine ring), 149.38 (*C*-N, pyridine ring), 158.75 (*C*-CH_2, pyridine ring), 159.78 (*C*=O).

S6-8 (1-(2-(pyridin-2-yl)ethyl)-3-octylurea) **^{1}H-RMN (DMSO-d6, 400 MHz)** δ (ppm) = 0,86 (t, 3H, **CH_3**CH_2) ; 1,24-1.34 (m, 12H, CH_3(**CH_2**)$_6$$CH_2$) ; 2,83 (t, 2H, NH$CH_2CH_2$) ; 2,95 (q, 2H, CH_2**CH_2**NH) ; 3,34 (q, 2H, **CH_2**CH_2NH) 5,79 (t, 1H, **NH**CH_2) ;5.84 (t, 1H, **NH**CH_2) ; 7,22 (m,2H,**CH** pyridine ring); 7,70 (td,1H,**CH** pyridine ring) 8,49 (dq,1H,CH pyridine ring). **^{13}C NMR (DMSO-*d6*, 100 MHz)** δ (ppm)= 14.45 (*CH_3*), 22.58, 26.88, 29.20, 29.26, 30.48, 31.73 (6x*CH_2*), 38.76 (*CH_2*NH), 40.11 (*C*H_2-Py, among DMSO pick), 40.54 (*CH_2*NH, among DMSO pick), 121.87 (*CH*, pyridine ring), 123.67 (*CH*, pyridine ring), 136.90 (*CH*, pyridine ring), 149.47 (*C*-N, pyridine ring), 158.47 (*C*-CH_2, pyridine ring), 159.98 (*C*=O).

S7-6 (3-(2-(pyridin-4-yl)ethyl)-3-hexylurea) **^{1}H-RMN (DMSO-d6, 400 MHz)** δ (ppm) = 0,87 (t, 3H, **CH_3**CH_2) ; 1,21-1.35 (m, 8H, CH_3(**CH_2**)$_4$$CH_2$) ; 2,70 (t, 2H, NH$CH_2CH_2$) ; 2,95 (q, 2H, CH_2**CH_2**NH) ; 3,26 (q, 2H, **CH_2**CH_2NH) 5,78 (t, 1H, **NH**CH_2) ;5.82 (t, 1H, **NH**CH_2) ; 7,22 (dd,2H,**CH** pyridine ring); 8,46 (dd,2H,CH pyridine ring). **^{13}C NMR (DMSO-*d6*, 100 MHz)** δ (ppm)= 14.37 (*CH_3*), 22.53, 26.44, 30.28, 31.46 (4x*CH_2*), 35.71 (*CH_2*NH), 40.03 (*C*H_2-Py, among DMSO pick), 40.16 (*CH_2*NH, among DMSO pick), 124.87 (2x*CH*, pyridine ring), 149.44 (*C*-CH_2, pyridine ring), 149.69 (2x*CH*, pyridine ring), 158.69 (*C*=O).

S7-8 (3-(2-(pyridin-4-yl)ethyl)-3-octylurea) **^{1}H-RMN (DMSO-d6, 400 MHz)** δ (ppm) = 0,87 (t, 3H, **CH_3**CH_2) ; 1,21-1.35 (m, 12H, CH_3(**CH_2**)$_6$$CH_2$) ; 2,70 (t, 2H, NH$CH_2CH_2$) ; 2,95 (q, 2H, CH_2**CH_2**NH) ; 3,26 (q, 2H, **CH_2**CH_2NH) 5,78 (t, 1H, **NH**CH_2) ;5.82 (t, 1H, **NH**CH_2) ; 7,22 (dd,2H,**CH** pyridine ring); 8,46 (dd,2H,CH pyridine ring). **^{13}C NMR (DMSO-*d6*, 100 MHz)** δ (ppm)= 14.37 (*CH_3*), 22.53, 26.44, 29.52, 30.28, 31.46, 31.73 (6x*CH_2*), 35.71 (*CH_2*NH), 39.69 (*C*H_2-Py, among DMSO pick), 40.16 (*CH_2*NH, among DMSO pick), 124.87 (2x*CH*, pyridine ring), 149.44 (*C*-CH_2, pyridine ring), 149.69 (2x*CH*, pyridine ring), 158.69 (*C*=O).

S8-6 (4-(2-(3-hexylureido)ethyl)benzenesulfonamide) **^{1}H-RMN (DMSO-d6, 400 MHz)** δ (ppm) = 0,87 (t, 3H, **CH_3**CH_2); 1,25-1.36 (m, 8H, CH_3**(CH_2)$_4$**CH_2); 2,75 (t, 2H, NH**CH_2**CH_2); 2,96 (q, 2H, CH_2**CH_2**NH); 3,24 (q, 2H, **CH_2**CH_2NH) 5,79 (t, 1H, **NH**CH_2); 5.83 (t, 1H, **NH**CH_2); 7.29 (s, **2H**, **H_2N**-SO_2-Ph); 7,38 (d, 2 H, **CH** benzene ring); 7,74 (d,1H, **CH** benzene ring). **^{13}C NMR (DMSO-*d6*, 100 MHz)** δ (ppm)= 14.42 (*CH_3*), 22.59, 26.54, 30.44, 31.52 (4x*CH_2*), 36.37 (*CH_2*NH), 40.20 (*C*H_2-Ph, among DMSO pick), 41.01 (*CH_2*NH), 126.13 (2x*CH* Benzene ring), 129.61 (2x*CH* Benzene ring) 142.40 (*C*-CH_2, Benzene ring), 144.56 (*C*-SO_2, Benzene ring) 158.43 (*C*=O).

S8-8 (4-(2-(3-octylureido)ethyl)benzenesulfonamide) **^{1}H-RMN (DMSO-d6, 400 MHz)** δ (ppm) = 0,86 (t, 3H, **CH$_3$**CH$_2$); 1,25-1.37 (m, 12H, CH$_3$**(CH$_2$)$_6$**CH$_2$); 2,75 (t, 2H, **NH**CH$_2$CH$_2$) ; 2,95 (q, 2H, **CH$_2$**CH$_2$NH) ; 3,23 (q, 2H, CH$_2$**CH$_2$**NH) 5,79 (t, 1H, **NH**CH$_2$) ;5.83 (t, 1H, **NH**CH$_2$) ; 7.29 (s, **2H**, **H$_2$N**-SO$_2$-Ph); 7,38 (d, 2 H, **CH** benzene ring); 7,74 (d,1H, **CH** benzene ring) **^{13}C NMR (DMSO-*d6*, 100 MHz)** δ (ppm)= 14.42 (*CH$_3$*), 22.54, 26.79, 29.13, 29.18, 30.33, 31.68 (6x*CH$_2$*), 36.25 (*CH$_2$*NH), 40.20 (*C*H$_2$-Ph, among DMSO pick), 41.00 (*CH$_2$*NH), 126.11 (2x*CH* Benzene ring), 129.66 (2x*CH* Benzene ring) 142.19 (*C*-CH$_2$, Benzene ring), 144.58 (*C*-SO$_2$, Benzene ring) 158.71 (*C*=O).

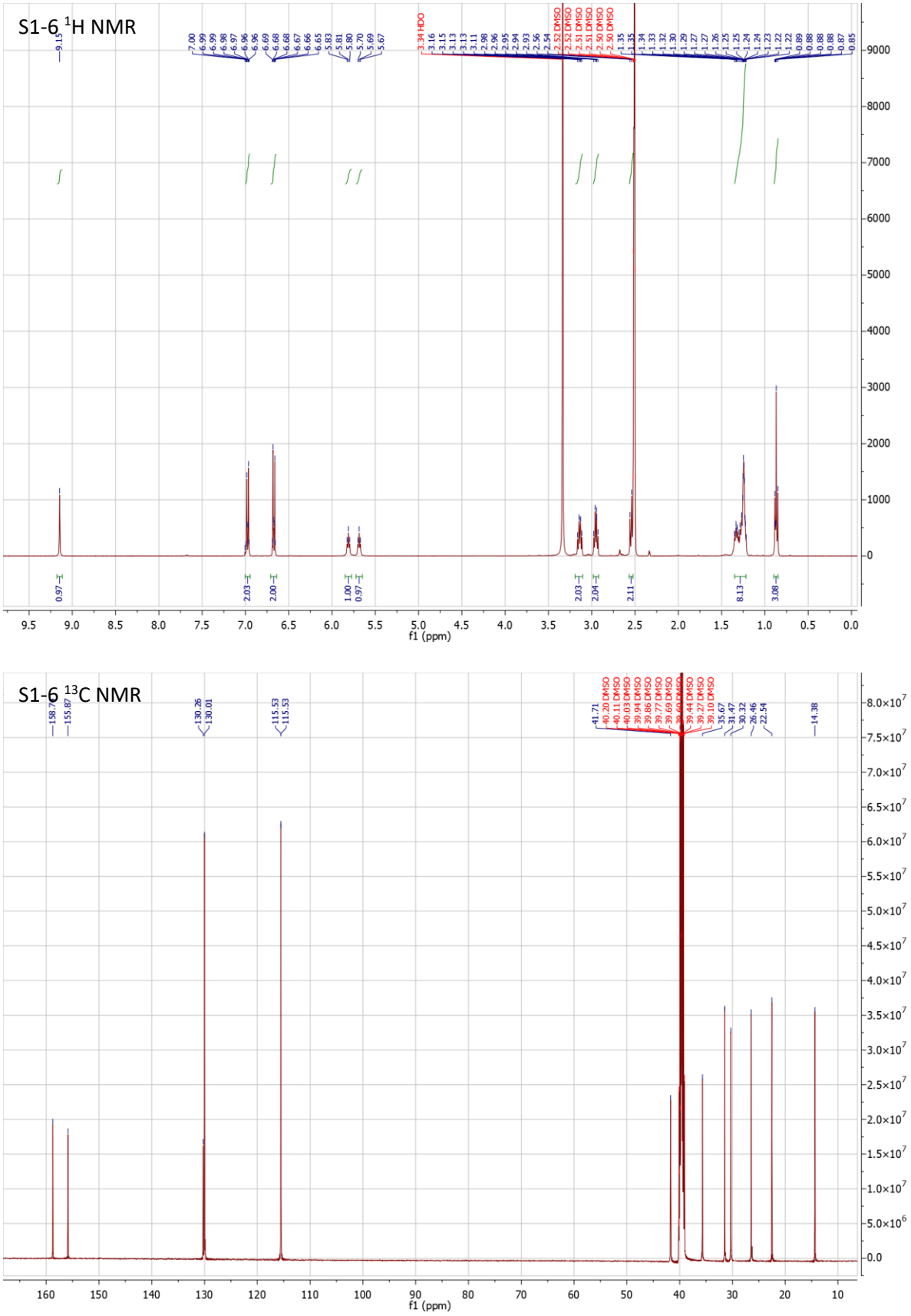

Figure S1. ^{1}H NMR (top) and ^{13}C NMR (bottom) spectra of S1-6

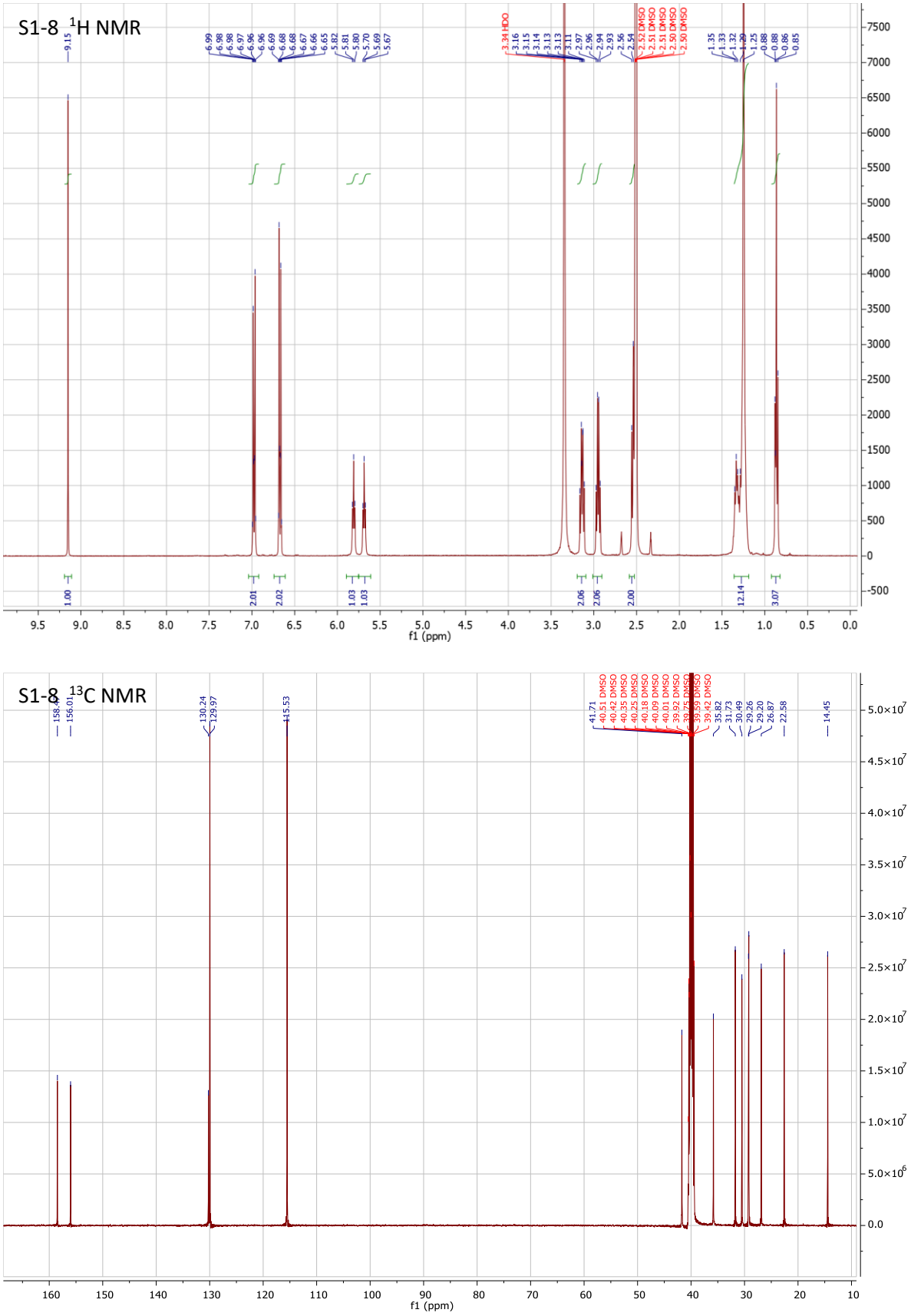

Figure S 1. ^{1}H NMR (top) and ^{13}C NMR (bottom) spectra of S1-8

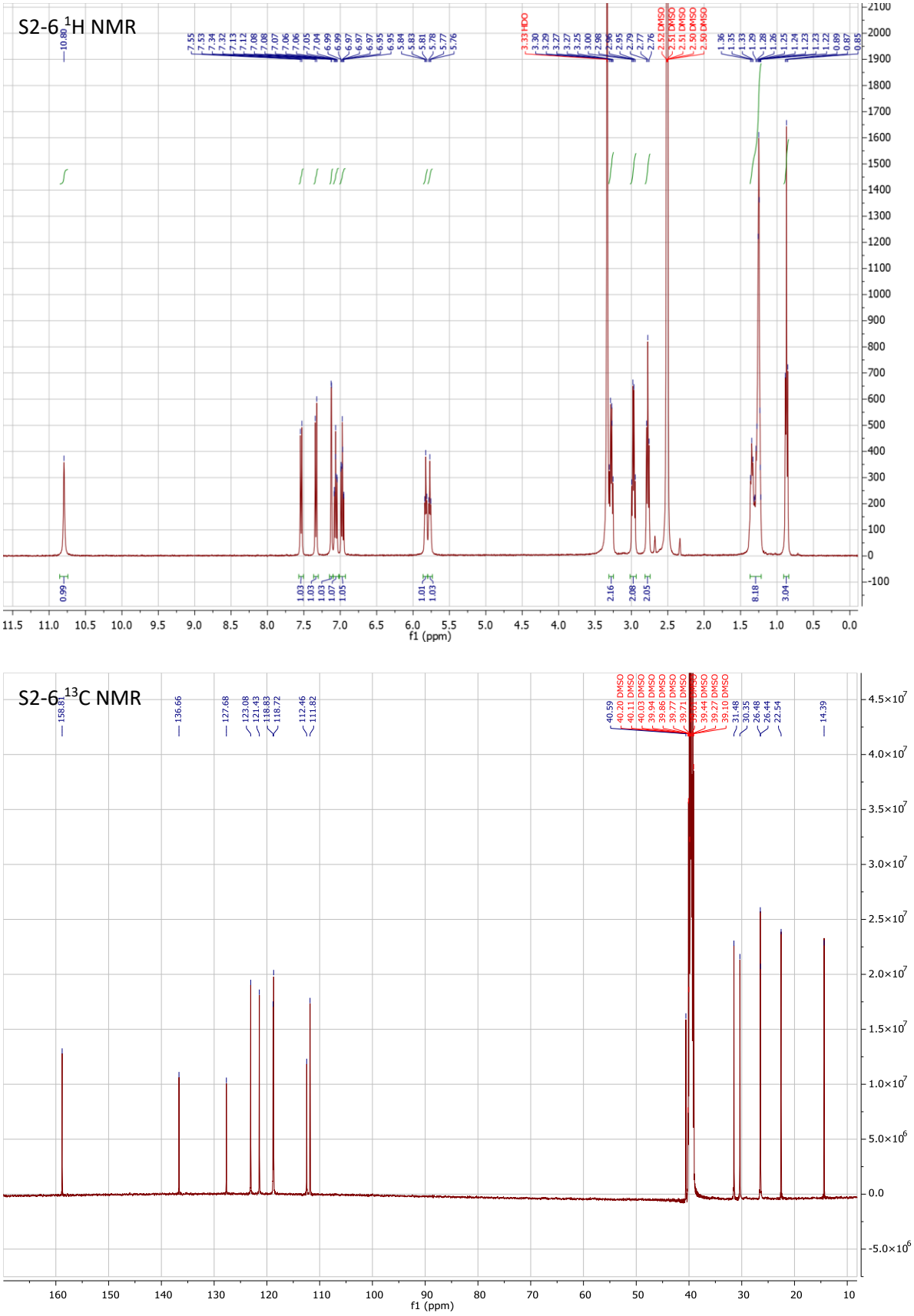

Figure S3. ^{1}H NMR (top) and ^{13}C NMR (bottom) spectra of S2-6

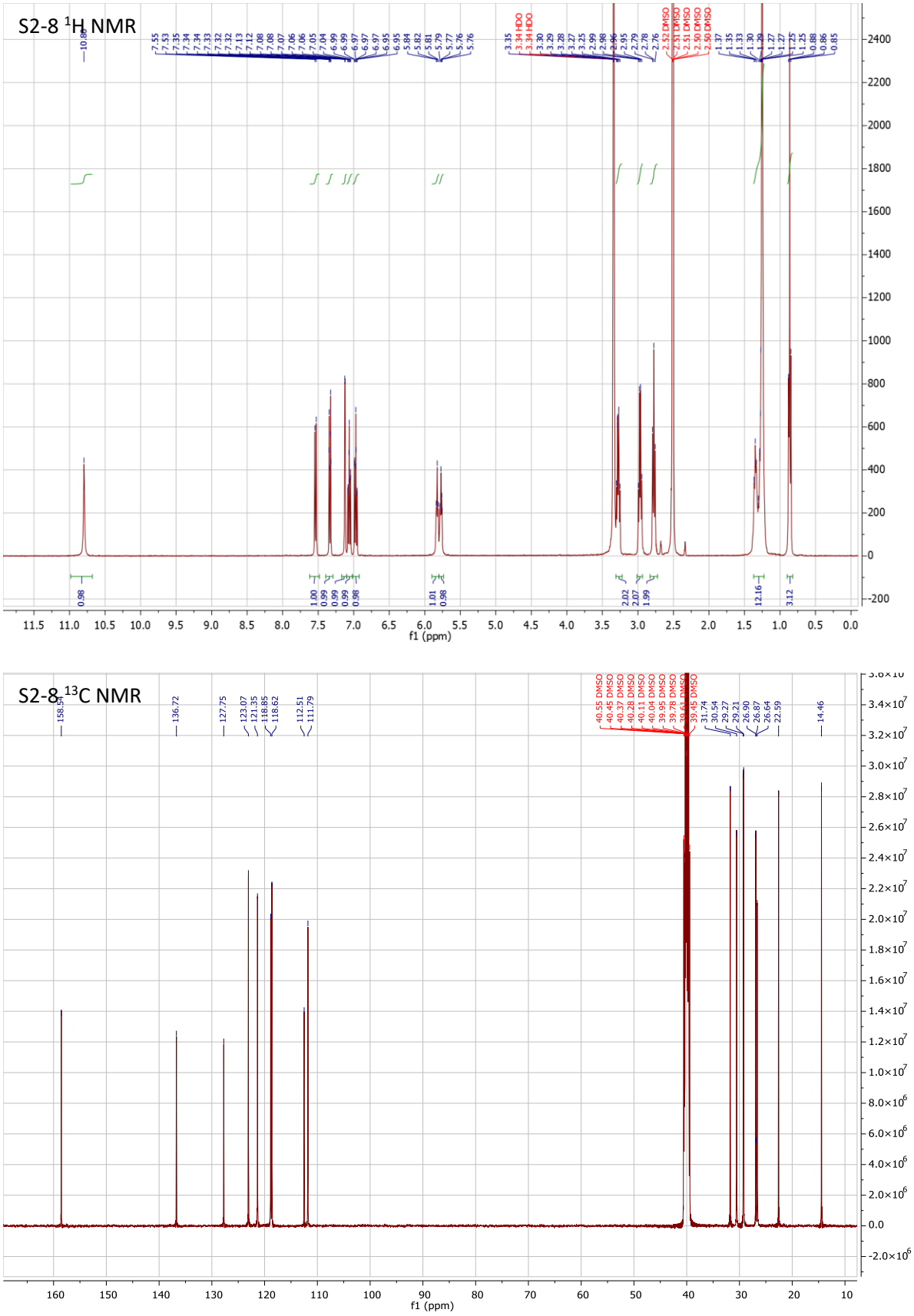

Figure S4. ^{1}H NMR (top) and ^{13}C NMR (bottom) spectra of S2-8

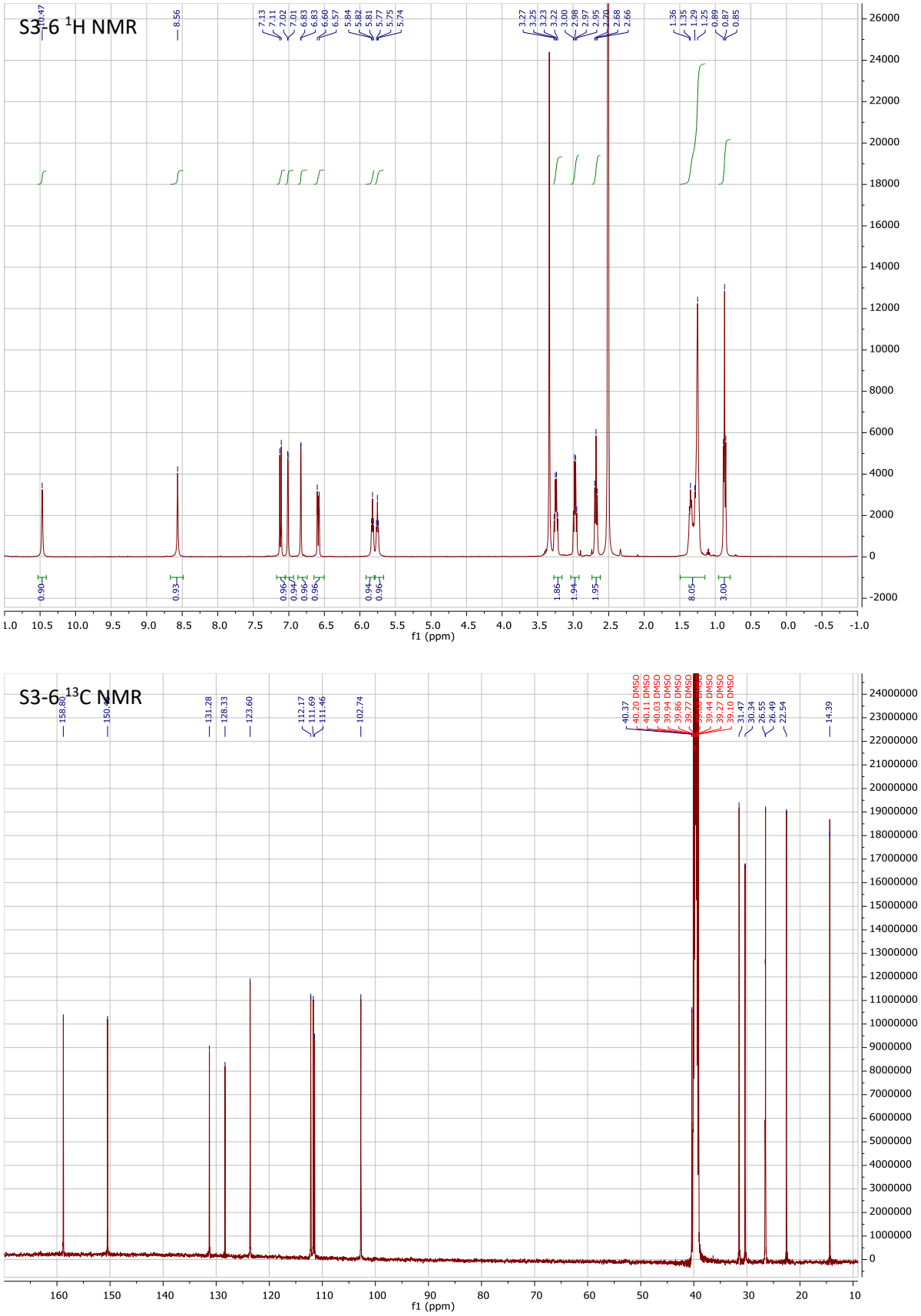

Figure S5. ^{1}H NMR (top) and ^{13}C NMR (bottom) spectra of S3-6

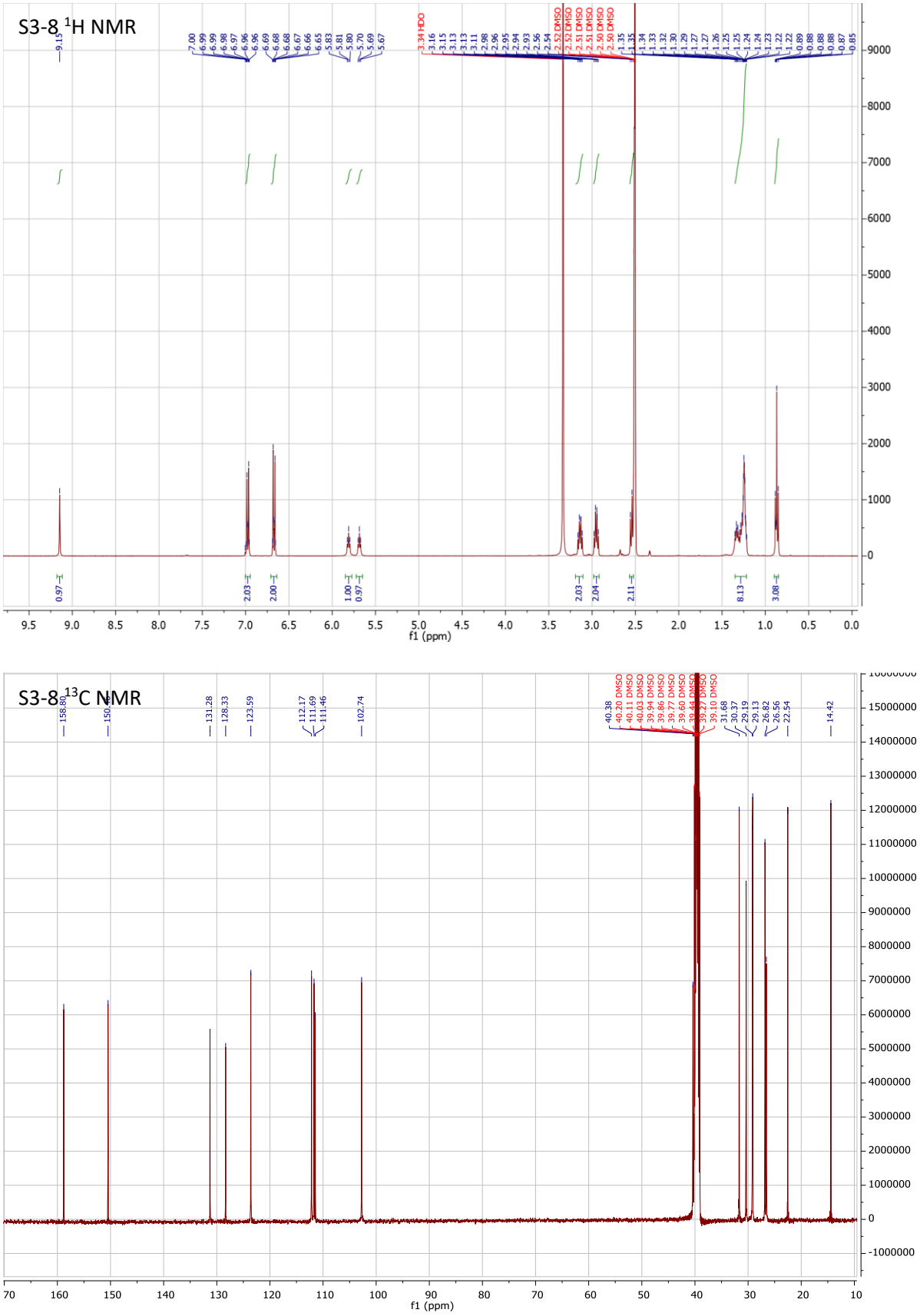

Figure S6. ^{1}H NMR (top) and ^{13}C NMR (bottom) spectra of S3-8

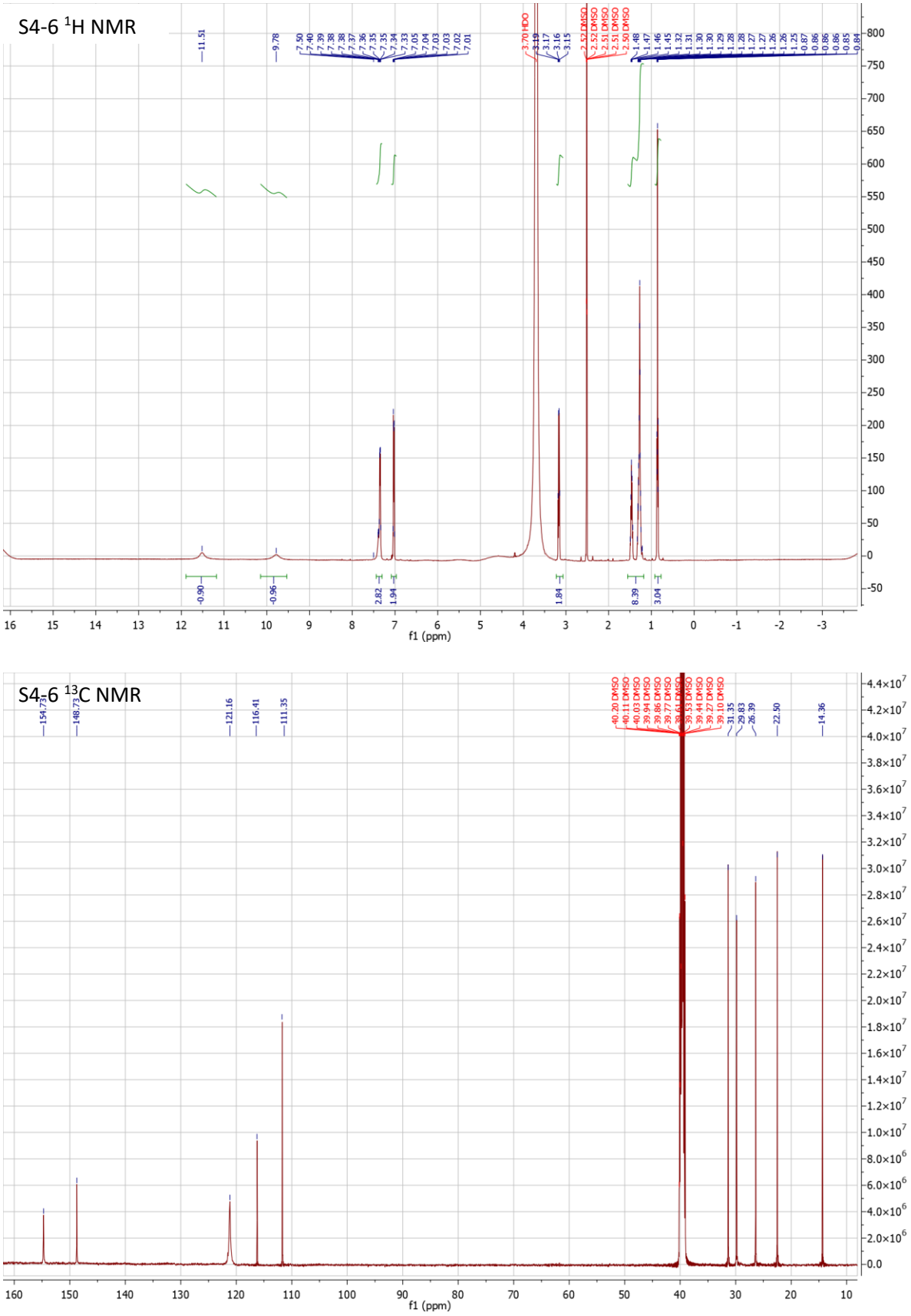

Figure S7. ^{1}H NMR (top) and ^{13}C NMR (bottom) spectra of S4-6

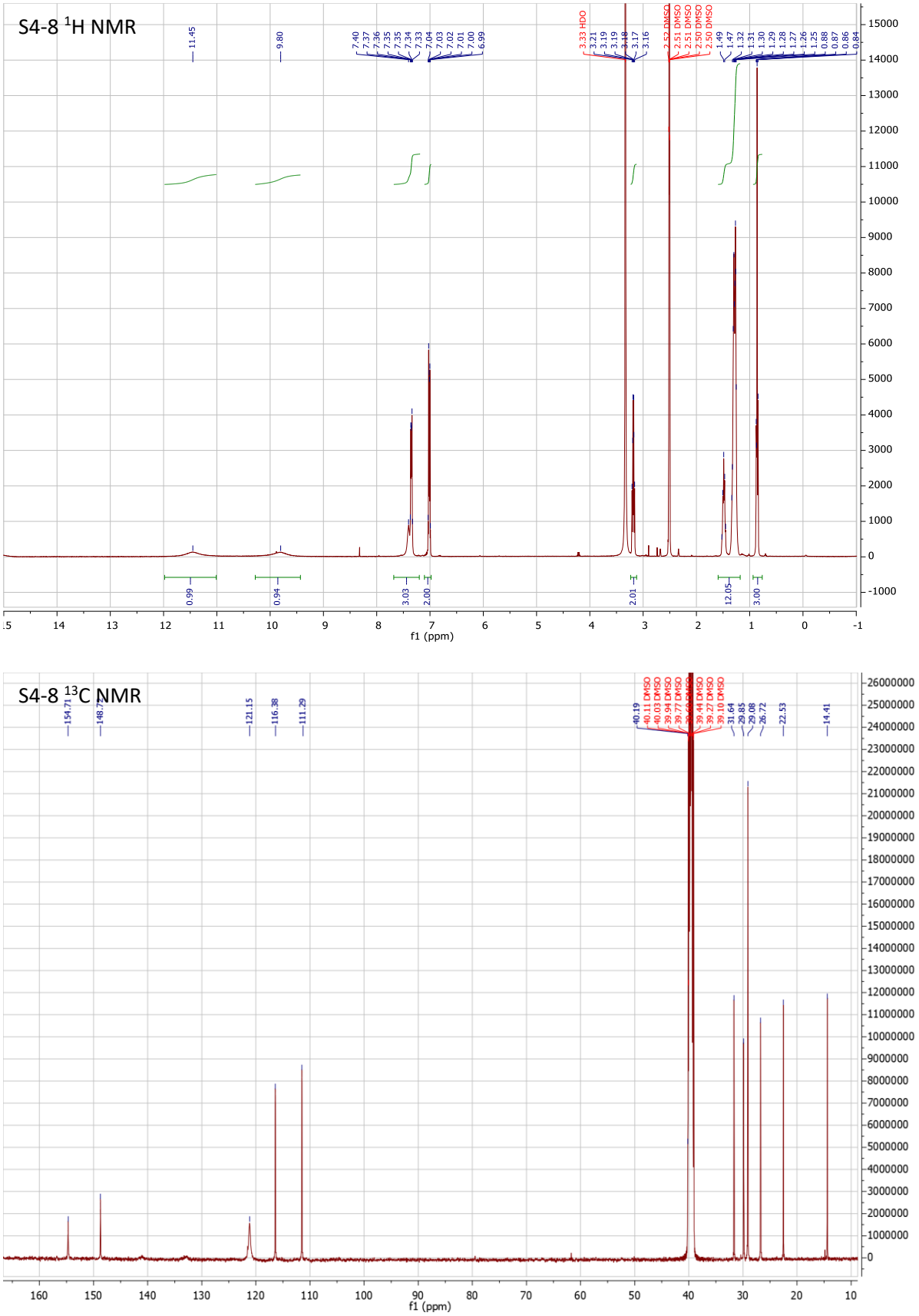

Figure S8. ^{1}H NMR (top) and ^{13}C NMR (bottom) spectra of S4-8

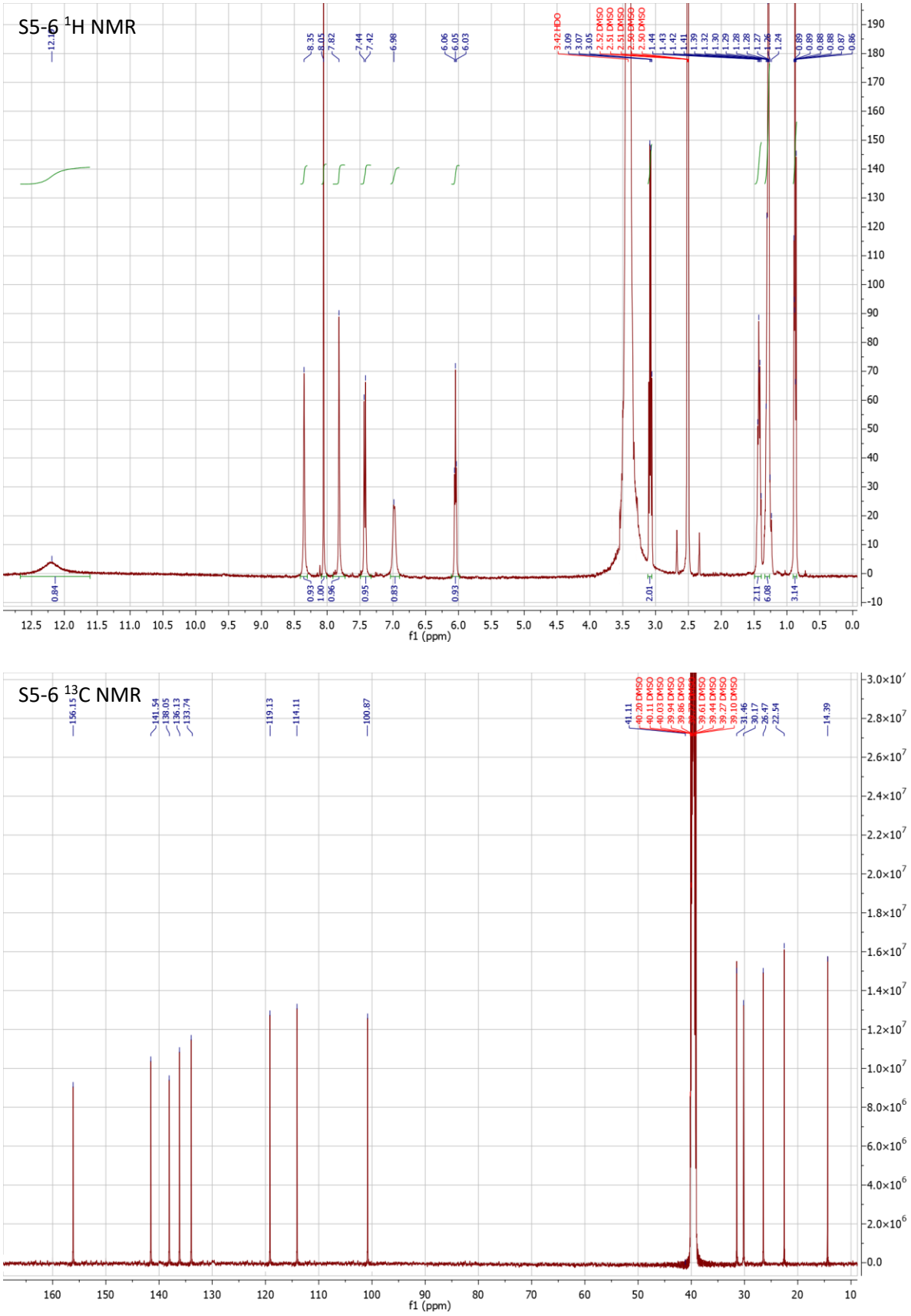

Figure S9. ^{1}H NMR (top) and ^{13}C NMR (bottom) spectra of S5-6

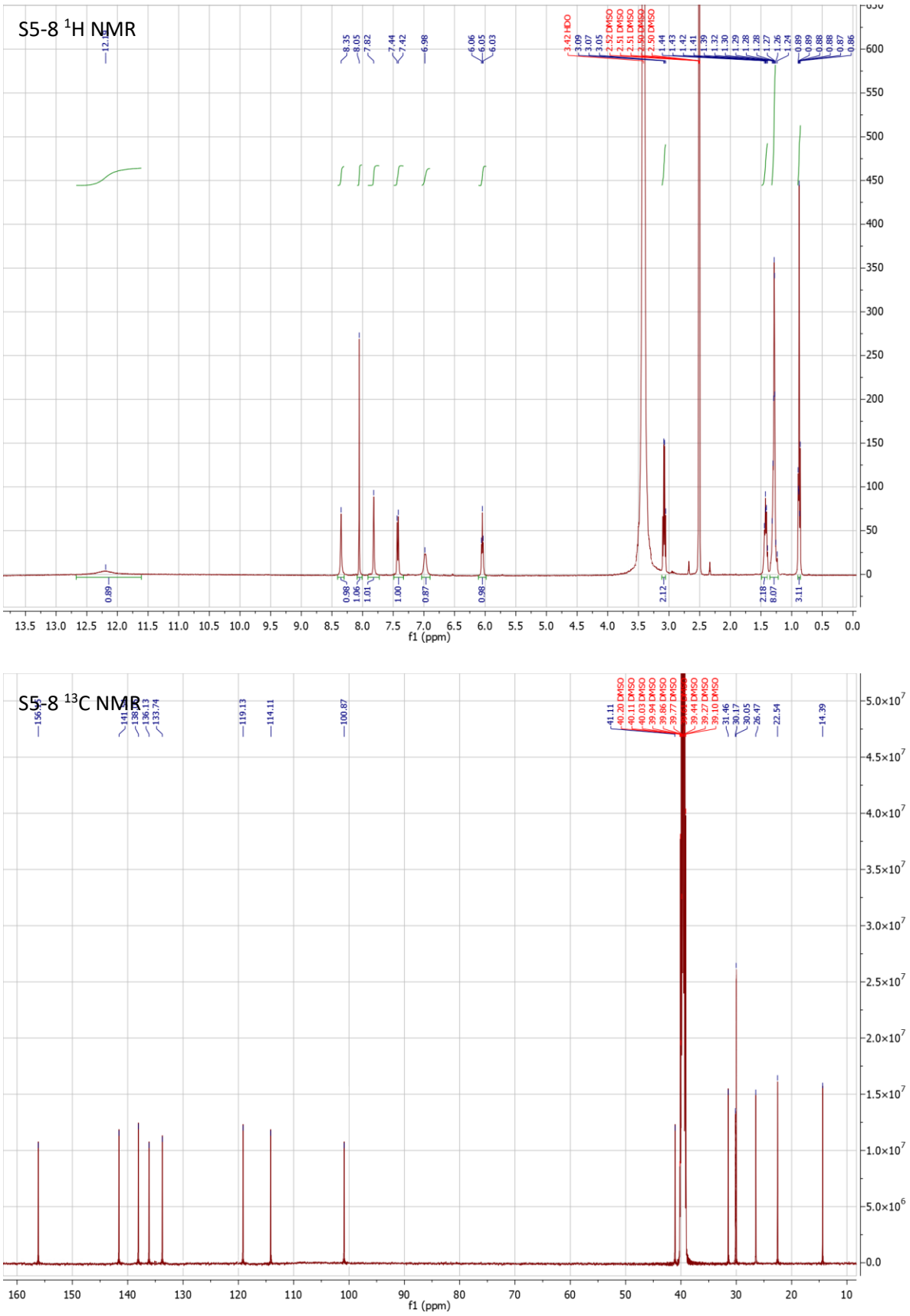

Figure S10. ^{1}H NMR (top) and ^{13}C NMR (bottom) spectra of S5-8

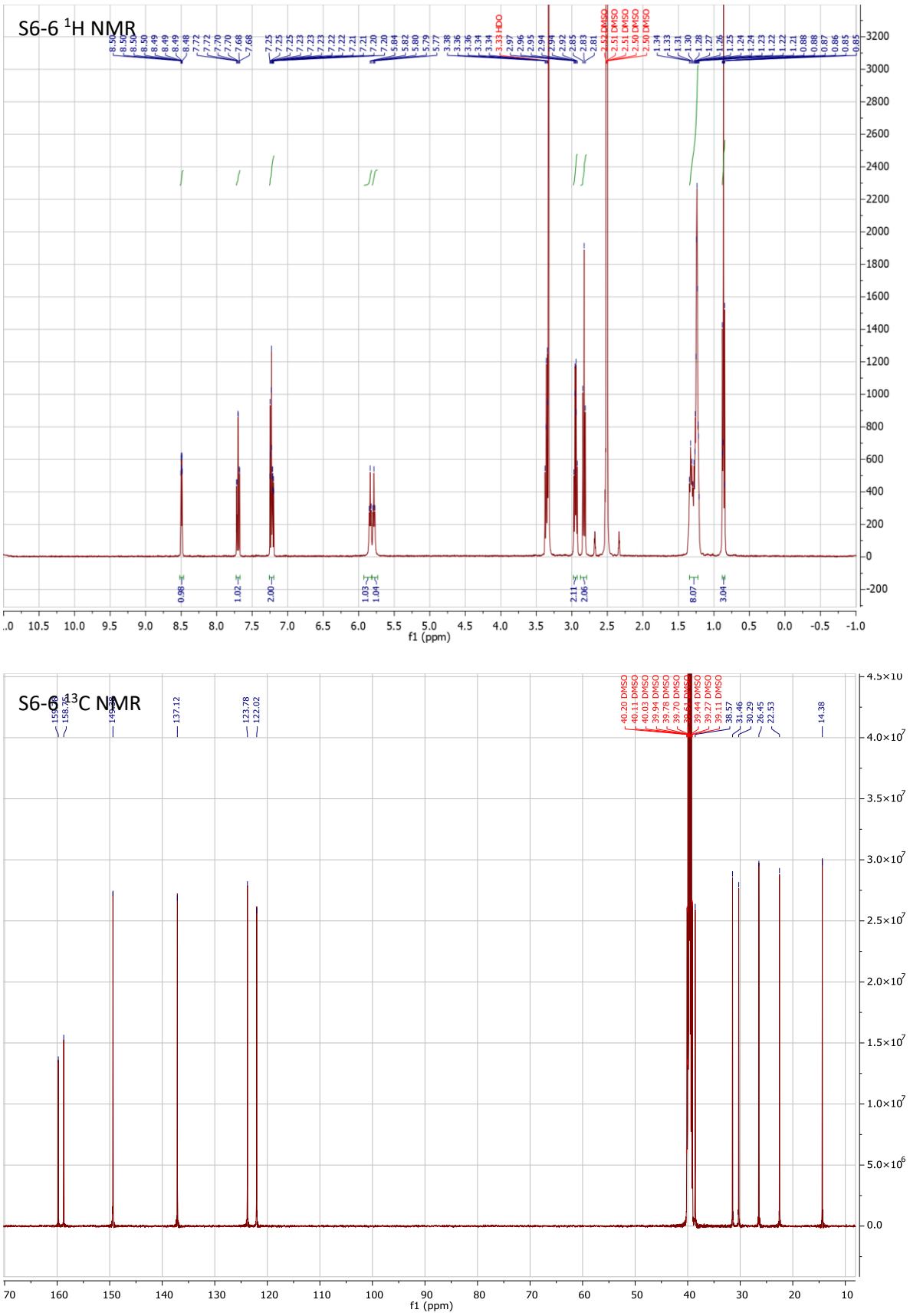

Figure S11. ^{1}H NMR (top) and ^{13}C NMR (bottom) spectra of S6-6

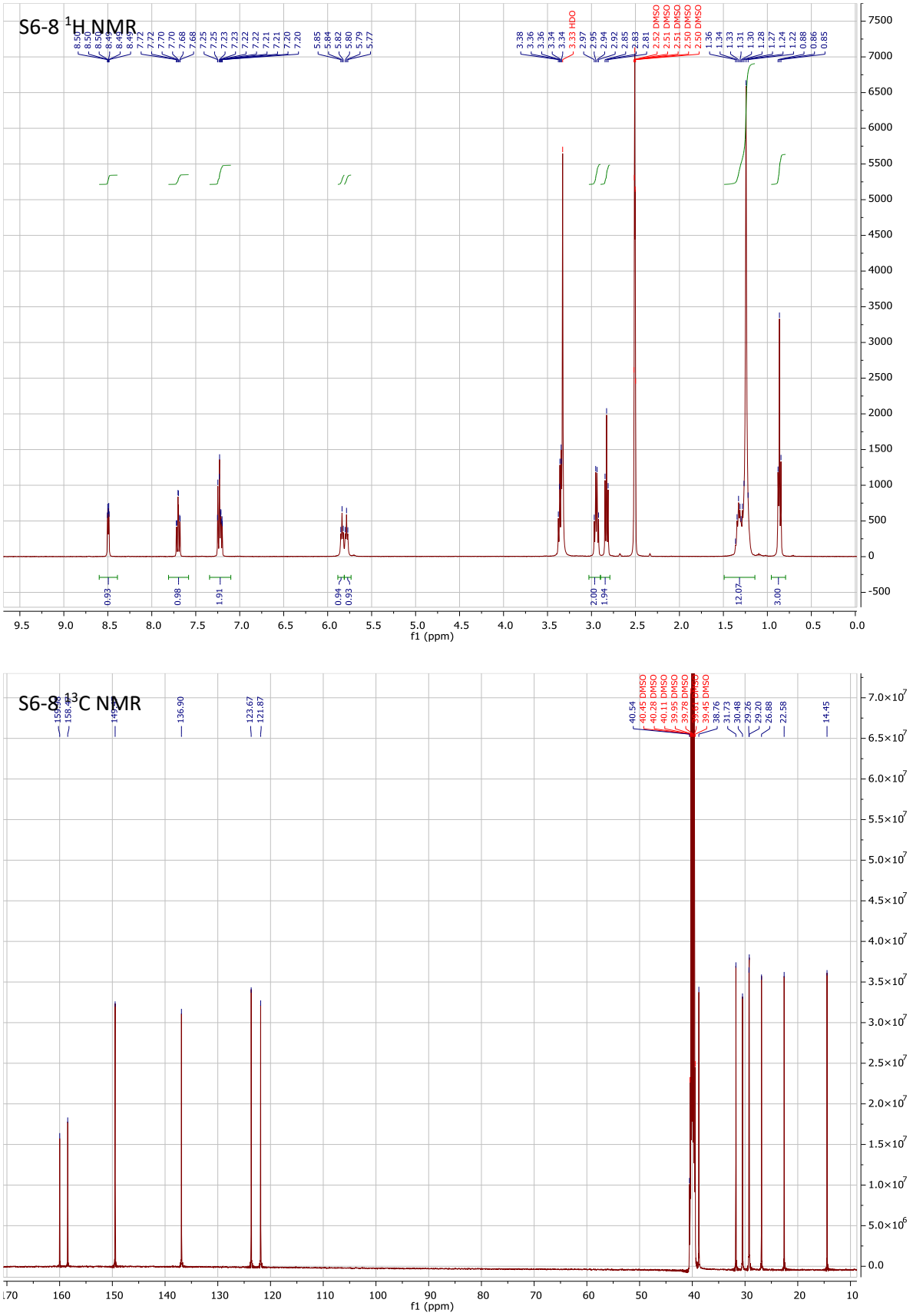

Figure S12. ^{1}H NMR (top) and ^{13}C NMR (bottom) spectra of S6-8

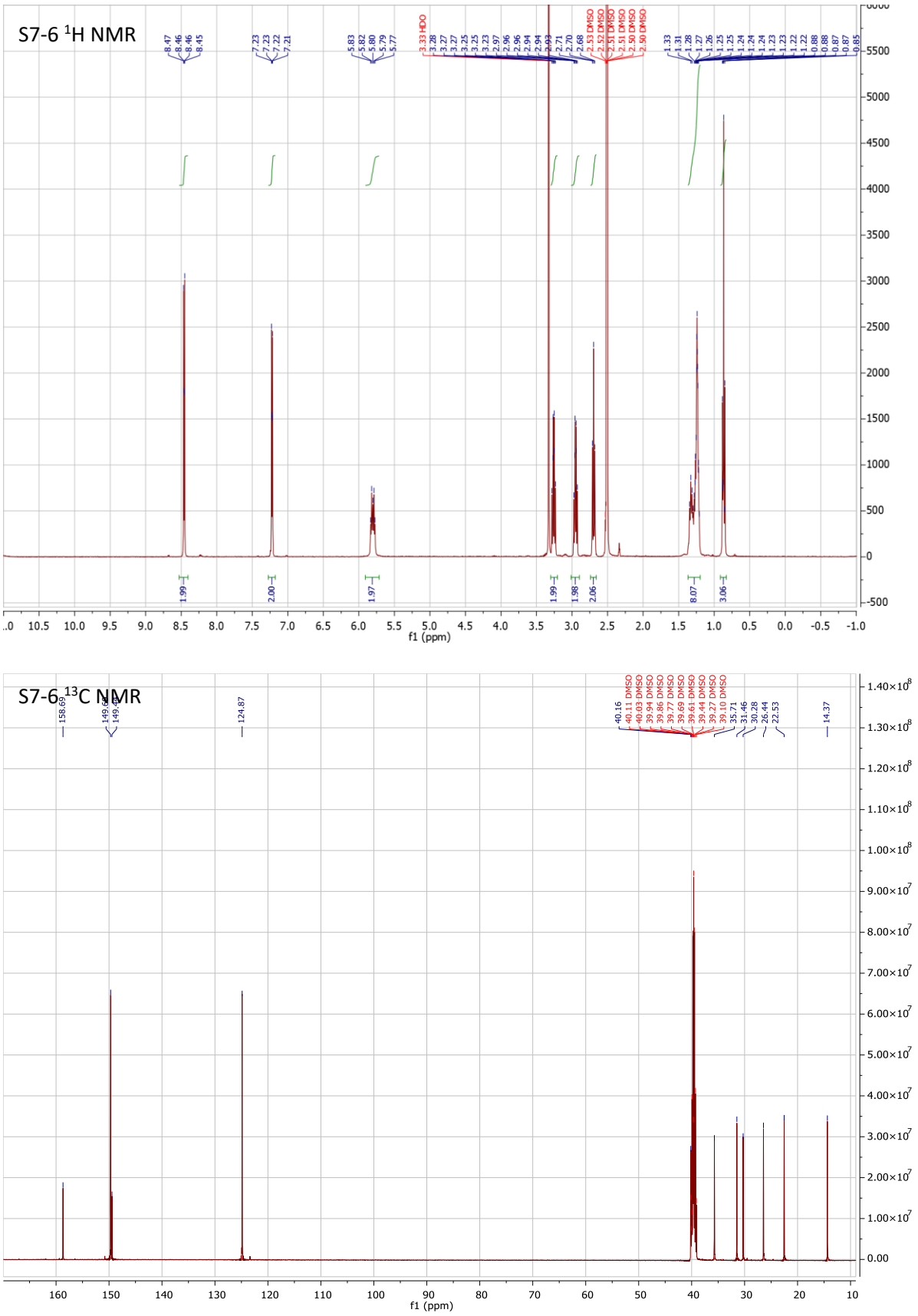

Figure S13. ^{1}H NMR (top) and ^{13}C NMR (bottom) spectra of S7-6

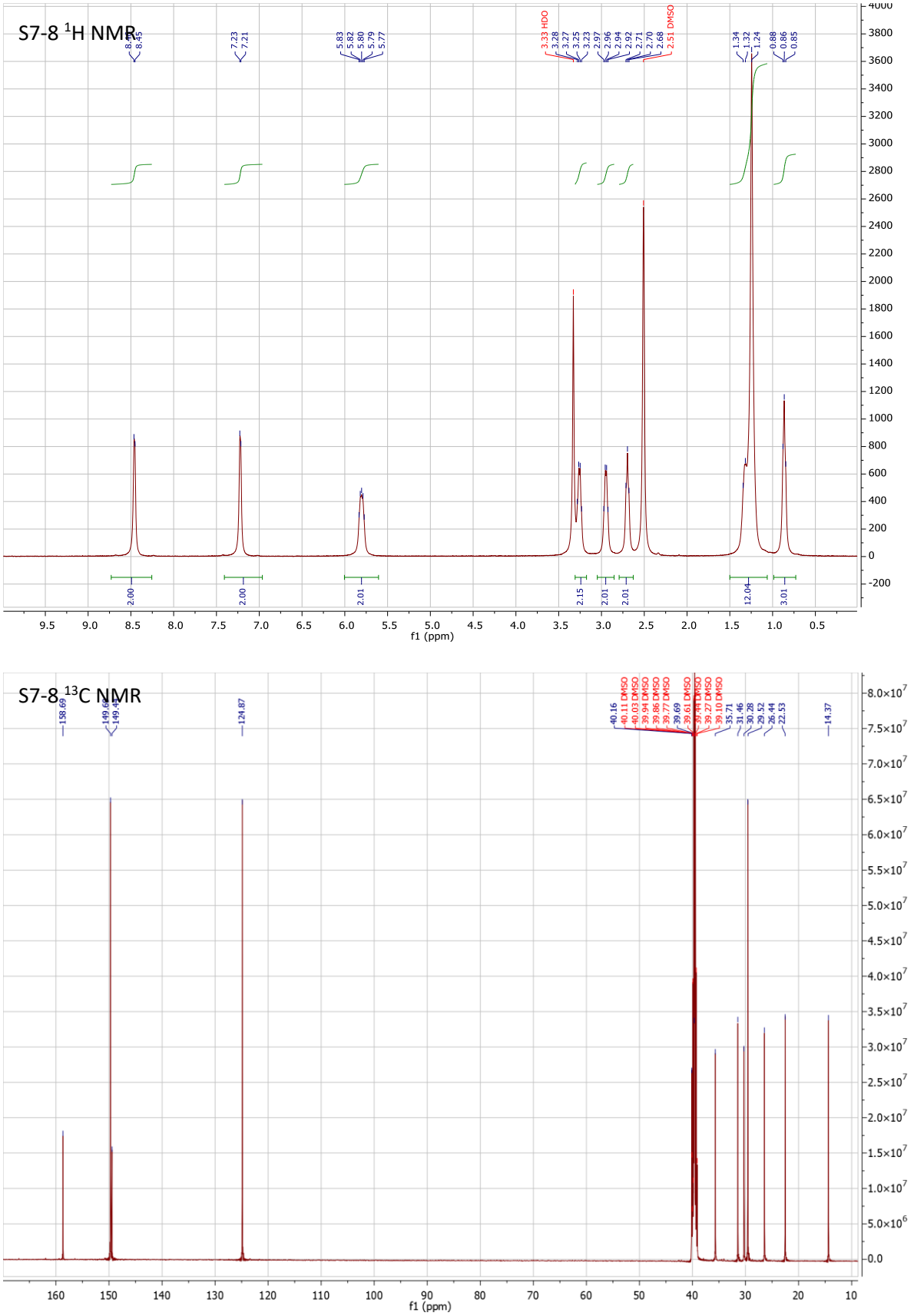

Figure S14. ^{1}H NMR (top) and ^{13}C NMR (bottom) spectra of S7-8

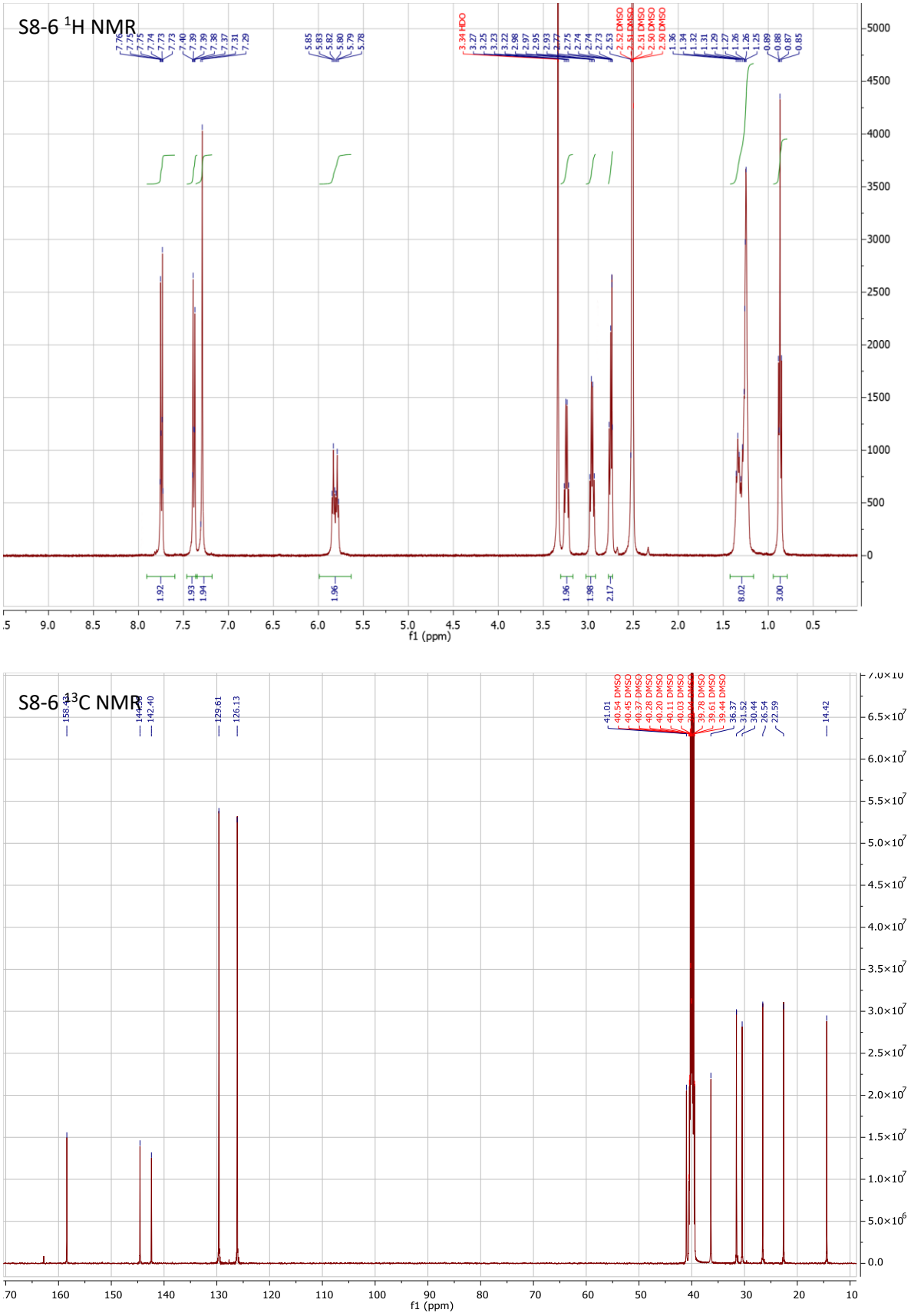

Figure S15. ^{1}H NMR (top) and ^{13}C NMR (bottom) spectra of S8-6

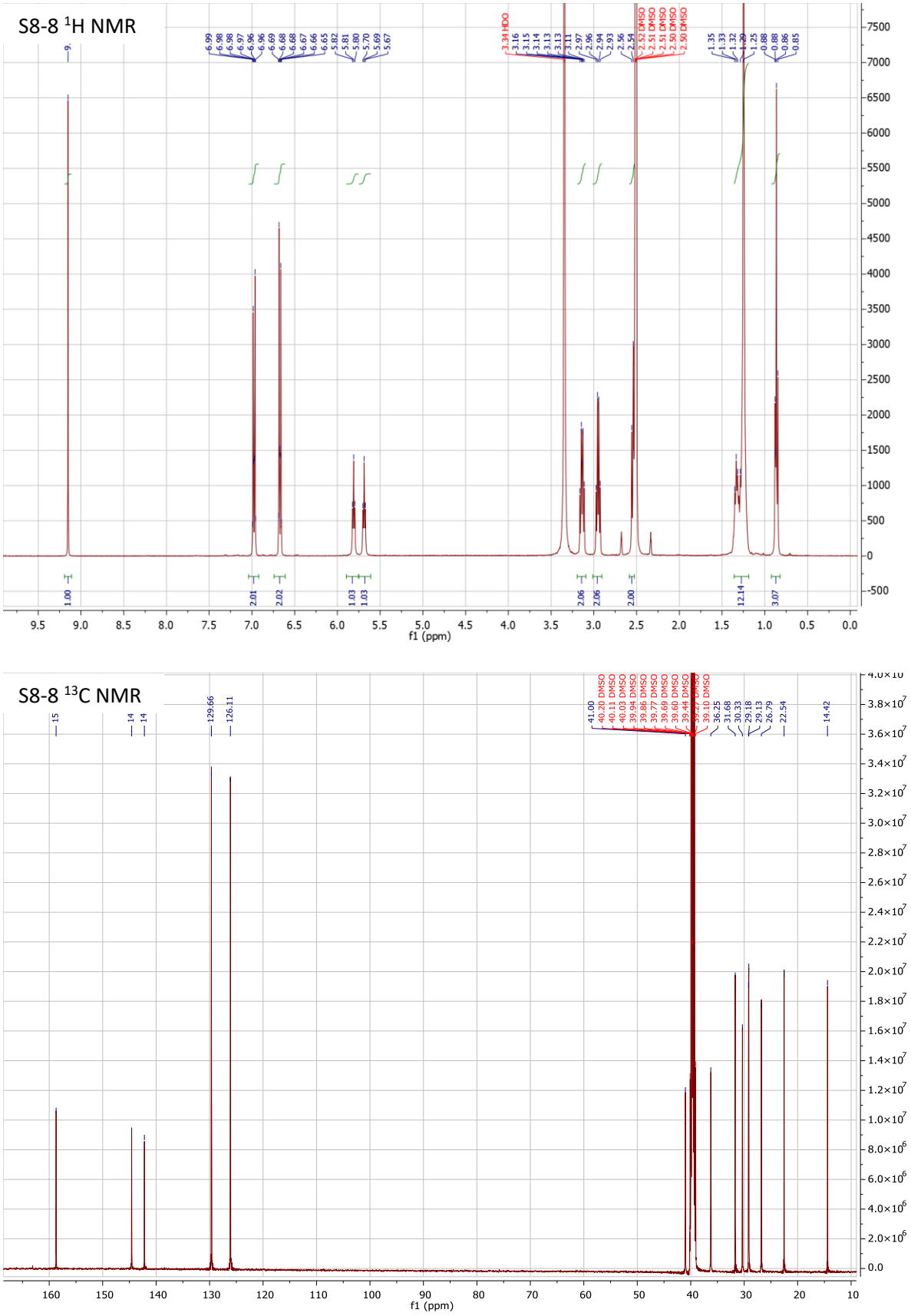

Figure S16. ^{1}H NMR (top) and ^{13}C NMR (bottom) spectra of S8-68

Methods

Water transport experiments

LUV preparation: Liposomes were prepared using the film rehydration method. A Phosphatidylcholine/Phosphatidylserine/Cholesterol mixture with a molar ratio of 4/1/5 was dissolved in chloroform/methanol mixture ($CHCl_3$/MeOH, v/v: 1/1). The solution was dried on a rotary evaporator and subsequently under high vacuum to remove residual solvent. After rehydration with 1 mL buffer containing 200 mM sucrose and 10 mM PBS (pH=6.4), the suspension was extruded through 0.1 μm track-etched filters for 21 times (Whatman, UK) to obtain monodisperse unilamellar vesicles.

Stopped-flow water transport experiment: Water permeability of channels was measured with the stopped-flow instrument (SFM3000+MOS450, Bio-Logic SAS, Claix, France) by using stopped-flow light scattering experiments. Generally, the compound solution or their combinations in DMSO (20 μL with required concentration) was added to the vesicle suspension (1.980 mL) to incorporate the channel molecules into the lipid bilayers. Then the vesicle sample and the hypertonic solutions (2.0 mL, 400 mM sucrose in PBS buffer, pH = 6.4) were loaded into two syringes. The size change of the vesicles was monitored through the light scattering intensity change with light of 365 nm wavelength at a detection angle of 90°. The osmotic permeability (P_f) was calculated as following:

$$P_f = \frac{k}{\left(\frac{S}{V_0}\right) \times V_w \times \Delta Osm}$$

where k is the exponential coefficient of the change in the light scattering; S and V_0 are the initial surface area and volume of the vesicles, respectively; V_w is the molar volume of water, and Δ_{osm} is the osmolarity difference.

***Single channel water permeability*:** The single channel permeability was calculated based on compound concentration and channel configuration in lipid bilayer. Take one sample of HC6/S5-6 with concentrations 5mM/5mM (HC6 and S5-6 respectively) as an example. The vesicles had diameter of 100 nm in average after extrusion, the sum of outer and inner surface areas is $4\pi \cdot r + 4\pi \cdot (r-5) = 55{,}522$ nm^2, assuming that the bilayer thickness was 5 nm. The average cross-sectional area of a lipid in average was 0.287 nm^2 (PC/PS/Chl lipids with a molar ratio of 4/1/5: the cross-sectional areas of PC and PS were ~0.35 nm^2 and that of cholesterol was 0.223 nm^2), and that of the I-quartet (not including the alkyl chain) was estimated at 0.7 nm^2

(taking into account that I-quartets play role of channel frame). The average molecular weight of lipid is 484 Da and the molecular weight of the channel quartet is 11964 Da (24 HC6 and 24 S5-6 molecules assembled as a channel). The lipids to channel molar ratio is 207.36. The insertion number of the channel was ~ 428 per vesicle. If the overall net permeability by channels in liposomes was 21.8 μm/s, the single-channel permeability was $1.56 \cdot 10^{-15}$ cm^3/s and $5.22 \cdot 10^6$ water molecules/s.

Table S2. Calculation of water transport for combinations of I-quartet and hydrophobic compounds

Compound/System	C, mM	k_i	$P_{f\,(1)}$, $\mu m \cdot s^{-1}$	Net permeability, $\mu m \cdot s^{-1}$	P_{SINGLE}, cm^3/s	P_{SINGLE}, molecules H_2O/Channel/s
Control	0	3.620	33.52			
HC6	5	3.862	35.76	2.24	$3.26 \cdot 10^{-16}$	$1.09 \cdot 10^{7}$
S3-6	5	4.295	39.77	6.25		
HC6/S3-6	10	4.569	42.31	8.79	$6.45 \cdot 10^{-16}$	$2.15 \cdot 10^{7}$
S5-6	5	4.783	44.28	10.76		
HC6/S5-6	10	5.921	54.82	21.30	$1.56 \cdot 10^{-15}$	$5.22 \cdot 10^{7}$
S6-6	5	4.616	42.74	9.22		
HC6/S6-6	10	4.722	43.72	10.20	$7.48 \cdot 10^{-16}$	$2.50 \cdot 10^{7}$
S7-6	5	4.739	43.88	10.36		
HC6/S7-6	10	4.115	38.11	11.80	$3.37 \cdot 10^{-16}$	$1.12 \cdot 10^{7}$
S8-6	5	3.619	33.51	-0.02		
HC6/S8-6	10	4.142	38.35	4.83	$3.55 \cdot 10^{-16}$	$1.18 \cdot 10^{7}$
Control		3.337	30.90			
HC8		3.623	33.55	1.00	$1.46 \cdot 10^{-16}$	$4.88 \cdot 10^{6}$
S6-8		3.933	36.42	5.51		
HC8/S6-8		3.991	36.95	6.05	$4.44 \cdot 10^{-16}$	$1.48 \cdot 10^{7}$
S7-8		3.880	35.92	5.02		
HC8/S7-8		4.002	37.06	6.16	$4.52 \cdot 10^{-16}$	$1.51 \cdot 10^{7}$
S8-8		6.038	55.90	25.00		
HC8/S8-8		6.923	64.10	33.20	$2.44 \cdot 10^{-15}$	$8.14 \cdot 10^{7}$

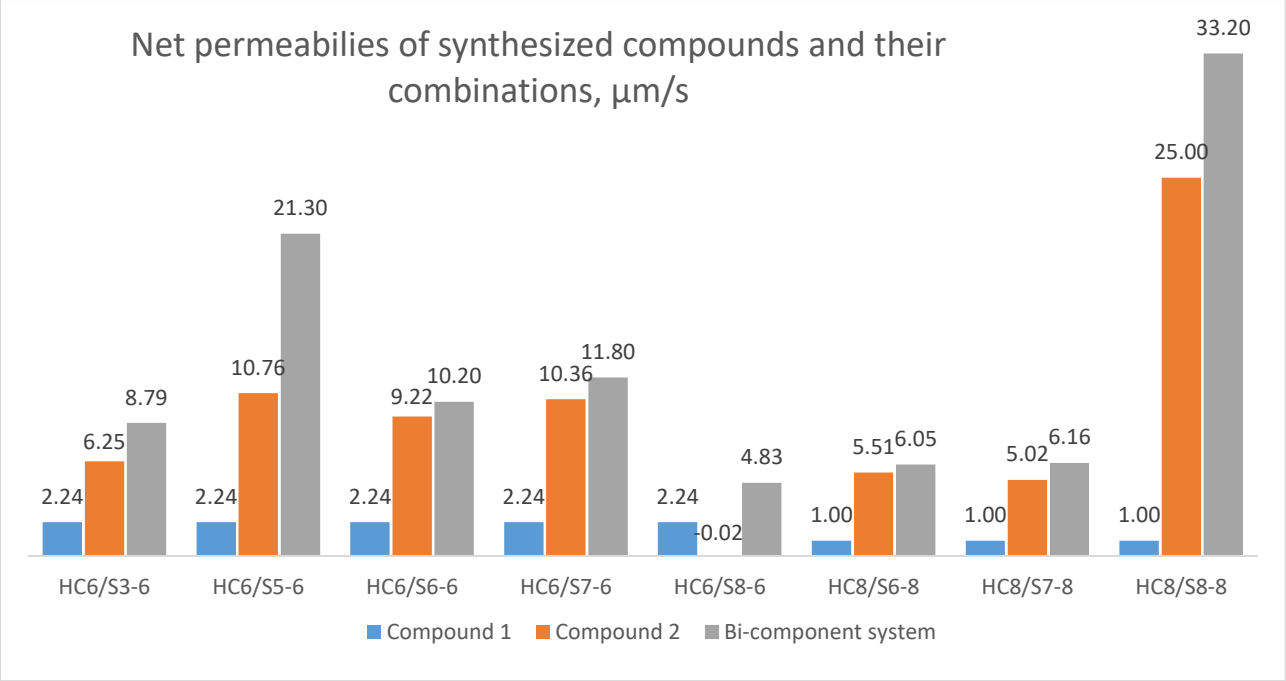

Figure S17. Net permeabilities of synthesized compounds and their combinations.

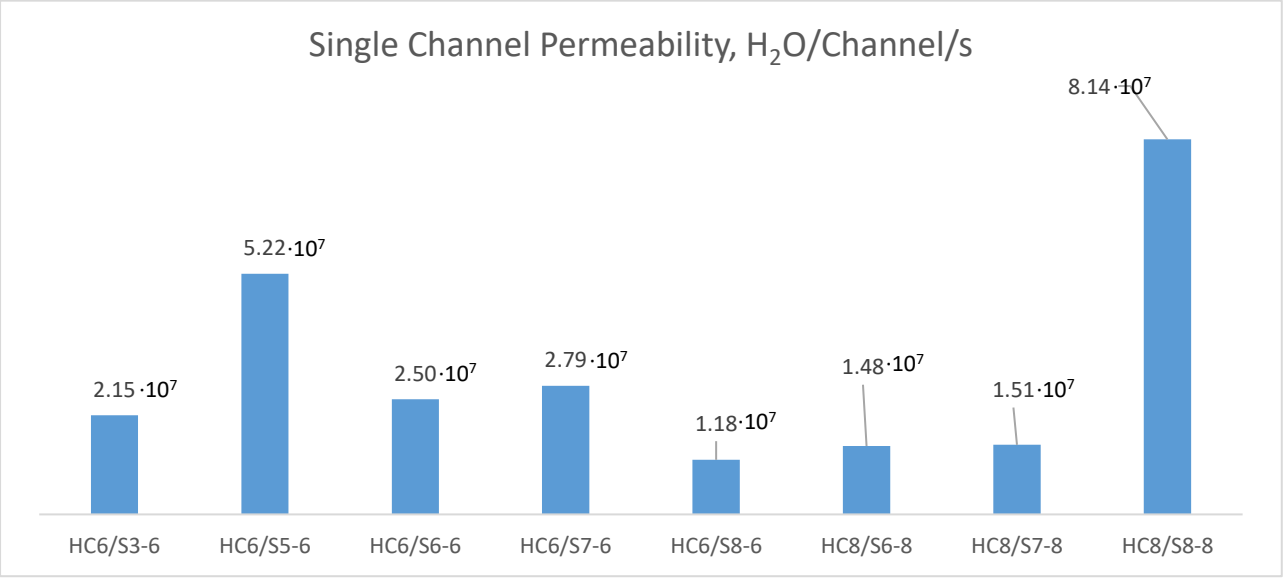

Figure S18. Comparison of single channel permeabilities of combined systems.

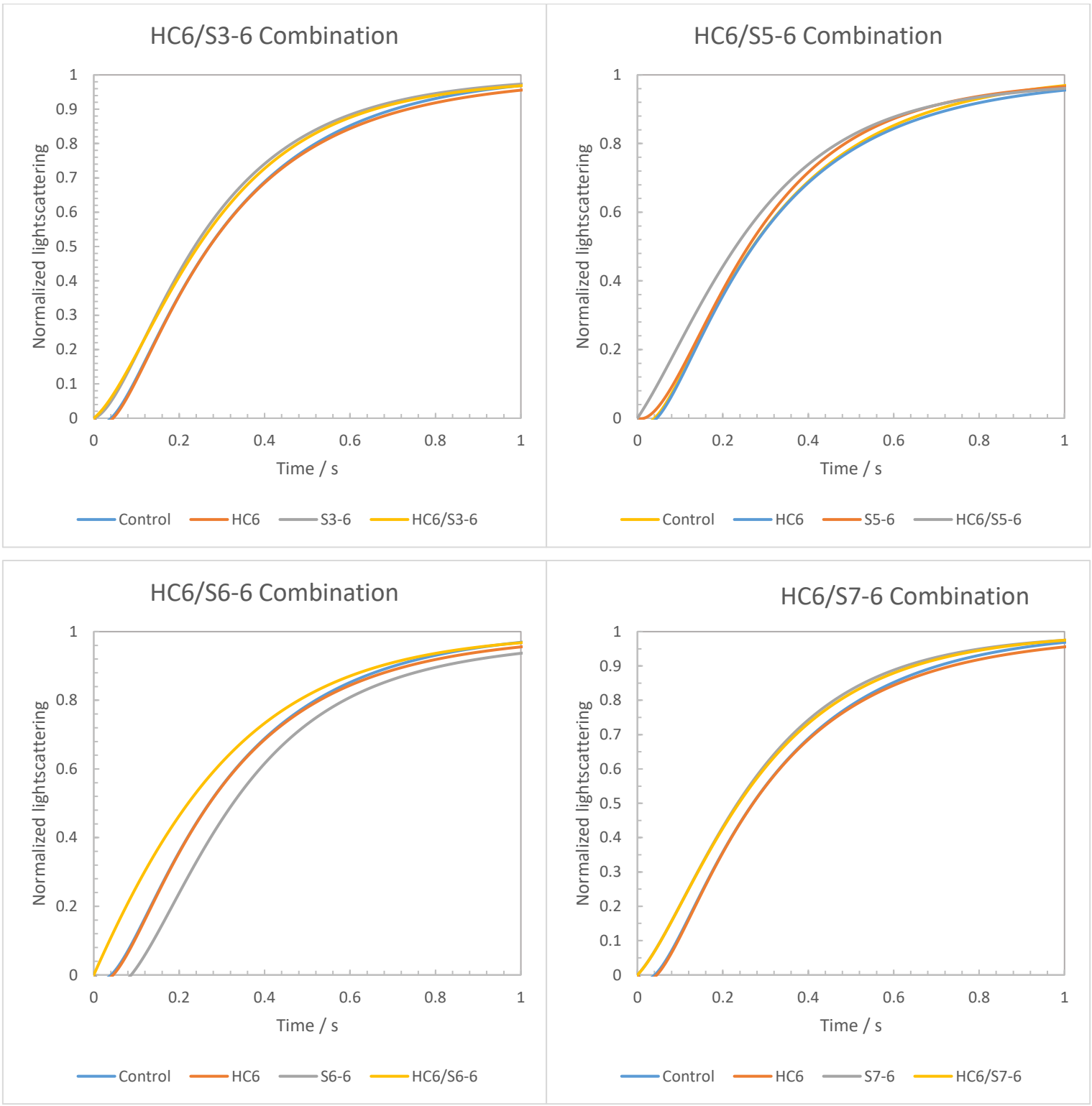

Figure S19. Stopped-flow traces of individual compounds and combined systems.

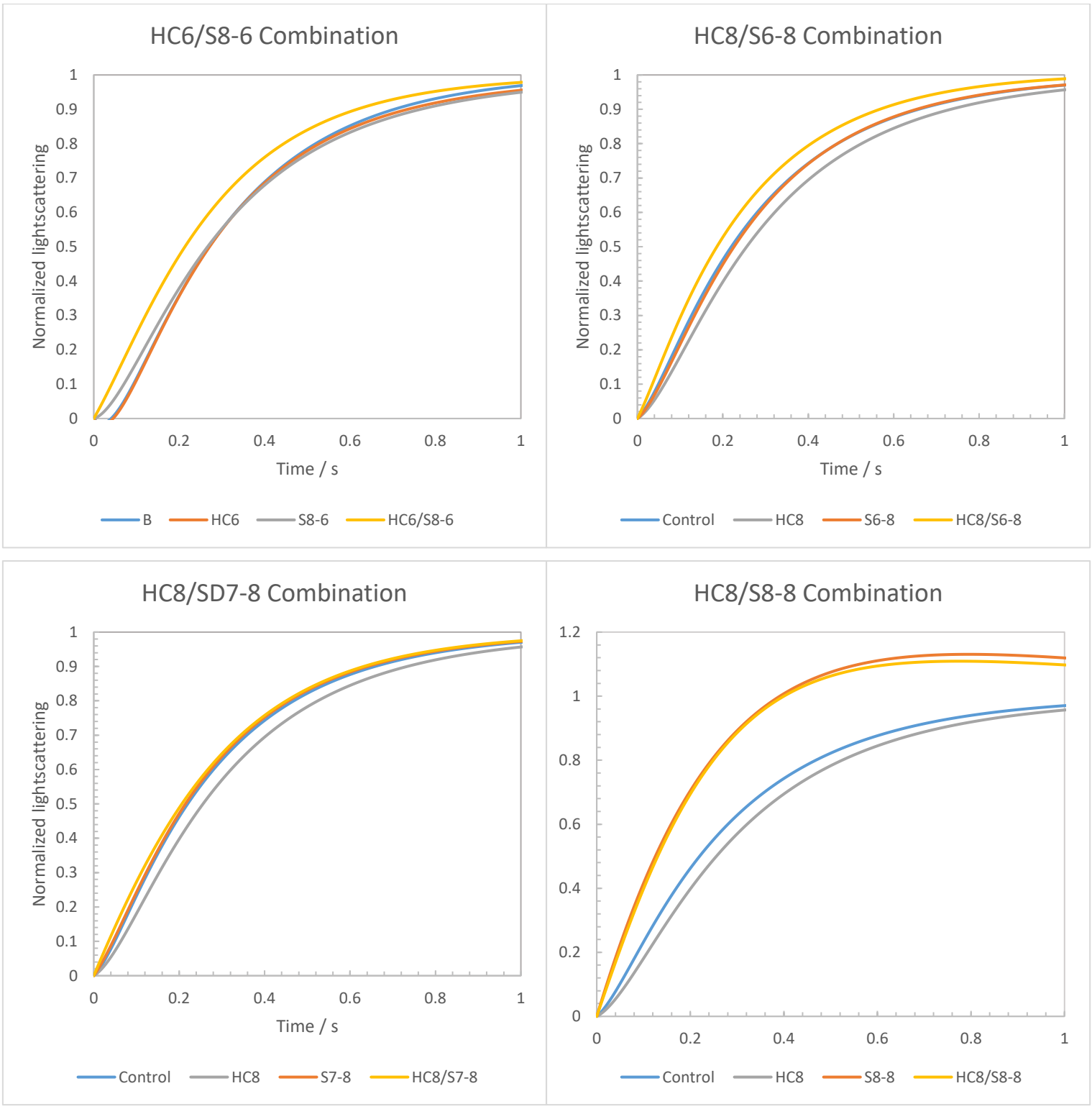

Figure S20. Stopped-flow traces of individual compounds and combined systems.

Ion transport experiments

LUV preparation for HPTS experiments: The large unilamellar vesicles (LUVs) were formed using egg yolk L-α-phosphatidylcholine (EYPC chloroform solution, 95%, 4 mL, 100 mg). To this solution was added 4 mL of MeOH and the solvent was slowly removed by evaporation under vacuum and dried overnight under high vacuum. The resulting thin film was hydrated with 2 mL of PBS buffer (10 mM sodium phosphate, pH 6.4, 100 mM NaCl) containing 10 μM HPTS (8-hydroxypyrene-1,3,6-trisulfonic acid trisodium salt). After hydrated for at least 30 minutes, the suspension was subject to 10 freeze-thaw cycles (liquid nitrogen and water at room temperature). The obtained white suspension was extruded 21 times through a 0.1 μm polycarbonate membrane in order to transform the large multi-lamellar liposome suspension (LMVs) into large unilamellar vesicles (LUVs) with an average diameter of 100 nm. The LUVs suspension was separated from extra-vesicular HPTS dye by using size exclusion chromatography (SEC, stationary phase Sephadex G-50, mobile phase: sodium phosphate buffer with 100 mM NaCl) and diluted with mobile phase to give 14 mL of 9.3 mM lipid stock solution (considering all the lipids have been incorporated).

HPTS assays for Ion Transport experiments: Here a fluorescent ratio data collection method was applied. 100 μL of stock vesicle solution was suspended in 1.85 mL of the corresponding buffer (10 mM sodium phosphate, pH 6.4, 100 mM of the analysed cation KCl or NaCl) and placed into a quartz fluorimetric cell. The emission of HPTS at 510 nm was monitored at two excitation wavelengths (403 and 460 nm) simultaneously. An experiment involved two main events: injection of 20 μL of analysed sample (at 20 s after the start of experiment), then 29 μL of aqueous NaOH (0.5 M) (at 40 s) was added, resulting in a pH increase of about one unit in the extra-vesicular media. Finally, the vesicles were lysed with detergent (40 μL of 5% aqueous Triton X-100), in order to equilibrate the intra-vesicular and extra-vesicular solutions.

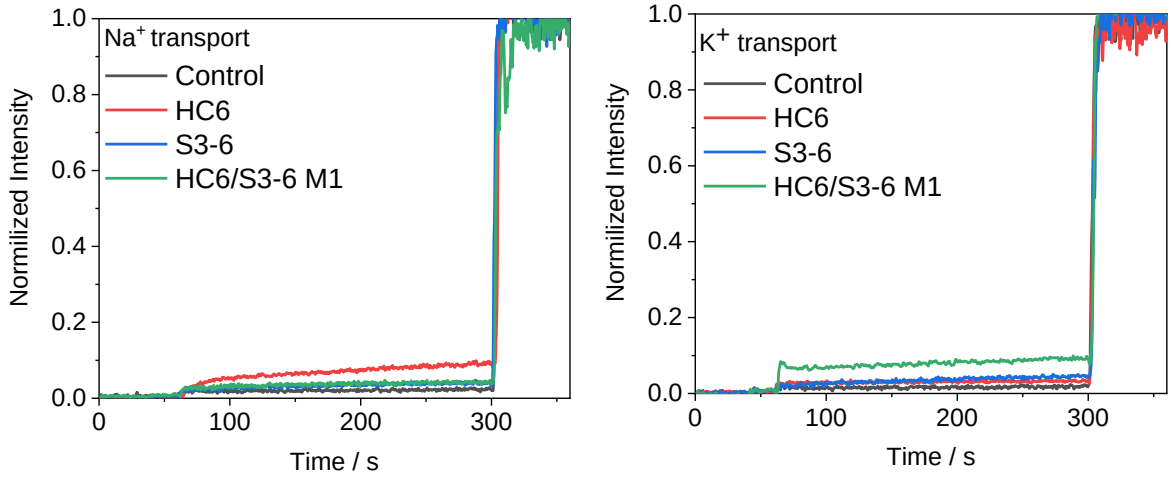

Figure S21. Comparison of cation transport activity expressed as normalized fluorescence intensity of 5 mM / 5 mM HC6/S3-6 system and individual compounds in the extra-vesicular medium containing 100 mM NaCl(left) or KCl (right).

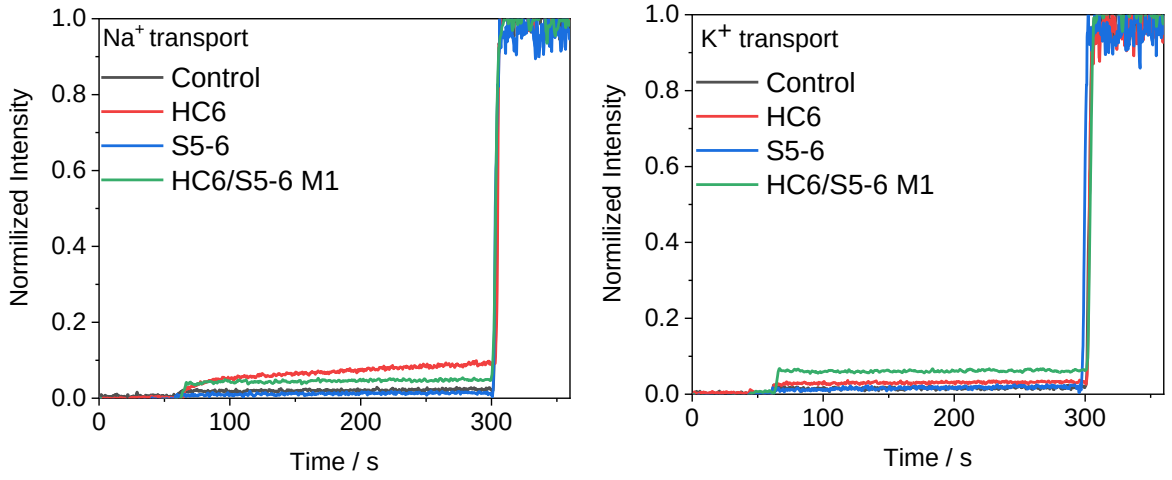

Figure S22. Comparison of cation transport activity expressed as normalized fluorescence intensity of 5 mM / 5 mM HC6/S5-6 system and individual compounds in the extra-vesicular medium containing 100 mM NaCl(left) or KCl (right).

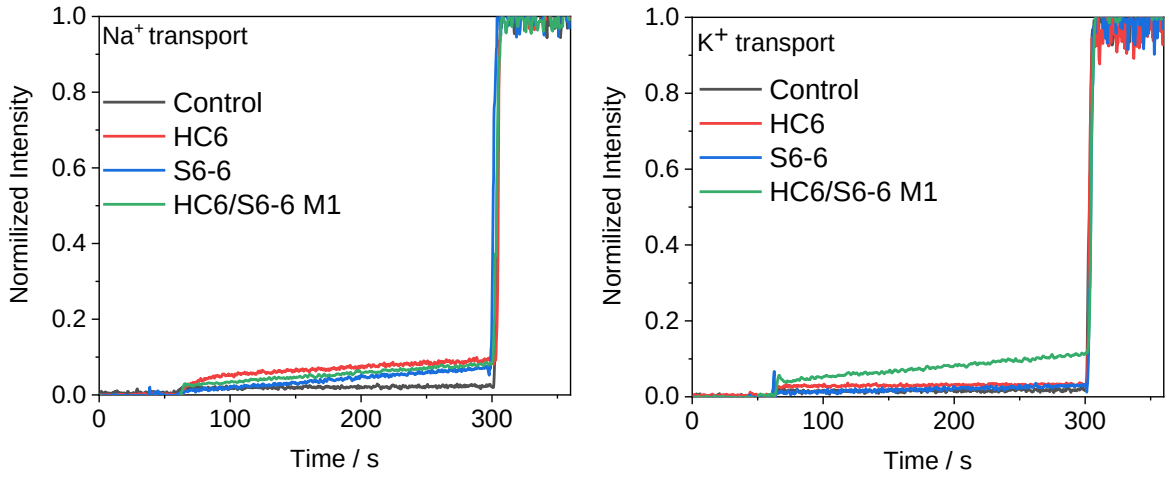

Figure S23. Comparison of cation transport activity expressed as normalized fluorescence intensity of 5 mM / 5 mM HC6/S6-6 system and individual compounds in the extra-vesicular medium containing 100 mM NaCl(left) or KCl (right).

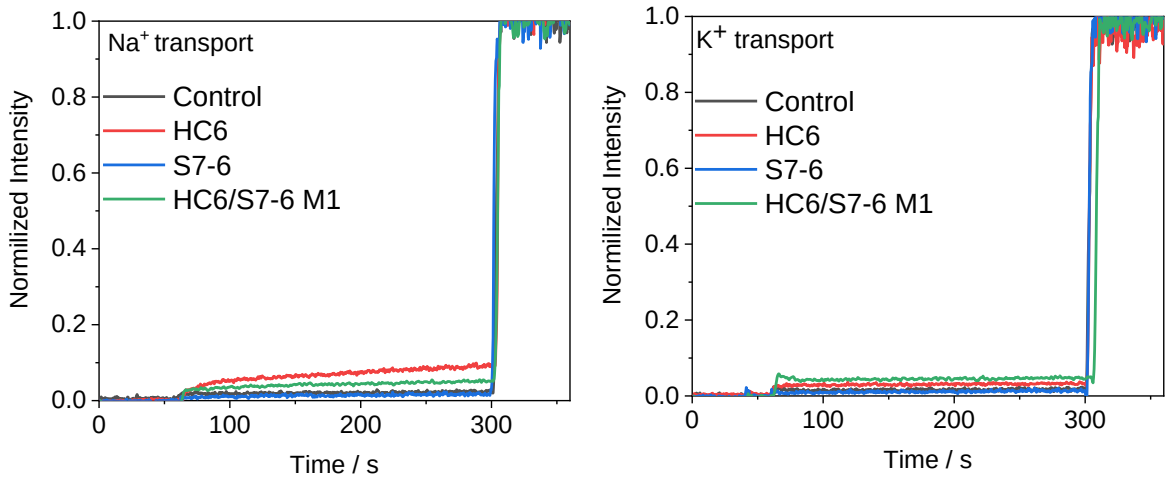

Figure S24. Comparison of cation transport activity expressed as normalized fluorescence intensity of 5 mM / 5 mM HC6/S7-6 system and individual compounds in the extra-vesicular medium containing 100 mM NaCl(left) or KCl (right).

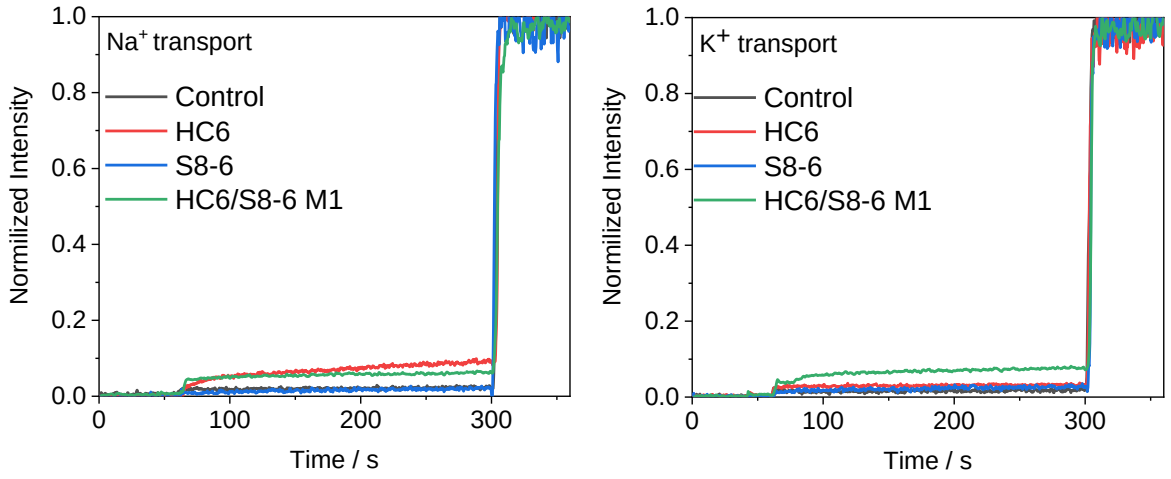

Figure S25. Comparison of cation transport activity expressed as normalized fluorescence intensity of 5 mM / 5 mM HC6/S8-6 system and individual compounds in the extra-vesicular medium containing 100 mM NaCl(left) or KCl (right).

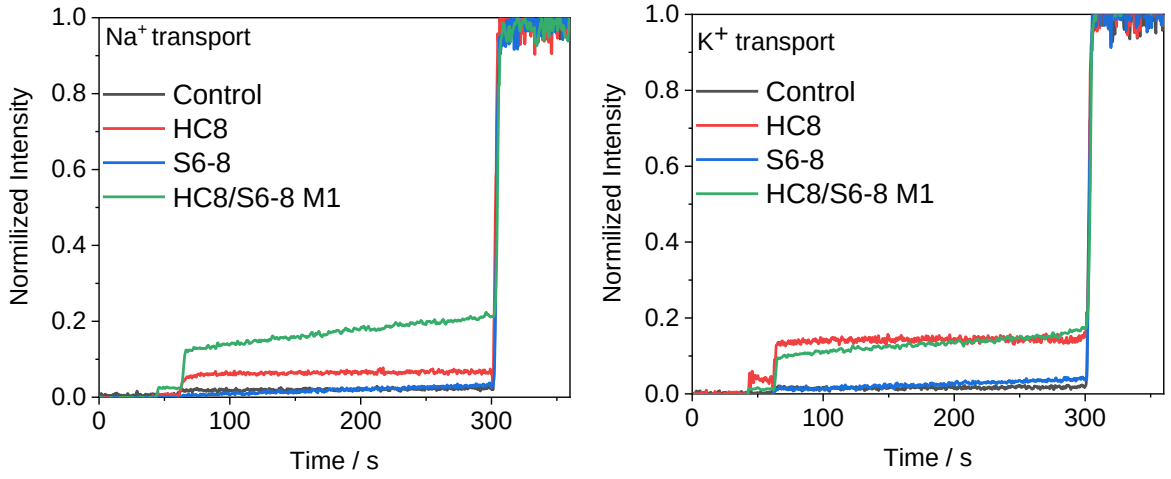

Figure 26. Comparison of cation transport activity expressed as normalized fluorescence intensity of 5 mM / 5 mM HC8/S6-8 system and individual compounds in the extra-vesicular medium containing 100 mM NaCl(left) or KCl (right).

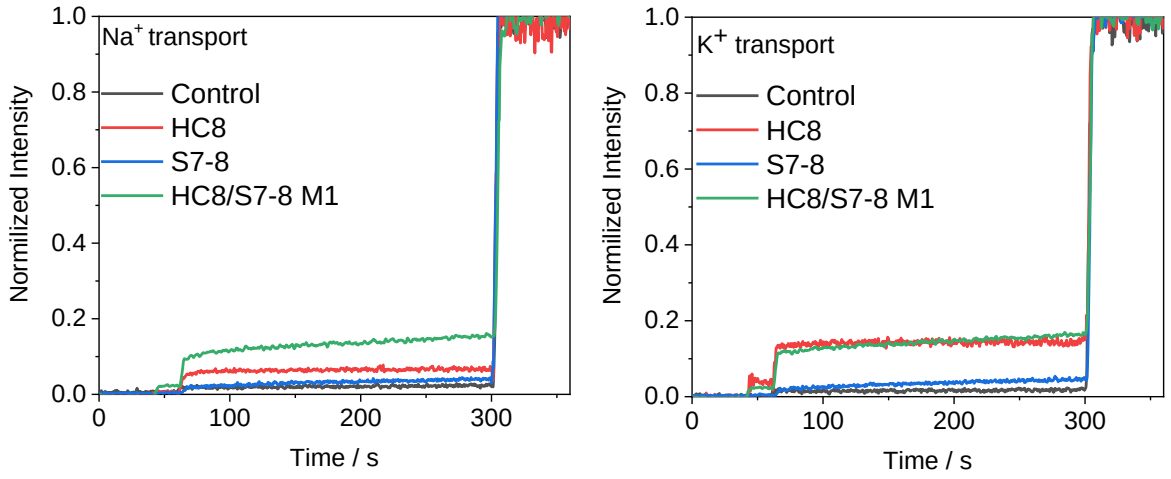

Figure 27. Comparison of cation transport activity expressed as normalized fluorescence intensity of 5 mM / 5 mM HC8/S7-8 system and individual compounds in the extra-vesicular medium containing 100 mM NaCl(left) or KCl (right).

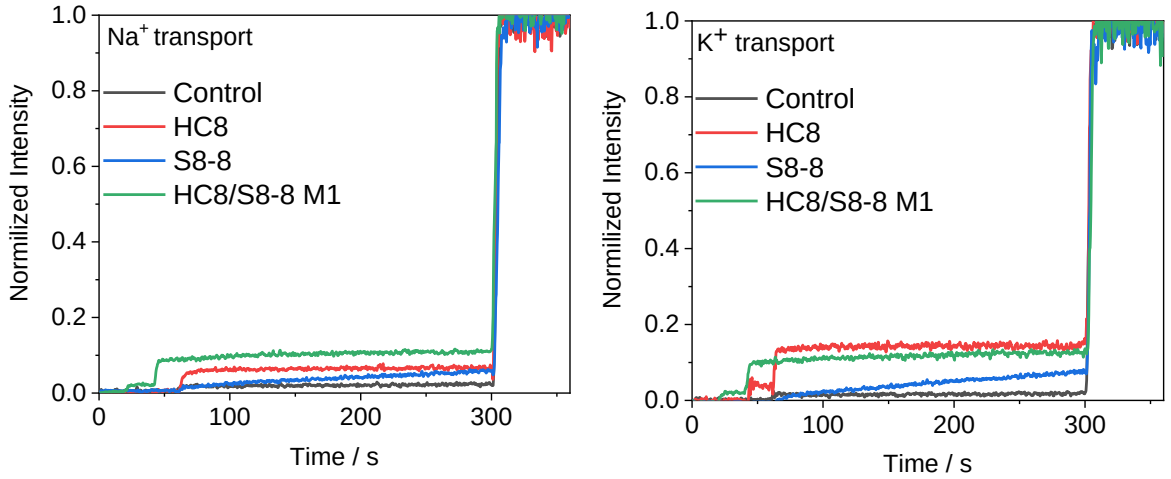

Figure 28. Comparison of cation transport activity expressed as normalized fluorescence intensity of 5 mM / 5 mM HC8/S8-8 system and individual compounds in the extra-vesicular medium containing 100 mM NaCl(left) or KCl (right).

Conclusions

Billions of years of evolution have contributed to the creation of ideal transport systems for living organisms. Discovered in 1992, Aquaporin-1 became the ancestor of the Aquaporin family of water transport proteins. This discovery contributed to the development of a new branch in water purification systems – Biomimetic membranes for desalination technologies. However, the complexity of the production of transport proteins at an industrial level, challenges with incorporation into synthetic membranes for desalination of water, as well as problems with membrane stability, prompted scientists to design systems that mimic the structure or/and properties of aquaporins – artificial water channels. As described in the first chapter, some systems have come close to achieving the goal of development of channels that have both extremely high water permeability and the ability to reject all kinds of ions, including the smallest one - the proton, nonetheless, this has been obtained through complex chemical syntheses, which makes large-scale production of these channels difficult. At the same time, there is no elegant, simple and effective solution, there is always a trade-off between water permeability, selectivity and system complexity, which is the main challenge for the design of new artificial water channels.

The PhD work described here contains results that include both fundamental and applicative researches towards the design of artificial water transport systems. From a fundamental point of view, the second chapter presents detailed work towards investigation of water transport mechanism of novel Pillar[5]arene-based artificial water channels. The pillar[5]arene platform was not chosen by chance; this relatively simple molecule has a number of advantages, such as a rather small pore size (~4.7 Å) and easy modification due to the presence of numerous functional groups on both sides of the ring. The discrete tubular dimers of rim-differentiated peralkyl-carboxylate-pillar[5]arenes – PAD systems – is a compromise solution between self-assembled and unimolecular AWCs, since these channels are formed due to the self-assembly of two large functionalized macrocycles. Investigation of the crystal structure showed that these systems can

form 2 types of pores via two different H-bonding vs hydrophobic binding modes. In addition, it was established that the narrowest part is formed *via* 15 hydrogen bonds between the carboxyl groups and water molecules together with closely spaced carboxy-phenyl groups with a fivefold helical conformation, which allows to reduce pore size from the characteristic for pillar[5]arene platform of 4.7 Å-pore diameter up to 2.8 Å, which in turn completely coincides with Aquaporin's ar/R selectivity filter. These observations correlated with ion transport results were obtained using fluorescence HPTS assay and single channel planar bilayer experiments. Thus, PAD channels did not show K^+ and Na^+ transport through lipid bilayer. High water transport ability of PAD channels (5.21×10^7 water molecules per second per channel for PAD8, one order of magnitude less than natural AQP) obtained by stopped-flow experiments could be explained due to that fact, that PAD channels have hybrid hydrophobic/hydrophilic nature in presence of alkyl chains (hydrophobic part) and numerous H-bonding sites from carboxylic groups (hydrophilic part) in the structure. MD simulation opened the door to understanding water transport through PAD channels. It was found that a H-bonding dimer formation is preferentially obtained and more stable in the membrane. The water translocation events led to the change in shape of the channel conduits in bilayer membranes from a single water-wirs to fully aggregated toroidal water clusters, which confers to these channels the self-adaptive behaviours and make it particularly self-protective against ions.

The third chapter of this thesis work was more directed towards the applicative side. Inspired by the results from chapter II, as object of research we chose non-modified pillar[5]arene, ancestor of the pillar[5]arene family of AWC. The ability of this macrocycles to form nanometric porous structure make it attractive to use as AWC for incorporation into well-developed PA matrix. We used *in-situ* aggregation-interfacial polymerization method of incorporation – *is*AGRIP – previously reported by our group, due to that fact that this method had already shown excellent results for I-quartet systems. By modification and optimisation of this method for pillar[5]arene, we succeeded in homogeneously incorporating PA[5] artificial water channels starting from their *in-situ* colloidal self-assembled superstructures into PA thin film composite

membranes. It was noticed, that concentration of PA[5] in ethanol-aqueous solution, as well as ethanol/water ratio of embedding colloidal solution impacted the performance of hybrid PA[5]-PA membranes, that may be related to a different distribution of PA5 nanoparticles in the PA layer due to different colloidal PA5 particles in the embedding solution. Thus, formation of large nanocrystals during IP process led to defects in the resulting PA layer, which is confirmed by experiments on incorporation using solid-state PA5 particles. This was proved by SEM imaging, Energy dispersive X-ray spectroscopy, as well as through ATR-FTIR analysis. Optimized hybrid PA5/PA TFC membranes with using 0.025% (w/w) of PA5 showed a ~40 % increase in water permeability with an excellent productivity of 50 L $m^{-2}h^{-1}$ under 17.5 bar applied pressure, while maintaining a high selectivity of 99.4 % during BWRO experiments.

In the fourth chapter, we have presented alternative design of self-assembled artificial water channels by using ideas of I-quartet systems. Inspired by natural transport proteins, it was decided to use hydrophobic heads instead of imidazole. Thus, a library of hydrophobic ureido derivatives was synthesized. Next step was focused on combining synthesized hydrophobic ureido derivatives with I-quartets in order to obtain synergistic combined hybrid AWC. I-quartet system was used as platform for new AWC due to its unique features, as narrow pore size (2.6 Å), relevantly high water permeability and selectivity. Besides, similarity of structures of both kinds of AWCs could form sequences of I-quartets and hydrophobic derivatives maintaining or even exceeding the original properties of imidazole-quartet systems. Water transport investigation performed by stopped-flow experiments showed that bi-component systems had multiplying times increased single channel permeability compared to single compound systems. Thus, the system HC8/S8-8 formed by combination for imidazole and benzosulfonamine derivatives had permeability of almost $8.2 \times \cdot 10^7$ water molecules per second, which is 16.7 times more than HC8 channels itself. Ion transport experiments did not show significant Na^+ and K^+ transport through lipid bilayer for selected systems.

The work done here opens up perspectives for future development in the field of artificial water channels. Despite the obtained results for pillar[5]arene-based channels, additional studies of the transport mechanism, as well as proton transport experiments are still necessary. Besides, the ability of rim-differentiated peralkyl-carboxylate-pillar[5]arenes to form a trimer with peralkylamino pillar[5]arene that could improve water permselectivity of those pillar[5]arene-based AWCs. Considering bi-component alkylureido AWC systems, crystal structures of hybrid channels were not investigated yet, as well as water transport mechanism. Future MD simulation of hybrid ureido derivative AWCs behaviour in lipid bilayer could solve this problem. For the fabrication of efficient membrane materials based on pillar[5]arene, other advanced physico-chemical characterization techniques as TEM and AFM could be used for additional confirmation of the presence of PA5 nanoparticles in the PA matrix and to examine the nanostructural features of the new membranes. In addition, performance and stability under SWRO conditions of hybrid PA5/PA TFC membranes should be done before the start of upscaling attempts in order to commercialize these membranes.

Here, we have described several AWC systems that successfully function as selective water filters both at molecular and macro levels. Further development of self-assembled AWC based on pillar[5]arene or ureido derivatives could lead to even more efficient and stable water channels. Thus, research in this area is essential if we have an aim to expand our knowledge of biomimetic systems.

List of Publications

This thesis is based on three scientific articles, represented in Chapter II-IV:

Chapter II **Biomimetic approach for highly selective artificial water channels based on tubular Pillar[5]Arene dimers**

D. Strilets, S. Fa, A. Hardiagon, M. Baaden T. Ogoshi*, **M. Barboiu***

Manuscript. Published in Angewandte Chemie, September 2020.

Reference: D. Strilets, S. Fa, A. Hardiagon, M. Baaden T. Ogoshi*, **M. Barboiu***, Biomimetic approach for highly selective artificial water channels based on tubular Pillar[5]Arene dimers" **Very Important paper**. *Angew. Chem*. **2020** DOI: 10.1002/ange.202009219; *Angew. Chem. Int. Ed.* **2020**, *59(51)*, 23213-23219. DOI: 10.1002/anie.202009219. *Copyright © 2020, Wiley*

Chapter III **Enhanced desalination polyamide membranes incorporating Pillar[5]arene via in-situ aggregation-interfacial polymerization-isAGRIP**

Dmytro Strilets, Sophie Cerneaux, Mihail Barboiu*

Manuscript. submitted to Angewandte Chemie, July 2021**.**

Chapter IV **Synergistic self-assembly of bi-component alkylureido systems into artificial water channels**

Dmytro Strilets, Sophie Cerneaux, Mihail Barboiu*

Manuscript in preparation.

Résume
L'objectif de ce travail est la conception des nouveaux types de canaux d'eau artificiels (AWC) auto-assemblés à haute efficacité, l'étude de leur permsélectivité vers l'eau et leur mécanisme de transport envisageant la transition de l'échelle nanométrique à l'échelle macroscopique. Pour celle-là on a évalué la possibilité de fabrication de membranes incorporent à l'AWC.
Le point de départ s'est concentrée sur l'étude des capacités de transport eau/ion et, de la nature du mécanisme de transport des dimères tubulaires discrets auto-assemblés de peralkyl-carboxylate-pilier [5]arènes (PAD). L'objectif était l'évaluation du transport et de la sélectivité du procès, la description du fonctionnement et de l'existence/stabilité structurelle des PAD dans les systèmes lipidiques comme potentiels canaux d'eau artificiel. En utilisant des méthodes avancées telles que la cristallographie aux rayons X et la simulation MD combinées à des techniques d'investigation du transport des ions d'eau comme la méthode Stopped Flow et la spectroscopie de fluorescence, on a montré que ces canaux sont capables à former des pores toroïdaux à l'intérieur de la bicouche lipidique. Ceux-ci ont pu transporter sélectivement les molécules d'eau jusqu'à 5,21 $\times 10^7$ H_2O/s/canal.
Inspirés par ces résultats, nous avons essayé, avec success, d'incorporer du pillier[5]arène dans des matrices polymères pour obtenir des matériaux fonctionnels pour des expériences de désalinisation de l'eau. La méthode utilisé est l'agrégation et de polymérisation interfaciale in situ - isAGRIP. Nous avons réussi à incorporer d'une manière homogène des canaux d'eau artificiels en PA[5], ce qui a conduit à une augmentation de ~ 40 % de la perméance de l'eau avec une excellente productivité de 50 L $m^{-2}h^{-1}$ sous 17,5 bar de pression appliquée, tout en maintenant une sélectivité élevée de 99,4 %. .
Dernièrement, on a réalisé l'expansion de la famille des canaux d'eau artificiels par la synthèse de nouveaux dérivés uréido hydrophobes. Par leur mélange avec des I-quartets hautement un nouveau canal d'eau supramoléculaire hybride auto-assemblé a été construit. Les études sur le transport de l'eau et des ions ont montré que les systèmes bi-composants ont multiplié quelques fois la perméabilité à un seul canal par rapport aux systèmes monocomposé, alors qu'aucun transport d'ions significatif n'a été détecté. La meilleure performance a été montrée par le système HC8/S8-8 formé entre les dérivés d'imidazole et de benzsulfonamine avec une perméabilité de près de 8,2 $\times \cdot 10^7$ H_2O/s/canal.
En conclusion ce travail a décrit plusieurs systèmes AWC qui fonctionnent comme filtres à eau de haute sélectivité à l'échelle nano bien que a l'échelle macro.
Mots-clés: canaux d'eau artificiels ; membranes biomimétiques; désalinisation de l'eau; Pilier[5]arène ; I-quatuors; auto-assemblage

Abstract
The objective of this work is the design new types of highly efficient self-assembled artificial water channels (AWC) and the investigation of their water permselectivity and transport mechanism aiming for the transition from nanoscale to macroscale by showing of possibility of AWC-incorporated membrane fabrication.
The starting point focused on the investigation of water/ion transport abilities and nature of transport mechanism of self-assembled discrete tubular dimers of rim-differentiated peralkyl-carboxylate-pillar[5]arenes (PADs). The objective was the assessment of water transport and selectivity of the transport, by describing the functioning and structural existence/stability of PADs in lipidic systems as perspective artificial water channels. By using advanced methods as X-Ray crystallography and MD simulation combined with water and ion transport investigation techniques such as Stopped-flow methods and fluorescence spectroscopy, it was proven that those channels able to form toroidal pores inside lipide bilayer, which could selectively transport water molecules up to 5.21 $\times 10^7$ H_2O/s/channel.
Inspired by those results, an attempt was made to incorporate pillar[5]arenes into polymeric matrices to obtain functional materials for water desalination experiments using in-situ aggregation-interfacial polymerization method – isAGRIP. We succeeded to incorporate homogeneously PA[5] artificial water channels, which led to a ~40 % increase in water permeance with an excellent productivity of 50 L $m^{-2}h^{-1}$ under 17.5 bar of applied pressure, while maintaining high selectivity of 99.4 %.
Finally, this work focused on expanding the artificial water channel family by synthesising new hydrophobic ureido derivative. These were combined with highly efficient I-quartets in order to construct novel hybrid supramolecular self-assembled water channels. Water and ion transport investigations showed that bi-component systems presents a multiple time increase single channel permeability compared to single compound systems, while no significant ion transport was detected. The highest performance was shown by the system HC8/S8-8 formed by combination of imidazol and benzsulfonamine derivatives with a permeability of almost 8.2 $\times \cdot 10^7$ H_2O/s/channel.
In conclusion, this work has described several AWC systems that function as selective water filters both on a molecular as well as on macro-level.
Keywords: artificial water channels; biomimetic membranes; reverse osmosis; water purification; thin-film composite, Pillar[5]arene, I-quartets, water permeability